Development of all-in-one CRISPR/Cas9 and CRISPRi AAV constructs to treat autosomal dominant retinitis pigmentosa

Caroline Frances Peddle BSc (Hons)

St Cross College

Thesis submitted for a DPhil in Clinical Neurosciences

Hilary Term 2021

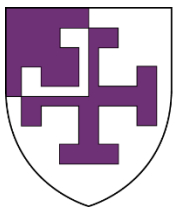

ST CROSS COLLEGE
UNIVERSITY OF OXFORD

NLO
Nuffield Laboratory of Ophthalmology

Acknowledgements

I would like to express my thanks to my primary supervisor Robert MacLaren, who helped guide this thesis throughout the past four years. He provided invaluable clinical insight, always encouraging me to relate my daily molecular experiments back to the wider goal of treating an incurable disease. I am immensely grateful to my secondary supervisor Michelle McClements for all her help and encouragement. She was always there to listen and advise, from troubleshooting experiments, to sharing in the highs and lows of this project on a daily basis.

I am extremely thankful to the Mabel Churn Scholarship who funded my PhD, without whom, this research could not have been conducted. I would also like to thank The Nuffield Department of Clinical Neurosciences and St Cross College for giving me to opportunity to study and learn in such an incredible environment.

I want to extend my gratitude to everyone in the MacLaren research team. Between training each other in new techniques, endless lunchtime discussions about the differences between mandarins and clementines, and incredible lab dinners, you created an easy working atmosphere in the lab full of comradery. Thank you to those who were there to help me at the beginning while I was finding my feet – Shaun Wood, Harry Orlans, Mark Hassall, Maria Patricio, Cristina Martinez, Alun Barnard, and Marco Bellini – and to those who kept me company on a daily basis – Imran Yusuf, Ahmed Salman, Federica Staurenghi, Jasleen Jolly, Ariel Kantor, Tina Storm, and Arantxa Bolinches Amoros. It has been a pleasure working with you all. To Team CRISPR – Michelle McClements, Lewis Fry, Elena Piotter, and Marta Stevanovic - thank you for embracing the sticker charts and indulging my excitement about having teammates. A special thanks goes to Laurel Chandler, my deskmate, who went above and beyond. She never let a bad day stymie the expansion of the “wall of fun”.

To my incredible friends and family, I am so grateful for your combined love and support, and I cannot thank you enough. To my parents, brother, and grandparents, thank you for nurturing my curiosity for

learning, whole-heartedly encouraging me to pursue my goals, and always believing in me. Thank you to my partner Ian for providing limitless patience and understanding, moving to Oxford to support me, and always making sure there was food in the house. Thank you to my amazing friends for all your support: for listening to my experimental woes and always cheering me along. To 24, thank you for teaching me to always look on the bright side of life.

Contents

Abstract

Dominant mutations in *RHO* (rhodopsin) are the most common cause of autosomal dominant retinitis pigmentosa (RHO-adRP). RHO-adRP causes progressive loss of rod cells, followed by cone cells, leading to blindness. This disease is a candidate for CRISPR gene editing, as reduction of mutant rhodopsin is associated with phenotypic rescue. This thesis optimises all-in-one CRISPR/Cas9 and CRISPRi adeno-associated viruses (AAVs) and explores their potential as RHO-adRP gene therapy vectors.

Following construct optimisation in vitro, a CRISPR/Cas9 and CRISPRi plasmid carrying SaCas9 and dSaCas9.KRAB, respectively, were generated. Both demonstrated knock down of endogenously expressed EGFP in a transgenic cell line. For allele-specific knock down of RHO, the CRISPR constructs must target a region unique to the mutant allele. Bioinformatic screening of *RHO* identified seven non-pathogenic single nucleotide polymorphisms (SNPs) that were targetable with SaCas9. Two of these SNPs could be targeted allele-specifically, with high CRISPR/Cas9 gene disruption and CRISPRi gene repression rates of 38.5-73.2 % and 43.1-65.8 %, respectively. In heterozygous patients, targeting the SNP on the mutant *RHO* offers a mutation-independent allele-specific targeting strategy.

As a proof-of-concept for targeting rod cells, the AAV were subretinally injected into Nrl-EGFP mice, in whom enhanced green fluorescent protein (EGFP) expression is limited to rod photoreceptors. To restrict Cas9 expression to rods cells only, a novel 154 bp rod cell-specific promoter was identified. This shortened promoter from the *PDE6B* gene was active in human retinal explants, the human retinoblastoma-derived cell line Y79, and drove strong rod cell-specific expression in mice. The CRISPRi AAV was unable to repress EGFP, despite high transgene expression. The CRISPR/Cas9 AAV however, drove strong EGFP disruption. It produced 4.1 % EGFP indels, resulting in a reduction of EGFP mRNA and fluorescence of 55.3% and 36.5 %, respectively. The all-in-one CRISPR/Cas9 AAV is therefore able to drive strong gene disruption in rod cells in vivo, making it a useful vector for the treatment of *RHO*-adRP.

This thesis describes in detail the development of these all-in-one CRISPR/Cas9 and CRISPRi AAV vectors from proof-of-concept to in vivo study and advances the potential for using such therapies in future treatments of RHO-adRP.

Publications

The work in this thesis contributed to the following published abstracts, journal articles, and book chapters:

First author publications:

1. The Application of CRISPR / Cas9 for the Treatment of Retinal Diseases. *Journal article: Yale Journal of Biology and Medicine (2017)*. See Appendix 9.10.
2. Evaluation of the efficiency and specificity of short variants of the human PDE6b promoter in photoreceptor-like cells in vitro and ex vivo. *Published abstract: IOVS (2017)*
3. Validation of Staphylococcus aureus Cas9 gRNAs targeting EGFP present in the rod cells of the Nrl-EGFP mouse line. *Published abstract: IOVS (2018)*
4. Effect of single guide nucleotide mismatch in CRISPR/Cas9-mediated disruption of the human rhodopsin gene in vitro. *Published abstract: IOVS (2019)*
5. CRISPR interference – potential application in retinal disease. *Journal article: International Journal of Molecular Sciences (2020)*. See Appendix 9.11.

Other authored publications:

6. Guide RNA orientation influences Cas9 expression in a single vector approach to CRISPR editing in a model system. *Published abstract: IOVS (2019)*
7. Promoter Orientation within an AAV-CRISPR Vector Affects Cas9 Expression and Gene Editing Efficiency. *Journal article: CRISPR Journal (2020)*
8. An analysis of the Kozak consensus in retinal genes and its relevance to gene therapy. *Journal article: Molecular Vision (2021)*
9. CRISPR Genome Engineering for Retinal Diseases. *Book chapter: Curing Genetic Diseases though Gene Reprogramming (to be published October 2021)*

Abbreviations

AAV	Adeno-associated virus
adRP	Autosomal dominant retinitis pigmentosa
CAG	CMV early enhancer fused to chicken beta-actin promoter
Cas9	CRISPR-associated protein 9
CRISPR	Clustered, regularly interspaced, short, pandromic repeats
CRISPR/Cas9	CRISPR/Cas9 gene disruption
CRISPRi	CRISPR interference
cSLO	Confocal scanning laser ophthalmoscopy
dCas9	Catalytically inactivate “dead” Cas9
dSaCas9	Catalytically inactivate “dead” Cas9 from *Staphylococcus aureus*
dSaCas9-KRAB	Catalytically inactivate “dead” Cas9 from *Staphylococcus aureus* fused with a KRAB repressor
EGFP	Enhanced green fluorescent protein
ERG	Electroretinogram
gRNA	single guide RNA
HEK293	Human embryonic kidney cell line 293
HMAR	Heat-mediated antigen retrieval
KRAB	Krüppel associated box
IHC	Immunohistochemistry
Indels	Small insertions and deletions
ITR	Inverted terminal repeats
MAF	Minor allele frequency
MFISH	Multicolour fluorescence in situ hybridisation
MOI	Multiplicity of infection
NTC	No template control
OCT	Optical coherence tomography
pA	Polyadenylation
PBS	Phosphate buffered saline

PCR	Polymerase chain reaction
PDE6B	Phosphodiesterase 6B
PDE6Bp	Phosphodiesterase 6B promoter
RHO	Rhodopsin
RHO-adRP	Autosomal dominant retinitis pigmentosa caused by rhodopsin mutations
RHOp	Rhodopsin promoter
RNP	Ribonucleoprotein
RP	Retinitis pigmentosa
SaCas9	Cas9 from *Staphylococcus aureus*
Scram	gRNA with a “scrambled” sequence
SNP	Single nucleotide polymorphism
SpCas9	Cas9 from *Streptococcus pyogenes*
TIDE	Tracking of indels by decomposition software
Untr	Untransfected or Untransduced sample

1 Introduction

1.1 Overview

Autosomal dominant retinitis pigmentosa (adRP) is an inherited retinal degeneration primarily affecting rod cells, a specialist light-sensing cell of the retina. The rod cells degenerate circumferentially, reducing patient's visual field and eventually resulting in complete blindness. adRP is caused by dominant mutations in a range of genes, the most common of which is rhodopsin (*RHO*)[1]. *RHO* is almost completely haplosufficient, meaning one working copy of the gene is able to provide sufficient levels of rhodopsin protein to sustain wild type function (although mild electroretinogram [ERG] changes have been reported in individuals carrying one null mutation)[2]. Disabling the mutant rhodopsin allele has been shown to alleviate adRP, preventing retinal degeneration and therefore further loss of vision[3].

CRISPR/Cas9 and CRISPRi are molecular techniques that are used to disrupt, or knock down, a gene of interest, respectively. Targeting these CRISPR techniques exclusively to the mutant *RHO* allele may reduce expression of the mutant rhodopsin protein, leaving the unaffected wild type rhodopsin to provide essential protein function. The CRISPR/Cas9 system from the bacterium *Staphylococcus aureus* can be packaged into a single adeno-associated virus (AAV), which acts as a delivery vehicle. If injected subretinally into a patient with adRP this could prevent further degeneration of the retina, halting the disease progression permanently with a single treatment. This thesis explores the potential use of a single CRISPR AAV gene therapy system as a treatment for adRP caused by *RHO* mutations (RHO-adRP).

1.2 Rhodopsin in the human retina

The retina is the innermost tissue layer at the back of the eye and is responsible for detecting light and converting it into an electrochemical signal. Light entering the eye is focused on the retina by the cornea and the lens. The retina contains multiple layers of cells, which can be distinguished under a microscope (Figure 1.1A, B). One of the retinal layers, called the photoreceptor layer, is made up of rod cells and cone cells, which contain photopigments allowing them to detect light and create a response, initiating the phototransduction cascade. This response is modulated as it passes through the retinal layers to the retinal ganglion cells, which form part of the optic nerve, ultimately sending the electrochemical signal to the brain.

Rod and cones cells are unevenly distributed throughout the retina. Rod cells, which have high sensitivity allowing the detection of low level light, are found around the peripheries of the retina and account for approximately 95 % of photoreceptors[4,5]. Cone cells, on the other hand, provide colour and detailed vision in bright light. They are sparsely distributed in the peripheries and are concentrated centrally in the retina within an area called the fovea, where rod cells are absent.

Rod cells and cone cells can be described in four sections: the synapse, the nucleus, the inner segment, and the outer segment (Figure 1.1C). In rod cells, this outer segment contains stacked internal membranes known as discs which each house between 10^4 and 10^6 rhodopsin molecules. Rhodopsin is a photopigment responsible for detecting light and is expressed exclusively in rod cells[6]. It is a combination of an opsin protein (henceforth referred to as simply "rhodopsin") and the chromophore retinal. Rhodopsin is 348 amino acids in length and consists of seven transmembrane α-helices. Correctly processed rhodopsin is essential for the survival of rod cells: *Rho* knockout mice do not develop outer segments and have progressive retinal degeneration[7]. When light interacts with retinal its chemical conformation changes, altering the shape of rhodopsin. This allows rhodopsin to interact with protein transducin which triggers the phototransduction cascade.

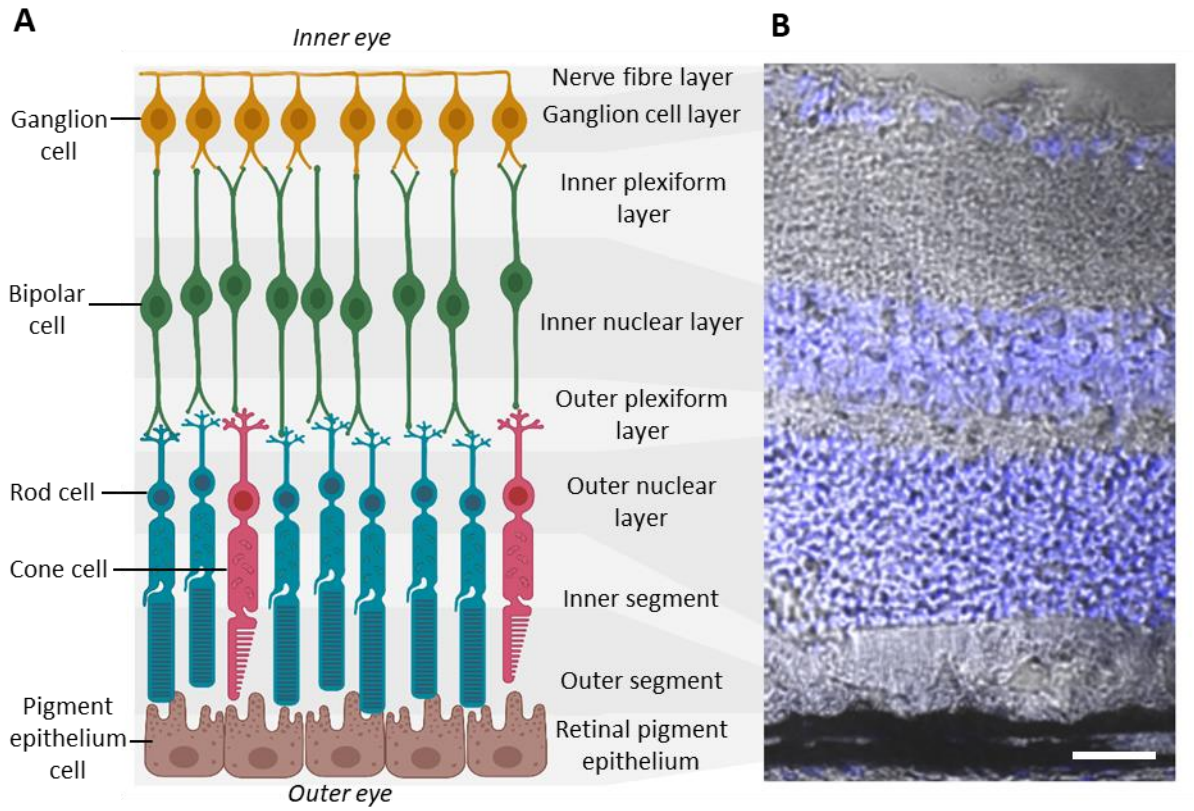

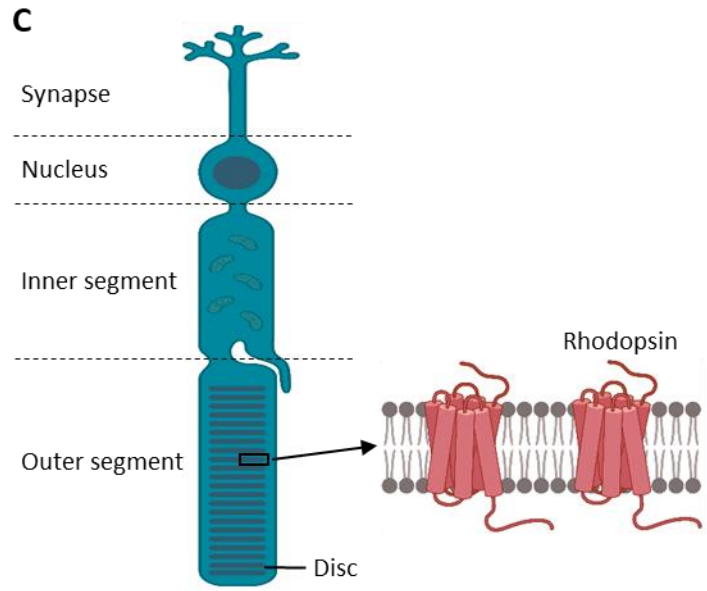

Figure 1.1 The human retina.
Diagrams not to scale. ***A)*** *Diagram of retinal cells and layers.* ***B)*** *Stained section of mouse retina showing retinal layers, DAPI (blue) stain is cellular nuclei. Scale bar is 5 µm.* ***C)*** *Rod cell morphology. Rhodopsin molecules are located in the disc membranes within the outer segment.*

1.3 Autosomal dominant retinitis pigmentosa

1.3.1 Retinitis pigmentosa pathophysiology

Retinitis pigmentosa is an inherited retinal degeneration that causes progressive sight loss over several years or decades, eventually resulting in complete blindness. The loss of vision experienced by these patients is life changing, and has been shown to negatively impact mental health, socialising, independence, and employment[8–11]. It affects approximately 1 in 4000 individuals, making it the most common inherited retinal dystrophy globally[12]. While disease progression is highly variable, classic retinitis pigmentosa symptoms begin in adolescence, becoming severe in middle age[1,13]. Genetic mutations cause the loss of rod cells from the periphery of the retina, gradually degrading towards the centre over time (Figure 1.2). This causes reduced low light vision, termed nyctalopia, and then tunnel vision as the loss of rod cells constricts the visual field[14]. As the disease progresses, the retinal pigment epithelial cells break down, and eventually central cone cells die, decreasing the patient's visual acuity. The pathways ultimately responsible for photoreceptor death are not fully understood and may be variable with the pathogenic gene[15]. Apoptosis, oxidative stress, inflammation, and necrosis have all been implicated[16–22].

Diagnosis of retinitis pigmentosa is based on patient's loss of night vision, constricted visual field, changes in morphology and response of the retina, family history, and retinal electrophysiology[14,25]. It

Figure 1.2 Fundus photographs of normal and retinitis pigmentosa-affected eyes.
Image of the right eye of a patient with no retinal degeneration "Normal", and with retinitis pigmentosa[23,24].

is important to note that retinitis pigmentosa can occur as a *de novo* mutation without a family history present[1,14,25].

1.3.2 Genetics of autosomal dominant retinitis pigmentosa

Retinitis pigmentosa can be inherited in an autosomal dominant, autosomal recessive or X-linked manner and is highly heterogeneous. Autosomal dominant retinitis pigmentosa (adRP) makes up 15-40 % of global cases and generally has the latest onset and slowest progression of the inheritance types[1,13,15] (Figure 1.3). As of June 2021, 30 pathogenic adRP genes have been identified, whose proteins have a wide range of functions, including rod cell structure, phototransduction, RNA processing, and amino acid synthesis, amongst others[1,26]. The most common pathogenic adRP gene is rhodopsin (*RHO*) which accounts for 20-40 % of cases[15,27]. This is approximately 59 000 to 312 000 individuals worldwide. Despite advancements in sequencing technology, and increasing routine genetic screening, the pathogenic mutation cannot be identified in 22-50 % of patients[1].

1.3.3 RHO mutations

RHO codes for the protein component of the rhodopsin molecule and there are over 150 point

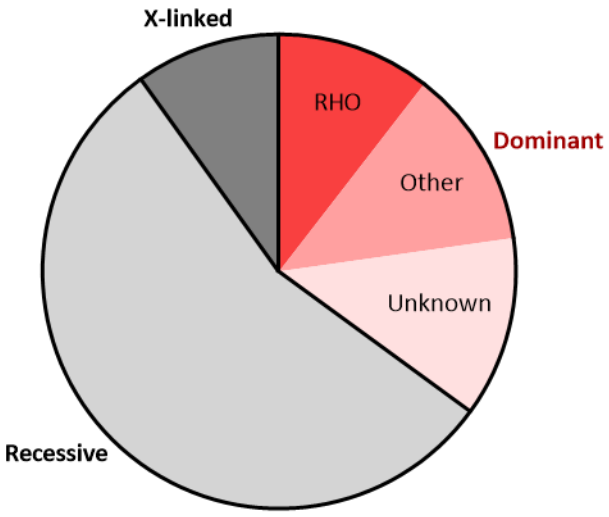

Figure 1.3 Approximate proportion of retinitis pigmentosa cases caused by mutations in RHO.

mutations in *RHO* which cause adRP[15]. Frequency of pathogenic *RHO* mutations are highly variable with geographic and ethnic populations and are strongly influenced by founder mutations[1,28–30]. For example, the Pro23His mutation accounts for about 10 % of adRP cases in the United States but is globally quite rare[31]. Pathogenic mutations are either toxic gain-of-function, where the mutant rhodopsin protein acquires a detrimental mechanism of action, or dominant-negative, where the mutant rhodopsin protein inhibits the activity of the wild type rhodopsin protein. Individual mutations have varied implications for rhodopsin, and subsequently affect rod cell structure and function differently. They have been categorised into seven classes based on their mechanism of effect (Table 1.1)[3,32]. While some classes are linked to the location of the mutation within the amino acid coding sequence, for example, Class I mutations are clustered in the C-terminus cytoplasmic domain of RHO, other classes, such as Class 2, are found throughout the RHO protein. The majority of *RHO* mutations affect either folding or trafficking of the protein, but mutations affecting post-translational modifications, stability, dimerization, and activation of the phototransduction cascade have also been identified. Many of these mutations result in the accumulation of mutant rhodopsin in inappropriate locations, inhibiting normal cellular function or causing cellular stress.

Identifying the disease mechanism and classifying these mutations is difficult. Approximately 40 % of mutations are unclassified, while the best studied mutation, Pro23His, has evidence to suggest its

Table 1.1 Classification of RHO mutations as described by Athanasiou et al. (2018)[3]

Class	Toxic mechanism
1	RHO is not transported to the outer segment
2	RHO is misfolded and retained in the endoplasmic reticulum
3	RHO is endocytosed and disrupts vesicular traffic
4	RHO post-translational modifications are affected, reducing stability
5	RHO activation of transducin is altered
6	RHO is constitutively activated
7	RHO cannot form essential dimers
Unclassified	Not yet identified

classification as both a Class 2 misfolding and a Class 4 dominant-negative mutation[3]. In some cases, the inheritance pattern of the disease is also unclear: both the E150K and M253I mutations have been described as both autosomal recessive mutations, and as autosomal dominant mutations which cause a clinically mild form of retinitis pigmentosa when present on only one allele[3,33]. Finally, infrequently cited mutations are often subsequently found to be benign rather than pathogenic[1,3].

1.3.4 Treatment strategies

Different treatment strategies are being explored for adRP caused by *RHO* mutations (RHO-adRP). These can be divided broadly into two approaches: preventing retinal degeneration or restoring lost vision. Strategies that restore lost vision treat late stage patients with severe retinal degeneration regardless of the pathogenic gene. These strategies provide a replacement for photoreceptors, creating a system for detecting light and generating an electrical response that stimulates the remaining retinal layers. This replacement can be retinal progenitor cells attached to a retinal grafts, electronic retinal implants (both of which are surgically fixed in the eye), or optogenetics. In optogenetics, a gene encoding a light-sensitive protein is delivered to retinal cells that do not naturally respond to light. All three techniques are involved in ongoing clinical trials, and multiple electronic retinal implants are approved for use in the USA and the EU. Electronic retinal implants and retinal grafts have demonstrated safety and some degree of improvement in vision, although they are still overcoming issues including adverse events and longevity[34–36].

If aiming to prevent retinal degeneration, patients need to be treated while there are remaining rod cells to preserve. Approaches have included delivering chaperone proteins to improve RHO folding, drugs to inhibit cell death mechanisms, histone deacetlyase inhibitors to reduce global *RHO* expression, or over-expressing wild type *RHO* to treat dominant negative mutations. These strategies have had variable results in vivo, and the success of the treatment is often mutation-dependent as they target the disease pathway[3,13].

RNA-based, or CRISPR-based techniques aim to reduce the levels of mutant rhodopsin by targeting *RHO* mRNA, or DNA, respectively[42]. Approaches can either target the mutant *RHO* exclusively, or target both the wild type and mutant *RHO*. Cellular rhodopsin levels below 50 % are toxic to rod cells, and therefore strategies targeting both alleles must also deliver a resistant copy of *RHO* by gene augmentation[38,43]. Following significant visual improvements in vivo, both strategies are currently being used in clinical trials[42,44–47].

Using gene disruption techniques such as CRISPR/Cas9 or CRISPRi to exclusively suppress the mutant *RHO* could provide a mutation-independent approach to preventing retinal degeneration. The exact disease pathway would not need to be understood, as removal of the mutant *RHO* allele would remove its toxic effects regardless of the mechanism. If delivered by AAV, which allow long-term expression, the disease could be treated with a single injection in each eye. Multiple in vivo studies have been conducted that use CRISPR/Cas9 or CRISPRi to knock down genes in the retina as a treatment for inherited retinal dystrophies[48,49]. These have achieved significant suppression of retinal

Table 1.2 In vivo experiments using CRISPR/Cas9 to treat animal models of RHO-adRP.

Reference	Gene Target	Model	Methodology	Results
Latella et al. 2016[37]	Removal of *Rho* P23H locus	*Rho*$^{-/-P23HTg}$ mice	Subretinal injection and electroporation of plasmid	16 % of reads contained the desired 24 bp deletion
Bakondi et al. 2016[38]	Allele-specific disruption of *Rho*^{S334}	*Rho*$^{S334ter-3}$ rats	Subretinal injection and electroporation of plasmid	Delayed loss of rod function and prolonged cone survival
Yu et al. 2017[39]	Disruption of *Nrl*	*Rho*^{P347S} mice	Subretinal injection of AAV	Increased retinal preservation and 35 % increased visual acuity
Li et al. 2018[40]	Allele-specific disruption of *Rho*^{P23H}	*Rho*$^{+/P23H}$ and *Rho*$^{P23H/P23H}$ mice	Subretinal injection and electroporation of plasmid	Allele-specific editing of mutant *Rho*. Increased outer nuclear layer thickness in treated areas.
Giannelli et al. 2018[41]	Allele-specific disruption of *Rho*^{P23H}	*Rho*$^{+/P23H}$ mice	Intravitreal injection of AAV	16.7-20.5 % editing of Rho^{P23H} in strongly transduced cells.

genes leading to improvements in photoreceptor morphology, retinal responses, and visual acuity in treated animals. Four of these studies used CRISPR/Cas9 to disrupt *Rho* in models of autosomal dominant retinitis pigmentosa; they demonstrate in vivo *Rho* disruption is achievable using a range of delivery methods, but none have explored a single AAV delivery method to date (Table 1.2). CRISPRi gene repression of *RHO* has not been attempted in vivo.

1.4 CRISPR

CRISPR/Cas9 and CRISPRi are gene modification techniques that can be used to edit genes, or repress genes, respectively. They offer a promising treatment for autosomal dominant diseases, including adRP, by silencing the pathogenic gene. Compared to previously used techniques for DNA editing, such as zinc finger nucleases, and TALENs, CRISPR/Cas9 has a wider targeting capability, higher efficiency, and is easier to deliver into cells[50–52]. CRISPRi reduces transcription of a chosen gene. Prior to CRISPRi, RNAi was the leading technique for gene repression in eukaryotic cells. RNAi targets mRNA and CRISPRi targets DNA; CRISPRi therefore has access to more potential binding sites in untranscribed regions. While the two techniques have comparable efficiencies, CRISPRi rarely reports any off-target effects, whereas off-target effects with RNAi are common[49]. The advantages and versatility of the CRISPR/Cas9 system has made it a game changer in gene editing and regulation, with rapid development of the technology since its discovery in 2012[53].

1.4.1 Mechanism

The CRISPR/Cas9 system is a naturally occurring bacterial defence mechanism against invading phages. The bacteria contain two specialized RNA molecules called crRNA and tracrRNA, which form a complex with the bacterial endonuclease protein Cas9. This complex is guided to invading phage DNA that shares sequence homology with crRNA. In order to bind to the DNA, Cas9 requires a short, 3-8 bp DNA element called a Protospacer Adjacent Motif (PAM) site immediately adjacent to the crRNA binding site. The exact sequence requirements of the PAM site vary with bacterial species. Following binding, Cas9 will cleave both strands, preventing phage colonization[53–56](Figure 1.4A).

This system is used within biological research to disrupt genes of interest. The target gene exons are screened for PAM sites, and then a single guide RNA (gRNA, which is an artificial amalgamation of crRNA and tracrRNA first created by Jinek et al in 2012[53]) is designed to match the region immediately

adjacent to the chosen PAM. By providing the cell with both the Cas9 and gRNA, Cas9 will induce a double stranded break in the target gene. The cell then attempts to repair this break through the non-homologous end joining pathway, but this process is extremely error prone. This causes small insertions and deletions (indels) to be incorporated into the DNA break site, resulting in frame shifts or premature stop codons within the DNA. When transcribed into mRNA, this is typically detected by the nonsense-mediated decay pathway and degraded, preventing translation into a protein[53,57](Figure 1.4B).

CRISPRi uses a modified version of the Cas9 protein. The native Cas9 protein contains two DNA cleavage domains called HNH and RuvC, which cleave the gRNA complementary and gRNA non-complementary DNA strands, respectively. By changing a single amino acid at each domain, the Cas9 becomes catalytically inactive. While it can no longer cleave DNA, the "dead" dCas9 still binds to DNA where it acts as a steric block, preventing access of other proteins. By targeting it to the transcriptional start site (-50 to +250 bp from the transcriptional start site ideally) dCas9 will block transcription initiation (Figure 1.4C). Binding dCas9 outside of the transcriptional start site will block transcription elongation, but the knock down achieved is highly variable and typically only successful when dCas9 is bound to the non-template strand of DNA (also called the sense strand, forward strand, or coding strand)[58–64].

The knock down achieved with CRISPRi can be increased by fusing dCas9 with the transcriptional repressor domain Krüppel Associated Box (KRAB), which influences the histone state of the gene[65]. Eukaryotic DNA is wound around histone proteins that can be chemically modified, influencing how closely they associate[66]. The KRAB repressor interacts with histone modifying proteins to create a tightly wound histone state which is inaccessible to RNA polymerase II and therefore reduces gene transcription[67](Figure 1.4D). This significantly increases CRISPRi gene repression at most sites. Unlike when using dCas9 alone to block transcription elongation, dCas9-KRAB can be targeted to either strand of the DNA, dramatically increasing the potential target sites[60,63].

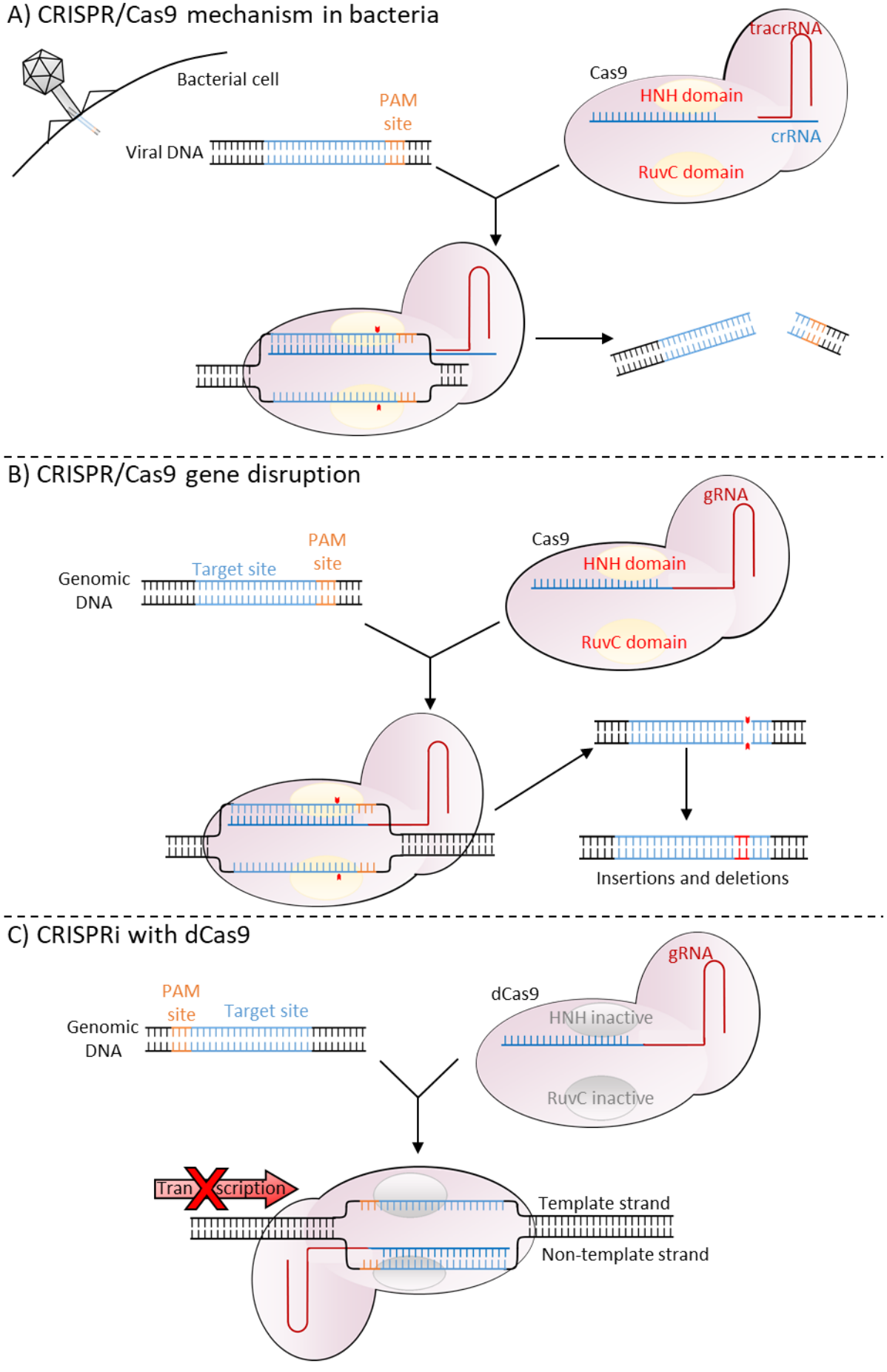
A) CRISPR/Cas9 mechanism in bacteria
Bacterial cell
Viral DNA
PAM site
Cas9
tracrRNA
HNH domain
crRNA
RuvC domain
B) CRISPR/Cas9 gene disruption
Genomic DNA
Target site
PAM site
Cas9
gRNA
HNH domain
RuvC domain
Insertions and deletions
C) CRISPRi with dCas9
Genomic DNA
PAM site
Target site
dCas9
gRNA
HNH inactive
RuvC inactive
Tran scription
Template strand
Non-template strand

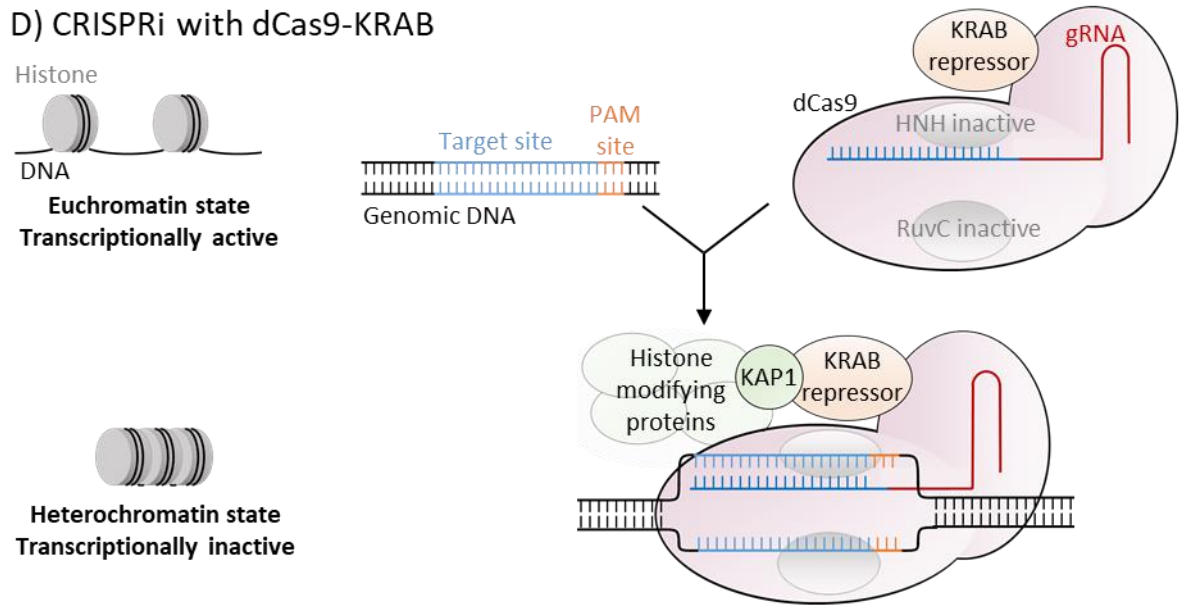

Figure 1.4 Mechanisms of CRISPR/Cas9 and CRISPRi.
***A)** CRISPR/Cas9 mechanism as a bacterial defence against invading viruses. **B)** Using CRISPR/Cas9 to disrupt target genes. **C)** Using CRISPRi with dCas9 to block transcription initiation or transcriptional elongation. **D)** CRISPRi using a dCas9-KRAB fusion protein to alter the chromatin state of a target gene.*

The CRISPR/Cas9 system exists in 48 % of bacterial species, and more are being discovered regularly[68]. While broadly very similar, the Cas9 protein and gRNA sequence can vary between species. Each Cas9 species also has its own PAM site requirements, and the ever-growing range of available Cas9 species increases the chances that a particular locus can be targeted with CRISPR. This thesis explores the use of the CRISPR/Cas9 system from the bacterium *Staphylococcus aureus* to treat retinal disease. This Cas9 species (called SaCas9) is 3159 bp long, and has the PAM site 5'-NNGRRT-3'[69]. SaCas9 was the first Cas9 species discovered that is small enough to be packaged into a single AAV alongside its gRNA. While other single AAV Cas9 species have been described since, including CjCas9 from *Campylobacter jejuni*[70], SaCas9 remains the best-characterised Cas9 species, justifying its use in this thesis.

While not directly relevant to this thesis, it is useful to know that the CRISPR system is very versatile and can be used to activate genes, edit DNA, and edit RNA, amongst other applications. For a recent review on this see Knott and Doudna (2018)[71].

1.4.2 CRISPR/Cas9 vs. CRISPRi

CRISPR/Cas9 causes permanent changes to the genome, whereas CRISPRi does not alter the DNA sequence, and only affects transcription while dCas9 and gRNA are present. If driven by an inducible promoter, the effects of CRISPRi have been shown to be reversible in vitro[58,60], providing safety benefits for potential therapeutic treatments using this technology.

CRISPR/Cas9 and CRISPRi have different optimal target requirements. CRISPR/Cas9 is most successful when targeted to the exon of a gene, as insertions and deletions in introns can be removed through splicing, leaving an unaltered coding sequence[48]. CRISPRi, on the other hand, can in theory be targeted anywhere in the transcribed region. In practice, however, the optimal target site for CRISPRi is quite narrow, at −50 to +250 relative to the transcriptional start site[58,59].

While CRISPRi can be highly efficient, it is generally accepted that CRISPR/Cas9 provides greater gene knock down[60,63,72]. This is likely because the efficiency of CRISPRi gene repression is not only dictated by the gRNA:DNA binding efficiency, as with active CRISPR/Cas9, but by the ability of that locus to successfully block transcription[58]. This makes the knock down rates seen with CRISPRi highly variable across the sequence of a gene[58–60].

CRISPRi may have greater specificity than CRISPR/Cas9. Off-target binding occurs when DNA with partial homology to the gRNA sequence is adjacent to a PAM site. CRISPR/Cas9 has shown variable tolerance for gRNA:DNA mismatches and off-target effects are common; some have been reported at sites with a 5 bp gRNA:DNA mismatch[53,73–76]. This has led to the development of “high-fidelity” Cas9 species, which are engineered to have reduced off-target activity[77–80]. CRISPRi, on the other hand, has very low tolerance for gRNA:DNA mismatches, with one bp mismatches often sufficient to prevent binding[53,54,58,74,75,81]. This might be due to the different mechanisms between CRISPR/Cas9 and CRISPRi: CRISPR/Cas9 may be able to cleave DNA whilst in contact with it only briefly, which might be the case with mismatched nucleotides, whereas for CRISPRi to be effective, it is likely to need to be in contact with the DNA target for considerably longer[49].

1.4.3 Allele-specific targeting of pathogenic genes for dominant diseases

Provided a gene is not haploinsufficient, disruption of the pathogenic allele provides a viable treatment strategy for dominantly inherited diseases. This can be achieved with the CRISPR system by targeting it to a unique DNA region on the mutant allele that is absent from the wild type allele. This is usually the pathogenic mutation but non-pathogenic single nucleotide polymorphisms (SNPs) can also be targeted[48,49].

If the unique region is in the gRNA binding site then the gRNA will have 100 % sequence homology with the mutant allele and a mismatch of at least one bp with the wild type allele (Figure 1.5). If this mismatch prevents gRNA binding then allele-specificity will be achieved. The precise nucleotide mismatch and location within the gRNA binding sequence determines whether the gRNA will bind[53,73–76]. PAM-proximal mutations are typically less tolerated than PAM-distal mutations.

Alternatively, the unique region on the mutant allele may generate a novel PAM site that is not present on the wild type allele. Cas9 will therefore only be able to bind to the mutant allele. With the ever-growing range of Cas9 species, and subsequent range of PAM requirements, it is increasingly likely that an individual mutation will generate a novel PAM site for one of these Cas9 species[48,82].

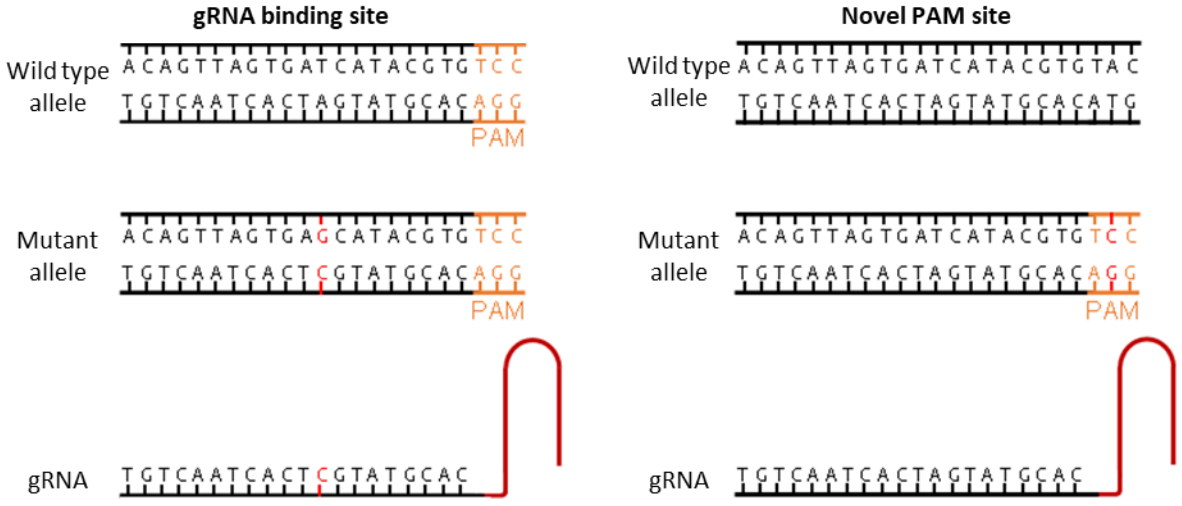

Figure 1.5 Allele-specific Cas9 targeting via gRNA binding site or novel PAM sites.
Cas9 can be targeted to the mutant allele by designing the gRNA to a unique region on that allele. The discrepancy between the gRNA sequence and the wild type allele may be sufficient to prevent binding. If the target mutation generates a novel PAM site this will allow Cas9 to bind exclusively to the mutant allele.

Both gRNA-binding and novel PAM sites have been targeted for allele-specific disruption of pathogenic genes in mouse models of adRP. In all cases, only the mutant allele was disrupted resulting in improved visual outcomes[38,40,41]. These experiments used either a plasmid, or dual AAV delivery method but a single AAV delivery had not been attempted prior to this thesis.

1.4.4 Clinical Application in Retinal Diseases

Promising in vivo results led to the first in situ CRISPR/Cas9 clinical trial, which aims to treat Leber congenital amaurosis 10, a severe retinal dystrophy. The BRILLIANCE trial began in 2020, and uses CRISPR/Cas9 packaged in an AAV to remove the pathogenic cryptic intronic splice site in *CEP290*[83,84]. While investigations into CRISPR treatments are progressing at a steady rate, there are still important factors that need to be considered when moving into clinical trials.

Off-target effects are an important hurdle with CRISPR treatments. Off-target knock down of essential genes results in cell dysfunction or death, while knock down of onco-suppressor genes can result in cancer[52]. Although CRISPRi is more specific than CRISPR/Cas9, off-target effects are still reported and remain an important consideration[49,58]. Bioinformatics screens can be used to predict which gRNAs might be the most specific and where they are likely to bind[85]. Despite this, off-target activity frequently occurs at unpredicted sites and so techniques such as Digenome-Seq and CIRCLE-Seq have been developed which use next-generation sequencing to identify sites of CRISPR/Cas9 activity within treated DNA[86,87]. Off-target effects with CRISPRi are identified with RNA-Seq, whole-transcriptome-Seq, or ChIP-Seq[58,60,88]. As off-target effects can vary between cell types, assessment of off-target activity should be conducted in cells as similar as possible to the therapeutic target[89].

The immune response to CRISPR constructs is a concern in the field. Although no serious responses have been reported, immune reactions could cause inflammation, reduced efficacy, and pose health risks to patients. Immune molecules against both Cas9 and gRNAs have been identified. Anti-Cas9

antibodies and cytotoxic T cells have been documented in healthy humans which could potentially destroy cells expressing Cas9, although this has not been observed[90–92]. Immune responses have also been seen against gRNAs which are transcribed in vitro – although these are not an issue with gRNAs delivered via AAV[93].

1.5 AAV gene therapy

Gene therapy is the introduction of genetic material into a cell to treat a disease. For successful cellular uptake, the genetic material must be packaged in a vector. Adeno-associated viruses (AAVs) are naturally occurring viruses in the parvovirus family and are a popular vector for gene therapy. They are composed of an icosahedral capsid protein shell containing a roughly 4.8 kb single-stranded DNA genome with a DNA sequence called an inverted terminal repeat (ITR) at either end. Their genome encodes three genes (called Rep, Cap, and App) which encode nine proteins involved in cell infection and viral assembly. AAVs enter cells via cell surface carbohydrates and then migrate to the nucleus. Here the second strand of viral DNA is synthesised using the inverted terminal repeat (ITR) as a primer, then the genome is expressed. In order to complete replication, AAVs require additional genes from other viruses (typically adenoviruses) to be present; they are therefore are not considered pathogenic on their own.

Recombinant AAV are modified AAV molecules used for delivery of genetic components during gene therapy. The wildtype AAV genome is removed and replaced with the chosen transgene cassette flanked by ITRs, which are needed to form palindromic loops that protect the ends of the single stranded DNA. The AAV cannot replicate as it lacks its native genome and the presence of additional helper viruses. In their absence, multiple copies of the transgenes link via the ITR sequences to form circular concatemers in the nucleus, where they are expressed if they contain a promoter recognised by the cell[94–96].

AAVs have several key features that have made them the vector of choice for retinal gene therapy trials. Firstly, as the transgene is expressed episomally in eukaryotes, they are non-integrating. This removes the safety concerns surrounding random integration of introduced genetic material into the genome. There are many identified serotypes of AAV and particular ones, such as AAV2 and AAV8, are able to transduce retinal cells with high efficiency. As different serotypes have different cellular tropisms, selection of viral serotype allows transduction to be limited to select tissue types, increasing

safety. It is also possible to combine genomes and capsids from different serotypes, in a process called "pseudotyping". The genome serotype is noted before the capsid serotype, for example AAV2/8 indicates the genome is taken from serotype 2 and the capsid from serotype 8. This can help avoid pre-existing immunity to certain AAV serotypes. Finally, clinical trials have demonstrated the effects of AAV transduction in the retina can last for several years after application, which could theoretically be indefinite, as retinal cells do not proliferate[95–97].

The main limitation of AAV gene delivery is its packaging capacity, which is limited to approximately 4.7 kb. While larger cassettes have been packaged, this typically reduces efficiency and can result in truncated sequences[98,99]. Another potential issue is immune responses to AAV. Although AAVs have low immunogenicity they can still produce an immune response. AAV-neutralising antibodies have been detected post-subretinal injection in vivo, and intraocular inflammation has been reported in multiple AAV gene therapy trials[100–104].

The eye is an ideal candidate for AAV gene therapy. It is easily accessible using ophthalmic surgical techniques; it is immune privileged, reducing the likelihood of immune responses; and the presence of the blood ocular barrier helps to prevent systemic spread of the introduced material[105–107]. These factors have driven dozens of gene therapy clinical trials, culminating in the first FDA approved ocular gene therapy treatment in 2017[108,109].

For in situ delivery of CRISPR components as a gene therapy, two main methods are favoured: AAV and a complex of Cas9 and gRNA called a ribonucleoprotein (RNP). While RNPs typically have higher editing rates, delivery to photoreceptors is not currently possible. Subretinally injected RNPs are rapidly degraded making them unsuitable for CRISPRi, which requires sustained expression[110]. AAV, on the other hand, have demonstrated retinal delivery of CRISPR components with high editing rates in transduced cells[48,49]. For a single AAV strategy, Cas9, gRNA and their regulatory elements must be packaged within the 4.7 kb limit of an AAV. While the most popular Cas9 species from *Streptococcus pyogenes* is too large (4104 bp) for this, multiple shorter variants of Cas9 have been identified,

including SaCas9 from *Staphylococcus aureus* which is used in this thesis[69].

1.6 Thesis scope

RHO-adRP is a dominantly inherited retinal degeneration with no treatment or cure[12]. Reducing the levels of mutant rhodopsin protein have been shown to delay photoreceptor degeneration and improve visual outcomes in vivo. CRISPR/Cas9 and CRISPRi can be used to disrupt, and repress target genes, and may be able to knock down retinal mutant rhodopsin, preventing disease progression[42]. Retinal gene therapy typically uses AAV to deliver transgenes. Most CRISPR/Cas9 systems have a large coding sequence and must be delivered across two AAV vectors. The CRISPR/Cas9 system from *Staphylococcus aureus*, however, has a smaller coding sequence, and can be packaged into a single AAV[69]. A single AAV strategy reduces the number of immunogenic AAV particles required and allows greater control over dose compared to a dual AAV strategy. This thesis focuses on the development of single AAV CRISPR/Cas9 and CRISPRi gene therapy constructs to treat RHO-adRP, and proposes the hypothesis that an all-in-one AAV is capable of driving significant CRISPR gene editing within rod cells.

Initially, a short, rod cell-specific promoter was validated which drives strong expression of SaCas9 and dSaCas9.KRAB in vivo. This limits the CRISPR activity to the target cell population and therefore improves the safety profile of the treatment. Following optimisation, the constructs were used to target non-pathogenic *RHO* SNPs in vitro. A selection of these target sites drove allele-specific knock down, identifying this as a viable strategy for a mutation-independent, allele-specific approach. Finally, these constructs were used to target the rod-specific EGFP gene in the Nrl-EGFP mouse. Significant EGFP disruption was measured, demonstrating their ability to target rod cell-specific genes within a retina. This thesis is broken down into four experimental chapters:

- Validation of a short, rod cell-specific, hPDE6B promoter (Chapter 3)
- Optimisation of CRISPR constructs in vitro (Chapter 4)
- Allele-specific *RHO* knock down by targeting non-pathogenic single nucleotide polymorphisms (Chapter 5)
- CRISPR/Cas9 gene disruption of rod cell-specific EGFP in vivo (Chapter 6)

2 Methods and Materials

2.1 Molecular

2.1.1 Polymerase Chain Reaction (PCR)

Primers were designed using the Primer3 online tool. Before beginning the reaction, the bench and pipettes were soaked in 10 % bleach for 30 min and all plasticware UV-treated for 10 min to remove any contaminants. A no template control was run with each reaction (NTC). PCR was performed using KOD Polymerase (Merck) unless stated otherwise. The reaction contained a final concentration of 1x KOD Hot Start Polymease Buffer, 1.5 mM $MgSO_4$, 0.2 mM of each dNTP, 0.3 µM forward primer, 0.3 µM reverse primer, and 1 unit KOD Hot Start DNA Polymerase in a 50 µl reaction volume. Template DNA was added at 10 ng if a plasmid, and 100 ng if genomic DNA. Samples were heated to 95 C for 2 min then went through 30-40 cycles of 95 C for 20 s, annealing temperature for 10 s, and then 70 C for 15 s per kilobase of PCR product length. The forward and reverse primers, annealing temperatures and any special conditions for PCR are detailed in Appendix 9.1.1. Following amplification in a thermocycler, all products were run on a 1 % agarose gel by electrophoresis along with a DNA ladder to check the size of the products and note any non-specific products or contaminants in the NTC.

2.1.2 TIDE analysis

TIDE (Tracking of Indels by Decomposition, Deskgen) is an online software that compares sequence traces of CRISPR-edited DNA and unedited control DNA to estimate the percentage of reads containing indels. PCR primers were designed to amplify a roughly 700 bp region, with one primer binding roughly 200 bp from the predicted cut site, and the other primer binding roughly 500 bp from the predicted cut site. Following PCR amplification using KOD polymerase (see 2.1.1 Polymerase Chain Reaction), the PCR product was sent for Sanger sequencing (Eurofins Genomics Ltd) using the primer closest to the predicted cut site. This was only done if the PCR NTC contained no contaminating bands. The

sequencing reads were viewed in the bioinformatics software Geneious, to assess their quality. Only reads with a high quality of sequencing before the cut site, and a consistent quality after the cut site were used for analysis; poor quality sequencing reads were either resent for sequencing or new primer pairs were designed. The chromatogram sequencing file (file extension .ab1) was uploaded into the TIDE online software (Deskgen) along with a control file of unedited DNA. The control DNA was extracted prior to the CRISPR experiments (therefore reducing the risk of contamination) and was PCR amplified and sequenced alongside the test samples (to ensure that read variability from PCR efficiency or sequencing run quality was as consistent as possible). The decomposition window was adjusted to the length of the high quality read on the control sample, if required. The indel size range was adjusted, where necessary, to improve the R^2 value of the alignment. All PCR primer combinations used are detailed in Appendix 9.1.

2.1.3 Restriction digestion

1 µg DNA and 20 units of each enzyme were mixed together with 1x rCutSmart Buffer and incubated in a thermocycler for the maximum recommended time (typically 1 hour). A no template control was also included containing no DNA template. If there was an optional heat inactivation step this was also conducted. Successful digestion was confirmed by running the products on a 1 % agarose gel.

2.1.4 cDNA synthesis

cDNA synthesis was conducted using SuperScript III First-Strand Synthesis System for RT-PCR (Invitrogen). 1000 ng RNA, 1.64 µM oligo$(dT)_{20}$ was made up to 29.5 µl with water. Samples were incubated at 65 C for 5 min. 23.5 µl mixture of 2.13x RT buffer, 21.3 mM DTT, 10.6 mM $MgCl_2$, 1.7 U RNaseOUT, 1.06 mM dNTP mix was added to each sample. Samples were incubated at room temperature for 2 min. 200 U SuperScript III was added and the samples were incubated at 85 C for 5 min. 2 U RNase H was added to each sample and they were incubated at 37 C for 20 min. When

reverse transcription of gRNA was required, the sequence-specific primer “sgRNA_R1” (5’-ATCTCGCCAACAAGTTGACG-3’) was added to the dNTP mixture. The cDNA was then purified using the QIAquick PCR Purification Kit, eluting the cDNA in 30 µl water.

2.1.5 qPCR

Prior to the qPCR, the workbench and pipettes were disinfected in 10 % bleach for 30 min. All plasticware and tips were UV-treated for 10 min. All reagents were thawed on ice and kept on ice throughout the protocol. Each sample was run in a technical triplicate and a “no template” control was run on each plate to monitor potential contamination of the reaction. If a semi-quantitative qPCR was conducted, samples were run with one or two primers against housekeeping genes for normalisation. Descriptions of the primers used are given in the methods section for each individual chapter.

When using Taqman (Thermofisher) probes, 1 µl of cDNA was added to the required wells. 10 µl TaqMan PCR Master Mix, 1 µl of TaqMan qPCR gene probe, and 9 µl water were added to each reaction. The plate was then run on the CFX Connect Real-Time PCR system (Bio-Rad) at 95 C for 20 s followed by 40 cycles of 95 C for 3 s then 60 C for 30 s. Taqman probes are given in Table 2.1.

When using SYBR Green probes (Thermofisher), 1 µl of cDNA was added to the required wells. 5 µl iTaq SYBR Green, 2 µl 2 µM forward primers, 2 µl 2 µM reverse primer, and 2 µl water were added to each reaction. The plate was then run on the CFX Connect Real-Time PCR system (Bio-Rad) at 95 C for

Table 2.1 Taqman qPCR probes

Target	Assay ID
Beta-actin (Human)	Hs01060665_g1
SaCas9/dSaCas9/dSaCas9.KRAB	APKA4TC (custom assay)
gRNA (SaCas9)	APH6A7E (custom assay)
GAPDH (Human)	Hs02786624_g1
EGFP	Mr04329676_mr
RHO (Human)	Hs04970106_m1

2 min followed by 40 cycles of 95 C for 10 s then 55 C for 30 s. If testing new primers for the first time, a melt curve analysis was also run to confirm only one product was being amplified.

When performing a semi-quantitative qPCR, the cT values for each technical replicate were averaged. If two housekeeping genes were used, the geomean of their cT values were calculated. The housekeeping mean was then subtracted from the sample mean to calculate ΔcT. Statistical analysis compared the ΔcT between groups of interest. For graphical representation of the results, the ΔcT of the control was subtracted from the ΔcT of the samples to calculate ΔΔcT. This data was then converted to a fold change and plotted on a graph with an axis in log base 2.

2.1.6 Protein extraction from cell pellets

Cells were pelleted as described in 2.2.8. Samples were kept on ice during the protein extraction protocol. The cell pellet was resuspended in 80 µl protein buffer. If the sample was analysed for fluorescence, the pellet was resuspended in complete FIPA buffer (NaCl 150 mM, Tris base 50 mM, EDTA 2 mM, 1 % TritonX-100; adjusted to pH 7.4 with HCl), otherwise it was resuspended in complete RIPA buffer. The sample was sonicated using a probe sonicator for 10 s at 20 % power. Samples were then centrifuged at 14 000 rpm for 10 min at 4 C. The supernatant containing the protein was transferred to a new tube and the pellet discarded.

2.1.7 Pierce BCA quantification assay

Bovine serum albumin standard was diluted with RIPA buffer to give eight standards with a protein concentration of 2000 µg/mL to 25 µg/mL. 25 µl of each standard and sample were transferred into a flat-bottomed 96 well plate in duplicate. The Pierce BCA protein assay kit (ThermoFisher) was used to create a working mixture of reagent A and B. 200 µl of this was added to each well and incubated in the dark at 37 C for 30 min, then in the dark at room temperature for 5 min. The absorbance of the

wells was measured at 563 nm using the iMark Microplate Absorbance plate reader. The standards were used to create a standard curve, from which the protein concentration of the samples could be calculated.

2.1.8 Western blot

All incubations with solution were done on a shaking platform. 2-20 µg of protein was mixed with 5x protein loading dye (National Diagnostics) and heated to 95 C for 5 min. They were then loaded into a 10 % polyacrylamide gel (BioRad Criterion TGX) in an electrophoresis tank and run until the proteins of interest were separated (the length of the run was dependent on the molecular weight of the key

Table 2.2 Primary and secondary western blot antibodies.

Target	Molecular weight (kDa)	Primary antibody	Primary antibody dilution	Secondary antibody	Secondary antibody dilution
Beta-actin (human)	42	ThermoFisher mouse anti-beta actin AM4302	1/10 000	Abcam Donkey anti-mouse ab98799	1/10 000
Beta-actin (mouse)	42	Abcam rabbit anti-beta actin ab8227	1/5 000	Abcam Donkey anti-rabbit ab97064	1/10 000
CRX (human)	37	ThermoFisher rabbit anti-CRX PA5-32182	1/1 000	Abcam Donkey anti-rabbit ab97064	1/10 000
Nrl (human)	33	Abcam rabbit anti-Nrl ab137193	1/1 000	Abcam Donkey anti-rabbit ab97064	1/10 000
RHO (human)	40	Mouse anti-rhodopsin 1D4 ab5417	1/1 000	Abcam Donkey anti-mouse ab98799	1/10 000
SaCas9	124	Abcam rabbit anti-SaCas9 ab203933 (amino acids 100-200)	1/20 000	Abcam Donkey anti-rabbit ab97064	1/20 000
SaCas9	124	Diagenode rabbit anti-SaCas9 N-terminus C15310260	1/10 000	Abcam Donkey anti-rabbit ab97064	1/20 000
SaCas9	124	Diagenode rabbit anti-SaCas9 C-terminus C15310259	1/10 000	Abcam Donkey anti-rabbit ab97064	1/20 000
Vinculin (human)	135	Abcam rabbit anti-vinculin ab219649	1/1 000	Abcam Donkey anti-rabbit ab97064	1/10 000

proteins). The gel was then layered onto a PVDF membrane (Transblot, BioRad), which had been pre-soaked in methanol, and the proteins transferred onto the PVDF membrane using the Trans-blot Turbo Transfer System (Bio-Rad) with a "Mixed Weight" programme at 2.5 A for 7 min. The membrane was washed in PBS-T for 7 min then incubated with 3 % BSA in PBS-T for 45 min. To allow the target protein and the loading control to be processed separately, the membrane was divided into two halves with scissors. This created two separate membranes - one containing the target protein and the other containing the loading control protein. Each membrane was incubated with its primary antibody in 3 % PBS-T overnight at 4 C. The membranes were washed in PBS-T for 7 min then incubated with the desired secondary antibody in 3 % BSA in PBS-T for 30 min. A WesternSure pen was used to mark the position of the protein ladder then the proteins developed using the Clarity Western ECL Substrate Kit (BioRad). The membrane was imaged on the Odyssey Fluorescence Imaging System (Licor) using the programme Licor Image Studio. The antibodies used and their dilutions are given in Table 2.2.

2.1.9 Plasmids

The plasmids used in this thesis were acquired from a range of different sources: gifted from research institutes (acquired from the non-profit plasmid repository AddGene), purchased from manufacturers, created in this thesis, or previously created within the research group (Table 2.3). All plasmids were transformed into XL10 Gold Ultracompetent Cells (Stratagene), and subsequent liquid bacterial cultures were mixed 1:1 with 50 % glycerol to create a glycerol stock, which was kept frozen at -80 C. The sequence of key plasmids are listed in Appendix 9.9.

2.1.10 General plasmid cloning

Vector and insert were ligated together using T4 Ligase (New England Biolabs) Kit. The vector to insert ratio was 1:3 unless stated otherwise. Multiple controls were included in the ligation reaction. Firstly, a "backbone only" control which contains the vector and ligase; colonies on this plate indicate the

plasmid has re-ligated to itself or the vector sample contains some undigested plasmid. Secondly, a "ligation positive control", which contains a linearized vector and ligase; colonies on this plate indicate the ligation reaction is successful. Finally, a "negative control" which contains no DNA; colonies on this plate indicate contamination of whole plasmid. Ligated products were then transformed into XL10 Gold Ultracompetent Cells (Stratagene). 50 µl cells were mixed with 2 µl β-mercaptoethanol in a chilled 15 ml falcon tube. The tubes were incubated on ice for 10 min, flicking the tubes at regular intervals to mix. 5 µl of ligation product was added to the cells and they were incubated on ice for 30 min. The cells were then heat shocked by placing them in a 42 C water bath for exactly 30 s then incubating on ice for 2 min. The cell solution was spread on Lyosogeny Broth agar plates (100 µg/ml ampicillin) at 37 C and incubated overnight. Two additional transformation controls were included: a positive control plasmid which confirms the transformation step is functional, and untransformed cells which ensure the antibiotic in the plates is successfully killing untransformed cells. A sterile pipette tip was used to transfer individual colonies to liquid Lyosogeny Broth 100 µg/ml ampicillin solution and incubated at 37 C overnight in a shaking incubator. The following day the plasmid was extracted from the liquid cultures using the Sigma-Aldrich Miniprep kit. To identify successfully ligated plasmids, a diagnostic restriction digestion was conducted (the enzymes selected varies with cloning strategy - see 2.1.3 Restriction digestion). Correctly-ligated plasmids were sent for Sanger Sequencing across the transgene using the primers in Appendix 9.1.2. Sanger Sequencing service provided by Eurofins Genomics.

2.1.11 Cloning gRNAs into SaCas9 plasmids

The gRNA scaffold was in the SaCas9 plasmid, but the target-homologous part of the gRNA needed to be cloned into the plasmid. The target insert was ordered as two separate oligonucleotides containing BsaI restriction digest overhangs. The forward oligonucleotide was 5'-CACC-gRNA sequence-3'. If the gRNA sequence did not start with a 5'-G, it was added to improve transcription from the U6 promoter.

Table 2.3 Plasmids.

Plasmid name	Plasmid construct	Source	Bacterial growth temperature
hRHOp.DsRed	ITR.hRHOp.DsRed.bGHpA.ITR	Research group	37 C
shorthPDE6Bp.DsRed	ITR.shorthPDE6Bp.DsRed.bGHpA.ITR	Created	37 C
longhPDE6Bp.DsRed	ITR.longhPDE6Bp.DsRed.bGHpA.ITR	Created	37 C
CAG.DsRed	CAG.DsRed.bGHpA.ITR	Created	37 C
Promoterless.DsRed	DsRed.bGHpA.ITR	Created	37 C
CAG.GFP.WPRE	ITR.CAG.GFP.WPRE.bGHpA.ITR	Research group	37 C
pDG	(Contains AAV2 repcap and helper genes)	Plasmid Factory	37 C
pAdDeltaF6	(Contains helper genes E4, E2a, VA)	James M Wilson (Addgene plasmid number 112867)	37 C
pAAV2/8(Y733F)	p5.AAV2-Rep.AAV8-Cap	Research group	37 C
SaCas9	ITR.CMV.SaCas9.bGHpA.U6.gRNA.ITR	Feng Zheng (Addgene plasmid number 61591)	37 C
dSaCas9	ITR.CMV.dSaCas9.bGHpA.U6.gRNA.ITR	Created	37 C
dSaCas9.KRAB	ITR.CMV.dSaCas9.KRAB.bGHpA.U6.gRNA.ITR	Created	34 C
CMV.dSaCas9.KRAB	ITR.CMV.dSaCas9.KRAB.bGHpA.ITR	Charles Gersbach (Addgene plasmid number 106219)	34 C
SaCas9.puro	ITR.CMV.SaCas9.bGHpA.U6.gRNA.ITR.puro	Research group	37 C
dSaCas9.puro	ITR.CMV.dSaCas9.bGHpA.U6.gRNA.ITR.puro	Research group	37 C
dSaCas9.KRAB.puro	ITR.CMV.dSaCas9.KRAB.bGHpA.U6.gRNA.ITR.puro	Research group	34 C
PDE6Bp.SaCas9	ITR.PDE6Bp.SaCas9.bGHpA.U6.gRNA.ITR	Created	34 C
PDE6Bp.dSaCas9.KRAB	ITR.PDE6Bp.dSaCas9.KRAB.bGHpA.U6.gRNA.ITR	Created	34 C
Psicheck2	T7.Renilla.pA.HSV-TK.Firefly.pA	Promega	37 C
CMV.CRX	ITR.CMV.CRX.WPRE.bGHpA.ITR	Research group	37 C
NRL	CMV.NRL.pA	Origene (catalogue number RC202237)	37 C
RHO	ITR.hRHOp.RHO.bGHpA.ITR	Research group	37 C

The reverse oligonucleotide was a 5'-AAAC-reverse complement of gRNA sequence-3'. 25 pmol of the forward and reverse oligonucleotides were combined into a tube. They were phosphorylated using the T4 PNK kit (New England Biolabs), then heated to 95 C for 4 min to denature the oligonucleotides and melt any secondary structures. They were then gradually cooled to 4 C in a thermocycler with 47 cycles of 1 min incubations decreasing in temperature by 1.5 C each cycle. This annealed the forward and reverse oligonucleotides together.

The SaCas9 plasmid was digested with BsaI (New England Biolabs)(2.1.3 Restriction digestion), and the products were separated by gel electrophoresis on a 1 % agarose gel. The linearised plasmid band was gel purified using the QIAquick Gel Extraction Kit (Qiagen). The digested plasmid and gRNA were ligated together with T4 ligase (New England Biolabs) at an insert:backbone ratio of 20:1 then transformed into XL10 Gold Ultracompetent Cells (Stratagene). Following bacterial culture and miniprep (Sigma-Aldrich), the successfully ligated plasmids were identified by digestion with BsaI: plasmids containing an insert will not digest with BsaI whereas SaCas9-plasmids that were never originally digested with BsaI, and plasmids which have re-ligated onto themselves, are linearised with BsaI.

The plasmids are named with the type of Cas9 (SaCas9, dSaCas9, or dSaCas9.KRAB) followed by the name of the gRNA. For example, the construct CMV.SaCas9.bGHpA.U6.gRNAF10 is referred to as SaCas9.F10 throughout the thesis.

2.1.12 Plasmid amplification for cell transfections

When the plasmid was required for cell transfection it was amplified with an endotoxin-free kit, or a low-endotoxin kit. Depending on the amount of plasmid required, the plasmid was extracted with the Zyppy Miniprep kit (Zymo), the PureLink Fast Low Endotoxin Midiprep kit (Invitrogen), the Qiagen Endotoxin-free Maxiprep kit, or the Qiagen Endotoxin-free Megaprep kit. All bacterial cultures were

incubated at 37 C except for plasmids containing the KRAB repressor, which were incubated at 30 C for longer periods (Table 2.3).

2.2 Cell and tissue culture

2.2.1 Cell culture

All cell culture work was performed in a designated tissue culture facility. Cell media and flasks were only opened within positive pressure ventilation hoods using aseptic technique. Cells were maintained in a humidified incubator at either 37 C or 34 C with 5 % carbon dioxide. Media added to cells was pre-warmed to 37 C. Immortalised cells were routinely passaged. Cells used in experiments were between passage 4 and 30 post-thawing. Cell maintenance conditions are listed in Table 2.4.

2.2.2 Resuspension of frozen cells

Immortalised cell lines were stored in liquid nitrogen. Frozen cell stocks were thawed in a 37 C water bath then centrifuged at 300 g for 5 min. The supernatant was discarded, the cell pellet resuspended in 6 ml media, and the cells transferred to a T25 flask. Once confluent, the cells were transferred to a T75 flask.

2.2.3 Cell passage

Adherent immortalised cells were maintained in T75 flasks. When cells reached 80-90 % confluency they were passaged as follows. The media was removed from the cells and the cells were washed with 5 ml PBS. The cells were incubated with 1 ml TypLE dissociation reagent (ThermoFisher) for 5 min at 37 C. 9 ml media was added to the cells and pipette mixed. A proportion of the cells was transferred to a fresh T75 flask to give the desired cell passage, and the volume made up to 10 ml with media.

Immortalised suspension cells were maintained in T175 flasks. Once a week, the cells were centrifuged at 100 g for 5 min and resuspended in fresh media. The cells were counted as described in 2.2.4 Cell seeding and reseeded into a fresh T175 flask at 5x10^5 cells/ml (this was approximately a 1 in 4 passage).

Table 2.4 Cell and tissue culture conditions.

Cell type	Description	Catalogue number	Culture type	Culture media	Passage requirements	Growth conditions
HEK293	Human embryonic kidney cell line transfected with adenoviral genes for efficient production of recombinant plasmid proteins	ECACC 85120602	Adherent	DMEM high glucose, 2 mM L-glutamine, 50 000 units penicillin, 100 µg/ml streptomycin, 10 % FBS	1:5 twice a week	37 C
HEK293-EGFP	HEK293 cell line expressing EGFP from the enhanced super CMV promoter	GenTarget SC001	Adherent	DMEM high glucose, 2 mM L-glutamine, 50 000 units penicillin, 100 µg/ml streptomycin, 1x non-essential amino acids (Sigma) 10 % FBS	1:10 twice a week	37 C
HEK293T	HEK293 cell line expressing SV40-T antigen for efficient production of proteins from plasmids with the SV40 origin of replication	ECACC 12022001	Adherent	DMEM high glucose, 2 mM L-glutamine, 50 000 units penicillin, 100 µg/ml streptomycin, 10 % FBS	1:10 twice a week	37 C
Y79	Retinoblastoma-derived cell line expressing some photoreceptor-specific markers	ECACC 86093003	Suspension	RPMI 1640, 2 mM L-glutamine, 50 000 units penicillin, 100 µg/ml streptomycin, 10 % FBS	Media change once a week. Passage 1:4 once a week	37 C
Human retinal explants	Retinal tissue cultured from consenting adults undergoing routine retinectomy	N/A	Adherent	Neurobasal A, 0.8 mM L-glutamine, 50 000 units penicillin, 100 µg/ml streptomycin, 1% 100x N2 supplement, 2% 50x B27 supplement	Media change every other day	34 C

2.2.4 Cell seeding

Cells were approximately 70-90 % confluent when harvested for seeding. Cells were washed with PBS, trypsinised and neutralised with media as described in 2.2.3 Cell passage. The cell suspension was then centrifuged at 300 g for 5 min, the supernatant removed, and the cells resuspended in fresh media. 100 µl of cells was mixed with 100 µl trypan blue (ThermoFisher) and 10 µl loaded into the BioRad TC20 automatic cell counter. The cells were then diluted to the desired concentration (detailed in each the methods and materials section of each individual chapter) and pipetted into the wells.

2.2.5 Cell line transfection

Unless stated otherwise, cells were forward transfected using the Trans*IT*-LT1 reagent (Mirus Bio). Cells were seeded 24 hours pre-transfection at a density that ensured the confluency reached 50-70 % on the day of transfection. Plasmid and Trans*IT*-LT1 reagent were mixture together at 1 µg plasmid to 3 µl Trans*IT*-LT1 unless detailed otherwise, and OptiMEM (Gibco) was used as the serum-free medium to dilute the DNA:reagent complexes. The mixture was incubated at room temperature for 20 min then added dropwise to the tissue culture plate well. The untransfected control was treated identically to the other samples but water was used instead of plasmid DNA. Unless stated otherwise, the cells were harvested 48 hours post-transfection. The specific cell seeding densities and plasmid quantities are detailed in the relevant chapter method.

2.2.6 Cell line transduction

For transduction of HEK293 cells, cells were grown in 96 well plate tissue culture wells until 80-90 % confluent. The cells in an individual well were counted to calculate the amount of virus required for a given multiplicity of infection, and the media removed from all the wells. For AAV8(Y733F) viruses, 50 µl DMEM high glucose, 2 mM L-glutamine, 50 000 units penicillin, 100 µg/ml streptomycin, 200 mM doxorubicin was added to the well and the viruses added to this. The cells were then incubated at 37

C for 1 hour, then 50 µl DMEM high glucose, 2 mM L-glutamine, 50 000 units penicillin, 100 µg/ml streptomycin, 20 % FBS added.

For transduction of Y79 cells, cells were seeded in the wells 24 hours before transduction. As they grow slowly they were not recounted before transducing. For AAV8(Y733F) viruses 1 mM hydroxyurea and 200 nM doxorubicin was added to the cells and incubated at 37 C for 4 hours. Then the virus was added directly to the media. Half the media in the well was changed every other day following transduction. The amount of AAV varied between experiments and is detailed in each specific chapter methods section.

2.2.7 Microscopy imaging

Transmission and fluorescence images of live cells were taken using the Invitrogen EVOS FL Auto 2 Cell Imaging System (ThermoFisher). The gain in each channel was adjusted to ensure the image was not saturated, and this was kept constant between channels and time points for each experiment. In different experiments, the images were taken either using brightfield or phase contrast depending on the cell type and which image provided to most useful representation of the cells.

2.2.8 Cell harvesting

The volumes of reagents used for cell harvesting varied depending on the size of the well. These volumes are details in Table 2.5. The media was removed from the well and the cells washed with PBS.

Table 2.5 Reagent volumes used for cell harvesting.

Reagent	Volume per well/µl				
	6 well plate	12 well plate	24 well plate	48 well plate	96 well plate
PBS (cell wash)	1000	500	250	125	62.5
TrypLE	300	150	75	37.5	18.75
Cell media	1000	500	250	125	62.5
PBS (pellet wash)	500	250	125	62.5	31.3

TrypLE was added to the well and the cells incubated at 37 C for 5 min. Media was added to the cells and pipette mixed to resuspend the cells. The cells were transferred to an Eppendorf and centrifuged for 5 min at 300 g. The supernatant was removed, the cells were resuspended with PBS and centrifuged for 5 min at 300 g. Finally, the PBS was removed and the cell pellet flash frozen on dry ice before being stored at -80 C.

2.3 AAV production

2.3.1 AAV production

The AAV used in this thesis were either created within this thesis, or previously created within the research group and gifted for use in this research (Table 2.6). All AAV were stored at -80 C. Before AAV production, all AAV plasmids were digested with XmaI to confirm the presence of both ITRs. HEK293T cells were grown in two hyperflasks in DMEM high glucose, 2 mM L-Glutamine, 50 000 units penicillin, 100 µg/ml streptomycin, 10 % FBS, until 90 % confluent. Viral production plasmids and transgene plasmid (see Table 2.3) were mixed together (total 500 ng DNA) in 10 ml 150 nM NaCl. When making AAV8(Y733F), the helper plasmid pAdDeltaF6 (contains genes E4, E2a, and VA from adenovirus) the pAAV2/8(Y733FF) plasmid (contains gene Rep and Cap) and the transgene plasmid were mixed together at a copy number ratio of 1:1:1. When making AAV2 the helper plasmid genes and RepCap plasmid genes were present on a single plasmid, called pDG, which was purchased from Plasmid

Table 2.6 AAV used throughout this thesis.

AAV name	Serotype	Construct	Source	Titre genome copies/ml
AAV8.shorthPDE6Bp	AAV2/8(Y733F)	shorthPDE6Bp.DsRed.bGHpA	Created	$2.65x10^{11}$ $3.16x10^{12}$
AAV8.longhPDE6Bp	AAV2/8(Y733F)	longhPDE6Bp.DsRed.bGHpA	Created	$2.04x10^{11}$
AAV8.CAG.GFP	AAV2/8(Y733F)	CAG.GFP.WPRE	Research group	$3.58x10^{12}$
AAV2.CAG.GFP	AAV2/2	CAG.GFP.WPRE	Research group	$1.25x10^{11}$
AAV8.hRHOp	Self-complementary AAV2/8(Y733F)	hRHOp.DsRed.bGHpA	Research group	$6.47x10^{11}$
AAV.SaCas9.scram	AAV2/8(Y733F)	shorthPDE6Bp.SaCas9.bGHpA.U6.scramgRNA	Created	$2.29x10^{12}$
AAV.SaCas9.F10	AAV2/8(Y733F)	shorthPDE6Bp.SaCas9.bGHpA.U6.F10gRNA	Created	$7.81x10^{12}$
AAV.dSaCas9.KRAB.scram	AAV2/8(Y733F)	shorthPDE6Bp.dSaCas9.KRAB.bGHpA.U6.scramgRNA	Created	$1.05x10^{12}$
AAV.dSaCas9.KRAB.F10	AAV2/8(Y733F)	shorthPDE6Bp.dSaCas9.KRAB.bGHpA.U6.F10gRNA	Created	$1.14x10^{13}$
AAV2.shorthPDE6Bp	AAV2/2	shorthPDE6Bp.DsRed.bGHpA	Created	$1.96x10^{12}$

Factory. This was added at a copy number ratio of 1:1 with the transgene plasmid. 10 ml 0.1 mg/ml polyethylenimine in 150 mM NaCl was added to the plasmid mixture dropwise and incubated for 20 min at room temperature. The plasmid DNA/PEI mixture was then added to a bottle of DMEM high glucose, 2 mM L-Glutamine, 50 000 units penicillin, 100 µg/ml streptomycin, 2 % FBS. The hyperflask media was removed and replaced with the media containing plasmid DNA. The cells were incubated at 37 C for 72 hours.

The cells were detached by shaking, transferred to a centrifuge bottle and centrifuged for 10 min at 1200 g at 20 C. The cell pellet was resuspended with 15 ml lysis buffer (1M Trizma base, 150 mM NaCl, pH 8.5) + half a Complete Mini EDTA-free protease inhibitor pellet (Roche). The cells were then frozen at -80 C for 1 hour and thawed in a 37 C water bath twice before storing at -80 C overnight or longer.

Lysed cells were thawed at 37 C for 15 min. 5 µl benzonase (200 U/µl) was added and the cells were incubated at 37 C for 45 min, vigorously shaking every 15 min. Cells were centrifuged for 20 min at 3700 G at room temperature. Iodixanol fractions were made up as in Table 2.7.

The iodixanol fractions were layered into an ultracentrifuge tube with an increasing iodixanol concentration going down the tube. After centrifugation, the cell supernatant was added on top of the iodixanol fractions (Figure 2.1). Samples were centrifuged at 59 000 rpm for 1 hour 30 min at 20 C.

Following centrifugation, the AAV particles containing the transgene collected in the 40 % fraction. This fraction was removed by piercing the ultracentrifuge tube at the 40 % fraction with an 18 G needle

Table 2.7 Reagents comprising iodixanol fractions.

Fraction	Iodixanol 60 %	5M NaCl	5 mM $MgCl_2$, 12.5 mM KCl, 5x PBS	H_2O	Phenol Red	Volume added to each ultracentrifuge tube
15%	8 ml	6.4 ml	6.4 ml	11.2 ml	-	7.2 ml
25%	10 ml	-	4.8 ml	9.2 ml	40 µl	4.8 ml
40%	13.4 ml	-	4 ml	2.6 ml	-	4 ml
60%	20 ml	-	-	-	40 µl	4 ml

attached to a syringe. The 40 % fraction was drawn out, transferred to a falcon tube, and stored at 4 C overnight.

5 ml PBS was added to an Amicon Ultra 100K filter and centrifuged at 3000 g for 15 min at 20C. The AAV was made up to 15 ml with PBS and added to the filter. It was centrifuged at 3000 G at 20 C until the volume was reduced to under 500 µl. 14 ml PBS was added to the filter, and re-centrifuged at 3000 G until the volume is reduced to under 500 µl. This is then repeated twice more. The final centrifugation was performed until the volume was reduced to under 250 µl. The purified AAV was removed from the filter and stored at -80 C. 500 µl PBS was added and repeatedly pipetted over the filter to release any remaining AAV. This sample was called the wash and typically has a much lower concentration. It was stored at -80 C.

2.3.2 SDS-PAGE

To confirm the presence of the viral capsid proteins VP1, VP2, VP3, the vector preparations were run on an SDS-PAGE. 20 µl vector suspension was mixed with 5x protein loading dye and incubated at 95 C for 15 min. After cooling on ice, it was run on a 10 % SDS PAGE gel. The SDS PAGE gel was then removed from the tank and washed with water 3 times. The SDS PAGE gel was incubated with EZ Blue

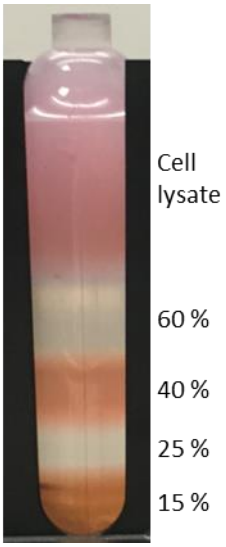

Figure 2.1 Iodixanol gradient.
Iodixanol percentage is given on the right hand side.

gel stain (Sigma-Aldrich) on a shaking incubator for 2 hours which stains all present protein bands, including AAV proteins. The gel was washed with water 3 times then imaged using the Licor Odyssey.

2.3.3 Viral titration

To remove any contaminating DNA, the vector preparations were digested with DNase at 37 C for 30 min then heated to 95 C for 10 min. Titration of the viral preparation was done via qPCR (2.1.5 qPCR), with Sybergreen primers amplifying the polyA sequence common in all plasmids used in this thesis (Table 2.8). A 1/10 serial dilution of the transgene plasmid was created, from 1 ng/µl to 0.0001 ng ng/µl. A standard curve of the target was created and used to estimate the number of viral genomes present.

Table 2.8 qPCR primers used for viral titration.

Primer name	Primer sequence 5'-3'
20F	CCAGCCATCTGTTGTTTGCC
91R	GAAAGGACAGTGGGAGTGGC

2.4 In vivo procedures

All animal procedures were conducted in accordance with the Animals (Scientific Procedures) Act 1986, UK under UK Home Office Personal License I229763D7 and Project License 30/3363. All mice used were *Mus musculus* and were housed and cared for at the Biomedical Sciences Division, University of Oxford. They were kept in a 12-hour light/dark cycle and had free access to food and water at all times.

2.4.1 Mouse anaesthesia

Mice were anaesthetised via an intraperitoneal injection of ketamine at 80 mg/kg body weight and xylazine at 10 mg/kg body weight. Anaesthesia was reversed via an intraperitoneal injection of atipamezole at 2 mg/kg body weight.

2.4.2 Subretinal injections

AAV used for subretinal injections were diluted with 0.001 % Pluronic™ F-68 Non-ionic Surfactant (Gibco) in PBS to reduce their attachment to the syringe and needle. All AAV were diluted at least 1:1. All mice used for subretinal injections were 6-8 weeks old. Following administration of anaesthesia (see 2.4.1 Mouse anaesthesia), the mouse pupils were dilated by applying 1 % tropicamide and 2.5 % phenylephrine hydrochloride, then proxymetacaine was applied as a topical anaesthetic. The cornea was punctured with a 33 G needle to lower intraocular pressure and minimize the risk of trans-scleral reflux. Carbomer gel was applied to the corneal surface of both eyes, and on top of this, a 5 mm glass coverslip was applied to allow the posterior pole to be visualised. A 35 G bevelled needle (Nanofil) was inserted into a 10 µl syringe (Nanofil). 1.5 µl of AAV was drawn up into the needle for injection. The superior rectus muscle was held with forceps to stabilise the eye, and the needle slowly inserted into subretinal space superiorly until the entire bevel was visible through the pupil. The needle contents

were then injected into the subretinal space, creating a bleb. The needle was withdrawn and the coverslip and carbomer gel removed. The location of the injection site, the bleb shape, and any bleeds were noted on a sketch. Eyes were not harvested for analysis if they had moderate or severe bleeds, or any bleeds in the subretinal space. The antibiotic chloramphenicol was applied to the treated eye, then carbomer reapplied, and the mouse recovered. The retinas were collected 4 weeks post-injection, unless detailed otherwise.

2.4.3 Harvesting retina

Mice were euthanized by Schedule One (UK Home Office) techniques. Forceps were used to grasp the optic nerve underneath the eyeball and the eye removed.

2.5 Tissue analysis

2.5.1 Retinal sectioning

Enucleated eyes were rinsed in PBS, placed in 4 % paraformaldehyde in PBS for 30 min, then transferred to 1 % paraformaldehyde in PBS and incubated overnight. The cornea and lens were dissected out in cold PBS, and then the eye was transferred into increasing sucrose concentrations of 10 %, 20 % and 30 % for 1 hour each. The eyes were frozen in Optimal Cutting Temperature compound and stored at -80 C. The tissue was cut into 18 µm sections using a cryotome.

2.5.2 Immunohistochemistry

To preserve fluorescence all incubation steps were conducted in the dark. Between each incubation step, the slides were washed in 0.01 M PBS for 5 min, 3 times. Slides were incubated at room temperature for 20 min then permeabilised in 0.2 % Triton-X 100 for 20 min. Sections were then blocked in 10 % BSA, 10 % serum, 0.1 % Triton-X 100 at room temperature for 1 hour. The serum used matched the animal that the secondary antibody was raised in. The slides were then incubated with the primary antibody in 1 % BSA, 1 % serum, 0.1 % Triton-X 100 overnight at 4 C. The following day the slides were washed in 0.05 % Tween-20, 0.01 M PBS for 5 min twice then incubated with the secondary antibody in 1 % BSA, 1 % serum, 0. 1% Triton-X 100 at room temperature for 2 hours. Slides

Table 2.9 Primary and secondary immunohistochemistry antibodies.

Target	Primary antibody	Primary antibody dilution	Secondary antibody	Secondary antibody dilution
Cone arrestin	Rabbit anti-cone arrestin (Millipore Ab15282)	1/1000	Donkey anti-rabbit Alexafluor647 (ThermoFisher A31573)	1/200
SaCas9	Rabbit anti-SaCas9 (Abcam ab203933)	1/500	Donkey anti-rabbit Alexafluor555 (Thermofisher A31572)	1/600
SaCas9 (anti-HA tag)	Rabbit anti-HA tag (Cell signalling 3724)	1/1600	Donkey anti-rabbit Alexafluor555 (Thermofisher A31572)	1/600

were again washed in 0.05 % Tween-20, 0.01 M PBS for 5 min twice, then washed in 0.01 M PBS for 5 min. SlowFade Diamond Antifade Mountant with DAPI (ThermoFisher) was applied to the slides then a coverslip laid on top of this. Nail varnish was used to seal the edges of the coverslip, and the slides were incubated at room temperature overnight before storage at 4 C. Primary and secondary antibodies used are detailed in Table 2.9.

2.5.3 Confocal microscopy

The LSM-710 inverted confocal microscopy system (Zeiss) was used with the Zen software 2009 (Leica) to image retinal sections. The fluorophores DAPI, GFP, DsRed, and Alexafluor647 were acquired using a 405 nm UV, 488 nm argon, 543 nm helium-neon, and 633 helium-neon laser, respectively. The Airy Disc Unit was set to 1 and the gain adjusted to ensure there was no saturation.

2.6 Statistical analysis and graphical representation

GraphPad Prism 8 was used to perform all statistical analysis and produce graphs. Data points on graphs represent mean, and error bars represent standard error of the mean, unless detailed otherwise. Graphs usually display the data normalised to an untreated control (Untr) as this is helpful for interpretation by the reader, but the statistics are performed on un-normalised data. The results of the statistical tests are detailed in the appropriate figure legend. If any multiple comparisons are not significant, their p values are not listed. When highlighting particular results in the body of the text the corresponding p value is given. Results with a p value of equal or less than 0.05 were considered significant, and are indicated graphically by a number of asterisks above the data point (Table 2.10).

The majority of this thesis uses parametric tests, predominantly t-test and ANOVA, to interpret results. Parametric tests rely on assumptions about the data set: that it is normally distributed, the variance is homogeneous, and the data points for each variable are independent from one another. While the variables are independent, the data sets are too small for normal distribution and homogeneity of variance to be assessed statistically. Parametric tests were therefore carried out when the data was assumed to behave in a parametric manner based on an understanding of the biochemistry of the test (e.g. the data points were distant from the upper and lower detection limits of the technique), and the biological characteristics of the trait being measured.

Table 2.10 Interpretation of graphical asterisks.

Symbol	Meaning
*	p≤0.05
**	p≤0.01
***	p≤0.001
****	p≤0.0001

3 Validation of a short, rod cell-specific, hPDE6B promoter

3.1 Introduction

Identification of a short, rod-cell specific promoter is crucial for the development of an AAV-delivered CRISPR/Cas9 gene therapy strategy to treat adRP. Gene therapy frequently uses cell-specific promoters to limit transgene expression to the target cell[109]. This improves the safety profile of the treatment, as any off target effects are limited to the diseased cell type. This is particularly important when using techniques that edit the human genome such as CRISPR/Cas9, as the effects of the treatment are permanent and concerns surrounding off-target effects have been raised in the literature[111].

CRISPR gene therapy requires the transcription of two components: Cas9 and gRNA. Expression of Cas9 can be tightly controlled with cell-specific RNA polymerase II promoters. RNA polymerase III promoters which drive gRNA expression are ubiquitous and will be active in any successfully transduced cells[112]. Thankfully, gRNA alone is unable to interact with genomic DNA and therefore the expression profile of Cas9 determines the edited cell population. Promoters specific to neurons,

Table 3.1 The elements in the CRISPRi construct.

Element	Size (bp)
ITR	130
N-terminus NLS	21
dSaCas9	3159
KRAB repressor	195
C-terminus NLS	47
bGHpA	208
U6 promoter	241
gRNA	98
ITR	141
Spaces between elements	190
Total	4430
Remaining space	270

muscle cells, and photoreceptors have all been used to limit expression of a CRISPR/Cas9 construct to the target cell type in vivo[39,113,114]. Driving Cas9 with a rod cell-specific promoter ensures that CRISPRi and CRISPR/Cas9 gene disruption will be limited to rod cells.

AAV have a packaging capacity limited to roughly 4700 bp and the coding requirements for CRISPR/Cas9 and CRISPRi gene therapy are quite large, with the SaCas9, gRNA, and regulatory elements totally 4235 bp and 4430 bp, respectively (Table 3.1). This leaves only 270 bp remaining for a Cas9 promoter. Commonly used rod cell-expressing promoters are detailed in Table 3.2. Several of these target both rods and cones, making them unsuitable for use in this construct. The human *RHO* promoter drives high transgene expression and is rod cell-specific but it is too large at >800 bp[115,116]. In 2001, a shortened 146 bp version of the human *PDE6B* promoter was identified which was shown to drive rod cell-specific expression in *Xenopus* embryo heads, and was functional in the human retinoblastoma cell line Y79[117]. The *PDE6B* gene codes for the beta subunit of PDE6. This protein complex is involved in the phototransduction pathway and is only present in rod cells[118,119]. Lerner et al. (2001) identified two regulatory elements within the 146 bp region[117]: the βAp1/NRE element which the rod cell transcription factor NRL interacts with, and the β/GC element which is believed to be a binding site for zinc finger transcription factors (Figure 3.1). Unfortunately, the efficiency and specificity of this shortened promoter was not assessed in mice or human tissue, which are crucial for this DPhil.

In this chapter, two novel, shortened versions of the *PDE6B* promoter (hPDE6Bp) were used to drive

Table 3.2 Commonly used rod-expressing promoters and their characteristics.

Promoter	Size	Human cell functionality	Mouse cell functionality	Specificity	References
Mouse *Nrl*	1700	Unknown	Yes	Rod cells	120, 121
Human rhodopsin (*RHO*)	807	Yes	Yes	Rod cells	115, 116
Mouse *Gnat1*	541	Unknown	Yes	Rod and cone cells	122, 123
Human Rhodopsin Kinase (*hGRK1*)	292	Yes	Yes	Rod and cone cells	39
Human *PDE6B*	146	Yes	Yes	Unknown	117, 124

expression of the reporter gene DsRed. The shortened versions included both the βAp1/NRE element and the β/GC element. The activity of these promoters was assessed in various cell lines in vitro, in mice in vivo, and in human retinal tissue ex vivo.

3.2 Materials and Methods

3.2.1 Plasmid cloning

Plasmid cloning was performed as detailed in 2.1.10 General plasmid cloning. The specifics of cloning each individual plasmid used in Chapter 3 are detailed below.

3.2.2 Cloning hPDE6Bp.DsRed plasmids

The hRHOp.DsRed plasmid was digested with *Kpn*I and *Fsp*AI to remove hRHOp and a 46 bp section of the DsRed gene. The desired 3890 bp fragment was gel purified using the QIAquick gel extraction kit (QIAGEN). Two lengths of hPDE6Bp were selected – a 154 bp "shorthPDE6Bp" from -108 to +46 and a 209 bp "longhPDE6Bp", from –163 to +46 (nucleotide number is relative to the transcriptional start site, NG_009839.1). These were PCR amplified from human DNA using KOD Polymerase with a 5'-*Kpn*I overhang on the forward primer and a 5'-61 bp overhang on the reverse primer which replaced the section of the DsRed coding sequence removed from the hRHOp.DsRed plasmid (see Appendix 9.1.1 for PCR primers). Following ligation, transformation and miniprep, a diagnostic restriction digestion was conducted with *Bsa*I. The full hPDE6Bp sequences are given in Appendix 9.9.

3.2.3 Cloning CAG.DsRed

Site-directed mutagenesis was conducted to create a restriction site at the 3' end of hRHOp in the hRHOp.DsRed plasmid. The Agilent QuikChange II XL kit was used to mutate two bases, turning 5'-TCATCC-3' into the *Bam*HI restriction site 5'-GGATCC-3', and creating the plasmid hRHOp.BamHI.DsRed. hRHOp.BamHI.DsRed was digested with *Kpn*I and *Bam*HI to remove hRHOp. The desired 3765 bp band was gel extracted. CAG was amplified from the CAG.GFP.WPRE plasmid using KOD polymerase with a 5' *Kpn*I and 5' *Bam*HI overhang on the forward and reverse primers, respectively (see 9.1.1 for PCR primers). Following ligation, transformation and miniprep, a diagnostic

restriction digestion was conducted with *Hind*III and *Kpn*I.

3.2.4 Cloning promoterless.DsRed

To create a promoterless.DsRed construct, the hRHOp.DsRed plasmid was amplified with KOD polymerase using a forward primer binding at the start of DsRed, and the reverse primer binding upstream of hRHOp. This produced a 3763 bp product plasmid, with no promoter driving DsRed. The product was gel purified, phosphorylated with T4 PNK (New England Biolabs), ligated with T4 ligase (New England Biolabs), transformed into XL-10 Gold Ultracompetent cells, and miniprepped (Sigma).

3.2.5 Cell line transfection and transduction

The general protocol for cell transfection and transduction is given in section 2.2.5 and 2.2.6, respectively. The specific seeding densities, plasmid transfection quantities and transduction multiplicity of infection (MOI) are detailed in Table 3.3.

3.2.6 AAV production

Production and description of the AAV used in this chapter are detailed in section 2.3.1, and Table 2.6, respectively.

Table 3.3 Cell transfection and transduction experiments performed in Chapter 3.

Figure	Cell line	Seeding density	Plasmid copy number transfected	Viral MOI
Figure 3.2B	HEK293	10^5 cells/well (96 well plate)	$2.44x10^{10}$	N/A
Figure 3.2C	Y79	1.375^5 cells/well (96 well plate)	$4.88x10^{10}$	N/A
Figure 3.3C	HEK293	10^4 cells/well (96 well plate)	N/A	10^4
Figure 3.3D	Y79	1.375^5 cells/well (96 well plate)	N/A	$2x10^4$

3.2.7 Subretinal injections

Subretinal injections were conducted as detailed in 2.4.2. The specific AAV quantities used are detailed in Table 3.4.

3.2.8 Co-localisation analysis

Three retinas per condition (AAV8.shorthPDE6Bp, AAV8.RHOp, sham) were sectioned, stained for anti-cone arrestin, and analysed under confocal microscopy as described in 2.5.1, 2.5.2, and 2.5.3, respectively. For each retina, three sections per slide that had high levels of DsRed expression were chosen for analysis. The outer nuclear layer of the retinas were imaged under 64x magnification to capture EGFP, DsRed, and Alexafluor647 expression (the secondary fluorophore used during anti-cone arresting staining). ImageJ was used to open and process the files. A "random dot" macro (taken from the imageJ macro list - see below[125]) was used to select 20 random nuclei in the EGFP and DsRed channel. All anti-cone arrestin-positive cells were assessed as there were under 20 of these per image. The co-expression of other fluorophores at this nuclei position was noted manually. All analysis was performed while blinded to the AAV condition of the retina.

Random dot macro:

```
dotSize = 5;
        width = getWidth();
        height = getHeight();
        for (i=0; i<25; i++) {
        x = random()*width-dotSize/2;
        y = random()*height-dotSize/2;
        makeOval(x, y, dotSize, dotSize);
        run("Fill");
        }
        run("Select None");
```

Table 3.4 Subretinal injection conditions used in Chapter 3.

AAV	Viral genomes injected
AAV8.shorthPDE6Bp	$1.53x10^9$
AAV8.RHOp	$4.85x10^8$

3.2.9 Human retinal explant culture and transduction

Human retinal tissue was harvested from a consenting adult patient undergoing a clinically indicated retinectomy, under the REC-approved study "Human retinal cell culture" (REC reference number 10/H0505/8, IRAS number: 37274, approved by the Oxfordshire NHS Research Ethics Committee) at the Oxford Eye Hospital, UK, and processed in the Nuffield Department of Clinical Neurosciences, Oxford University. The tissue was handled in accordance with the Human Tissue Act 2004.

Harvesting, culturing, and fixation of the human retinal explant followed the protocol outlined by Orlans et al (2018), with imaging and fixation performed 20 days post-transduction[126]. The area of the explants was estimated using the image-processing programme ImageJ by drawing a "region of interest" around the edge of the explant and calculating its internal area.

3.3 Results

3.3.1 hPDE6Bp is functional in the retinal cell line Y79

Two lengths of hPDE6Bp were selected for testing and were cloned into a reporter plasmid driving DsRed expression. These were “shorthPDE6Bp” and “longhPDE6Bp” which covered the region from -108 to +46, and -163 to +46 of the PDE6B gene, relative to the transcriptional start site, respectively (Figure 3.1). These regions include both the βAp1/NRE and β/GC DNA regulatory elements. Positions -163 and -108 were selected because these are sites of convenient PCR primers for construct cloning. As the DsRed reporter plasmid already contained a functional kozak sequence, +46 was selected as the end of the promoter to exclude the native kozak sequence.

Following cell line transfection, DsRed expression was qualitatively compared to a ubiquitously expressing CAG.DsRed plasmid, a rod cell-specific hRHOp.DsRed plasmid, and the negative control promoterless.DsRed plasmid which contains no promoter upstream of DsRed (Figure 3.2A). Neither hPDE6Bp plasmid drove DsRed expression in the non-retinal HEK293 cells but both were able to drive DsRed expression in retinoblastoma-derived Y79 cells (Figure 3.2B-C). As expected, the promoterless.DsRed, and hRHOp.DsRed plasmids were unable to drive expression in either cell line (Y79 cells express only low levels of *RHO*[127]), while the CAG.DsRed plasmid successfully drove DsRed expression in both cell lines.

AAV2/8(Y733F) viral constructs were made of both shorthPDE6Bp.DsRed and longhPDE6Bp.DsRed

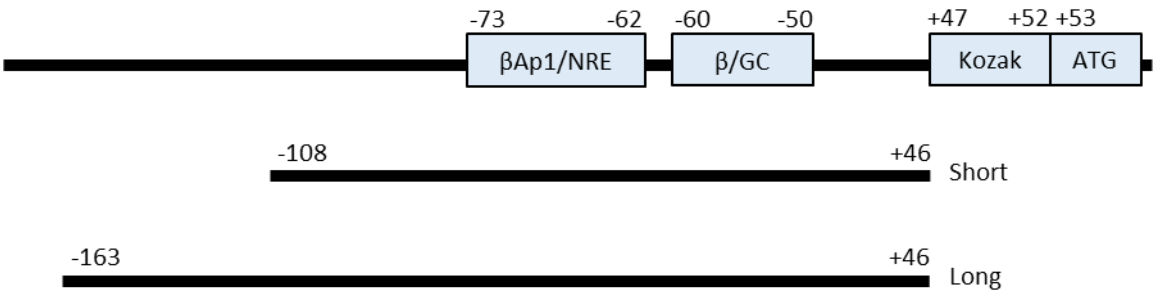

Figure 3.1 The human PDE6B promoter and regions selected for analysis.

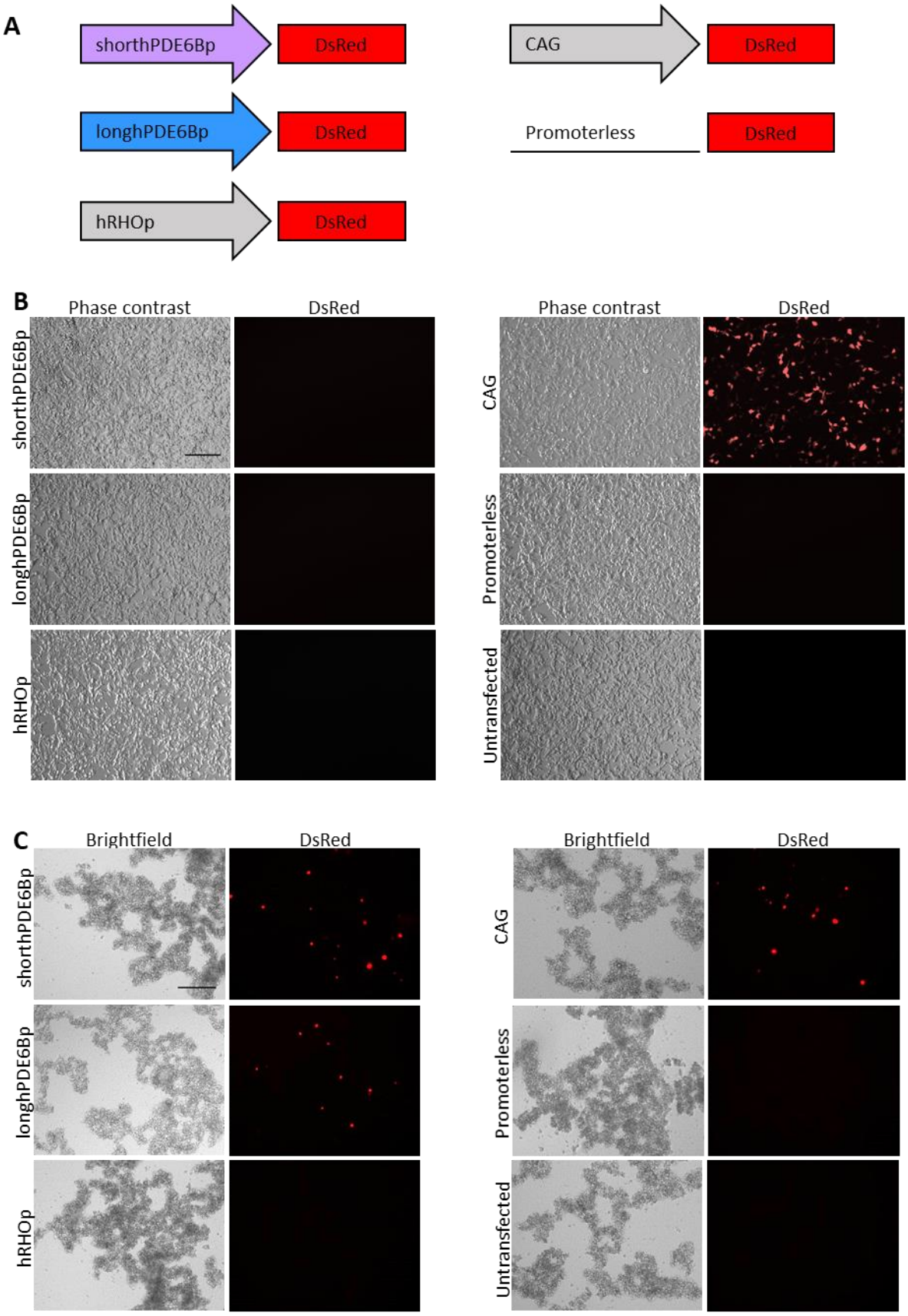

Figure 3.2. hPDE6Bp plasmids are active in Y79 cells.
A) *DsRed plasmid constructs driven by different promoters.* ***B)*** *Transfection of DsRed constructs in HEK293 cells.* ***C)*** *Transfection of DsRed constructs in Y79 cells. Scale bars represents 250 µM.*

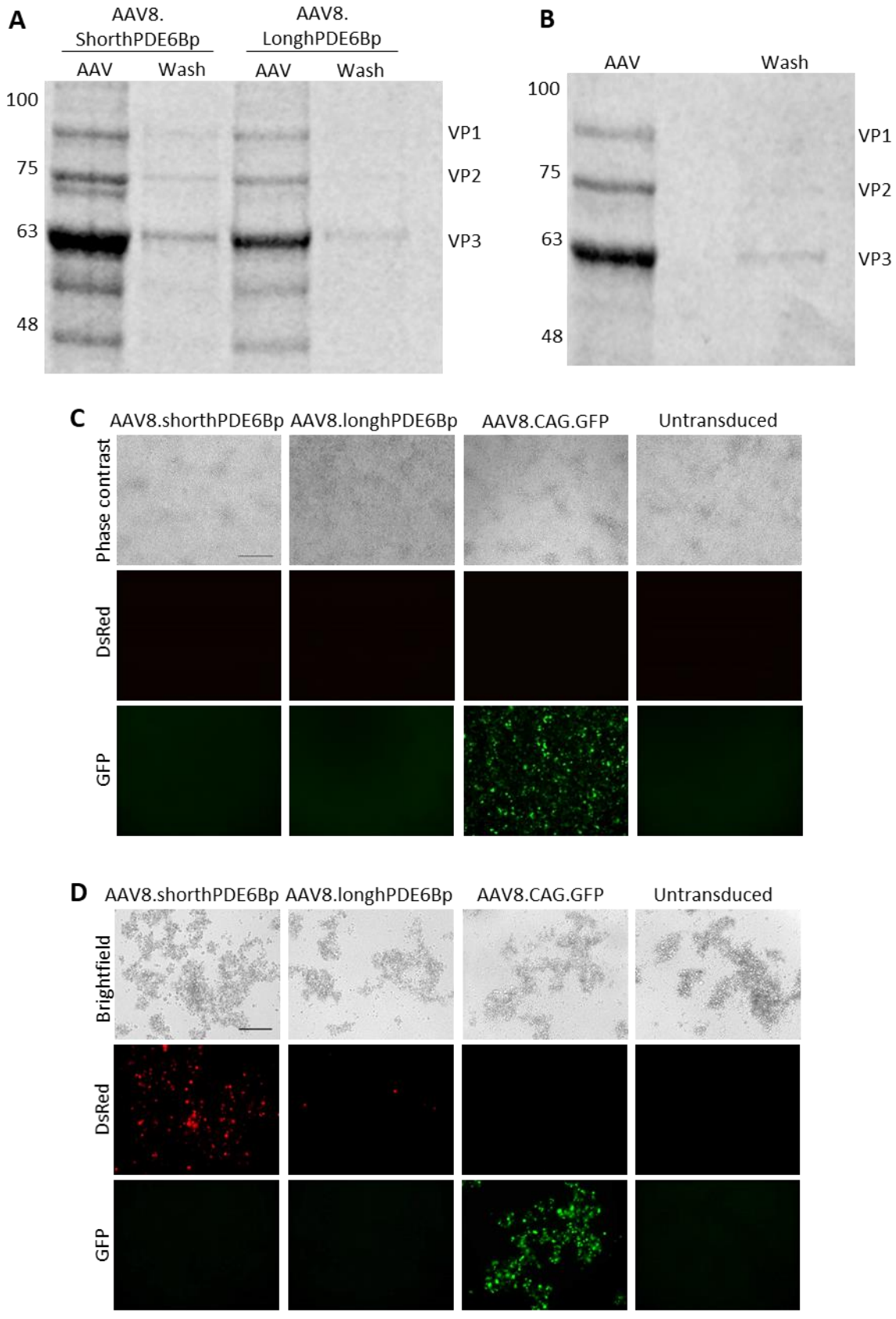

Figure 3.3 AAV8.shorthPDE6Bp drives strong expression in Y79 cells.
A) *SDS-PAGE of AAV8.hPDE6Bp viruses showing the three viral capsid proteins among contaminating bands.* ***B)*** *SDS-PAGE of second batch of AAV8.shorthPDE6Bp virus showing the three viral capsid proteins.* ***C)*** *Viral transduction in HEK293 cells.* ***D)*** *Viral transduction in Y79 cells. Scale bars represents 250 µm.*

constructs (named AAV8.shorthPDE6Bp and AAV8.longhPDE6Bp). The Y733F mutant capsid was selected as it is highly efficient at transducing photoreceptors following subretinal injection, and has driven rescue in multiple models of autosomal recessive retinitis pigmentosa[118,128–131]. SDS-PAGE showed strong viral capsid protein bands at 87 kDa, 73 kDa, and 62 kDa as expected, with some additional contaminating bands (Figure 3.3A). These proteins were not identified but protein contamination in AAV preps typically originate from the HEK293T cells used in AAV manufacturing[132]. These AAV were transduced into HEK293 and Y79 cells along with a ubiquitously-expressing AAV2/8(Y733F).CAG.GFP.WPRE positive control (named AAV8.CAG.GFP). DsRed expression was again seen with both promoters in the Y79 cells but not the HEK293 cells (Figure 3.3C-D). In AAV form, shorthPDE6Bp appeared to drive stronger gene expression than longhPDE6Bp, with more DsRed-positive cells. AAV8.shorthPDE6Bp was therefore taken forward into in vivo experiments.

3.3.2 hPDE6Bp is rod cell-specific in mice

A second batch of AAV8.shorthPDE6Bp was produced which was of higher purity, with no contaminating bands seen on the viral SDS-PAGE (Figure 3.3B). This was subretinally injected into Nrl-EGFP mice, which express EGFP in their rod cells[121]. The self-complementary AAV2/8(Y733F).hRHOp.DsRed (named AAV8.hRHOp) was injected as a rod cell-specific control, while a sham injection of PBS was used as a negative control. AAV8.shorthPDE6Bp was injected at $1.53x10^9$ genome copies per eye, as this was the highest dose possible (for the achieved titre), while AAV8.hRHOp was injected at $4.85x10^8$ genome copies per eye, as this dose demonstrated transduction by previous members of the research group. The eyes were harvested, sectioned and viewed under a confocal microscope. DsRed expression was observed in both the AAV8.shorthPDE6Bp and AAV8.hRHOp-injected eyes and not in the sham-injected eyes. The signal was strongest at the superior of the retina, where the injection took place, and diffused away from this point (Figure 3.4A-B). The

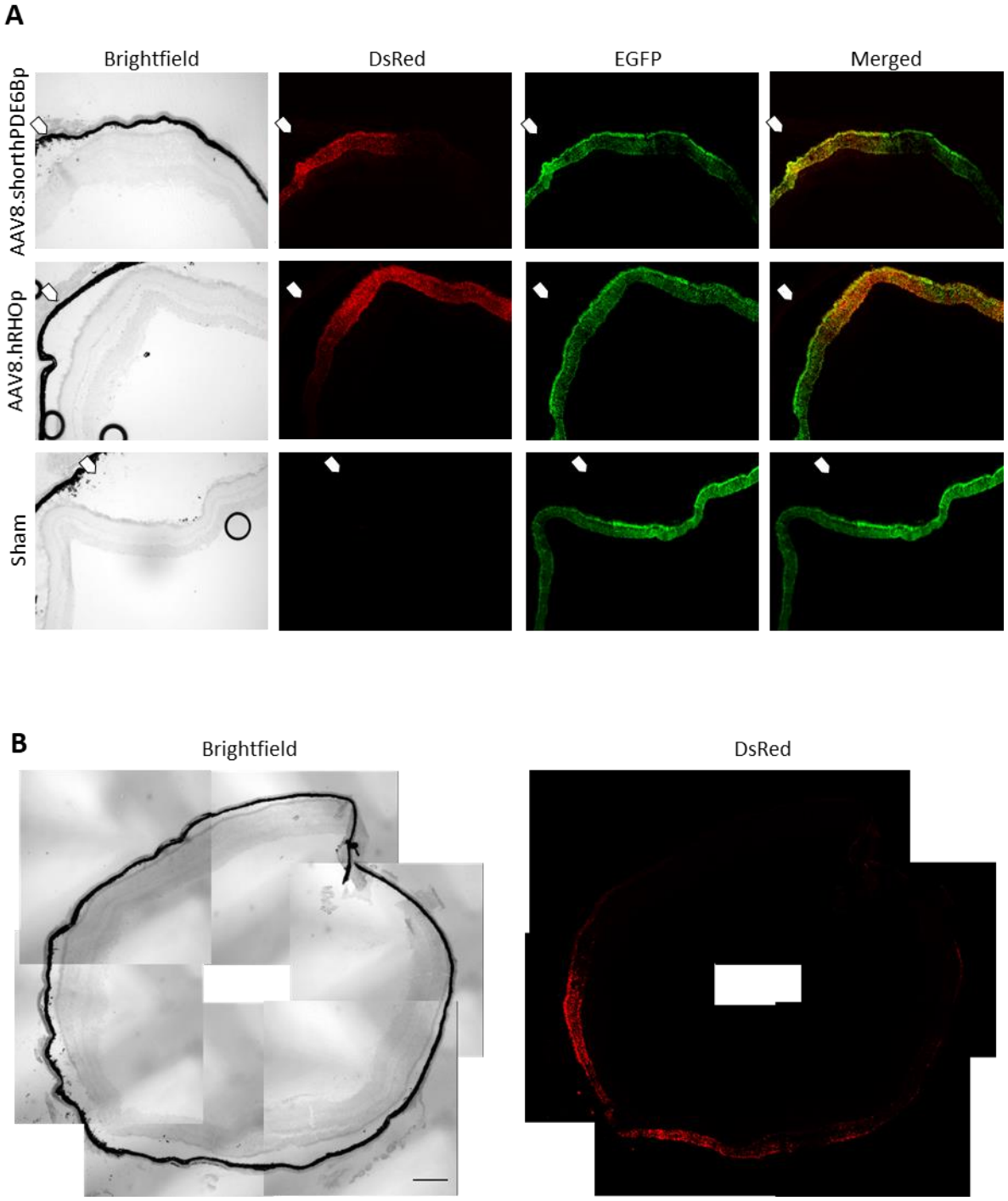

Figure 3.4 AAV8.shorthPDE6Bp efficiently transduces the murine retina.
A) *Confocal microscopy images of transduced mouse retina. The arrow indicates the approximate subretinal injection site.* ***B)*** *Whole retina image of eye injected with AAV8.shorthPDE6Bp. Scale bar represents 250 µm.*

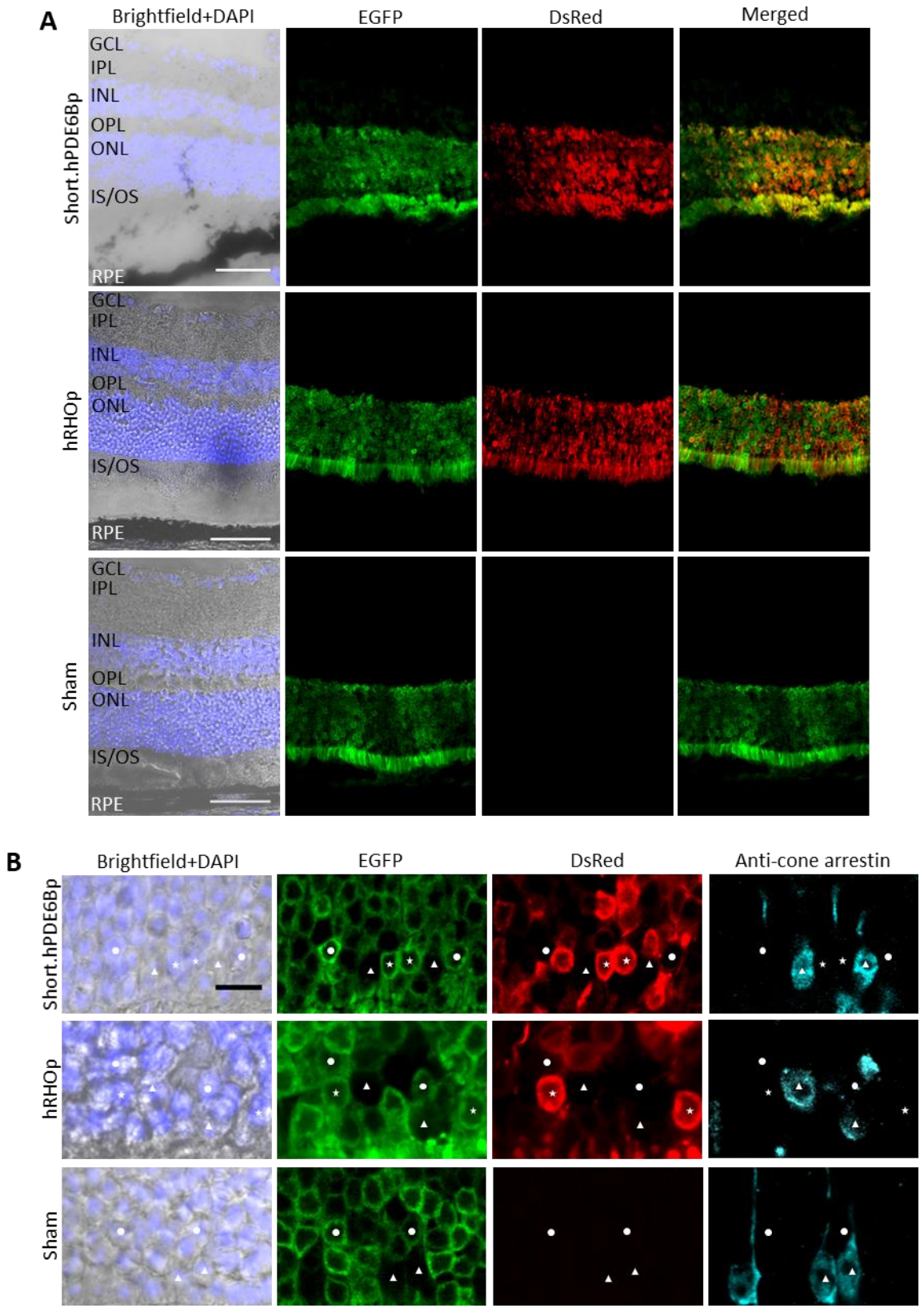

Figure 3.5 Transgene expression is exclusive to rod cells.
A) *Expression of EGFP and DsRed is limited to the photoreceptor layer of sectioned retinas following subretinal injection. GCL = ganglion cell layer, IPL = inner plexiform layer, INL = inner nuclear layer, OPL = outer plexiform layer, ONL = outer nuclear layer, IS/OS = inner segment/outer segment, RPE = retinal pigment epithelium. Scale bar represents 60 µm.* ***B)*** *Outer nuclear layer of injected eyes stained for anti-cone arrestin. Circle indicates untransduced rod cell, star indicates transduced rod cell, triangle indicates cone cell. Scale bar is 10 µm.*

expression pattern of both viruses were similar, with DsRed expression observed only in layers of the retina where photoreceptors are present – the outer nuclear layer, the inner segment, and the outer segment. This aligned with the native EGFP expression (Figure 3.5A).

To determine the specificity and efficiency of the constructs, EGFP-positive (indicating a rod cell), DsRed-positive (indicating promoter activity), and anti-cone arrestin-positive (indicating a cone cell) cell nuclei were selected at random within a region of high DsRed expression, and the co-expression of other fluorophores were noted. In both the AAV8.shorthPDE6Bp and AAV8.hRHOp-treated retinas, 100% of all 180 DsRed-positive cells examined were also positive for EGFP, indicating they are rod cells (Figure 3.5B). AAV8.hRHOp virus drove significantly higher levels of expression, with an average of 74.4 % of EGFP-positive cells expressing DsRed, compared to 55.0 % in the AAV8.shorthPDE6Bp-treated eyes (Unpaired t-test, F=16.71, p=0.0347). Of 256 anti-cone arrestin-positive cells, 251 were for negative for EGFP (98.05 %), indicating good distinction between rod and cone cell populations. In the AAV8.shorthPDE6Bp-treated retinas 0/92 of the anti-cone arrestin positive cells were DsRed positive, and in the AAV8.hRHOp-treated retinas 2/90 (2.22 %) of the anti-cone arrestin positive cells were DsRed positive. Importantly, the two cells positive for both DsRed and anti-cone arrestin were also positive for EGFP. This could indicate inappropriate staining or overlapping cells rather than a lack of specificity with hRHOp.

3.3.3 hPDE6Bp is functional in human retinal explants

Fragments of human retinal tissue were harvested from an NHS patient undergoing routine retinectomy to treat retinal detachment, and cultured in the laboratory. They ranged in size, from roughly 0.073 mm^2 to 0.935 mm^2. Transduction was initially attempted with AAV8(Y733F).CAG.GFP but this did not produce significant fluorescence (Figure 3.6A). AAV2 has been reported to drive strong transduction of human retinal explants so AAV2.shorthPDE6Bp.DsRed was produced (Figure 3.6B, named AAV2.shorthPDE6Bp)[133,134].

Following transduction with AAV2.shorthPDE6Bp or AAV2.CAG.GFP, fragments were cultured for 20 days, and then examined for expression of fluorescence. Both fragments transduced with 10^9 AAV2.CAG.GFP viral genomes demonstrated expression of GFP in multiple areas of the tissue. AAV2.shorthPDE6Bp was applied at $5x10^9$, 10^{10}, and $5x10^{10}$ viral genomes per explant and DsRed expression was seen in 0/3, 1/3, and 1/1 of explants, respectively (Figure 3.6C). When present, DsRed expression was only visible in a small region of the tissue compared to the AAV2.CAG.GFP-transduced explants. As native hPDE6Bp is rod cell-specific, the successfully transduced region could possibly

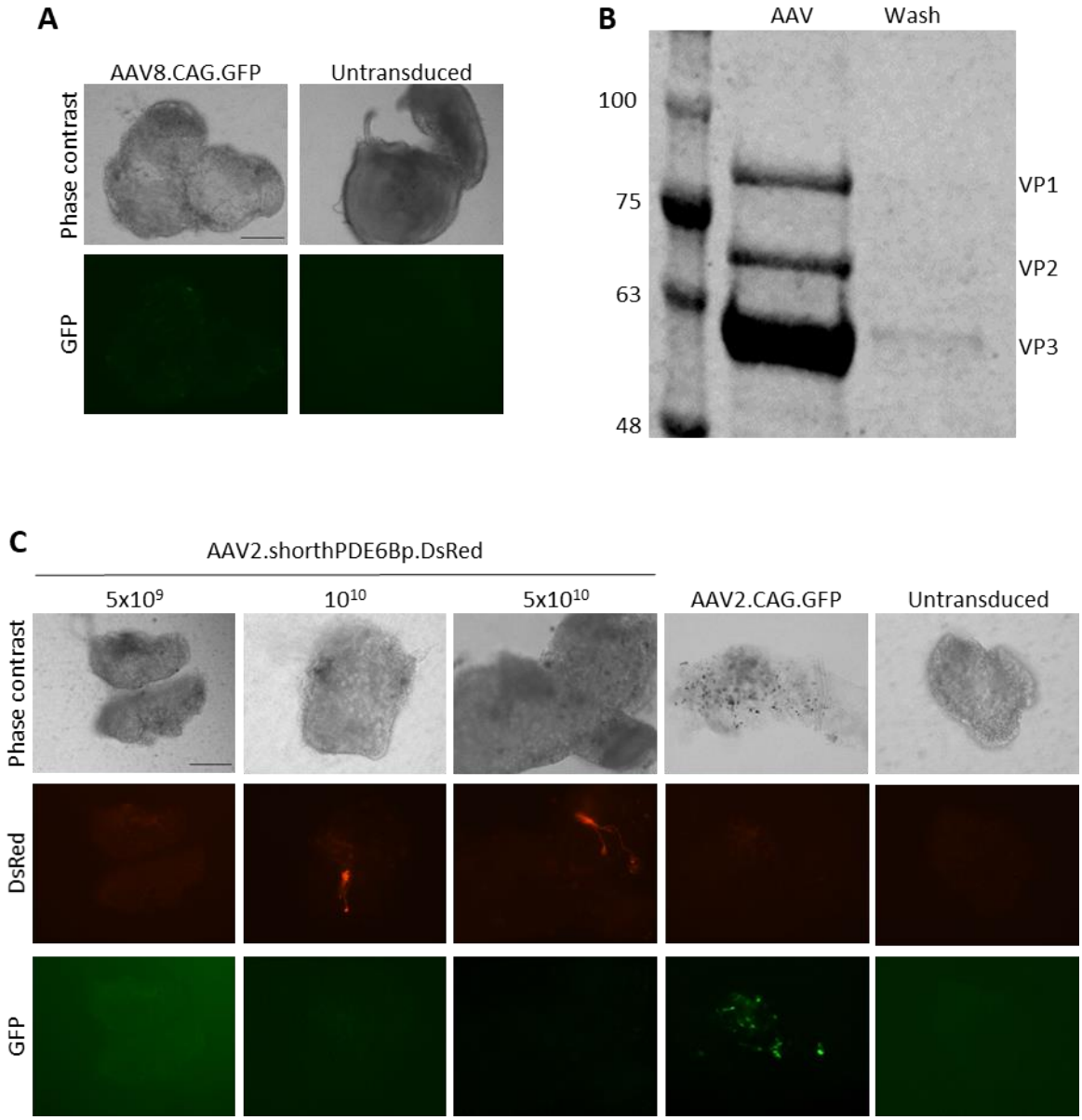

Figure 3.6 AAV.hPDE6Bp.DsRed transduces human retinal explants.
***A)** Representative images of human retinal explants unsuccessfully treated with AAV8.CAG.GFP. **B)** SDS-PAGE of AAV2.shorthPDE6Bp.DsRed virus showing the three viral capsid proteins. **C)** Representative images of human retinal explants transduced with different AAV2 and their transduction quantity. Scale bar represents 250 µm.*

correspond with areas containing viable rod cells. The explants were fixed for sectioning but unfortunately, the sections were unuseable.

3.4 Discussion

When selecting a promoter to drive expression in an AAV construct, the most important features are efficiency and specificity. Driving transgene expression with a target cell-specific promoter dramatically improves the safety of a potential AAV gene therapy treatment[109]. This chapter assessed the specificity and efficiency of shortened hPDE6B promoters to determine their suitability in an AAV gene therapy construct to treat adRP.

The in vitro activity of the hPDE6B promoters matched the expression profile of the tested cell lines: promoter activity was present in Y79 cells, which express PDE6B, and absent from HEK293 cells, which do not express PDE6B[127,135–137]. While this suggests that both promoters retained the required regulatory features to ensure cell-specificity, expression in other non-retinal cell lines cannot be ruled out, particularly as immortalised cell lines often express tissue-inappropriate genes[135,138,139]. Interestingly, the "short" 154 bp promoter (-108 to +46) drove higher in vitro expression than the "long" 209 bp promoter (-163 to +46) in an AAV construct, but both promoters were comparable when using a plasmid. Similar results have been previously described. When driving a reporter construct in plasmid form, Di Pollo et al (1997) found there was little difference in in vitro activity between promoters beginning at -93 and -167 (relative to the transcriptional start site of PDE6B)[124]. Conversely, Lerner et al. (2001) found that a shorter -93 to +53 promoter appeared to drive higher, and more specific, expression in transgenic *Xenopus* than a significantly longer -1356 to +53 promoter[117]. It is possible that longhPDE6Bp contains regulatory elements absent from shorthPDE6Bp which are influencing gene expression but none were identified in papers investigating DNA elements in this region[117,124].

ShorthPDE6Bp was found to be rod cell-specific in vivo, with an expression pattern matching hRHOp. Assessment of fluorophore co-localisation in vivo was performed manually. Rod cells and cone cells were identified by presence of EGFP, and anti-cone arrestin (stained with Alexafluor 647), respectively. As distinct cell groups, these fluorophores were expected to have a complete lack of co-localisation

but 4 out of 256 cells expressed both EGFP and anti-cone arrestin. While it is possible that this demonstrates inappropriate staining or gene expression, it is likely this was due to sub-optimal imaging using the confocal microscope. Background fluorescence, autofluorescence, bleed through from other channels, fluorescence from out of focus cells, or excessive image depth could all explain the misleading presence of both fluorophores at a given position[140]. Automated assessment of co-localisation was also attempted using Mander's Co-localisation Coefficient on the known rod cell-specific AAV8.hRHOp-treated samples but - likely due to the image quality - no meaningful correlation could be found between EGFP and DsRed.

The specificity of retinal promoters is frequently determined by ocular injection of promoter constructs driving a reporter gene, then identification of active cell types through microscopy analysis[116,141]. While this allows assessment of specificity within the retina, it does not exclude the possibility that the promoter is active in tissue outside the eye. Low levels of activity have been observed in the brain and spinal cord of transgenic *Xenopus* when using a 1409 bp version of the hPDE6B promoter. This non-specific activity was not present in a 146 bp version of hPDE6Bp, highlighting the importance of whole body tissue assessment[117]. AAV capsids exhibit tropism for particular tissue types, and therefore the AAV serotype will influence transgene expression in whole body assessments[142]. AAV8 has displayed strong transduction of liver, skeletal muscle, retina, heart, and pancreas tissue, but is less efficient in other tissue, including the kidney, making it difficult to assess promoter activity in these locations[79,104,142–147]. It is frequently cited that the human blood-ocular barrier should prevent subretinally injected AAV gene therapy constructs from leaving the eye but studies in non-human primates have detected presence of gene therapy AAV in the blood, urine, nasal secretions and tearfilm following subretinal injections[97,108,148,149]. The blood retina barrier is also not impenetrable and can break down in the course of some retinal diseases[100,150].

Despite moderate levels of transgene expression, AAV8.shorthPDE6Bp was outperformed by AAV8.hRHOp. Although the DNA sequences varied only in the choice of promoter, AAV8.hRHOp is self-

complementary whereas AAV8.shorthPDE6Bp is single-stranded. Self-complementary vectors contain both the forward and reverse strand of the AAV genome. As they do not have to undergo second strand synthesis, they are associated with stronger and more rapid transduction, an effect which is particularly pronounced in retinal tissue[151]. As the retinas were all harvested 4 weeks post-injection, higher expression levels would be expected in a self-complementary AAV compared to a single stranded AAV. A comparison of these AAV is therefore not a direct comparison of promoter activity.

shorthPDE6Bp activity was confirmed ex vivo in human retinal tissue harvested from a patient with a retinal detachment. While expression was not seen consistently throughout replicates this is not surprising as the rod containing outer retina is often damaged or lost in cases of retinal detachment. Detached tissue can also be diseased and dying; this justifies its clinical removal but cell death prevents successful transduction[134]. Some samples could therefore contain no living rods cells. Prior to using shorthPDE6Bp in clinical trials, confirmation of specificity within the human retina is recommended. To overcome the poor health of ex vivo human retinal tissue, human retinal organoids could be explored. Human retinal organoids broadly mimic human retinal structure and contain photoreceptor cells expressing rod- and cone-specific markers, including PDE6B[152–154]. They can be generated from both healthy and adRP patients which would allow promoter specificity to be determined in the target phenotype[155].

This chapter demonstrates that shorthPDE6Bp drives strong rod cell-specific expression in vivo. At just 154 bp in length, it could be used to drive expression of an SaCas9 or dSaCas9.KRAB construct (estimated at approximately 4235 bp and 4430 bp, respectively) within a single AAV, making it extremely useful for CRISPR gene editing studies in rod cells. As it is functional in both mouse and human tissue, transitioning from in vivo studies to human trials would be simple, as the vector would not require any modification between species.

4 Optimisation of CRISPR constructs in vitro

4.1 Introduction

Gene therapy relies on the activity of introduced transgenes to create clinically beneficial changes in a target cell. The design of the AAV gene therapy construct plays a critical role, influencing AAV packaging, AAV transduction, and expression of the delivered transgene[98,99,156–162]. This thesis describes the first CRISPR research conducted within the Clinical Ophthalmology Research Group at Oxford University. This required the development and optimisation of multiple AAV CRISPR constructs and laboratory techniques. While this could be done targeting a clinically relevant gene, it is common for initial proof of concept experiments to target a reporter gene[39,113,163,164]. These genes are well characterised and allow more efficient screening, and comparisons between different research studies. This thesis uses the reporter gene EGFP, and targets it first in a HEK293-EGFP cell line, then in a transgenic mouse model with rod cell-specific EGFP expression (see Chapter 6[121]).

Successful CRISPR gene editing requires a Cas9 endonuclease protein and a target-specific gRNA to be present in a cell. The px601 plasmid encodes *Staphylococcus aureus* Cas9 and gRNA, driven by the ubiquitous CMV and U6 promoters, respectively[69]. The transgene is flanked by ITRs, allowing the sequence to be packaged into an AAV. Px601 was created in 2015 and has demonstrated high levels of CRISPR-mediated gene disruption both as a plasmid in vitro, and an AAV in vivo, with in vivo editing rates of 40 %[69].

CRISPRi uses a modified version of Cas9 called dead Cas9 (dCas9). dSaCas9 differs from SaCas9 by two amino acid substitutions: D10A and N580A, which inactivate its two cleavage sites, removing its ability to cut DNA[165]. The catalytically inactive dCas9 in combination with the gRNA, binds to the target gene, blocking the access of regulatory proteins, and reducing the transcription rate[60].

While dCas9 can cause gene repression alone, studies have found that creating a fusion protein with

repressor domains can improve the knock down[58]. The Krüppel Associated Box (KRAB) repressor is a common regulatory domain found in eukaryotic zinc finger nucleases. It binds to the native cellular protein KRAB-associated protein 1, which interacts with a range of histone remodelling proteins (Figure 1.4D). This causes a change of chromatin conformation, converting open and transcriptionally active euchromatin, to more closed and transcriptionally inaccessible heterochromatin, resulting in gene silencing[166]. Addition of the KRAB repressor to dCas9 can increase the repression rates up to 15-fold, although this is highly variable with target sequence[58,65].

Selection of gRNAs begins with in silico gRNA software. These software predict gRNA:DNA binding efficiency based on algorithms derived from large-scale screens using SpCas9 gene disruption[167,168]. This thesis uses SaCas9 rather than SpCas9, and the translatability of the results between Cas9 species is unknown. This thesis also explores CRISPRi, which was not included in the prediction algorithms at the time of analysis (CRISPRi gRNA screening has since been added[169]), and is highly influenced by the position of gRNA within the gene as well as the gRNA:DNA binding efficiency (see 1.4.2 CRISPR/Cas9 vs. CRISPRi)[58]. For both these reasons, it is important that multiple gRNAs are screened in vitro to identify the best candidates.

The efficiency of knock down by a given gRNA can be measured at a DNA level, an mRNA level, or a protein level. This chapter will compare four different methods of measuring CRISPR/Cas9 and CRISPRi gene knock down efficiency: TIDE (Tracking of Indels by Decomposition) analysis to measure indels in DNA, qPCR to measure the impact on an mRNA level, and fluorescence images and fluorescence spectroscopy to measure the impact on EGFP protein function.

Not only are the elements of the construct important to consider but also their position and orientation. In bi-cistronic constructs (a single construct expressing transgenes from two promoters), the arrangement of promoters in relation to one another can influence the expression rate of the transgenes[156–159]. The mechanism for this is currently unknown, but it is possible that transcriptional interference could be the result of the transcriptional complexes colliding or blocking one another's

passage through the DNA. The orientation of U6-gRNA in bi-cistronic CRISPR constructs has been shown to impact gene editing rates, and so this chapter tests two orientations of the CRISPR/Cas9 construct [69,170,171].

This chapter describes the creation, validation, and optimisation of the CRISPR/Cas9 and CRISPRi constructs that will be used throughout this thesis. Px601 is used as the all-in-one SaCas9 construct for CRISPR/Cas9 gene disruption. This plasmid is used as a template for the creation of a dSaCas9, and then dSaCas9.KRAB construct for CRISPRi gene repression.

4.2 Materials and Methods

4.2.1 Sequencing Nrl-EGFP

DNA was extracted from an ear notch of an *Nrl*-EGFP mouse using the QIAamp DNA Mini Kit. Primer3 was used to design a range of sequencing and PCR primers to the transgene sequence (see 9.1.2 and 9.1.1). PCR was conducted on the region of interest using KOD Polymerase Master Mix (Merck). The target bands were excised from the gel, purified using the QIAQuick Gel Extraction Kit, and Sanger sequenced (Eurofins Genomics Ltd). The sequencing reads were aligned with the reference sequence using the bioinformatic software Geneious. The confirmed sequence is given in Appendix 9.2.

4.2.2 Screening the EGFP sequence for gRNAs

The bioinformatics programme Benchling, was used to screen the confirmed *Nrl*-EGFP sequence for 21 bp gRNAs with the SaCas9 PAM site 5'-NNGRRT-3'. The *Mus musculus* genome was used to calculate the off-target effects. gRNAs were selected from a range of positions within the EGFP sequence.

4.2.3 Characterisation of the HEK293-EGFP cell line

Both karyotyping analysis and MFISH analysis were conducted on the HEK293-EGFP cell line by the Wellcome Centre for Human Genetics. 15 cells were karyotyped and their chromosome numbers and any translocations were noted. MFISH analysis was performed on 50 cells in metaphase using a lentiviral vector carrying EGFP as a probe. Integration sites were noted.

4.2.4 Sequencing the EGFP transgene in HEK293-EGFP cells

HEK293-EGFP cell pellets were harvested by centrifugation (see 2.2.8 Cell harvesting) and DNA was

extracted using the QIAamp DNA Mini Kit. PCR was conducted using KOD polymerase and primers that amplify a few hundred bases upstream and downstream of EGFP. Sanger sequencing was conducted (Eurofins Genomics Ltd) and the sequence noted. Primer sequences are detailed in Appendix 9.1.2.

4.2.5 Creating the all-in-one dSaCas9 plasmid

Two site-directed mutagenesis reactions were performed using the QuikChange II XL Site-Directed Mutagenesis Kit (Agilent). The first introduced the A>C mutation at nucleotide 77 of SaCas9 (D10A) into px601 to create px601.D10A, and the second introduced the AA>GC mutations at nucleotides 1786-1787 of SaCas9 (N580A) into px601.D10A to create the CMV.dSaCas9.bGHpA.U6.gRNA plasmid. 5 µl 10x Reaction Buffer, 10 ng plasmid, 125 ng forward plasmid, 125 ng reverse plasmid, 1 µl dNTP mix, and 1 µl *PfuUltra* High Fidelity DNA polymerase were combined in a 50 µl reaction volume. The samples were run on a thermocycler at 95 C for 1 min followed by 18 cycles of 95 C for 50 s, 60 C for 50 s, 68 C for 7 min 24 s, and finally 68 C for 7 min. The primers are detailed in Appendix 9.1.4. The products were transformed into XL10 Gold Ultracompetent Cells (Stratagene). Colonies were miniprepped using the GenElute Sigma Miniprep Kit (Sigma) and successfully modified plasmids analysed by Sanger sequencing.

4.2.6 Cloning the CMV.dSaCas9.KRAB.U6.gRNA plasmid

The general protocol for plasmid cloning is detailed in 2.1.10. The CMV.dSaCas9.KRAB plasmid was a gift from Charles Gersbach (Addgene plasmid # 106219). It was digested with *Hind*III and *Eco*RI (New England Biolabs), and the KRAB-containing fragment was purified by gel extraction (QIAquick Gel Extraction Kit, Qiagen). The CMV.dSaCas9.U6.gRNA plasmid was digested with the same enzymes and the large backbone purified. The two fragments were ligated together to create the all-in-one plasmid CMV.dSaCas9.KRAB.U6.gRNA. The KRAB coding sequence unfortunately contained a *Bsa*I restriction site, which is the enzyme used to clone the gRNA into the plasmid. Another member of the team used

site-directed mutagenesis to change one nucleotide within the KRAB sequence; this removed the *Bsa*I restriction site without changing the amino acid coding sequence of KRAB.

4.2.7 Cloning gRNAs into SaCas9, dSaCas9, dSaCas9.KRAB plasmids

gRNA cloning is described in 2.1.11. The "scrambled gRNA" sequence is the sequence already present in the unmodified plasmid and has the sequence GGAGACCACGGCAGGTCTCA.

4.2.8 Cell line transfection

The general protocols for cell maintenance and transfection are given in sections 2.2.1 and 2.2.5, respectively. The specific seeding densities, plasmid transfection quantities, and viral transduction quantities used in this chapter are given in Table 4.1.

4.2.9 Puromycin treatment

Cells were seeded and transfected as described in 2.2.4 and 2.2.5, respectively. 24 hours post-transfection, 5 µg of puromycin was added directly to the wells (12 well plate). The cells were checked daily for signs of death in the untransfected well. 3 days post transfection there was complete cell detachment and death in the untransfected well and the cells were harvested as described in 2.2.8.

4.2.10 Trypan blue viability assay

Cells were trypsinised to detach them from the wells, neutralised with cell media, then diluted 1:1 with a 1/10 dilution of trypan blue (Merck). After a 3-minute incubation at room temperature, the living (non-blue) and dead (blue) cells were counted using a haemocytometer.

4.2.11 Western blot

Protein was extracted from cell pellets by sonication (see 2.1.6), and quantified using the Pierce BCA assay (see 2.1.7). Western blot was conducted as described in 2.1.8 using the anti-SaCas9 antibodies ab203933, C15310260, or C15310259 to detect SaCas9, dSaCas9, and dSaCas9.KRAB, with an anti-beta-actin antibody as a positive control (Table 2.2).

Table 4.1 Cell transfection experiments in Chapter 4.

Figure	Cell line	Seeding density	Plasmid quantity transfected	Viral particles transduced
Figure 4.4D-F	HEK293-EGFP	$9.5x10^5$ cells/well (6 well plate)	1000 ng, 1500 ng, 2000 ng	N/A
Figure 4.5A-E	HEK293-EGFP	$8x10^5$ cells/well (6 well plate)	2 µg	N/A
Figure 4.6A-E	HEK293-EGFP	$8x10^5$ cells/well (6 well plate)	1 µg	N/A
Figure 4.7A-C	HEK293-EGFP	$8x10^5$ cells/well (6 well plate)	1 µg	N/A
Figure 4.8B	HEK293-EGFP	$5x10^5$ cells/well (12 well plate)	500 ng	N/A
Figure 4.8C	HEK293-EGFP	$5x10^5$ cells/well (12 well plate)	dSaCas9 – 500 ng, 250 ng, 125ng. dSaCas9.KRAB – 500 ng	N/A
Figure 4.8D-E	HEK293-EGFP	$5x10^5$ cells/well (12 well plate)	500 ng	N/A
Figure 4.9A, B, C, E, G	HEK293-EGFP	$5x10^5$ cells/well (12 well plate)	$1.05x10^{11}$ copies	N/A
Figure 4.9D	HEK293T	$8x10^5$ cells/well (6 well plate)	2000 ng	N/A
Figure 4.9H	Y79	$1.375x10^5$ cells/well (96 well plate)	N/A	$2.75x10^9$
Figure 4.10A-C	HEK293-EGFP	$8x10^5$ cells/well (6 well plate)	1 µg, 2 µg, 2.5 µg	N/A
Figure 4.11B	HEK293-EGFP	$1.6x10^5$ cells/well (24 well plate)	125 ng, 250 ng, 500 ng, 750 ng	N/A
Figure 4.11C	HEK293-EGFP	$1.6x10^5$ cells/well (24 well plate)	500 ng	N/A

4.2.12 qPCR

RNA was extracted using the RNeasy Plus Mini Kit (Qiagen) and cDNA synthesis was performed using the SuperScript III First-Strand Synthesis Kit (Invitrogen) with the modified protocol for gRNA (see 2.1.4). qPCR was conducted using Taqman probes (see 2.1.5). EGFP, SaCas9, dSaCas9, dSaCas9-KRAB, and gRNA levels were expressed relative to human beta-actin levels.

4.2.13 TIDE analysis

DNA was extracted from cell pellets using the QIAamp DNA Mini Kit (Qiagen). The region of interest was PCR amplified using KOD polymerase (Merck Millipore) and TIDE analysis conducted as described in 2.1.2. The untransfected samples were PCR amplified and sequenced with the primer pairs for each tested gRNA, then run through TIDE analysis. This provided a "background" measurement. Primers are detailed in Appendix 9.1.3.

4.2.14 Mean grey value

Mean grey value is a measure of the brightness of an image in which the grey value of each pixel (0 indicates black, 1 indicates white) is averaged. To analyse the mean grey value of wells containing HEK293-EGFP cells, the automated imaging programme in the EVOS FL Auto Cell Imaging Software was used to image a proportion of the well (20 % of the well in a 6 well plate, 30 % of the well in a 12 well plate) at 4x magnification. The gain was set to ensure there was limited saturation of EGFP. This programme takes overlapping images of each area of the well then produces a stitched image. The stitched image was opened in ImageJ. The Region of Interest was set to exclude regions outside of the well, which therefore contain no cells (Figure 4.1), and the mean grey value of the region of interest was measured.

4.2.15 Fluorescence spectroscopy

10 µg of protein was added to each well of a 96 well black microplate (Greiner Bio-one) and the volume was made up to 300 µl with complete FIPA buffer (NaCl 150mM, Tris base 50mM, EDTA 2mM, 1% TritonX-100; adjusted to pH7.4 with HCl). The outermost wells of the plate were not used. The Victor^3 1420 Multilabel Plate Reader (Perkin Elmer) was used to assess the fluorescence (in Arbitrary Fluorescence Units) with excitation at 485 nm, detection at 535 nm and a 1.0 s exposure time. A technical average of each sample was calculated and the background control (containing only complete FIPA buffer) was subtracted from each of these to get the fluorescence per sample.

4.2.16 Immunocytochemistry

Three 13 mm circular coverslips were placed inside each well of a 6-well cell culture plate, overlapping as little as possible. The coverslips were moved using sterile disposable forceps. The plate was then UV treated for 10 min. HEK293T cells were counted and seeded on top of these coverslips at 8x10^5 cells/well (see 2.2.4). Cells were transfected 24 hours after seeding with 2 µg plasmid (see 2.2.5), then processed for immunocytochemistry 48 hours after transfecting. The coverslips were removed and placed into wells of a 24 well plate. All reagents were added into the wells on top of the coverslips. Approximately 0.2-0.5 ml reagent used per step. To preserve fluorescence all incubation steps were conducted in the dark. Between each incubation step, the coverslips were washed in 0.01 M PBS, 3

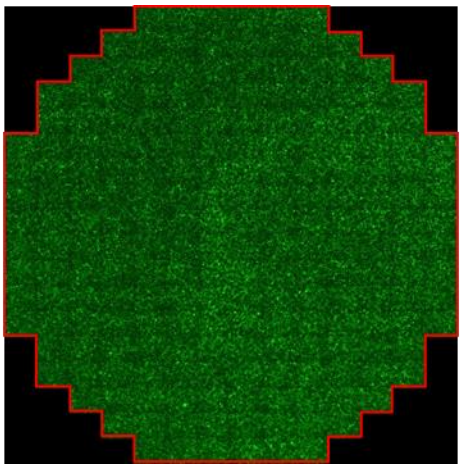

Figure 4.1 The region analysed for mean grey value of stitched fluorescence imaged (red line).

times. Coverslips were fixed in 4 % paraformaldehyde for 15 min at 4 C, then permeabilised in 0.2 % Triton-X 100 for 20 min. Coverslips were then blocked in 10 % BSA, 10 % donkey serum, 0.1 % Triton-X 100 at room temperature for 1 hour. The coverslips were then incubated with the primary anti-SaCas9 antibody (rabbit anti-SaCas9 abcam ab203933, diluted 1/250) in 1 % BSA, 1 % donkey serum, 0.1 % Triton-X 100 overnight at 4 C. The following day the coverslips were washed in 0.05 % Tween-20, 0.01 M PBS for 5 min twice then incubated with the secondary antibody (Alexafluor488 donkey anti-rabbit A21206, diluted 1/500) in 1 % BSA, 1 % donkey serum, 0.1 % Triton-X 100 at room temperature for 2 hours. Coverslips were again washed in 0.05 % Tween-20, 0.01 M PBS for 5 min twice, then washed in 0.01 M PBS for 5 min. To stain the nuclei, coverslips were incubated in Hoescht stain diluted 1/1000 with 0.01 M PBS for 25 min at room temperature. Finally, the coverslips were mounted onto glass slides using a drop of ProLong Diamond mounting medium and left to dry overnight in the dark. Edges were sealed with nail varnish and allowed to dry before imaging.

4.2.17 Restriction digest

Restriction digest was conducted as described in 2.1.3 using *Xma*I.

4.3 Results

4.3.1 Selection of EGFP-targeting gRNAs

The *Nrl*-EGFP mouse transgene was Sanger sequenced using ear notch DNA from a single mouse. Sequencing revealed that of the 1740 bases of the Nrl promoter examined (out of a total of 2500), there were 18 nucleotide substitutions and 4 nucleotide insertions compared to the predicted sequence (Table 4.2). There was also a 130 bp insertion between the end of the *Nrl* promoter and the start of EGFP. The EGFP gene had 100 % homology with the reference sequence. The full sequence is given in Appendix 9.2. As only one mouse transgene was sequenced, it is unclear whether these mutations in the *Nrl* promoter are consistent throughout the colony or are specific to this individual.

The confirmed Nrl-EGFP sequence was screened for potential SaCas9 gRNA sequences targeting EGFP. 18 potential gRNAs were generated (see Appendix 9.3). The bioinformatics screens produce two scores, for specificity and efficiency. Higher scores indicate a higher predicted specificity and efficiency, with a range of 0 to 100[85]. Of these 18 potential gRNAs, 9 were selected for in vitro screening (Table 4.3, Figure 4.2). These were chosen because they targeted the range of the EGFP coding sequence and had specificity scores of over 60.0 %.

4.3.2 Characterising the HEK293-EGFP cell line

To allow quick and efficient screening of EGFP-targeting gRNAs, the CRISPR constructs were tested in a HEK293-EGFP cell line. This commercially available cell line expresses EGFP constitutively from a CMV promoter. Sanger sequencing of the EGFP gene in HEK293-EGFP cells revealed 8 nucleotide substitutions compared to their reference sequence, which created 5 amino acid changes (Table 4.4). While this did not affect EGFP functionality (as the cells are visibly expressing EGFP), the C>T mutation at position +198 removes the PAM site from gRNA F11. This gRNA was subsequently used as a “no PAM” control for in vitro screening in HEK293-EGFP cells and was expected to produce no disruption of EGFP. The confirmed sequence is detailed in Appendix 9.4.

Table 4.2 Discrepancies between the predicted Nrl-EGFP transgene and the confirmed Nrl-EGFP transgene sequence.
+1 indicates the first nucleotide of the EGFP coding sequence.

Nucleotide position	Mutation type	Nucleic acid change
-1231	Substitution	TATCGTCACGGAACC > GGAACCATAGCAGTG
-1196	Insertion	G
-1139	Substitution	C > G
-825	Insertion	G
-254	Insertion	CT
-175	Substitution	AA > CC
-1	Insertion	TGTTCTGAATACAGGGACGACACCAGCCCCTGCTCTATGGAGTATTTAGCC TCCAGGGAAGCTGTGCCTTTCTGGTTCTGACAGTGACTACGTCATCTCTGCC ATTACATCGGATCCACCGGTCGCCACC

Table 4.3 EGFP targeting gRNAs selected for in vitro analysis.
+1 indicates the first nucleotide of the EGFP coding sequence. The gRNA sequence is homologous to the listed DNA strand.

Name	Position	DNA strand	Sequence 5' to 3'	PAM	Specificity Score	Efficiency Score
F9	+26	Plus	CAAGGGCGAGGAGCTGTTCAC	CGGGGT	86.5	15.3
F10	+138	Minus	GCCGGTGGTGCAGATGAACTT	CAGGGT	82.0	19.3
F11 (No PAM)	+198	Minus	GAAGCACTGCACGCCGTAGGT	CAGGGT	97.2	21.2
F12	+417	Minus	GTTGTACTCCAGCTTGTGCCC	CAGGAT	79.4	15.9
F13	+510	Minus	GCTGCCGTCCTCGATGTTGTG	GCGGAT	92.5	18.1
F14	+680	Plus	GCTGGAGTTCGTGACCGCCGC	CGGGAT	98.8	5.9
F15	+699	Minus	CTTGTACAGCTCGTCCATGCC	GAGAGT	91.8	9.8

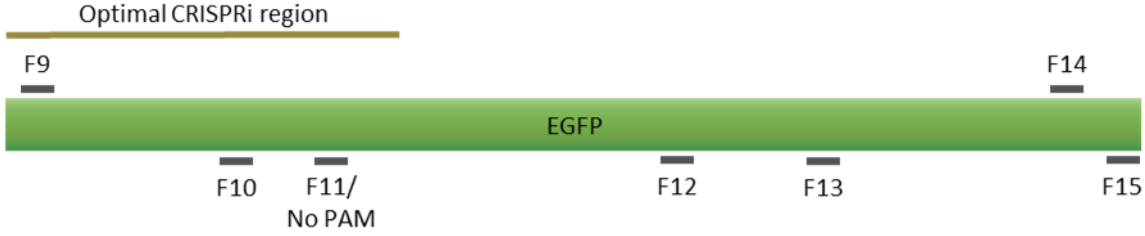

Figure 4.2 EGFP-targeting gRNAs selected for in vitro analysis.

The HEK293-EGFP cell line was sent for karyotyping analysis to identify its chromosomal arrangement. The analysis revealed a highly heterogeneous cell population. Of the 15 karyotyped cells, 14 had a total chromosome number between 61 and 70, making the cells near-triploid (Figure 4.3A). The remaining cell had 48 chromosomes. Individual chromosomes copy numbers varied between 0 and 5 per cell (Figure 4.3C). As expected there was no Y chromosome detected, as this cell line originates from a female embryo[172]. 6 common translocation events were detected in this cell line (Table 4.5, Figure 4.3D). 22 less common translocation events were also identified, which is typical of the genomic instability of the HEK293 cell line[172].

Multicolour fluorescence in situ hybridisation (MFISH) analysis identified the integration sites of the EGFP transgene in the HEK293-EGFP cell line. Integration site and number were inconsistent between cells, suggesting that the cell line did not derive from a single transduced clone. Of the 50 cells analysed, 44 % had one transgene integration site, 34 % had two transgene integration sites, 20 % had three transgene integration sites and 2 % had four transgene integration sites. Five separate EGFP integration sites were identified (named A-E), which created 14 different integration combinations in the examined cells (Table 4.6). Some of the sites had a greater signal intensity than others, suggesting that the number of integrated copies at each site may be variable (Figure 4.3B).

Table 4.4 Discrepancies between the EGFP transgene in the HEK293-EGFP cell line and the EGFP reference sequence.
+1 indicates the first nucleotide of the EGFP coding sequence.

Nucleotide Position	Mutation type	Nucleic acid change	Amino acid change
+193	Substitution	C > T	Leu > Phe
+195	Substitution	G > C	None
+217	Substitution	A > G	Ser > Ala
+218	Substitution	G > C	None
+450	Substitution	C > G	Asn > Lys
+461	Substitution	T > C	Met > Thr
+462	Substitution	G > C	None
+503	Substitution	T > C	Ile > Thr

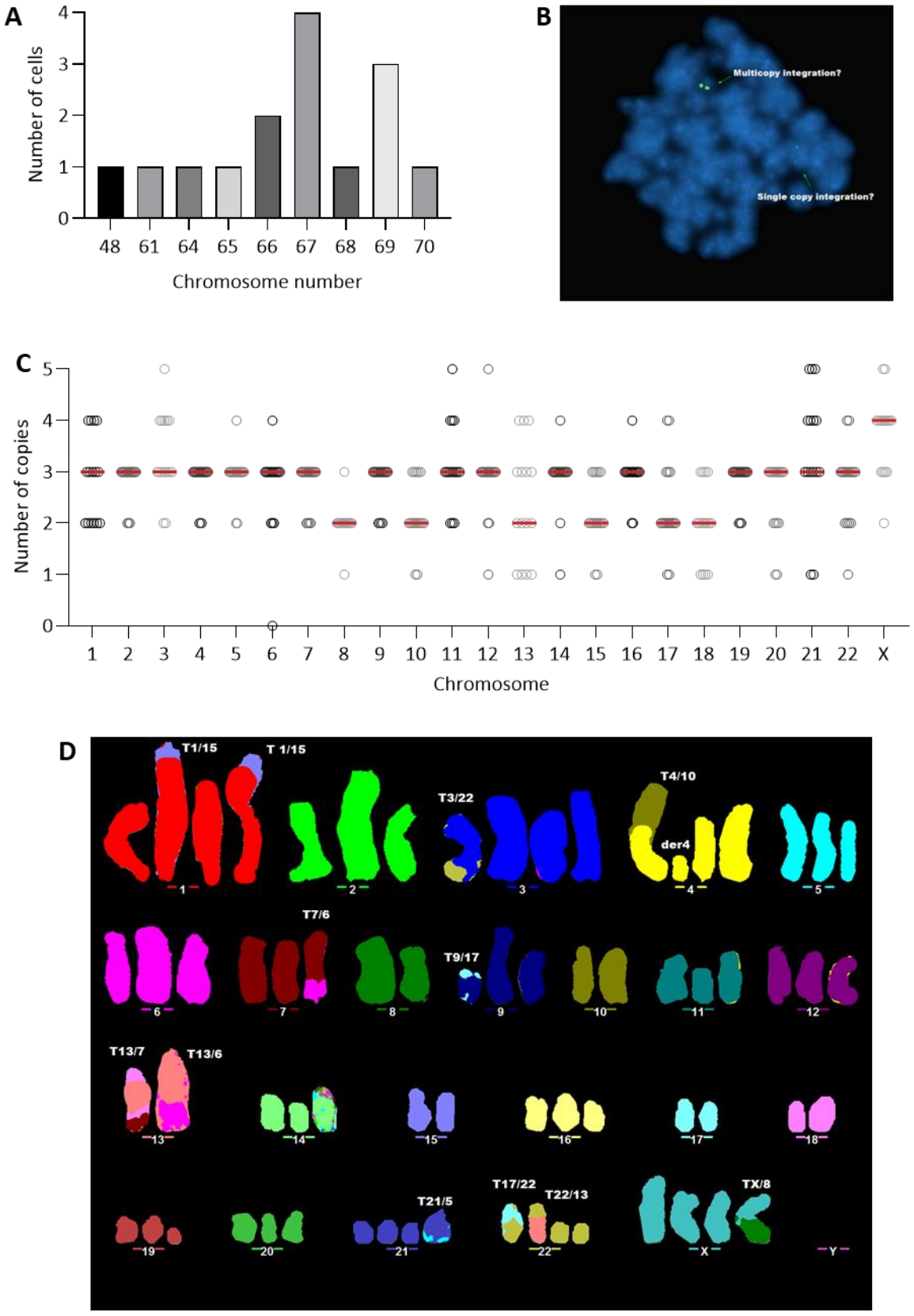

Figure 4.3 The HEK293-EGFP cell line has a variable genetic profile.
A) *Total chromosome number of 15 analysed cells.* ***B)*** *Stained chromosomes of a HEK293-EGFP cell showing a potential single copy integration and multicopy integration of the EGFP transgene.* ***C)*** *Chromosomal copy number of 15 analysed cells.* ***D)*** *Example karyotype of a cell containing the 6 most frequent translocation events detailed in Table 4.6.*

Table 4.5 Common chromosomal translocations in HEK293-EGFP cells. Frequency indicates proportion of cells carrying the translocation.

Translocated chromosomes	Frequency %
9 and 17	86
8 and X	80
1 and 15	73
4 and 10	67
17 and 22	47
13 and 7 (Robertsonian chromosome 13)	33

Table 4.6 Frequency of EGFP transgene integration patterns in HEK293-EGFP cells.

Type of EGFP integration	Frequency
A only	22 %
C only	16 %
A+C	12 %
A+B+C	12 %
B+C	8 %
A+B	6 %
A+C+D	6 %
A+D	4 %
B only	4 %
A+B+C+D	2 %
B+D	2 %
C+D	2 %
D only	2 %
A+C+E	2 %

4.3.3 Creating an inactive dSaCas9 plasmid using site-directed mutagenesis

The all-in-one px601 CMV.SaCas9.bGHpA.U6.gRNA plasmid (henceforth called SaCas9) was a gift from Feng Zhang (Addgene plasmid # 61591). Site-directed mutagenesis was used to introduce the D10A and N580A mutations into this plasmid to remove its catalytic activity and convert it into dSaCas9 (Figure 4.4A-C). To confirm the plasmids drove SaCas9 and dSaCas9 expression in a dose dependent manner, they were transfected into HEK293-EGFP cells at 1 µg, 1.5 µg, and 2 µg, and the cellular protein was extracted. Three anti-SaCas9 antibodies, binding to the N-terminus, C-terminus, and middle of the protein, were used to detect SaCas9 and dSaCas9 on a western blot. All three detected Cas9 in the transfected samples, indicating the full-length protein was produced. SaCas9 and dSaCas9 band density increased as the amount of transfected plasmid increased (Figure 4.4D-F).

To assess the CRISPR activity of these constructs, EGFP-targeting gRNAs F10, F13, and the control no PAM gRNA were cloned into the SaCas9 and dSaCas9 plasmids. The plasmids were transfected into HEK293-EGFP cells and the knock down of EGFP was measured using multiple methods. Both SaCas9.F10 and SaCas9.F13 significantly reduced the mean grey value of fluorescence images, by 19.8 % ($p<0.0001$) and 21.8 % ($p<0.0001$), respectively, and arbitrary fluorescence units of extracted protein, by 29.6 % ($p=0.0028$) and 36.5 % ($p=0.0004$), respectively. With dSaCas9, however, only gRNA F10 achieved significant knock down of 8.1 % when measured by mean grey value ($p=0.0354$), and 26.3 % (0.0071) when measured by fluorescence spectroscopy (Figure 4.5A-C). The No PAM gRNA did not have significant knock down with either Cas9 by either measure. None of the gRNA/Cas9 combinations drove significant knock down when measured by qPCR (Figure 4.5D).

TIDE analysis was used to measure the indels present in the EGFP sequence, which form following DNA cleavage by Cas9. 13.8 % and 13.6 % of EGFP reads contained indels following treatment with SaCas9.F10 and SaCas9.F13, respectively. Indel percentages detected with dSaCas9 were not statistically significant from the untransfected cells, indicating that the newly created dSaCas9 has lost the ability to cleave DNA (Figure 4.5E).

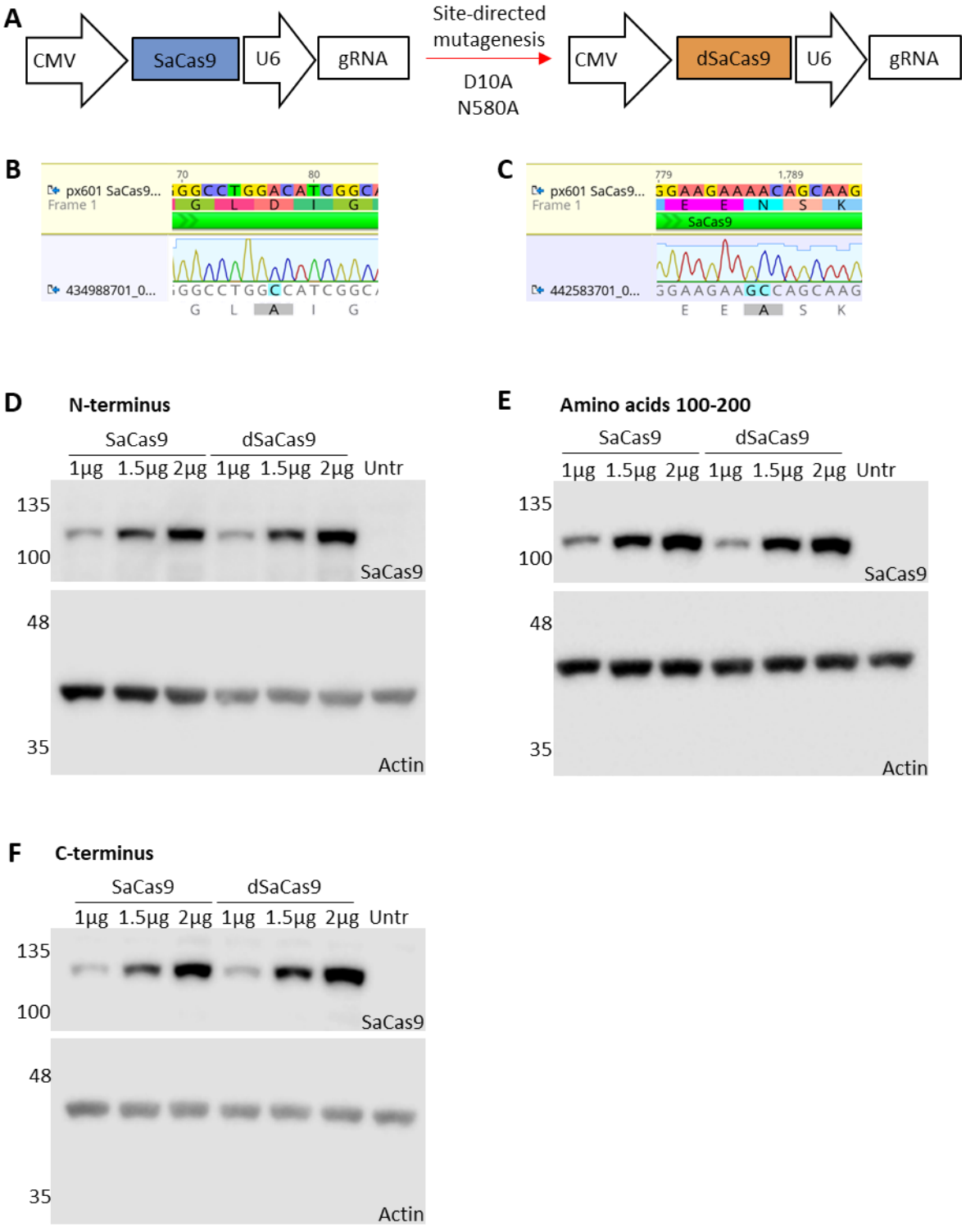

Figure 4.4 Creating and testing SaCas9 and dSaCas9 plasmids.
A) *Creation of the all-in-one dSaCas9 plasmid through site directed mutagenesis of the all-in-one SaCas9 plasmid.* ***B)*** *Sanger sequencing showing successful site directed mutagenesis introducing the D10A mutation to SaCas9.* ***C)*** *Sanger sequencing showing successful site directed mutagenesis introducing the N580A to SaCas9.* ***D-F)*** *Western blot of protein extracted from cells transfected with the SaCas9 or dSaCas9 plasmid, or untransfected (untr) at 1 µg, 1.5 µg, and 2 µg with three different antibodies. SaCas9 and dSaCas9 are 124 kDa. Anti-actin antibody is used as a positive control; actin is 42 kDa* ***D)*** *Anti-SaCas9 antibody binding to the N-terminus of SaCas9.* ***E)*** *Anti-SaCas9 antibody binding between amino acids 100 and 200 of SaCas9.* ***F)*** *Anti-SaCas9 antibody binding at the C-terminus of SaCas9.*

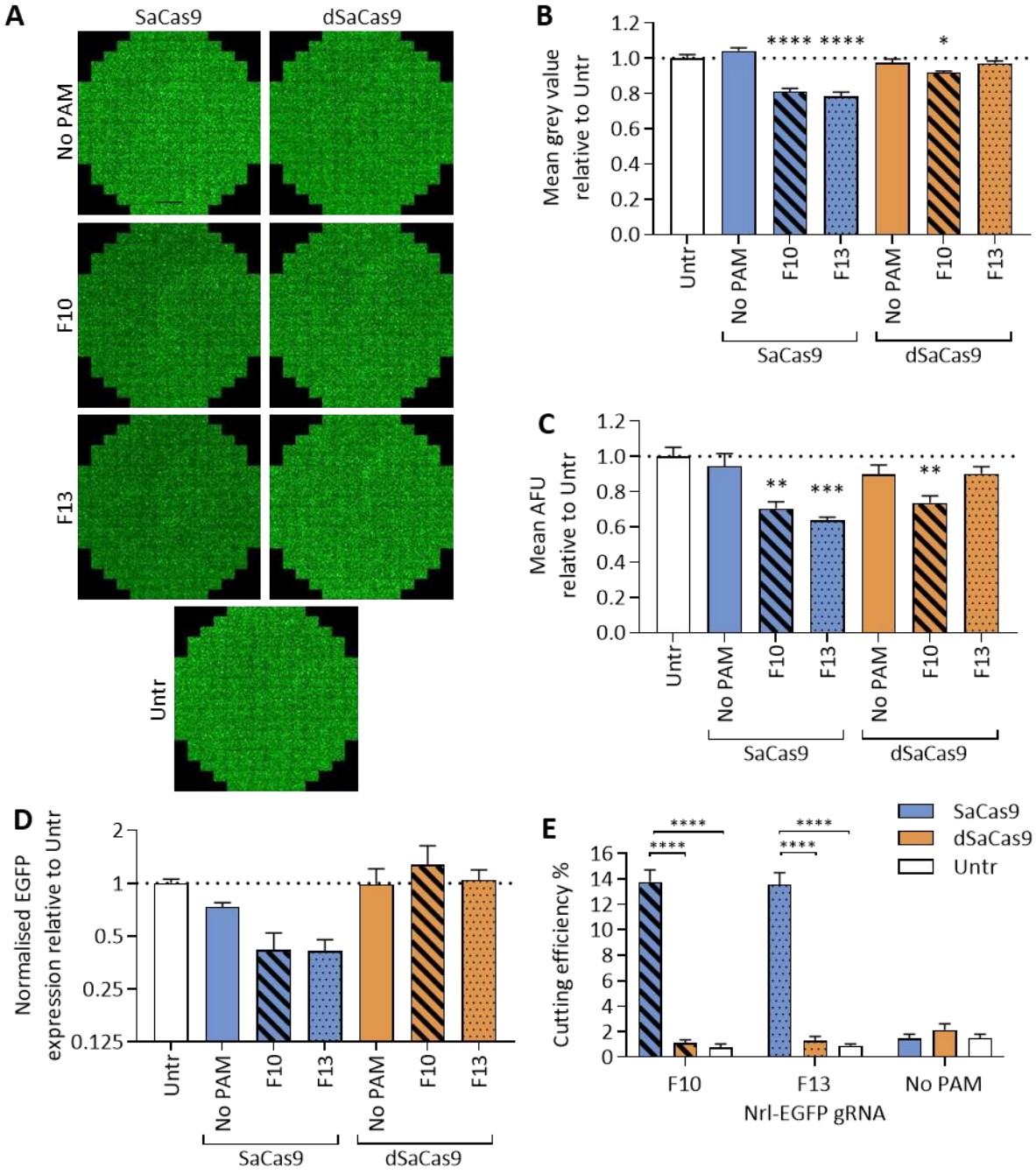

Figure 4.5 dSaCas9 has lost cleavage activity and drives CRISPRi.
Cells were untransfected (untr) or transfected with plasmid containing SaCas9 or dSaCas9 and one of three gRNAs, "No PAM", F10 or F13, ***A)*** *Representative spliced fluorescence microscopy images of transfected HEK293-EGFP cells. Scale bar is 2.3 mm.* ***B-D)*** *Knockdown of EGFP as measured by different methods. One-way ANOVA was conducted with multiple comparisons comparing the means to that of the Untr, n = 3.* ***B)*** *Mean grey value of fluorescence cell images, F(6, 14) = 27.75, p<0.0001. Untr vs SaCas9.F10 p=0.0001, Untr vs SaCas9.F13 p=0.0001, Untr vs dSaCas9.F10 p = 0.0354.* ***C)*** *Fluorescence spectroscopy of cell lysates. AFU stands for arbitrary fluorescence units. F(6, 14) = 8.547, p = 0.0005. Untr vs SaCas9.F10 p = 0.0028, Untr vs SaCas9.F13 p = 0.0004, Untr vs dSaCas9.F10 p = 0.0071.* ***D)*** *qPCR measuring EGFP expression normalised to human beta-actin. F(6,14) = 3.422, p = 0.0271.* ***E)*** *On-target editing efficiency measured by TIDE analysis. Two-way ANOVA with factors of SaCas9 and gRNA. Effect of SaCas9 F(2, 18) = 257.6 p<0.0001, effect of gRNA F(2, 18) = 46.19 p<0.0001, effect of interaction F(4, 18) = 69.83 p<0.0001. Multiple comparison compared SaCas9, dSaCas9 and Untr indels for each gRNA site. SaCas9.F10 vs dSaCas9.F10 p<0.0001, SaCas9.F10 vs Untr (F10) p<0.0001, SaCas9.F13 vs dSaCas9.F13 p<0.0001, SaCas9.F13 vs Untr (F13) p<0.0001.*

4.3.4 Screening EGFP-targeting gRNAs with SaCas9 and dSaCas9

All EGFP-targeting gRNAs, along with a "scrambled" (scram) non-targeting gRNA and the No-PAM gRNA were cloned into the SaCas9 and dSaCas9 plasmids and transfected into HEK293-EGFP cells. The scram sequence has no targets in the human or mouse genome (identified by searching the sequence in NCBI BLAST nucleotide alignment tool) and therefore functions as a negative control. The impact of CRISPR/Cas9 gene disruption was measured by mean grey value of fluorescence images, fluorescence spectroscopy, qPCR, and TIDE analysis. Each method of assessing CRISPR/Cas9-mediated gene disruption measured different degrees of knock down. Measured by mean grey value, four EGFP-targeting gRNAs had a significant reduction compared to scram. These were F9, F10, F14, and F15, with 14.3 %, 12.4 %, 9.2 %, and 16.0 % reduction, respectively ($p=0.0002$, $p=0.0010$, $p=0.0185$, $p<0.0001$, respectively) (Figure 4.6A-B). Fluorescence spectroscopy detected higher and more consistent levels of knock down across all six EGFP-targeting gRNAs, with knock down ranging from 28.7 % to 36.7 % ($p>0.0001$ for all)(Figure 4.6C). When knock down was measured at an mRNA level using qPCR, no gRNA provided significant knock down compared to scram, despite it measuring the greatest knock down of the three techniques (Figure 4.6D). This is likely because qPCR produced the most variable results, with the greatest data spread. All six EGFP-targeting gRNAs had detectable gene disruption by TIDE analysis, ranging from 14.20 % with F9 to 18.54 % with F10 (Figure 4.6E). The No PAM control had an indel rate of 1.48 %, which represents the baseline.

The same gRNAs were assessed for CRISPRi-mediated gene knock down with dSaCas9. Evaluation of the gRNA efficiency with dSaCas9 did not include qPCR as this was non-significant in the prior experiment (Figure 4.5), or TIDE analysis as dSaCas9 does not introduce indels into the target gene. Compared to CRISPR/Cas9 gene disruption, fewer gRNAs had significant knock down and the knock down measured was lower. Using dSaCas9, F10 was the only gRNA with significant reduction of mean grey value compared to scram (Figure 4.7A-B). With SaCas9, F10 drove 12.4 % knock down, whereas with dSaCas9 this was only 7.0 % ($p=0.0003$). gRNAs F10 and F14 significantly reduced fluorescence

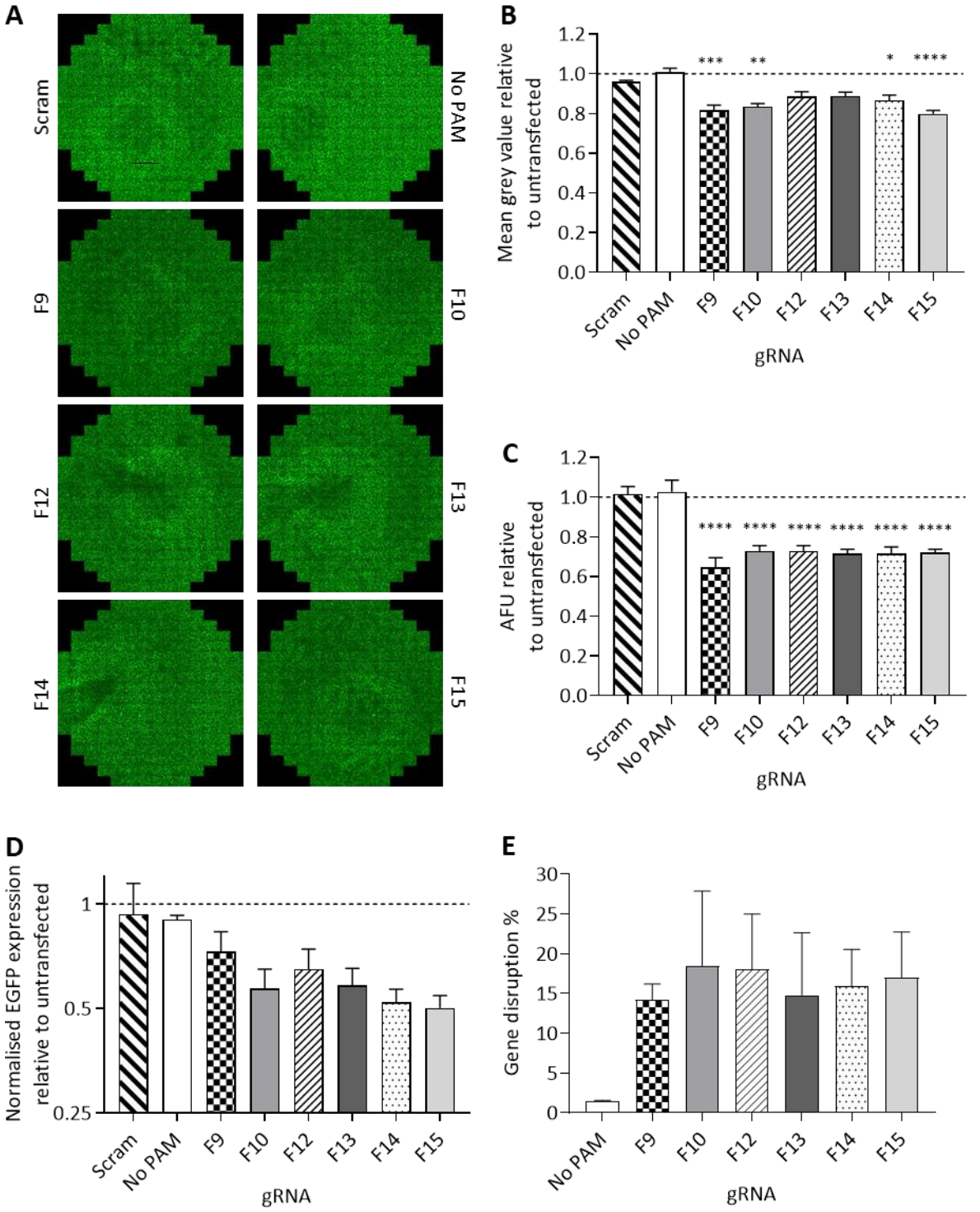

Figure 4.6 Testing EGFP-targeting gRNAs with SaCas9.
SaCas9 plasmids were transfected into HEK293-EGFP cells and knock down assessed by various methods. Values normalised relative to the untransfected control. ***A)*** *Representative fluorescence microscopy images of transfected cells. Scale bar represents 2.3 mm.* ***B-D)*** *One-way ANOVA was conducted with multiple comparisons comparing the means of the gRNAs to that of the scrambled gRNA (scram), n=5.* ***B)*** *Mean grey value of fluorescence images. F(7,32)=12.19 p<0.0001. Scram vs F9 p=0.0002, Scram vs F10 p=0.0010, Scram vs F14 p=0.0185, Scram vs F15 p<0.0001.* ***C)*** *Fluorescence spectroscopy. AFU stands for arbitrary fluorescence units. F(7,32)=16.48 P<0.0001. Scram vs F9 p<0.0001, Scram vs F10 p<0.0001, Scram vs F12 p<0.0001, Scram vs F13 p<0.0001, Scram vs F14 p<0.0001, Scram vs F15 p<0.0001.* ***D)*** *qPCR comparing normalised EGFP expression relative to human beta actin F(7,32)=2.438 p=0.043.* ***E)*** *Gene disruption measured by TIDE analysis.*

compared to scram, with 7.7 % and 12.1 % knock down, respectively (p=0.0225 and p=0.0157, respectively) (Figure 4.7C). Again, this was lower than the knock down measured with SaCas9, at 28.7 % with F10 and 29.9 % with F14.

Interestingly, both dSaCas9 control plasmids (dSaCas9.Scram and dSaCas9.NoPAM) have reduced mean grey value relative to the untransfected control (at 0.91 relative to untransfected) but

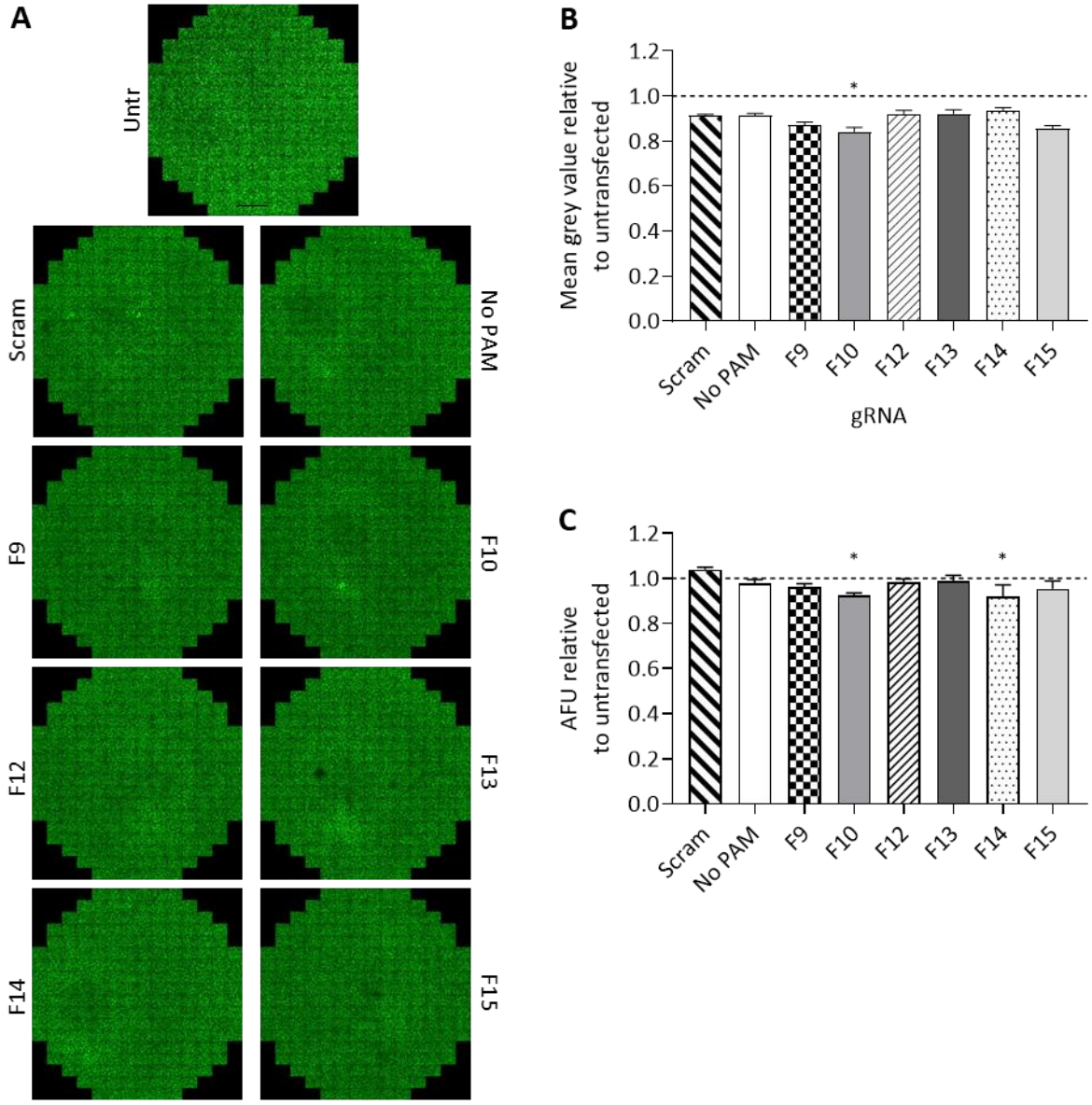

Figure 4.7 Testing EGFP-targeting gRNAs with dSaCas9.
dSaCas9 plasmids were transfected into HEK293-EGFP cells and knock down assessed by various methods. Values normalised relative to the untransfected control (Untr). ***A)*** *Representative fluorescence microscopy images of transfected cells. Scale bar represents 2.3 mm.* ***B-C)*** *One-way ANOVA was conducted with multiple comparisons comparing the means of the gRNAs to that of the scrambled gRNA (scram), n=5.* ***B)*** *Mean grey value of fluorescence images. F(7,32)=5.539 p=0.0003. Scram vs F10 p=0.0110.* ***C)*** *Fluorescence spectroscopy. AFU stands for arbitrary fluorescence units. F(7,32)=2.144 p=0.0670. Scram vs F10 p=0.0225, Scram vs F14 p=0.0157.*

comparable arbitrary fluorescence units (1.04 and 0.98 relative to untransfected, respectively). This suggests that the dSaCas9 plasmids could be having a toxic effect on the cells, reducing the number of cells present in the well, and therefore causing a reduction in mean grey value. Fluorescence spectroscopy is normalised to total protein amount so it is unaffected by the number of viable cells. This trend was not present with SaCas9: the control plasmids had a relative mean grey value and arbitrary fluorescence units close to 1 (Mean grey value: SaCas9.Scram=0.96, SaCas9.NoPAM=1.01. Arbitrary fluorescence units: SaCas9.Scram=1.02, SaCas9.noPAM=1.03).

4.3.5 Addition of the KRAB repressor increases CRISPRi knock down

Fusing a repressor domain to dCas9 has been shown to improve the level of CRISPRi gene repression achieved[65]. The KRAB repressor from plasmid CMV.dSaCas9.KRAB (Addgene plasmid #106219) was cloned into the dSaCas9 plasmid to create the all-in-one plasmid CMV.dSaCas9.KRAB.U6.gRNA (henceforth referred to as dSaCas9.KRAB) (Figure 4.8A). This newly created construct codes for dSaCas9.KRAB and gRNA, and is surrounded by ITRs. To ensure the KRAB repressor was correctly incorporated into the dSaCas9 protein, dSaCas9 and dSaCas9.KRAB were transfected into HEK293-EGFP cells and the protein extracted. A western blot was performed with an anti-SaCas9 antibody binding to amino acids 100-200 of SaCas9 (see Figure 4.4E). In an initial western blot, the band from dSaCas9 was significantly denser than the dSaCas9.KRAB band, making comparison difficult (Figure 4.8B). To overcome this, HEK293-EGFP cells were transfected with the dSaCas9 plasmid at 500 ng, 250 ng, and 125 ng, and the dSaCas9.KRAB plasmid at 500 ng. The addition of the KRAB repressor increased the molecular weight of the dSaCas9 protein from 124 kDa to 134 kDa, which is visible on the western blot when comparing the dSaCas9 125ng sample and the dSaCas9.KRAB 500ng sample (Figure 4.8C).

Three EGFP-targeting gRNAs (F10, F13, F15) and the “no PAM” control gRNA were cloned into both the dSaCas9 plasmid and the dSaCas9.KRAB plasmid. These were transfected into HEK293-EGFP cells and EGFP knock down was assessed by mean grey value of fluorescence images and fluorescence

spectroscopy. The KRAB repressor had a significant effect on the mean grey value of the fluorescence images (p=0.0009), with the knock down rate of F10 and F15 increased from 9.1 % to 12.5 % and from

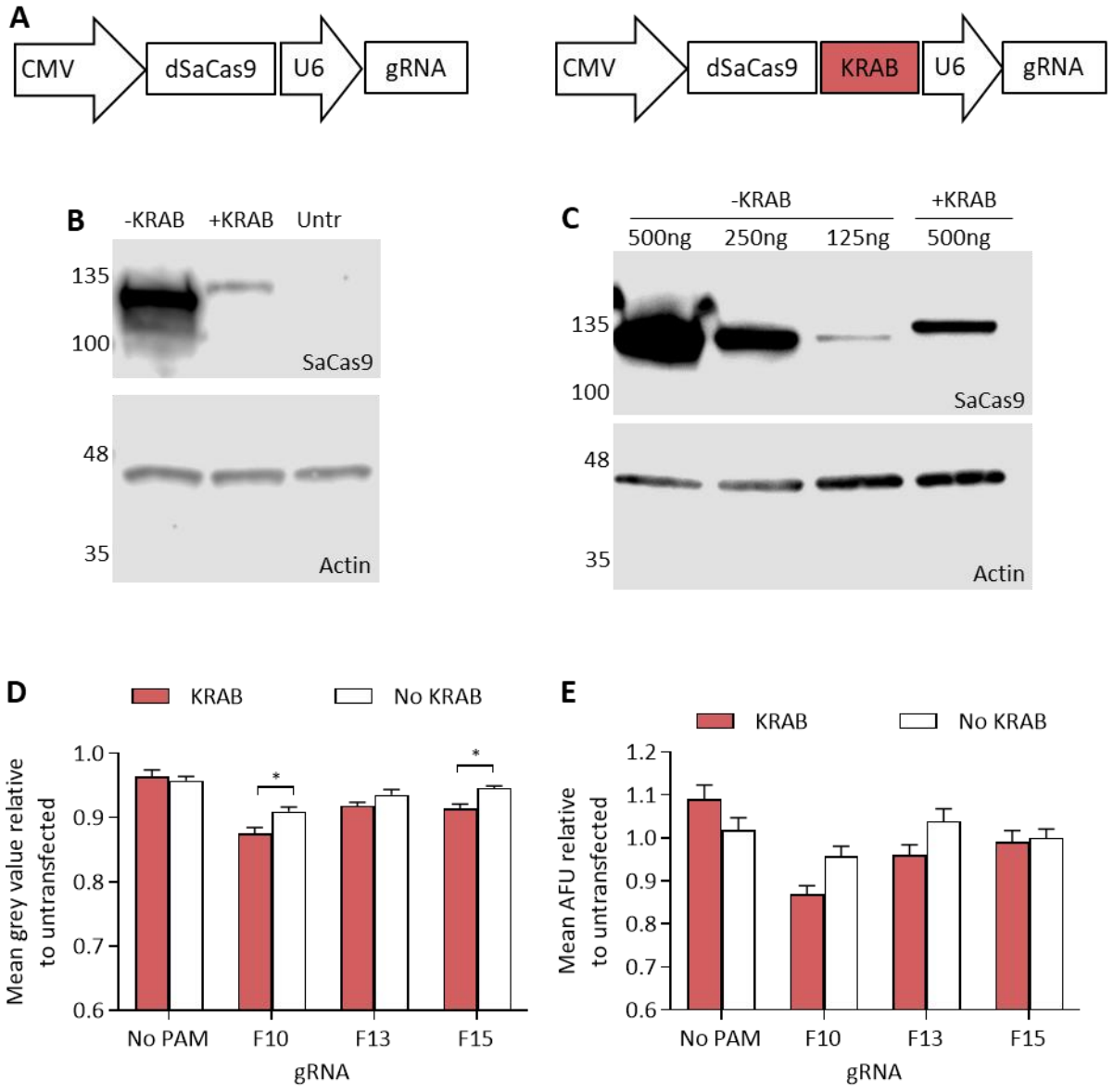

Figure 4.8 dSaCas9.KRAB has greater EGFP knock down than dSaCas9.
***A)** dSaCas9 and dSaCas9.KRAB plasmids. **B-C)** Western blots of protein extracted from cells transfected with different quantities of dSaCas9 plasmid (-KRAB), dSaCas9.KRAB plasmid (+KRAB), or untransfected (untr). Anti-SaCas9 detects dSaCas9 (124 kDa) and dSaCas9.KRAB (134 kDa) in corresponding samples, anti-actin antibody is used as a positive control (42 kDa). **B)** Plasmids transfected at 500 ng. **C)** dSaCas9 plasmid transfected at 125 ng, 250 ng, and 500 ng, dSaCas9.KRAB plasmid transfected at 500 ng. **D-E)** Knock down of EGFP with dSaCas9 compared to the dSaCas9.KRAB plasmid. Two-way ANOVA with factors of KRAB and gRNAs were conducted with multiple comparisons comparing dSaCas9 and dSaCas9.KRAB for each gRNA, n = 5. **D)** Mean grey value of fluorescence cell images. Effect of KRAB $F(1, 32) = 13.31$ $p=0.0009$, effect of gRNA $F(3, 32) = 27.17$ $p=0.0009$, effect of interaction $F(3,32) = 2.99$ $p=0.0455$. dSaCas9.F10 vs dSaCas9.KRAB.F10 = 0.0122, dSaCas9.F15 vs dSaCas9.KRAB.F15 = 0.0195. **E)** Fluorescence spectroscopy of extracted protein. Effect of KRAB $F(1, 32)$ $p=0.1609$, effect of gRNA $F(3, 32) = 10.17$, $p<0.0001$, effect of interaction $F(3, 32) = 4.102$ $p=0.0143$.*

5.4 % to 8.6 %, respectively (p=0.0122 for gRNA.F10, p=0.0195 for gRNA.F15) (Figure 4.8D). When measuring fluorescence spectroscopy there was no significant difference in the knock down of the plasmids with or without KRAB, although there does appear to be a trend of greater knock down with the KRAB repressor in the EGFP-targeting gRNAs (Figure 4.8E).

4.3.6 KRAB repressor causes reduction in Cas9 and gRNA expression in plasmid form

The western blot experiments with dSaCas9 and dSaCas9.KRAB revealed an unexpected phenomenon; the dSaCas9.KRAB-transfected samples had a significantly sparser Cas9 band than the dSaCas9-transfected samples, despite the actin band remaining consistent throughout samples (Figure 4.8B-C). It was possible that the addition of the KRAB domain was affecting the ability of the dSaCas9 protein to dissolve fully in RIPA buffer (the buffer used to dissolve proteins prior to western blot). HEK293-EGFP cells were transfected with SaCas9, dSaCas9, or dSaCas9.KRAB plasmids and the subsequent cellular protein dissolved in either RIPA buffer or 5 % SDS, which is a stronger denaturing agent. Although the 5 % SDS buffer appeared to increase the amount of Cas9 availability for the antibody, the dSaCas9.KRAB bands were still sparser than the SaCas9 or dSaCas9 bands (Figure 4.9B).

During cloning, the KRAB domain was fused to the C-terminus of dSaCas9. For the initial western blots, a monoclonal anti-SaCas9 antibody that binds to amino acids 100-200 was selected, as this is distal from the KRAB domain, which begins at amino acid 1096. It was possible, however, that the KRAB domain was blocking the reactive epitope of the antibody in the western blot. Immunocytochemistry uses antibodies to detect proteins within a sample of fixed cells. During immunocytochemistry, the protein is in its native three-dimensional conformation, whereas on a western blot it is linearised. Despite this change in conformation, immunocytochemistry with this antibody replicated the western blot results; with significantly reduced antibody binding in the dSaCas9.KRAB-transfected cells (Figure 4.9D). Western blots with polyclonal N-terminus and C-terminus antibodies revealed the same pattern

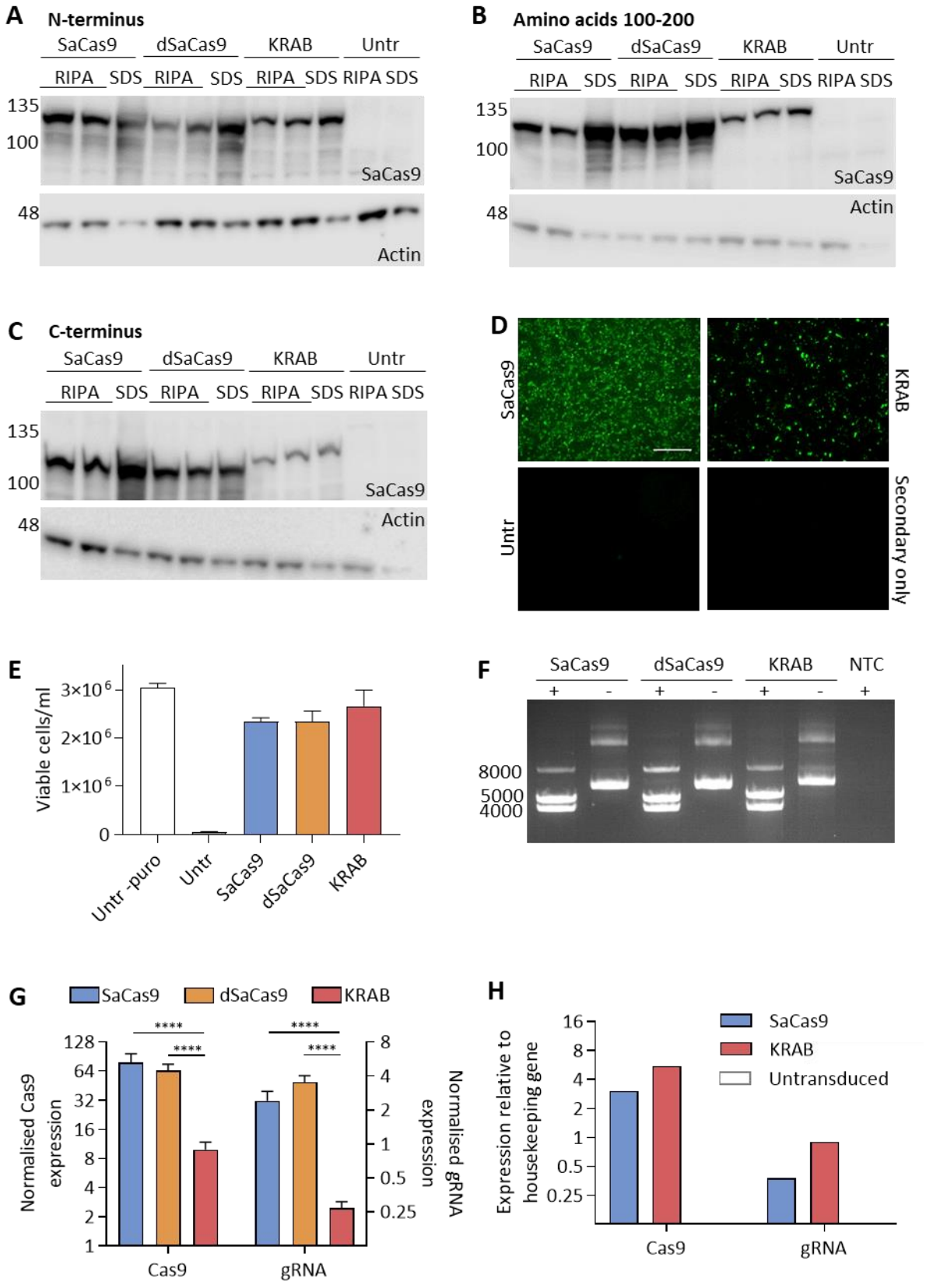

Figure 4.9 dSaCas9.KRAB plasmids have reduced transcription of Cas9 and gRNA, causing a reduced antibody response.

A-C) *Western blot of protein extracted from HEK293-EGFP cells transfected with SaCas9, dSaCas9, KRAB plasmids, or untransfected (Untr). Proteins were dissolved in either RIPA buffer or 5% SDS. SaCas9 and dSaCas9 are 124 kDa, KRAB is 134 kDa. Anti-actin antibody is used as a positive control; actin is 42 kDa.* ***A)*** *Anti-SaCas9*

antibody binding to the N-terminus of SaCas9. ***B)*** *Anti-SaCas9 antibody binding between amino acids 100 and 200 of SaCas9.* ***C)*** *Anti-SaCas9 antibody binding to the C-terminus of SaCas9.* ***D)*** *Immunocytochemistry staining for SaCas9 in HEK293T cells transfected with SaCas9, KRAB, or Untr. Scale bar is 250 µm.* ***E)*** *Number of viable HEK293-EGFP cells following transfection with puromycin resistance plasmids containing SaCas9, dSaCas9, KRAB or Untr, and subsequent puromycin treatment, n=3. One-way ANOVA was conducted with multiple comparisons comparing the means to that of the KRAB plasmid $F(4, 10)=40.91$ $p<0.0001$. Untr vs KRAB $p<0.0001$.* ***F)*** *SaCas9, dSaCas9, and KRAB plasmids digested with XmaI (+) or undigested (-), plus a no template control (NTC).* ***G)*** *Cas9 and gRNA expression normalised to human beta-actin expression in cells transfected with SaCas9, dSaCas9, or KRAB, n=3. Two-way ANOVA with factors of plasmid and transcript. Effect of plasmid $F(2, 12) = 79.45$ $p<0.0001$, effect of transcript $F(1, 12) = 415.6$ $p<0.0001$, effect of interaction $F(2, 12) = 1.637$ $p=0.2352$. Multiple comparison compared transcript expression of SaCas9 and dSaCas9 to KRAB. Cas9 levels: SaCas9 vs KRAB $p<0.0001$, dSaCas9 vs KRAB $p<0.0001$. gRNA levels: SaCas9 vs KRAB $p<0.0001$, dSaCas9 vs KRAB $p<0.0001$.* ***H)*** *Cas9 and gRNA expression normalised to human beta-actin expression, in Y79 cells transduced with PDE6Bp.SaCas9 (SaCas9) and PDE6Bp.dSaCas9.KRAB (KRAB) AAV.*

as the monoclonal mid-protein antibody; the Cas9 band was sparser in the dSaCas9.KRAB samples and proteins dissolved in 5 % SDS had a denser band than those dissolved in RIPA (Figure 4.9A, C). This appeared to rule out epitope availability as the cause of the reduced band density in dSaCas9.KRAB-transfected cells.

To investigate whether the dSaCas9.KRAB plasmids had reduced transfection efficiency, SaCas9, dSaCas9, and dSaCas9.KRAB plasmids containing a puromycin resistance gene in the backbone were acquired. Following transfection of these plasmids into HEK293-EGFP cells, they were puromycin treated, and 3 days later the number of viable cells were counted using the Trypan Blue assay. 98.3 % of untransfected cells were killed by the puromycin treatment, demonstrating that the number of viable cells represents the number of successfully transfected cells. The number of viable cells in the SaCas9, dSaCas9, and dSaCas9.KRAB-transfected samples were not significantly different from one another; this suggested there are comparable transfection rates between plasmids (Figure 4.9E).

Sanger sequencing of the plasmids confirmed that the transgene sequence was as expected. Digestion of the plasmids with *Xma*I, which cuts inside the ITRs, produced the two expected bands, confirming the transgene and backbone regions were of the correct size and there were no large re-arrangements of the plasmid (backbone band length 4037 bp, transgene band length 4758 bp for SaCas9 and dSaCas9, and 4986 bp for dSaCas9.KRAB). The comparable size of the undigested plasmid bands also suggests there had been no large re-arrangements (Figure 4.9F). Interestingly, an additional band was

observed at roughly 9000 bp. This is the approximate length of the plasmids, and indicates the plasmids have been cut once and linearised. The samples likely contain a mixed population of plasmids, some of which have lost one ITR. This is a common occurrence when growing bacterial cultures containing plasmids with ITRs as their homologous regions can result in mutations or recombinations that remove an ITR. Unfortunately, due to the high 70.8 % GC content and repetitive sequence of the ITRs, Sanger sequencing was not possible to identify which ITR was lost.

Finally, the Cas9 and gRNA transcript levels were assessed by qPCR following transfection with the three plasmids, and puromycin treatment. The dSaCas9.KRAB-transfected cells had significantly lower Cas9 and gRNA transcript levels than both the SaCas9- and dSaCas9-transfected cells (Figure 4.9G). The dSaCas9-KRAB transcript was 7.9-fold and 6.6-fold lower than the SaCas9 and dSaCas9 transcript, respectively ($p<0.0001$ for both), while the gRNA expression in the dSaCas9.KRAB-transfected cells was 8.9-fold and 13.0-fold lower than in the SaCas9-transfected and dSaCas9-transfected cells, respectively ($p<0.0001$ for both). Interestingly, in Chapter 6, the PDE6B promoter was used to drive SaCas9 and dSaCas9.KRAB expression in AAV8(Y733F). When this was transduced in Y79 cells, the levels of SaCas9 and gRNA transcript were no longer different between SaCas9 and dSaCas9.KRAB (Figure 4.9H).

4.3.7 Optimising plasmid transfection

Initial gRNA-screening experiments were performed with 1 µg plasmid DNA per well (6 well plate) (Figure 4.6, Figure 4.7). To try to improve the level of gene disruption achieved, the SaCas9.F13 plasmid was transfected into HEK293-EGFP cells at three concentrations in a 6-well plate: 1 µg, 2 µg, 2.5 µg. All three concentrations resulted in a significant reduction of mean grey value of fluorescence images (Untr vs 1 µg $p=0.0043$, Untr vs 2 µg $p=0.018$, Untr vs 2.5 µg $p=0.0014$) and expression of EGFP measured by qPCR (Untr vs 1 µg $p=0.0324$, Untr vs 2 µg $p=0.0400$, Untr vs 2.5 µg $p=0.0274$) compared to the untransfected control (untr). However, there was no significant difference between the plasmid

concentrations (Figure 4.10A, B). Despite this, gene disruption measured by TIDE analysis increased with plasmid quantity, with 9.45 %, 16.25 %, and 21.55 % gene disruption seen with 1 µg, 2 µg, and 2.5 µg plasmid, respectively (Untr vs 1 µg p=0.0006, 1 µg vs 2 µg p=0.0016, 2 µg vs 2.5 µg p=0.0002) (Figure 4.10C). Increasing plasmid dose may therefore improve CRISPR gene disruption in future in vitro experiments.

4.3.8 Reversing the U6-gRNA does not affect gene disruption using plasmid DNA

The arrangements of promoters in a bi-cistronic construct can affect expression of the transgenes, and

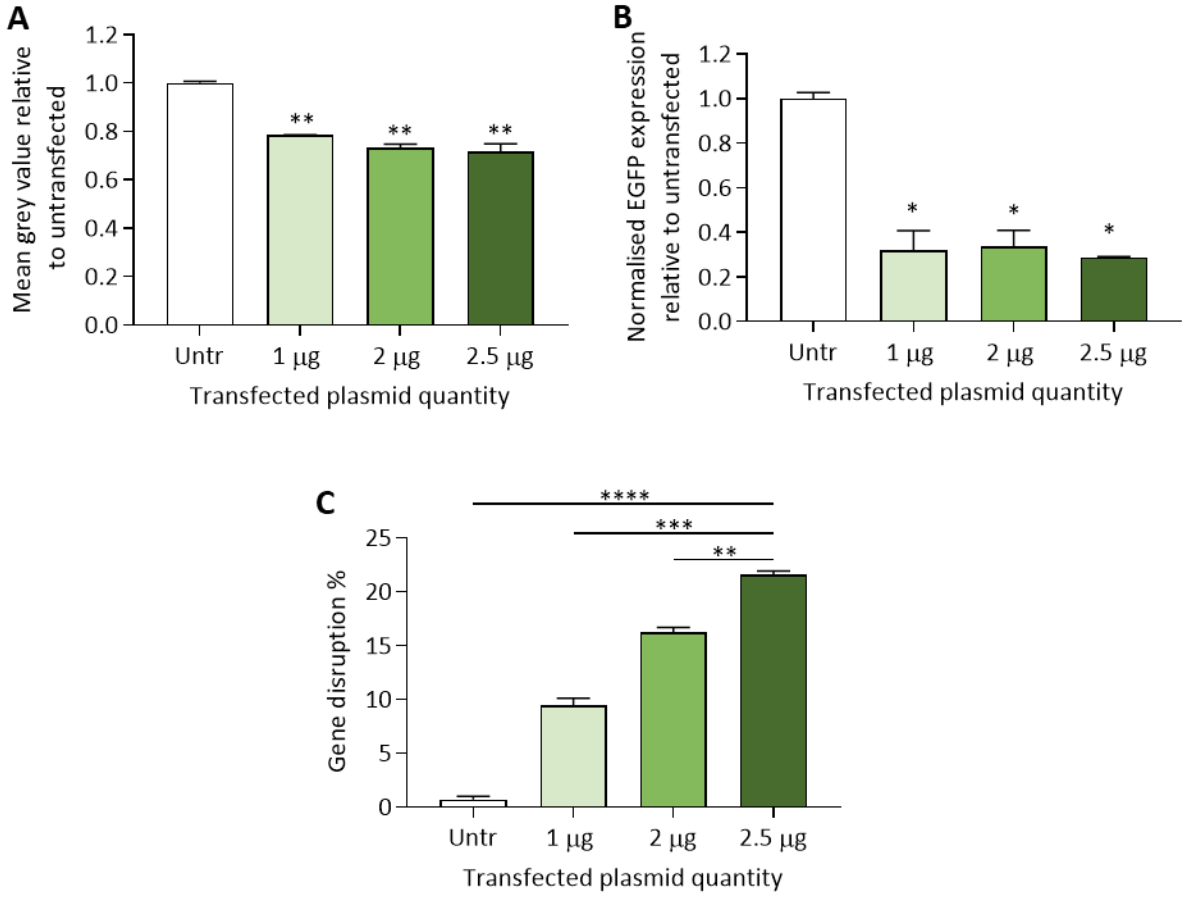

Figure 4.10 CRISPR/Cas9 gene disruption increases with transfected plasmid dose.
HEK293-EGFP cells were transfected with the SaCas9.F13 plasmid at 1 µg, 2 µg, and 2.5 µg plasmid or were untransfected (Untr). One-way ANOVA was conducted, comparing the means of each category in all combinations, n=2. ***A)*** *Mean grey value of fluorescence images. F(3,4)=49.90, p=0.0013. Untr vs 1 µg p=0.0043, Untr vs 2 µg p=0.0018, Untr vs 2.5 µg p=0.0014.* ***B)*** *qPCR measuring expression of EGFP normalised to human beta actin. F(3,4)=10.80, p=0.0218, Untr vs 1 µg p=0.0324, Untr vs 2 µg p=0.0400, Untr vs 2.5 µg p=0.0274* ***C)*** *Gene disruption measured by TIDE analysis. F(3,4)=387.6, Untr vs 1 µg p=0.0006, Untr vs 2 µg p<0.0001, Untr vs 2.5 µg p<0.0001, 1 µg vs 2 µg p=0.0016, 1 µg vs 2.5 µg p=0.0002, 2 µg vs 2.5 µg p=0.0042.*

so an alternate arrangement of the promoters was tested to try to maximise editing rates. The SaCas9 plasmid has both the CMV and the U6 promoter on the sense strand (called the "Forward" plasmid). The same plasmid was acquired that had the U6 promoter and the gRNA on the antisense strand (called the "Reverse" plasmid) (Figure 4.11A).

Three gRNAs were cloned into the Forward plasmid and transfected into HEK293-EGFP cells at a range of doses. Two of the gRNAs target *RHO* (RHO+28 and RHO+2300) and were selected because they bind to *RHO* exons and have a high predicted on-target efficiency (50.0 for RHO+28 and 69.4 for RHO+2300). The third gRNA targets VEGFA (VEGFA_val). This published gRNA demonstrated over 30 % VEGFA indels in vitro in a 2015 paper[173]. gRNA RHO+28 did not have any significant gene disruption at any plasmid quantity. gRNA RHO+2300 and VEGFA_val had a dose-dependent response with gene disruption increasing with transfected plasmid quantity. The highest recorded gene disruption was at

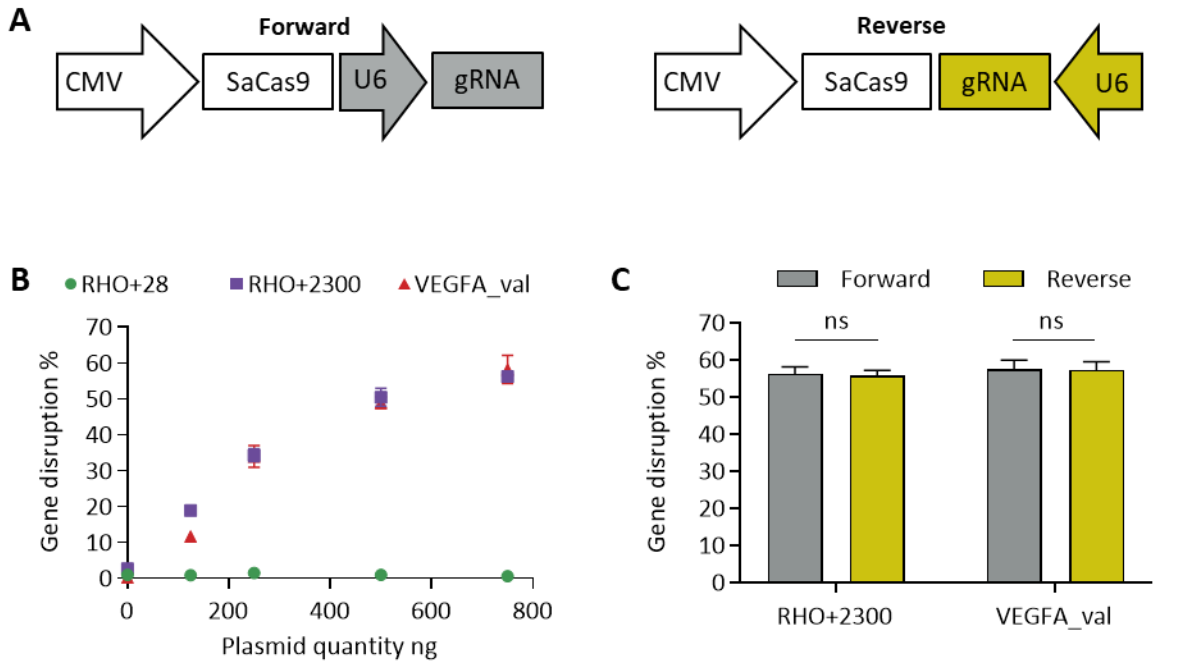

Figure 4.11 Reversing the U6-gRNA structure in the SaCas9 plasmid does not influence CRISPR/Cas9 gene disruption.
***A)** The SaCas9 plasmid with the U6-gRNA in the "Forward" and "Reverse" direction. **B)** Gene disruption achieved with three gRNAs targeting clinically relevant genes in the Forward plasmid transfected at a range of quantities into HEK293-EGFP cells, n=3. **C)** Forward and reverse plasmids have no significant difference in gene disruption using the RHO+2300 or VEGFA_val gRNAs. Two-way ANOVA conducted with multiple comparisons comparing Forward and Reverse for each gRNA, n=6. Effect of orientation F(1, 20)=0.03270 p=0.8583, effect of gRNA F(1, 20)=0.4881 p=0.4928, effect of interaction F(1, 20)=0.002432 p=0.9612. ns= not significant.*

750 ng transfected plasmid (24 well plate of cells), with 56.2 % and 58.2 % gene disruption for gRNAs RHO+2300 and VEGFA_val, respectively (Figure 4.11B).

gRNA RHO+2300 and VEGFA_val were cloned into both the Forward and Reverse SaCas9 plasmid, transfected at 500 ng, and gene disruption compared. There was no significant difference between the gene disruption measured for the Forward and Reverse SaCas9 plasmid for either gRNA (Figure 4.11C).

4.4 Discussion

This chapter details the creation and testing of the all-in-one dSaCas9 and dSaCas9.KRAB plasmids, using the SaCas9 plasmid as a template. These plasmids were then used to drive CRISPR/Cas9 and CRISPRi knock down of EGFP in the HEK293-EGFP cell line. The introduction of the well-characterised D10A and N580A mutations caused a complete loss of DNA cleavage activity in dSaCas9. Previous studies have demonstrated that dCas9 retains its ability to bind to DNA through analysing protein:DNA interactions using techniques such as electrophoretic mobility shift assays, or ChIP-Seq[53,69]. Although this was not employed here, the loss of indel formation alongside the reduction in target protein expression indicates that CRISPRi is taking place.

4.4.1 HEK293-EGFP cell line

In vitro models allow large numbers of gRNAs to be screen and are therefore a useful tool for selection of gRNAs before in vivo studies[71]. In vitro screening requires the gene of interest to be present and transcriptionally active. The HEK293-EGFP cell line was created by GenTarget Inc by transforming HEK293 cells with a lentivirus driving EGFP from a ubiquitous CMV promoter. Chromosomal analysis revealed that these cells are highly heterogeneous, suggesting the cell line did not derive from an isolated clone but rather a collection of transduced cells. As is typical with HEK293 cells, the HEK293-EGFP cell line has a varied karyotype, with a near-triploid number of chromosomes (typically 61-70)[172]. The number and location of transgene integration sites also varies between one and four, with some integration sites possibly containing multiple copies of the transgene. This EGFP copy number variation will influence the level of CRISPR gene editing achieved within each cell, even if each cell receives the same number of CRISPR constructs.

The EGFP sequence in this cell line contains eight nucleotide substitutions compared to the reference plasmid used in their creation. These mutations may have been present in the reference plasmid, in

the lentiviral sequence, or have occurred upon integration. If the latter, it is possible that the EGFP sequence could be slightly different at each integration site. Although there was no evidence of a mixed population in the Sanger sequencing reads, it could be present in quantities below the approximate 20 % limit of detection with this technique[174–176].

The activity of each EGFP integration in the HEK293-EGFP cells is unknown. While lentiviruses favour integration into transcriptionally active regions, integration into inactive regions is possible, and reduces the expression of the viral transgene[177]. Transcriptionally inactive regions have also been shown to have lower CRISPR/Cas9 editing rates[178]. This may contribute to the discrepancy between indel rate (14.2 % to 18.54 %) and fluorescence reduction (28.7 % to 36.7 %) seen in these experiments: If a cell contains EGFP transgenes that cannot produce EGFP proteins and cannot be accessed by Cas9, they will dilute the estimated indel rate but have no impact on cell fluorescence. A more appropriate EGFP-expressing cell line would be derived from an isolated clone with a known number of EGFP integration sites, all of which were confirmed as active. Unfortunately, at the time this was the only cell line available that expressed EGFP ubiquitously. Creating a stable clonal cell line within the thesis was an option but due to time constraints, it was not pursued.

4.4.2 Methods of measuring CRISPR activity

The gene editing rates of CRISPR were measured by four different techniques: TIDE analysis, qPCR, fluorescence spectroscopy, and mean grey value of fluorescence images, all of which produced varying estimations of knock down. Both fluorescence spectroscopy and mean grey value measure fluorescence and are therefore affected by the degradation rate of EGFP. The treated cells were assessed 48 hours post-transfection, while EGFP has an estimated half-life of 26 hours[179]. Even if there were no new EGFP proteins produced following transfection, approximately 27.8 % of EGFP molecules would remain after 48 hours. To overcome this issue, the in vitro assay could have been further optimised to increase the time post-transfection. If harvested at 72 or 96 hours, only 14.3 % and 7.5

% of pre-transfection EGFP molecules would remain, respectively. While these in vitro experiments may underestimate gene editing, prolonged in vivo experiments would not suffer from this limitation.

When measuring mean grey value, cells are imaged with a fluorescence microscope and the mean grey value of the pixels in the image is calculated. While this method is time-efficient and produced low variation between replicates, it measured lower EGFP knock down than fluorescence spectroscopy. This underestimation is possibly due to cells growing on top of each other, masking the CRISPR-driven reduction in fluorescence. Mean grey value also correlates with cell number, and therefore cell death can be misinterpreted as EGFP knock down. This was seen with the dSaCas9 plasmids, as both negative control gRNAs measured a significant reduction in mean grey value compared to the untransfected control, indicating plasmid toxicity. The cause of this toxicity are unknown, and is unlikely to be linked to the plasmid prep, as this was consistent between SaCas9 and dSaCas9 plasmid. To investigate this further, the toxicity should be confirmed with a cell viability assay.

Measuring indels by TIDE analysis offers the most direct measure of CRISPR/Cas9-mediated disruption and is a relatively quick and cheap method[180]. The indel rates in this experiment were lower than the measured fluorescence knock down. This was surprising, particularly as small insertions or deletions, which contribute to the indel rate, may still be able to produce a fluorescing EGFP molecule[181–184]. While this could be due to transgene integration in inactive sites, as discussed above, it could also be due to an underestimation of indel rate. TIDE is known estimate gene disruption at 12-20 % lower than with next generation sequencing[180]. In Chapter 5, TIDE analysis was compared to subcloning analysis (another method of measuring indels), and found to estimate 37.4 % lower editing rates for one particular gRNA.

The chosen method of analysis for a given experiment is likely to depend on the target of CRISPR gene editing. If therapeutic approaches rely on reducing the level of a mutant protein or toxic RNA, then a measure of protein or mRNA function, respectively, should be included. In this chapter, qPCR measured high levels of knock down in some experiments but it showed variability between replicates.

It was often unable to produce a statistically significant result, despite a clear trend indicating reduced EGFP mRNA following CRISPR treatment.

4.4.3 EGFP knock down

Across the gRNA screens, the highest level of EGFP knock down achieved with CRISPR/Cas9 and CRISPRi was 36.7 % and 26.3 % using gRNAs F9, and F14, respectively. gRNAs F10 and F13 were tested across three different experiments: with SaCas9 and dSaCas9 when assessing dSaCas9 inactivity, with SaCas9 and dSaCas9 when screening gRNAs, and with dSaCas9 and dSaCas9.KRAB when assessing the KRAB repressor. Although the knock down was measured relative to different controls, it was broadly comparable between experiments. EGFP disruption measured by TIDE analysis differed by 1.22-4.74 %, mean grey value differed by 2.1-14.6 %, and fluorescence spectroscopy differed by 0.9-22.1 % for gRNAs F10 and F13 between experiments. A 2019 paper used the same HEK293-EGFP cell line and found comparable EGFP knock down rates of approximately 10-50 % using 4 of the gRNAs screened in this chapter[163].

The predicted on-target efficiency score of the screened EGFP-targeting gRNAs (except for F11, which could not be used in this cell line) was between 5.9 and 19.3, and the indel rate achieved was 14.2 % to 18.54 %. By contrast, the RHO-targeting gRNA RHO+2300 had a predicted on-target efficiency score of 69.4 and achieved indel rates of 34.3% when transfected at a comparable plasmid dose. It's possible that the gRNAs screened here may have weak gRNA:DNA binding efficiencies, as predicted by the gRNA software, which are limiting the CRISPR/Cas9-mediated gene disruption.

Increasing the plasmid dose significantly increased the level of CRISPR/Cas9-driven gene disruption when targeting EGFP, VEGFA, and RHO. Surprisingly, the increasing indels did not correlate with increasing EGFP mRNA or protein knock down. This result was unexpected but may be influenced by transcript site integration, mRNA and protein half-life, indel types, or sensitivity of the assays, as discussed above. The impact of dose on CRISPRi was not explored but it is possible that increasing the

plasmid dose would have improved the EGFP knock down with this in vitro screening technique[165].

Although CRISPRi can drive high gene knock down, it is generally weaker than CRISPR/Cas9 gene disruption[60,63]. This is reflected in this chapter, with greater knock down seen with CRISPR/Cas9 than CRISPRi using the same gRNAs. While both SaCas9 and dSaCas9 rely on sequence homology between their gRNA and the DNA target in order to bind, dSaCas9-mediated gene knock down also depends on the ability of that locus to effectively block transcription initiation or elongation[58]. This means the knock down rate using CRISPRi is generally more locus-specific. Gene repression with CRISPRi is typically most effective in the region -50 to +250 relative to the transcriptional start site, and in the absence of a KRAB repressor is usually only effective with gRNAs homologous to the minus strand[58–63,185]. Significant dSaCas9 CRISPRi was achieved with gRNAs F10 and F14. gRNA F10 binds within the optimal region at +138. gRNA F14, however, binds outside the optimal region at +680 and is homologous to the plus strand, but was still able to significantly reduce EGFP fluorescence.

The addition of the KRAB repressor to dCas9 was associated with only a mild increase in target gene knock down. Analysis revealed that despite a comparable level of transfection, there were significantly fewer Cas9 and gRNA transcripts in cells treated with dSaCas9.KRAB plasmid compared to the equivalent SaCas9 and dSaCas9 plasmids. As only the KRAB repressor was tested, it is not known if this effect is specific to the KRAB repressor or if it would occur following the introduction of any C-terminus repressor. The reasons behind the reduced transcript levels are unknown and may explain the limited improvement in knock down seen when adding the KRAB repressor. Hypothetically, the reduced transcript level could be caused by increased transcript degradation but as the gRNA construct is identical between plasmids, this is unlikely. It is also possible that the addition of the KRAB repressor resulted in transcriptional interference between the CMV-driven Cas9 and the U6-driven gRNA. This effect was absent in AAV constructs driven by the hPDE6B promoter: the Cas9 and gRNA transcripts were comparable between SaCas9 and dSaCas9.KRAB.

The KRAB repressor increased EGFP knock down in two of the three tested gRNAs. Interestingly, gRNA

F13 did not drive CRISPRi with dSaCas9, or with dSaCas9.KRAB, suggesting that binding at this locus may always be ineffective at gene repression. Using dSaCas9, gRNA F15 had no impact on EGFP, but it was able to cause significant repression with dSaCas9.KRAB. It is possible that re-screening all the gRNAs following the addition of the KRAB repressor could have highlighted gRNAs that outperformed F10 and F15. While the KRAB repressor is the most commonly used CRISPRi repressor, attempts have been made to improve the level of CRISPRi. This led to the identification of a triple dCas9-KRAB-MeCP2 fusion protein in 2018. It drives greater knock down compared to dCas9-KRAB, but MeCP2 is 891 bp long and is therefore too large for a single AAV strategy[63]. Recently, Alerasool et al. (2020) screened 57 human KRAB repressors revealing that the commonly used *KOX1* KRAB repressor present in this thesis is a relatively weak KRAB repressor. Substituting it for the KRAB repressor from the *ZIM3* gene significantly improved CRISPRi, outperforming the KRAB-MeCP2 fusion protein[186]. At 300 bp in length, it is 105 bp longer than the *KOX1* KRAB repressor used in this thesis, but it could still be packaged into a single CRISPRi AAV using the hPDE6B promoter identified in Chapter 3 (construct would total 4689 bp in length).

4.4.4 Potential transcriptional interference

Transcriptional interference is well documented in bi-cistronic constructs[156–159]. Data from this thesis chapter was incorporated into a 2020 paper which investigated the impact of promoter orientation on CRISPR construct transcription and editing rates[187]. The U6-gRNA element was placed in a "forward" or "reverse" orientation relative to the CMV-SaCas9 element on SaCas9 and dSaCas9.KRAB plasmids (dSaCas9.KRAB data unpublished). This had no impact on transcription or editing rate as a plasmid. When converted to an AAV however, the "reverse" SaCas9 construct had significantly lower transgene expression and gene disruption, suggesting transcriptional interference may be occurring in this conformation.

As the "forward" transcript is associated with improved editing rates in AAV, plasmids in the forward

orientation were used in subsequent experiments. Although the reduced transcript levels in the dSaCas9.KRAB plasmids may cause an underestimation of gene repression in vitro, future in vivo work will use an AAV driving dSaCas9.KRAB with the hPDE6B promoter. These AAV constructs have comparable transgene expression between Cas9 species and therefore in vivo work will be unaffected by the transcriptional interference observed in vitro.

4.4.5 Conclusion

This chapter described the creation and validation of the CRISPR/Cas9 and CRISPRi constructs that are used throughout this thesis. Targeting EGFP in the HEK293-EGFP cell line demonstrated the constructs could disrupt and repress an endogenous gene in vitro. While SaCas9-mediated gene disruption and dSaCas9-mediated gene repression had been previously described, an all-in-one dSaCas9 plasmid was not commercially available. Site-directed mutagenesis was used to introduce the D10A and N580A mutations into the all-in-one SaCas9 plasmid, and TIDE analysis confirmed this dSaCas9 plasmid had lost its DNA editing ability. The addition of the KRAB repressor improved CRISPRi gene repression but was associated with transcriptional interference in plasmid form. The benefits of the KRAB repressor had been previously reported with SpCas9 but had limited research with SaCas9 when conducting this thesis.

Four different methods of measuring CRISPR gene editing were compared – to the authors knowledge this was the first comparison of knock down across DNA, RNA, and protein analysis. Estimated knock down varied between techniques, revealing their strengths and limitations. In particular, the genotype of the target gene, and half-life of the protein of interest were highlighted as important factors for selecting a method of measuring knock down.

Six EGFP-targeting gRNAs were screened: all drove CRISPR/Cas9 gene disruption, and two drove CRISPRi gene repression with dSaCas9.KRAB. gRNA F10 will be used to target EGFP in vivo in Chapter 6 as this demonstrated significant EGFP knock down with both CRISPR/Cas9 and CRISPRi.

5 Allele-specific *RHO* knock down by targeting non-pathogenic single nucleotide polymorphisms

5.1 Introduction

Mutations in *RHO* are the most common cause of autosomal dominant retinitis pigmentosa, contributing to an estimated 20-40 % of cases globally[1,13,15]. *RHO* mutations typically result in either a dominant-negative effect, interfering with the processing of wild type rhodopsin, or a toxic gain-of-function. This ultimately results in the death of rod photoreceptors, and therefore loss of vision in affected individuals[3].

CRISPR/Cas9 gene disruption and CRISPRi gene repression can be used to reduce rhodopsin expression, and have been shown to rescue the diseased phenotype in *Rho* models of adRP by preventing photoreceptor degeneration[38,39,41,188]. As wild type rhodopsin is essential for the survival of rod cells, successful treatments should target the mutant allele of *RHO* specifically, or involve a knock down and replace strategy[7]. While knockdown and replace strategies have shown benefits in vivo, over-expression of rhodopsin results in rod cell toxicity, and therefore dosing remains a concern[189].

To discriminate between strands, the CRISPR system must be targeted to a novel region present exclusively on the mutant *RHO* allele. Targeting the pathogenic mutation is possible, and has been used successfully in vivo to drive allele-specific knock down of mutant *Rho* in an adRP mouse model[15]. However, as there are over 150 pathogenic mutations in *RHO*[3], this would treat far fewer patients than a mutation-independent approach. Single-Nucleotide Polymorphisms (SNPs) are DNA nucleotides at a given position whose base can vary between individuals and between an individual's chromosomes. There are approximately 4-5 million SNPs in the human genome, making them one of the most frequent sources of genetic variation[190]. If an individual with adRP is heterozygous for a non-

pathogenic SNP occurring within *RHO*, this creates a discrepancy between the *RHO* strands, which may be sufficient to allow allele-specific targeting. This was demonstrated in *Rho*^{S334} rats, where targeting a non-pathogenic SNP on the mutant allele resulted in editing exclusively on the mutant strand[38].

If a SNP occurs in a gRNA-binding region, it creates a one bp mismatch between the gRNA and the wild type DNA sequence. Depending on the CRISPR strategy, the gRNA sequence, the precise nucleotide mismatch, and the position of the mismatch within the gRNA, a one bp mismatch may be sufficient to prevent binding, leading to allele-specific knock down[38,53,54,58,74,75,191]. Alternatively, the SNP may generate a novel PAM site on mutant *RHO*. As this ensures Cas9 will bind exclusively to the mutant strand, it is a more reliable strategy for allele-specificity, but it is only useful if the targetable SNP occurs on the mutant strand[192,193].

For this strategy to be a viable treatment for the prevention of retinal degeneration in adRP, multiple targetable SNPs would need to be identified and assessed for allele-specific targeting. A patient with an identified pathogenic mutation would require gene sequencing to identify heterozygous SNPs, then determine which SNPs are associated with the pathogenic strand (e.g. through next-generation sequencing, allele-specific PCR, or CRISPR-hapC[41,192,194]). The CRISPR construct targeting their pathogenic *RHO* strand would then be administered to drive allele-specific knock down.

This chapter explores the potential of a SNP-targeting strategy to knock down *RHO*. Firstly, common RHO SNPs are identified which can be targeted with SaCas9. Secondly, CRISPR/Cas9-driven *RHO* disruption identifies the SNPs with high levels of on-target editing in vitro. Finally, the allele-specificity of the gRNAs is assessed using a luciferase assay.

5.2 Materials and Methods

5.2.1 Screening for *RHO* target sites

The Eukaryotic Promoter Database was used to identify the transcriptional start site of *RHO*. The NCBI SNP database was then used to find SNPs occurring at an MAF of 0.1 or higher within *RHO* or its promoter (-1500 to -1 relative to the transcriptional start site). The chromosomal location searched was 3:129527140-3:129535169 (assembly GRCh38.p12). As there were multiple MAFs listed, the MAF from the 1000 genomes project was used. SaCas9 gRNAs in *RHO* were identified using the Benchling CRISPR Design tool and the PAM NNGRRT. These results were cross-referenced with the list of SNPs to identify SNPs that occurred in a gRNA binding region or PAM site. The PAM site SNPs were examined to see if the SNP removed the PAM site. Then, to identify SNPs that created a novel PAM site, the SNPs were introduced to the *RHO* sequence and re-screened for gRNA binding sites. Any new gRNAs were noted. Probability of SNP heterozygosity was calculated using the Hardy-Weinberg Equilibrium.

5.2.2 Genotyping *RHO* SNPs in HEK293-EGFP cells

Cells were harvested by centrifugation and DNA extracted from the cell pellet using the QIAamp DNA Mini Kit (Qiagen). All *RHO* SNPs except rs200054443 and rs2410 were PCR amplified using KOD polymerase, PCR purified (QIAquick PCR purification kit) then Sanger Sequenced (Eurofins Genomics Ltd). SNPs rs200054443 and rs2410 were analysed by subcloning. PCR primers are detailed in 9.1.1.

5.2.3 Subcloning analysis

The region surrounding the expected cut site was PCR amplified using GoTaq (as this polymerase generates a 3' A-tailed PCR fragment), ligated into the pGEM-T Easy Vector, then transformed into XL10 cells and plated using IPTG and X-Gal for white-blue selection. Following culturing and miniprep as described in 2.1.10, the plasmids were digested to determine the orientation of the insert relative

to the vector. Because the SNPs and cut site can only be successfully Sanger sequenced from one side of the PCR product (due to a repetitive region in the sequence), it is important to know the orientation of the ligated insert. Restriction sites were identified which cut once inside the PCR product, and once in the pGEM-T Easy Vector near the ligation site. For SNP rs200054443 (gRNA RHO+1841/RHO+1844) this was BspMI and for SNP rs2410 (gRNA RHO+5317) this was StyI. The direction of insertion did not need to be determined for SNP rs2855557 (gRNA RHO+4447) as the insert could be fully sequenced from either direction. The restriction digest generates different products depending on the orientation of the insert (Table 5.1). Once the orientation of the insert was confirmed, the plasmid was sent for sequencing using the appropriate primer, ensuring the sequence trace went through the gRNA region before the unsequenceable region.

When using subcloning analysis for genotyping, 20 clones were analysed. If only one allele was present, the cell line was deemed homozygous for that SNP. If two alleles were present, the cell line was deemed heterozygous.

When using subcloning analysis to determine the cutting efficiency, 24 clones per sample were analysed, and 3 replicates were analysed per condition. Following sequencing, the sequence trace was aligned with the unedited plasmid sequence and any discrepancies around the cut site were noted.

5.2.4 Cloning gRNAs into SaCas9, dSaCas9, dSaCas9.KRAB plasmids

gRNA cloning is described in 2.1.11.

Table 5.1 Subcloning sequencing for SNPs rs200054443 (RHO+1841/RHO+1844) and rs2410 (RHO+5317). Predicted restriction digestion products and subsequent sequencing primers for inserts cloned into the pGEM-T Easy Vector in the forward or reverse direction.

Insert orientation	rs200054443 (RHO+1841/RHO+1844)		rs2410 (RHO+5317)	
	Digestion products	Sequencing primer	Digestion products	Sequencing primer
Forward	117 bp, 3662 bp	T7 promoter	224 bp, 3511 bp	T7 promoter
Reverse	685 bp, 3094 bp	M13 rev (-29)	538 bp, 3197 bp	M13 rev (-29)

5.2.5 Cloning gRNA targets into PsiCheck2 plasmids

The gRNA target region was cloned into the PsiCheck2 plasmid in between the SV40 promoter and the renilla luciferase gene. The gRNA target region is a 50 bp region of DNA containing the gRNA binding site at its centre (*i.e.* 25 bp upstream and downstream from the centre of the gRNA binding site, Appendix 9.7). The insert was ordered as two separate oligonucleotides with *Nhe*I restriction digest overhangs. The forward oligonucleotide sequence was 5'- CTAGC-*gRNA target*-G' and the reverse oligonucleotide was 5'- CTAGC-*reverse complement of gRNA target*-G'.

25 pmol of the forward and reverse oligonucleotides were combined into a tube. They were phosphorylated using the T4 PNK kit (New England Biolabs), then heated to 95 C for 4 min to denature the oligonucleotides and melt any secondary structures. They were then gradually cooled to 4 C in a thermocycler with 47 cycles of 1 min incubations decreasing in temperature by 1.5 C each cycle. This annealed the forward and reverse oligonucleotides together.

The PsiCheck2 (Promega) vector was digested with *Nhe*I-HF (New England Biolabs) and dephosphorylated with rSAP (New England Biolabs), then PCR purified (QIAquick PCR Purification Kit).

The digested plasmid and gRNA were ligated together with T4 ligase (New England Biolabs) at an insert:backbone ratio of 20:1, then transformed into XL10 Gold Ultracompetent Cells (Stratagene). Following bacterial culture and miniprep (Sigma-Aldrich), the successfully ligated plasmids were identified by digestion with *Nhe*I-HF: plasmids containing an insert will not digest with *Nhe*I-HF whereas SaCas9-plasmids that were never originally digested with *Nhe*I-HF, and plasmids which have religated onto themselves are linearised with *Nhe*I-HF. For general cloning methods, see 2.1.10.

5.2.6 Cell line experiments

The general protocols for cell maintenance and transfection are given in sections 2.2.1 and 2.2.5, respectively. The specific seeding densities and plasmid transfection quantities used in this chapter

are given in Table 5.2.

5.2.7 Luciferase assay

HEK293T cells were seeded into a white, flat-bottomed, clear, 96 well plate (Corning catalogue 3610) in phenol red-free media (seeding every well in the plate) and transfected with 50 ng of dSaCas9.KRAB plasmid and 100 ng of luciferase plasmid 24 hours later. None of the outer wells were transfected as an edge effect influences the luciferase readout. 48 hours after transfection, the renilla and firefly luciferase expression were measured using the Dual-Glo Luciferase Assay (Promega). Luminescence was measured using the FLUOstar Omega plate reader.

When assessing knock down and allele-specificity of gRNAs, the normalised renilla expression achieved with each PsiCheck2/dSaCas9.KRAB combination was compared to the normalised renilla expression for the same PsiCheck2 plasmid with dSaCas9.KRAB.scrambled.

5.2.8 Seeding Y79 cells onto coated plates

The general protocols for cell seeding are described in 2.2.4. In this chapter, Y79 cells were seeded onto coated plates to improve adherence. 500 µl 1 mg/ml poly-D-lysine was added to each well of an

Table 5.2 The details of the cell transfection and transduction experiments performed in Chapter 5.

Figure	Cell line	Seeding density	Plasmid quantity transfected
Figure 5.2	HEK293-EGFP	$1.6x10^5$ cells/well (24 well plate)	500 ng
Figure 5.3B, D, E	HEK293T	$4x10^4$ cells/well (96 well plate)	25 ng dSaCas9.KRAB 50 ng PsiCheck2
Figure 5.4	Y79	$5x10^5$ cells/well (24 well plate)	500 ng
Figure 5.5A-B	Y79	$5x10^5$ cells/well (24 well plate)	0-1500 ng
Figure 5.5C-E	Y79	$5x10^5$ cells/well (24 well plate)	500 ng of each plasmid
Figure 5.6A-B	HEK293T	10^5 cells/well (24 well plate)	0-1500 ng of each plasmid
Figure 5.6C-E	HEK293T	$3x10^5$ cells/well (24 well plate)	500 ng of each plasmid

adherent 24 well plate and incubated at 37 C for 7 min. The poly-D-lysine was removed and the well washed in molecular grade water. 500 µl 1 mg/ml human fibronectin was added to each well and incubated at room temperature for 30 min. The human fibronectin was removed and the plate left in a positive pressure ventilation hood for 2 hours, with the lid removed, to dry. The coated plates were then kept in the fridge for up to 1 day before use.

5.2.9 Y79 cell transfection

For forward transfections, Y79 cells were transfected 24 hours after seeding in a poly-D-lysine and human fibronectin-coated plate. For reverse transfections, the transfection reaction was added to the coated plate and the cells added on top on the same day. Transfection was conducted with TransIT-LT1 (MirusBio), FuGENE (Promega), Viafect (Promega), or Lipofectamine 3000 (ThermoFisher). In all cases, Opti-MEM was used as transfection media.

5.2.10 Imaging DsRed expression in HEK293T cells

HEK293T cells were imaged as described in 2.2.7. In Figure 5.6, the same cells were imaged using a "short" DsRed channel exposure and a "long" DsRed channel exposure. Cells were imaged on the Invitrogen EVOS FL Auto 2 Cell Imaging System (ThermoFisher) at 10 x magnification. DsRed brightness was set to 0.0001 for the "short" exposure and 0.2 for the "long" exposure.

5.2.11 qPCR

RNA was extracted using the RNeasy Plus Mini Kit (Qiagen) and cDNA synthesis was performed using the SuperScript III First-Strand Synthesis Kit (Invitrogen). qPCR was conducted using Taqman reagents (ThermoFisher)(see 2.1.5 qPCR). RHO levels were expressed relative to human beta-actin levels.

5.2.12 Western blot

Protein was extracted from the cell pellet by sonication (see 2.1.6), and quantified using the Peirce BCA assay (see 2.1.7). Western blot was conducted as described in 2.1.8 using an anti-CRX, anti-Nrl, and anti-RHO antibody to detect CRX, NRL, and RHO, respectively, and an anti-vinculin antibody as a positive control (Table 2.2).

5.2.13 TIDE analysis

DNA was extracted from cell pellets using the QIAamp DNA mini kit. TIDE was conducted as described in 2.1.2 TIDE analysis.

5.3 Results

5.3.1 Identification of target sites

The *RHO* sequence and its promoter were screened for common SNPs with a minor allele frequency (MAF) of 0.1 or over. This signifies that the less common variant is present in 10 % of global alleles. Using the Hardy-Weinberg Equilibrium, this gives an estimated 0.18 probability that an individual will be heterozygous for the SNP. 11 SNPs, and 3 deletion events were found (Appendix 9.5, 9.6). *RHO* was then screened for SaCas9 target sites and the locations cross-referenced to find SNPs which occurred in the gRNA binding region, or created or removed a PAM site. Seven SNPs and one 10 bp deletion were targetable with 10 different gRNAs (Table 5.3).

The location of the SNP within the gRNA binding region is crucial to the tolerance of mismatches between the gRNA and DNA, with PAM-proximal mismatches less tolerated. SNPs rs6803468 and rs2855558 were therefore promising candidates for allele-specificity with the SNP 3 bp and 2 bp from a PAM site in gRNAs RHO+2781 and RHO+5991, respectively. SNP rs200054443 is a 10 bp deletion that removes the PAM site from gRNA RHO+1844 and deletes bases 7-16 of gRNA RHO+1841. With no PAM site, Cas9 should be unable to bind to *RHO* containing the minor allele of this SNP. The deletion of half the binding site for RHO+1841 also makes it unlikely Cas9 will bind successfully.

CRISPR/Cas9 gene disruption is most successful when targeted to the coding region of DNA, allowing it to disrupt the protein sequence. No gRNAs occur in a coding region as gRNA RHO+50 in exon 1 is before the start codon, and the gRNAs in exon 5 are in the 3' untranslated region. CRISPRi, on the other hand, can theoretically reduce gene transcription when bound anywhere within the gene, though is most successful when it binds near the TSS to block transcription initiation. The only gRNA in the "ideal" CRISPRi region is RHO+50.

Table 5.3 SNP-targeting gRNAs in rhodopsin that were tested in vitro.
Red text indicates the SNP. The position is relative to the transcriptional start site of RHO.

Position		Strand	Sequence	PAM	Specificity Score	Efficiency Score	SNP ID	SNP mutation	Distance of SNP from PAM	SNP MAF	Probability of heterozygosity
-677	Promoter	1	CAACCTCACAG**CC**CACCCTGGA	CGGAAT	63.80	14.12	rs2625955	C>A	10	0.47	0.50
+50	Exon 1	1	GCTCAGGCCTTC**G**CAGCATTC	TTGGGT	84.81	1.11	rs2269736	G>A	9	0.17	0.29-0.50
+1841	Intron 1	-1	AGAATG**CATCCTAATG**TGGGG	CAGAGT	80.52	51.38	rs200054443	Del of gRNA bases 7-16	6-15	0.15	0.26
+1844	Intron 1	1	ACAAGGAACTCTGCCCC**ACAT**	**TAGGAT**	74.54	8.06	rs200054443	Del of PAM and gRNA bases 19-21	1-3	0.15	0.26
+2781	Intron 2	1	CCATATTGTGGCCCCTTG**G**AA	CTGGGT	87.78	7.45	rs6803468	G>T	3	0.10	0.18
+4447	Intron 4	1	AAAGTCAGAAGG**A**CCCAAGTC	GGGAAT	73.85	8.41	rs2855557	A>T	9	0.48	0.50
+4452	Intron 4	1	CAGAAGG**A**CCCAAGTCGGGAA	TGGGAT	85.52	5.48	rs2855557	A>T	14	0.48	0.50
+5317	Exon 5	1	TCCCACGTTCCCC**A**AGGCCAG	CGGGAT	74.89	21.20	rs2410	A>G	8	0.27	0.39
+5991	Exon 5	1	GGTGAAGGCCAAGTTCCCA**AT**	GAGGGT	81.05	46.41	rs2855558	A>G	2	0.48	0.50
+6009	Exon 5	1	CAATGAGGGTGAGAT**T**GGGCC	TGGGGT	73.87	20.71	rs60645924	T>C	6	0.11	0.20

5.3.2 SaCas9 drives *RHO* disruption in HEK293-EGFP cells

Each *RHO* SNP in the HEK293-EGFP cell line was genotyped and found to be homozygous for the most common variant in every case (Table 5.4). The gRNAs targeting these SNPs, along with RHO+2300 from Chapter 4 (Figure 4.11) which will be called RHO_PTC for this chapter, were cloned into the all-in-one SaCas9 plasmid and transfected into HEK293-EGFP cells. Indel rate was assessed by TIDE analysis for most gRNAs. Unfortunately, SNPs rs200054443 and rs2410 are adjacent to highly repetitive nucleotide regions that cannot be Sanger sequenced. This means gRNAs RHO+1841, RHO+1844, and RHO+5317 cannot be measured by TIDE analysis, and so instead the indels were assessed by subcloning (Figure 5.1). In this method, the region around the target site was PCR amplified and cloned into the pGEM-T Easy Vector. The cloned plasmids were digested with an enzyme that cuts within the insert to determine the orientation of the ligated insert. Based on this orientation, they were Sanger sequenced with the primer that allows the sequencing reaction to pass through the predicted cut site before encountering the unsequenceable region. Any indels present in the sequencing trace were noted.

TIDE analysis detected *RHO* disruption with all gRNAs, from 16.4 % with RHO+50 to 62.8 % with RHO_PTC (Figure 5.2A). Subcloning analysis measured high and consistent disruption between 66.6 % and 73.3 % (Figure 5.2B). These are all higher than the measured TIDE disruption using RHO_PTC,

Table 5.4 SNPs present in the HEK293-EGFP cell line

SNP ID	Major allele	Minor allele	gRNA	HEK293-EGFP genotype
rs2625955	C	A	hRHO-677	C
rs2269736	G	A	hRHO+50	G
rs200054443	Ins	Del	hRHO+1841 hRHO+1844	Ins
rs6803468	G	T	hRHO+2781	G
rs2855557	A	T	hRHO+4447 hRHO+4452	A
rs2410	A	G	hRHO+5317	A
rs2855558	A	G	hRHO+5991	A
rs60645924	T	C	hRHO+6009	T

which was selected as it had one of the highest predicted efficiencies in the entire *RHO* coding sequence. To allow comparison between the two techniques, RHO+4447 was also measured by subcloning analysis. TIDE analysis measured 30.2 % gene disruption with RHO+4447, but subcloning measured 67.4 % gene disruption. This 37.4 % difference may be due to the indel detection limits of TIDE analysis. By default, TIDE analysis searches for indels up to 10 bp long, but subcloning analysis

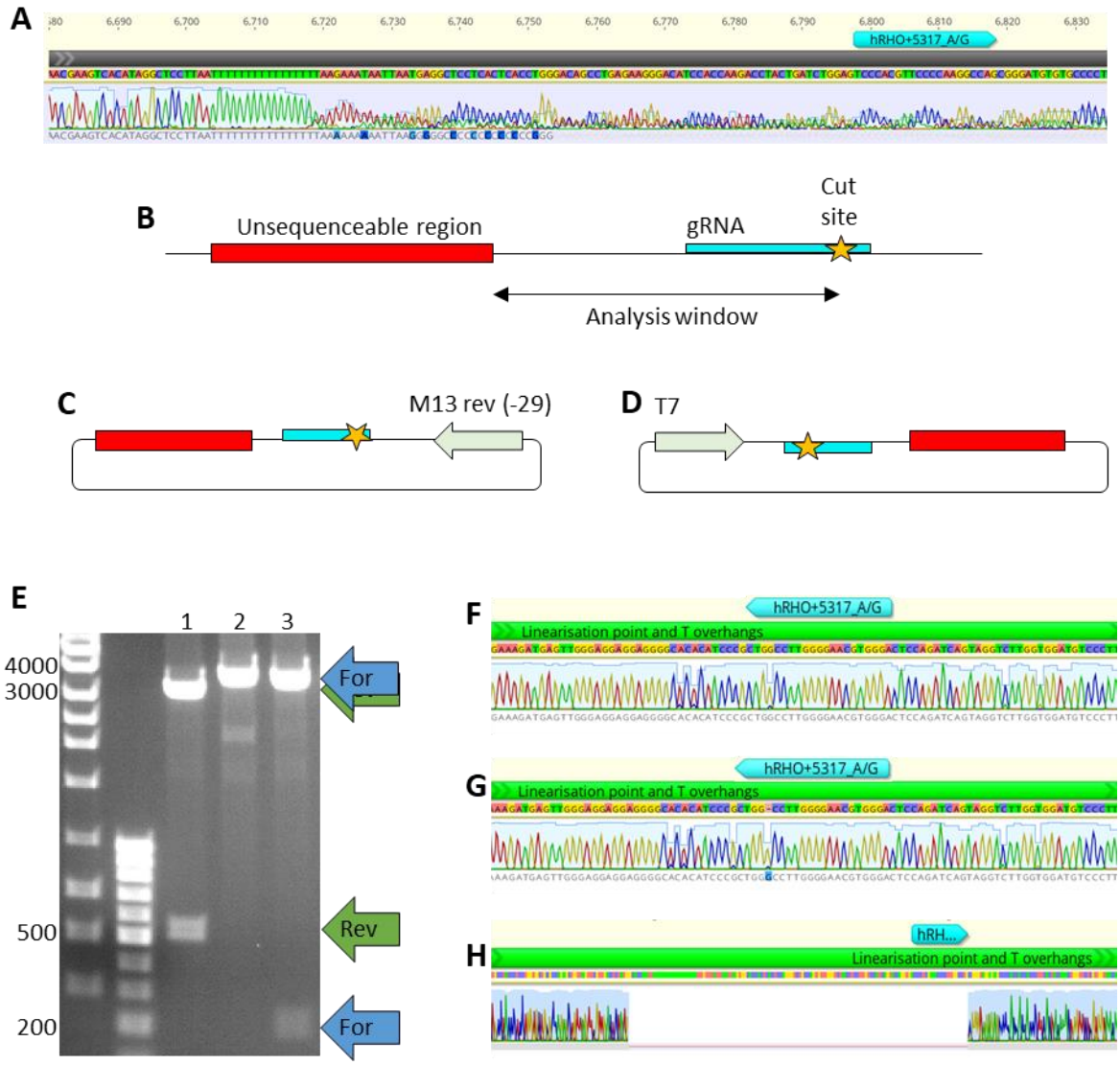

Figure 5.1 Workflow of subcloning analysis using gRNA RHO+5317 as an example.
***A)** Sequencing trace showing poly-T region that could not be sequenced. **B)** Diagram showing the region of DNA for indel analysis between the predicted cut site and the unsequenceable region of DNA. **C-D)** Sequencing primer used if the insert is cloned into the pGEM-T Easy Vector in the **C)** forward or **D)** reverse orientation. **E)** Example of a diagnostic restriction digest with StyI. For and Rev indicate the expected bands if the insert clones into the forward or reverse orientation, respectively. Well 1: Insert is in the reverse direction, well 2: Insert is in the forward direction but has a 124 bp deletion causing the loss of the 224 bp band, well 3: Insert is in the forward direction. **F-H)** Example of a sequencing trace with **F)** no indels, **G)** a 1 bp insertion, **H)** a 124 bp deletion. This is the sample from well 2 of E.*

revealed that indels over 10 bp long were responsible for an additional 29.3 % RHO disruption with RHO+4447. These >10 bp indels were common across samples, accounting for 20.7-46.0 % of all edited reads. The indel range of TIDE analysis can be increased to 50 bp but, surprisingly, when applied to RHO+4447-treated samples this only increased the disruption by 0.1 %.

All DNA insertions of over 10 bp were analysed to identify their origin (Table 5.5). The insertions were aligned to the SaCas9 plasmid, and if this was unsuccessful, it was aligned to the human genome using BLAST (Basic Local Alignment Search Tool from NIH)[195]. All identified inserts came from the SaCas9 plasmid, with the largest being a 230 bp insertion of the SaCas9 coding sequence. Two of the inserts

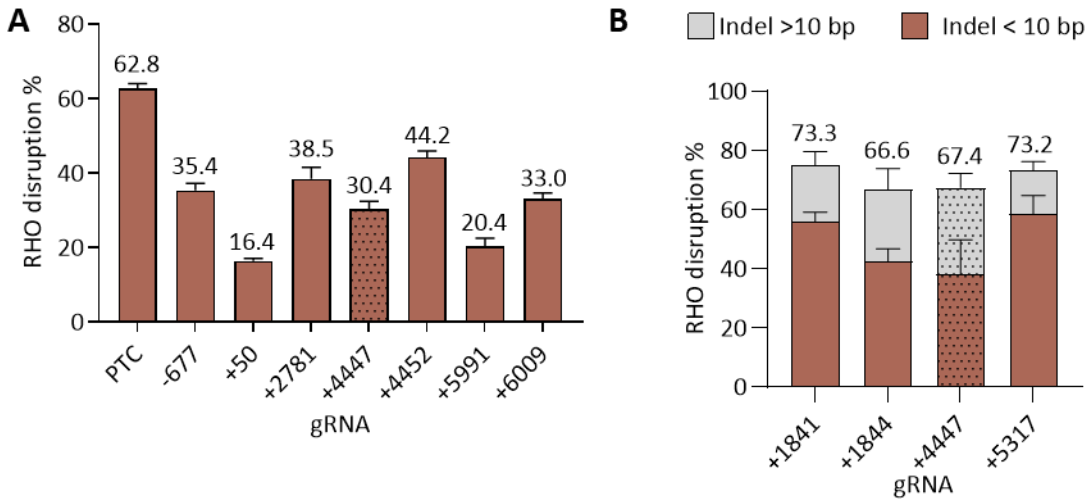

Figure 5.2 RHO disruption with different gRNAs.
***A)** TIDE analysis, n=6. **B)** Subcloning analysis, n=3.*

Table 5.5 Insertions over 10 bp in length in RHO following SaCas9 disruption.

gRNA	Size of insert/bp	Insert description	Insert origin
hRHO+1841	230	SaCas9	SaCas9 plasmid
	89	ITR	SaCas9 plasmid
	29	Puromycin resistance gene	SaCas9 plasmid
hRHO+1844	14	Unknown	Unknown
	114	Origin of replication	SaCas9 plasmid
	53	Origin of replication	SaCas9 plasmid
hRHO+4447	51	ITR	SaCas9 plasmid
hRHO+5317	38	Origin of replication	SaCas9 plasmid
	45	Unknown	Unknown

could not be successfully aligned to either the SaCas9 plasmid or the human genome, so their origin is unknown.

5.3.3 Allele-specificity of SNP-targeting *RHO* gRNAs

A luciferase assay was used to determine the allele-specificity of the SNP-targeting gRNAs (Figure 5.3A). The target sites for the SNPs were cloned into the PsiCheck2 plasmid between the SV40 promoter and the renilla luciferase gene that it regulates. PsiCheck2 also contains firefly luciferase driven by the HSV-TK promoter. The gRNAs were cloned into the dSaCas9.KRAB plasmid and the two plasmids co-transfected into HEK293T cells. If the gRNA successfully bound to the target, dSaCas9.KRAB reduced transcription of renilla luciferase relative to firefly luciferase. The assay was initially tested with both dSaCas9 and dSaCas9.KRAB using EGFP-targeting gRNA F11, which has been previously validated in house. dSaCas9.F11 and dSaCas9.KRAB.F11 reduced renilla expression by 17.8 % and 47.9 % relative to dSaCas9.scram, respectively ($p=0.0157$ and $p=0.0001$, respectively)(Figure 5.3B). Therefore, dSaCas9.KRAB was used in the subsequent experiment.

Initially, each dSaCas9.KRAB plasmid (containing each of the different gRNAs) was co-transfected with an unmodified PsiCheck2 plasmid. The normalised renilla expression did not vary with dSaCas9.KRAB plasmid, confirming that the different dSaCas9.KRAB plasmids had no impact on renilla or firefly expression from the PsiCheck2 plasmid (Figure 5.3D). Unfortunately, RHO+4447_A could not be included in the analysis due to an experimental error.

To assess the allele-specificity of the gRNAs, the dSaCas9.KRAB plasmids were co-transfected with the PsiCheck2 plasmid containing the target SNP of the gRNA or the non-target version of the SNP. If a gRNA was allele-specific it would reduce the normalised renilla expression when co-transfected with its target SNP but not its non-target SNP (Figure 5.3A).

All tested gRNAs had normalised renilla expression that was comparable to, or lower than, their

corresponding scrambled control; no gRNAs had an increased renilla expression, indicating the assay is producing relevant data (Figure 5.3E). 14 of the 19 tested gRNAs significantly knocked down their target SNPs. 7 of these were previously screened by TIDE analysis in the HEK293-EGFP cells using equivalent SaCas9 constructs (Figure 5.2). There was poor correlation between the measured CRISPR activity between the techniques (Figure 5.3C, $R^2 = 0.04140$), and interestingly gRNAs RHO+50_G and RHO+6009_T measured no knock down with the luciferase assay but significant CRISPR/Cas9-driven *RHO* disruption in HEK293-EGFP cells. For RHO+50_G it is possible that poor gRNA:DNA binding prevented detectable knock down in the luciferase assay, as only 16.4 % RHO disruption was measured by TIDE analysis. RHO+6009_T however, produced 33.0 % RHO-disruption by TIDE analysis, indicating that the binding efficiency is moderate in a genomic context. As well as having no detected knock down of its target SNP, RHO+6009_T knocked down its non-target SNP (PsiCheck2RHO+6009_C) by 38.8 % ($p<0.0001$). This result was unexpected as a site with 100 % homology is anticipated to have greater gRNA:DNA binding than a site with a mismatch 6 bp from the PAM site. The dSaCas9.KRAB and PsiCheck2 plasmid dilutions used for transfection were sent for sequencing which confirmed there had not been a mix up in the plasmids.

Of the 14 gRNAs with significant target SNP knock down, 9 of these were specific, with no knock down of their non-target SNP. These included gRNAs RHO+1841_ins, RHO+1844_ins, RHO+2781_G/T and RHO+5991_A, which were identified as strong candidates for allele-specificity due to the location of the SNP within the gRNA binding region. The other specific gRNAs were RHO+4447_A, RHO+4452_T, and RHO_5317_A/G with SNPs 9, 14, and 8 bp from the PAM site, respectively. Interestingly, specificity was not always consistent between gRNAs targeting different versions of the same SNP: for example, gRNA RHO+4447_A was allele-specific but gRNA RHO+4447_T knocked down both the target and non-target SNP.

The most therapeutically useful strategy involves identification of multiple SNPs, both versions of which can be targeted in an allele-specific manner. Provided a patient was heterozygous for a given

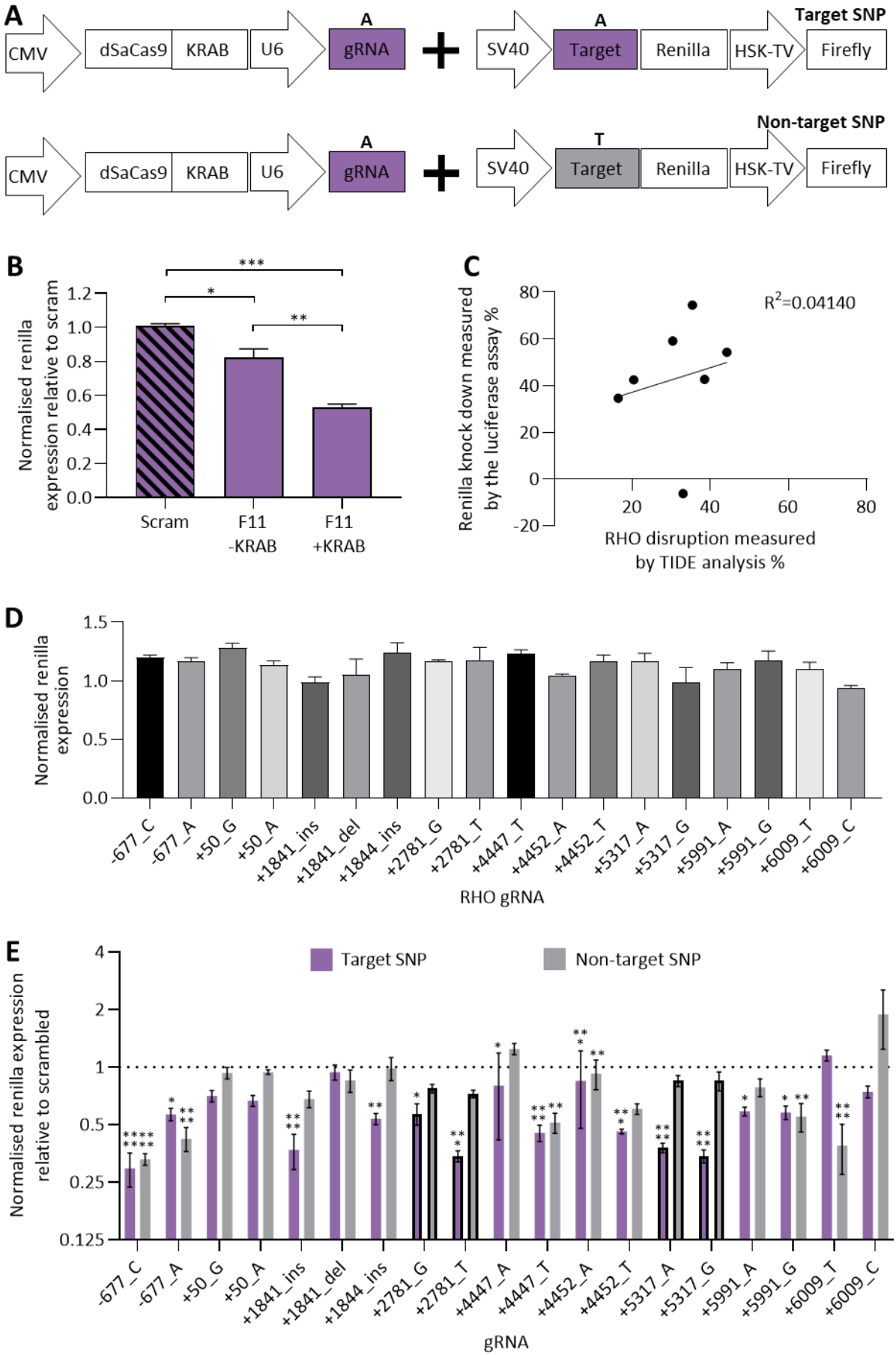

Figure 5.3 Luciferase assay testing allele-specificity of SNP-targeting RHO gRNAs.

A) *Dual transfection of dSaCas9.KRAB and luciferase reporter plasmids to assay allele-specificity. gRNA targeting SNP A is tested against the luciferase assay carrying the corresponding target SNP A and the alternative target SNP B.* ***B)*** *Luciferase assay knock down is greater when transfected with the dSaCas9.KRAB plasmid (+KRAB) than the dSaCas9 plasmid (-KRAB), n=3. One-way ANOVA with multiple comparisons comparing the means of normalised renilla expression. F(2,6)=55.07, p=0.0001. Scram vs F11-KRAB p=0.0157, Scram vs F11+KRAB p=0.0001, F11-KRAB vs F11+KRAB p=0.0017* ***C)*** *Correlation between gene knock down measured by the luciferase assay and gene disruption measured by TIDE analysis. Line indicates linear regression.* ***D)*** *Co-transfection of unmodified PsiCheck2 plasmid with each dSaCas9.KRAB plasmid. One-way ANOVA compared the normalised renilla expression between plasmids. F(17, 34)=1.873 p=0.0586 (not significant).* ***E)*** *Measuring knock down with different combinations of gRNA and target sequence. Two-way ANOVA with factors of PsiCheck2 plasmid and gRNA were conducted with multiple comparisons comparing normalised renilla expression between test gRNA and scrambled gRNA, n = 5. Effect of PsiCheck2 plasmid F(37, 148)=66.44 p<0.0001, effect of gRNA F(1, 4)=148.6 p=0.0003, effect of interaction F(37, 148) p<0.0001. Significant multiple comparison results are detailed in Table 5.6. gRNAs outlined in bold indicate the most promising target sites. These loci can be targeted allele-specifically regardless of which SNP is present.*

Table 5.6 Significant One-way ANOVA multiple comparison results of the luciferase assay experiment in Figure 5.3E.

gRNA	PsiCheck2 plasmid	p value
RHO-677_C	RHO-677_C	<0.0001
RHO-677_C	RHO-677_A	<0.0001
RHO-677_A	RHO-677_A	0.0161
RHO-677_A	RHO-677_C	<0.0001
RHO+1841_ins	RHO+1841_ins	<0.0001
RHO+1844_ins	RHO+1844_ins	0.0053
RHO+2781_G	RHO+2781_G	0.0134
RHO+2781_T	RHO+2781_T	<0.0001
RHO+4447_A	RHO+4447_A	0.0202
RHO+4447_T	RHO+4447_T	<0.0001
RHO+4447_T	RHO+4447_A	0.0011
RHO+4452_A	RHO+4452_A	0.0003
RHO+4452_A	RHO+4452_T	0.0038
RHO+4452_T	RHO+4452_T	0.0002
RHO+5317_A	RHO+5317_A	<0.0001
RHO+5317_G	RHO+5317_G	<0.0001
RHO+5991_A	RHO+5991_A	0.0398
RHO+5991_G	RHO+5991_G	0.0262
RHO+5991_G	RHO+5991_A	0.0025
RHO+6009_T	RHO+6009_C	<0.0001

SNP, the mutant *RHO* could then be targeted regardless of which SNP was present on the mutant strand. Out of the 10 possible gRNAs, RHO+2781 and RHO+5317 fulfil this requirement as both SNP variants at rs6803468 and rs2410 can be targeted allele-specifically, with gene knock down ranging from 43.1 % to 65.8 % (Figure 5.3E, columns outlined in bold).

5.3.4 Transfection of CRX and Nrl transcription factors into Y79 and HEK293T cells does not induce significant endogenous *RHO* expression

To measure the impact of these RHO-targeting gRNAs at a protein level, a cell line expressing the full-length *RHO* gene from its native regulatory elements is required. There is conflicting information on the RHO-expression in Y79 cells, with no expression, or low-level expression reported[127,196]. In Chapter 3, a reporter construct containing a human *RHO* promoter was unable to drive expression of DsRed in transfected Y79 cells. Transfection of Y79 cells with the transcription factor CRX has previously been shown to activate endogenous *RHO*[196]. Y79s have a low transfection efficiency so the transfection protocol was first optimised with the CAG.DsRed plasmid (see Chapter 3). Reverse transfection had greater efficiency than forward transfection, with more DsRed-positive cells (Figure 5.4A). Four different transfection reagents were reverse transfected at a range of doses (Figure 5.4B). Viafect (Promega) had the greatest level of transfection, with DsRed transgene expression increasing with transfection reagent dose. Even at the highest transfection efficiency, the transfection rate is still lower than other immortalised cell lines such as HEK293-derived lines. A dose of 6 µl Viafect per µg of DNA was selected for subsequent experiments.

Y79 cells were reverse transfected with a ubiquitously expressing CRX plasmid (CMV.CRX) at a range of doses. The cells natively express CRX and transfection with CRX plasmid did not increase their levels of CRX protein, or the level of *RHO* expression, which remained extremely low (Figure 5.5A-B). Rhodopsin protein was undetectable by western blot across all doses (Figure 5.5B). The cells were then transfected with CMV.CRX and/or hRHOp.RHO (RHO expression driven by the RHO promoter)

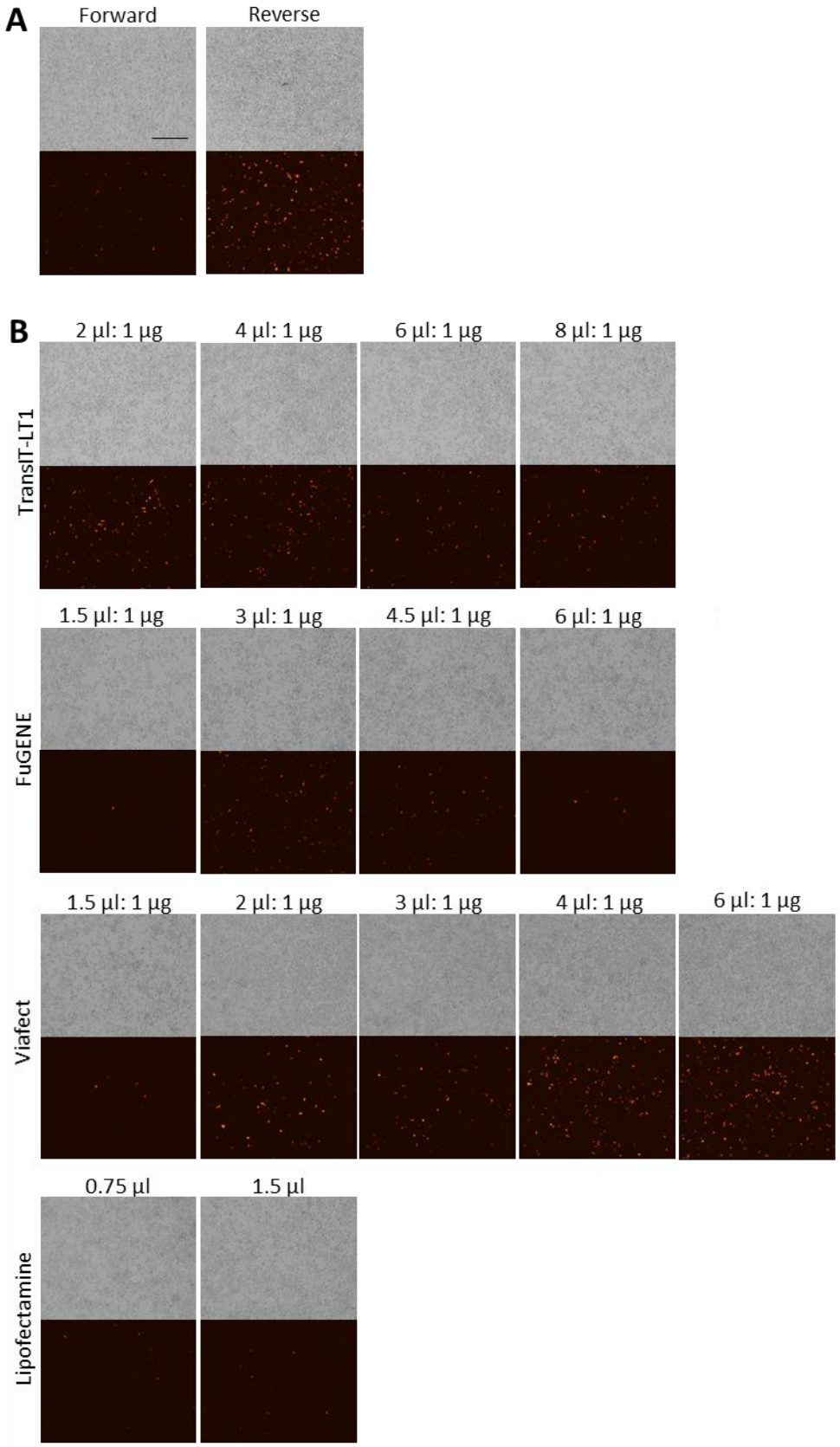

Figure 5.4 Optimising transfection of Y79 cells with CAG.DsRed.
***A)** Forward and reverse transfection of Y79 cells. **B)** Four different transfection reagents tested at different volumes using reverse transfection. µl indicates the amount of transfection reagent added, µg indicates the amount of DNA added. Scale bar is 250 µm.*

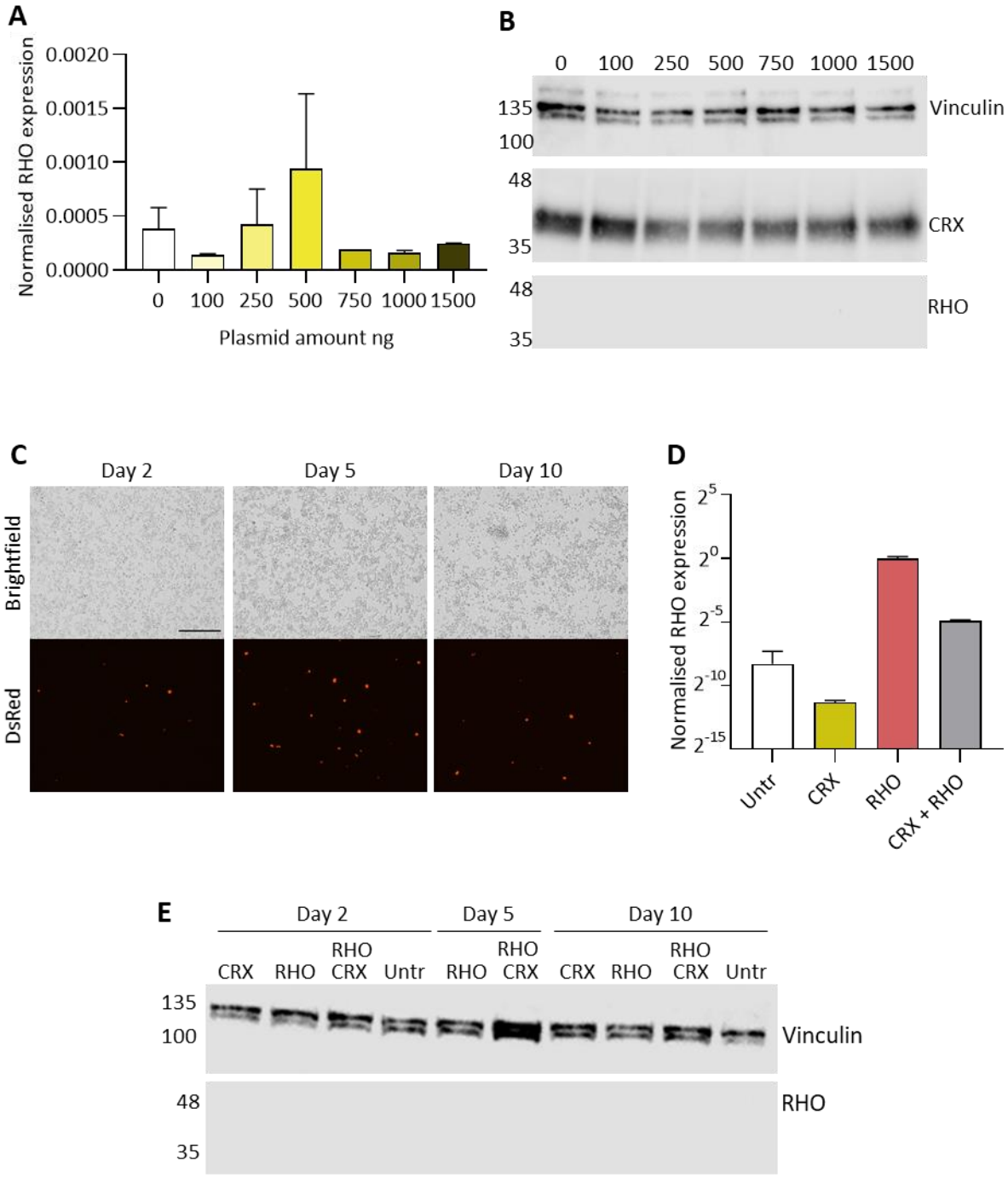

Figure 5.5 Transfecting Y79 cells with CMV.CRX does not induce significant RHO expression.
A-B) *Y79 cells reverse transfected with a range of CMV.CRX plasmid doses from 0 to 1500 ng detected no increase in RHO expression.* ***A)*** *qPCR measuring RHO expression normalised to human beta-actin. n=2. One-way ANOVA F(6, 7)=0.8753 p=0.5565.* ***B)*** *Western blots staining for vinculin (135 kDa), CRX (37 kDa), and RHO (40 kDa).* ***C-E)*** *Y79 cells transfected with CMV.CRX (CRX), hRHOp.RHO (RHO), CMV.CRX & hRHOp.RHO, CAG.DsRed or untransfected (Untr) and harvested at day 2, day 5, or day 10 post-transfection produced no dectable increase in RHO expression.* ***C)*** *Microscopy images of CAG.DsRed-transfected cells at harvesting. Scale bar is 250 µm.* ***D)*** *qPCR measuring RHO expression normalised to human beta-actin in the samples harvested 10 days post-transfection. One-way ANOVA with multiple comparisons compared the means to that of Untr. F(3, 4)=4.231, p=0.0986* ***E)*** *Western blot staining for vinculin (135 kDa) and RHO (40 kDa).*

and harvested at 2 days (as before), 5 days, and 10 days post-transfection. The impact of prolonged culture on transgene expression was assessed with the ubiquitously expressing CAG.DsRed plasmid, which showed comparable levels of DsRed expression on all three days (Figure 5.5C). Rhodopsin protein could not be detected under any of these conditions (Figure 5.5E) and there was no increase in *RHO* mRNA levels on day 10 post-transfection (Figure 5.5D).

RHO expression has been previously induced in HEK293T cells following transgenic expression of CRX and Nrl[197]. CMV.CRX and CMV.NRL plasmids were transfected into HEK293T cells, both individually and simultaneously, at 6 doses from 100 ng to 1500 ng. A dose-dependent increase in expression of CRX and Nrl protein was observed (Figure 5.6B). Unfortunately, no significant expression of *RHO* could be seen at an mRNA or protein level (Figure 5.6A-B). As with the Y79 cells, the time post-transfection was increased to 2, 5, and 10 days to see if this impacted expression. Again, no *RHO* expression was induced at an mRNA level at 10 days post-transfection or a protein level at any time point (Figure 5.6D-E). Prolonged culture times was associated with a reduction in Nrl protein (Figure 5.6E). Due to low protein yield, a western blot for CRX could not be conducted on these samples but it is possible that the prolonged culture times tested are not beneficial for transgene expression in this cell line.

CRX- and Nrl-mediated activation of *RHO* in HEK293T cells was previously only detected using reporter plasmids, and the impact on endogenous *RHO* was not investigated[197,198]. Activation of *RHO* may therefore be possible on an introduced plasmid. To investigate this, HEK293T cells were transfected with hRHOp.DsRed (DsRed driven by the human *RHO* promoter, see Chapter 3) and hRHOp.RHO (RHO driven by the human *RHO* promoter). hRHOp.DsRed alone did not express DsRed but when co-transfected with CRX and NRL plasmids the HEK293T cells expressed low levels of DsRed that were detectable with longer imaging exposure times (Figure 5.6C). Transfection of hRHOp.RHO did not produce detectable RHO mRNA or protein either alone or when co-transfected with CRX and NRL plasmids (Figure 5.6D-E).

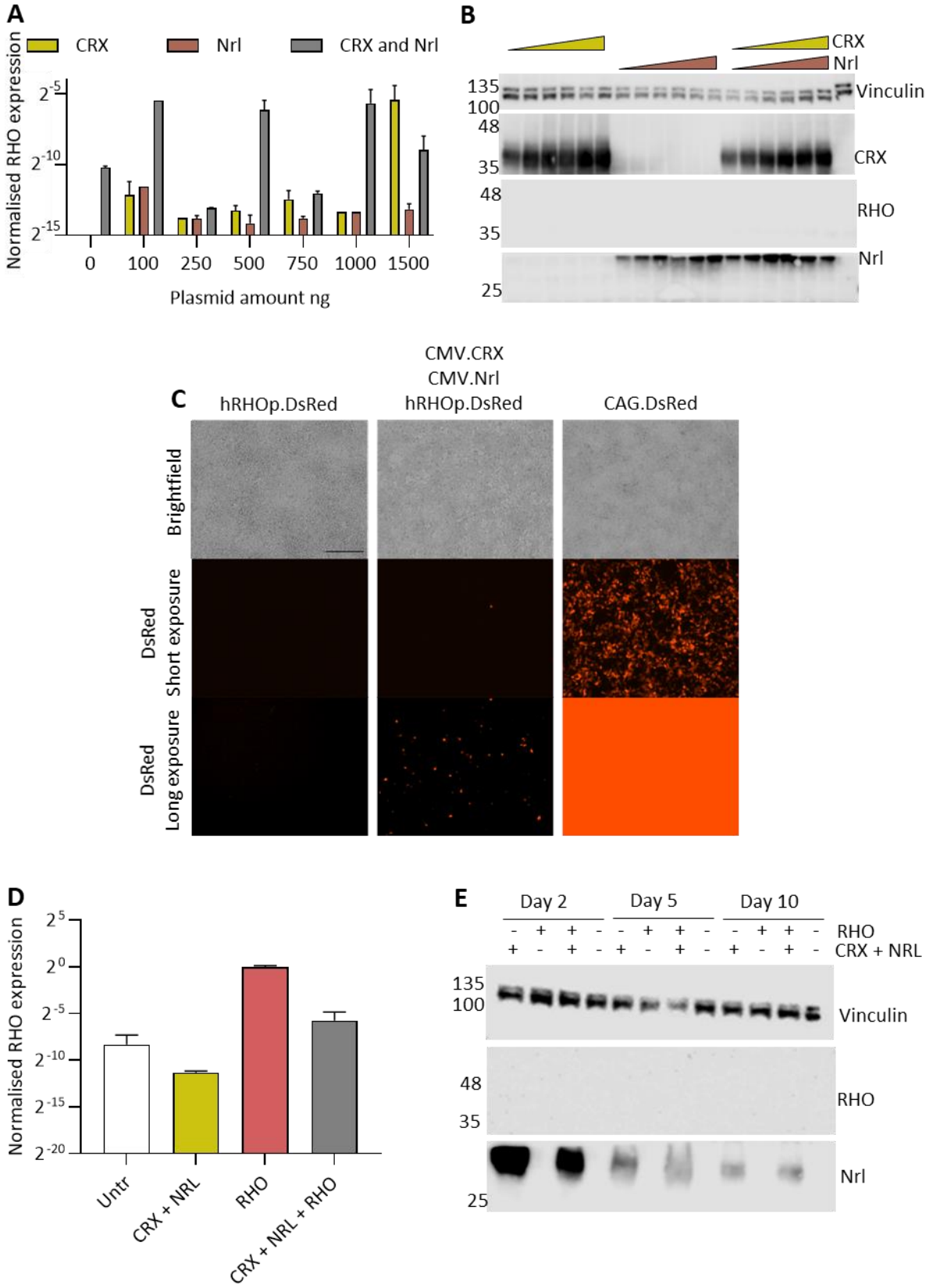

Figure 5.6 Transfecting HEK293T cells with CMV.CRX (CRX) and CMV.Nrl (NRL) drives low levels of expression from the hRHO promoter.

A-B) *Cells transfected with a range of CRX and NRL plasmid doses, separately and combined, from 0 ng to 1500 ng detected no RHO expression.* ***A)*** *qPCR measuring RHO expression normalised to human beta-actin, n=2. One-way ANOVA with multiple comparisons comparing all sample means to the untransfected control.*

F(18, 14)=2.158, p=0.0747. ***B)*** *Western blots staining for vinculin (135 kDa), CRX (37 kDa), RHO (40 kDa), and Nrl (33 kDa). The triangle above the well indicates transfection with CRX or Nrl with increasing dose from left to right.* ***C-E)*** *Cells were transfected with CRX, NRL, hRHOp.RHO (RHO), hRHOp.DsRed, or untransfected (Untr), and harvested at 2, 5, and 10 days post-transfection. Scale bar is 150 µm.* ***C)*** *DsRed expression is visible following co-transfection of CMV.CRX, CMV.Nrl, and hRHOp.DsRed. Cells were imaged 10 days post-transfection with a long and short DsRed exposure time.* ***D)*** *qPCR measuring RHO expression normalised to human beta-actin in samples harvested 10 days post-transfection did not detect an increase in expression. One-way ANOVA with multiple comparison comparing the means to Untr. F(3, 4)=4.231, p=0.0986.* ***E)*** *Western blot staining for vinculin (135 kDa), RHO (40 kDa), and Nrl (33 kDa) detected no RHO protein in any condition.*

5.4 Discussion

5.4.1 Selection of SNPs

CRISPR gene therapy targeted to a *RHO* SNP could allow mutation-independent yet allele-specific treatment of adRP. In order to create a strategy that could target a large number of patients, SNPs were selected if they were relatively common, with a global MAF of over 0.1 (and could be targeted with SaCas9). Seven SNPs and one deletion were identified. As SNPs are highly variable with human population, the MAFs were taken from the 1000 genomes project, as this large-scale study sequenced 2504 genomes across 26 distinct human populations. Subsequent analysis on the data has determined that it is highly accurate for variants with an MAF of over 0.01, but unfortunately some groups, including Middle-Eastern populations, were absent from this study and are therefore not represented in this data[199–202].

The variable distribution of SNPs means that some targets have greater clinical application in particular human populations. One of the allele-specific gRNAs identified in this chapter targets SNP rs6803468, which has a relatively low global MAF of 0.10 (17.8 % chance of heterozygosity). In African populations, however the MAF is 0.21, giving a 33.2 % chance that a given individual will be heterozygous for this mutation (ALFA Allele Frequency Aggregator accessed 10/02/2021). The frequency of pathogenic mutations also varies with population due to founder effects. This means it is possible that certain pathogenic mutations and SNPs will be linked by haplotype[1,28–30], which will influence the chances that an individual is heterozygous, and therefore targetable with a given gRNA.

RHO MAFs were taken from a dataset of unaffected individuals and as the SNPs investigated in this chapter are common in the global population, they are not expected to be linked to adRP[3]. The variant frequencies in this unaffected population are therefore expected to be approximately representative of adRP individuals. Founder mutations are likely to influence the SNP distribution however, and so SNP frequencies should be confirmed in the target patient population in the future.

The HEK293-EGFP cell line was found to be homozygous for all 7 SNPs and 1 deletion examined. This was unexpected, but is potentially influenced by two factors. The HEK293 cell line originated from embryonic kidney cells harvested from a female foetus. Little is known about the origins of the foetus, including the ethnicity; it is possible that it is from a human population in which the SNPs occur at low rates[172]. The HEK293-EGFP cell line was karyotyped in Chapter 4 and found to be highly re-arranged and heterogeneous. Chromosome 3, which contains the *RHO* gene had a chromosome number between 2 and 5 copies per cell. It is possible that heterozygous SNPs could be diluted out of the detection limit of Sanger sequencing following replication of one of the chromosomes[172,174–176].

This SNP-targeting strategy relies on knowing the pathogenic *RHO* mutation of an adRP patient to determine the target allele. For common mutations such as P23H this would be straightforward but there are many rare *RHO* mutations which are not as well-studied. Non-pathogenic SNPs have previously been mischaracterized as adRP-causing mutations, which could lead to the treatment of the incorrect allele in this strategy[1,3]. As well as treating adRP, this strategy may be able to treat some recessive retinitis pigmentosa cases. *RHO* mutations E150K and M253I are believed to be mild gain-of-function mutations that are only pathogenic when present on both alleles[3,33]. Targeting a heterozygous SNP on either allele could potentially slow disease progression in these patients, as a single copy of these mutations are not pathogenic.

5.4.2 Measuring on-target activity

TIDE analysis and subcloning analysis were used to measure the on-target gene disruption of each *RHO* gRNA with CRISPR/Cas9. Subcloning produced a higher estimation of gene disruption than TIDE analysis. TIDE is known to report common indels accurately, with estimations comparable to those achieved with next-generation sequencing. However, indels with a frequency of under 1-2 % are below the limit of detection, which causes TIDE to underestimate the overall editing rate by approximately 10-20 %. TIDE is particularly poor at estimating the presence of indels over 10 bp long, which made up

20.7-46.0 % of edited *RHO* reads according to the subcloning analysis conducted in this chapter. This underestimation was not improved by increasing the indel detection range from 10 bp to 50 bp in the software, suggesting this is the limitation of TIDE sensitivity. While subcloning allowed detection of all indels, it may potentially be biased against insertion events as the PCR and ligation processes are more efficient with smaller fragments[180,203–205].

Subcloning analysis is significantly more expensive and time-consuming than TIDE analysis: it relies on over 20 sequencing reactions per replicate and takes 3 days, whereas TIDE uses one sequencing reaction per replicate and can be completed within a single day. The main advantage of subcloning analysis is it reveals the sequence of inserted DNA fragments. Large insertions into the cut site in this experiment originated from the CRISPR plasmid, with integrations of the SaCas9 coding sequence, the ITR, the bacterial origin of replication, and the puromycin resistance gene. These made up 4.12 % of all edited reads. Integration of AAV genomes into CRISPR cut sites is well documented, with in vitro rates estimated between 13.8-36.5 % in one study[205–207]. In AAV, this integration is thought to be dependent upon ITR loops but these secondary structures are absent from plasmids carrying ITR sequences and the majority (5 out of 7) of the integration events did not involve the ITRs. To the author's knowledge, integration analysis of plasmid DNA into the cut site following CRISPR treatment has not been previously investigated.

Contrary to the results in this chapter, Giannelli et al. (2018) found comparable rates of editing with subcloning and TIDE analysis targeting *Rho*. They transduced both wild type, and *Rho*-P23H knock in mouse embryonic fibroblast cells with a lentivirus carrying SpCas9-VQR and a P23H-targeting gRNA. In the wild type cell line, they detected 6 % editing with TIDE analysis and no editing by subcloning, while in the P23H cell line they detected 65 % and 66 % editing by TIDE and subcloning, respectively[41].

CRISPRi repression measured with the luciferase assay correlated poorly with endogenous CRISPR/Cas9 disruption measured by TIDE analysis. While the luciferase assay is a more direct measure of dCas9 binding to the target site, TIDE is influenced by additional factors, such as the gene

accessibility, the SaCas9 cleavage rate after binding, and the error-rate of the NHEJ repair pathway[178].

5.4.3 Allele-specificity of gRNAs

Allele-specificity of the gRNAs was assessed using a luciferase reporter assay. In the initial optimisation of this assay, dSaCas9.KRAB improved the repression seen with dSaCas9 alone. This effect has been seen previously, with reporter plasmid knock down used to compare different CRISPRi repressors[63]. As the KRAB plasmid alters the histone state of the gene, this suggests the transfected plasmids are interacting with histone molecules, which was previously proposed by Mladenova et al. in 2009[208].

The tolerance of Cas9 for mismatches between the gRNA and DNA target are known to be variable with position and nucleotide change of the mismatch. Broadly speaking, the closer to the PAM site the mismatch is, the less it will be tolerated[53,73–76]. Based on this, seven promising gRNA candidates were identified which either had a SNP 2-3 bp from the PAM or included a large deletion of the gRNA binding region or PAM site. Of these seven gRNAs, five were allele-specific. An additional four gRNAs were allele-specific with mismatches 8 bp, 9 bp, and 14 bp from the PAM site. In 2013, a screen was conducted to identify which gRNA:DNA mismatches were tolerated[74]. Unfortunately, this was conducted with SpCas9 and the results do not appear to translate to SaCas9 well: in this experiment they do not explain the specificity of the gRNA:DNA mismatch combinations (Figure 5.7).

Out of ten gRNAs initially screened, two were able to drive allele-specific targeting for both SNP variants. These screens used both the native SaCas9 coding sequence, and gRNAs 21 bp long, which have been shown to be the most optimal for SaCas9, producing the greatest knock down[170]. Some studies have demonstrated that reducing the gRNA length for the *Streptococcus pyogenes* CRISPR system from 20 bp to 17 bp was associated with a decreased tolerance for mismatches[76]. Li et al (2018) targeted *RHO* in the mouse retina using SpCas9 and a gRNA that spanned the P23H mutation in *Rho*[40]. The P23H mutation caused a single nucleotide mismatch between the gRNA and wild type strand, four bases from the PAM site. A 20 bp gRNA was unable to discriminate between the strands, knocking

down both wild type and mutant *Rho*. When the gRNA was truncated to 17 bp in length, it drove 28 % *Rho* cleavage in homozygous P23H knock in mice and no editing in wild type mice. It is possible that truncating the SaCas9 gRNA may also improve specificity but in the initial study optimising SaCas9 gRNA length, lengths of 17 bp were associated with near-complete ablation of editing[170].

In the luciferase assay, gRNA RHO+6009_T produced an unexpected result: it was unable to knock down its target SNP but repressed its non-target SNP by 67.0 %. This was particularly surprising as it caused 33.0 % CRISPR/Cas9 mediated disruption of its target SNP in endogenous *RHO*. All other gRNAs with CRISPR/Cas9 gene disruption of over 20 % were able to drive significant gene repression with the luciferase assay. Plasmid sequencing confirmed there was no mix up in plasmids during transfection. A screen with unmodified luciferase plasmids confirmed that the gRNA RHO+6009_T plasmid does not influence baseline luciferase expression. This suggests the issue could be with the luciferase RHO+6009_T plasmid. This plasmid could not be repressed using either the gRNA RHO+6009_T or RHO+6009_C. It is possible that secondary structure in the luciferase plasmid prevents gRNA or Cas9

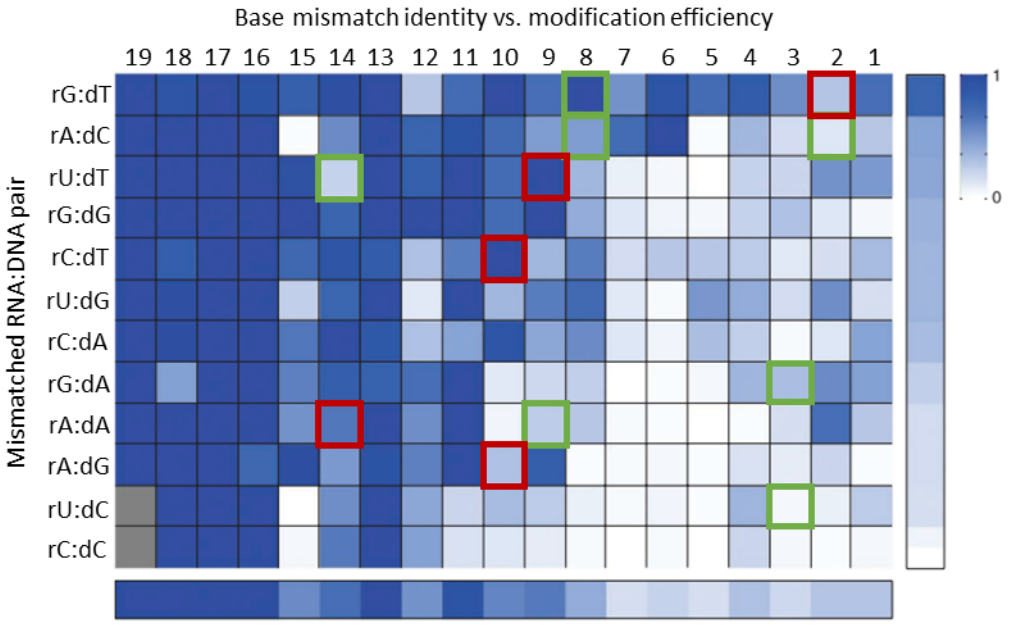

Figure 5.7 gRNA specificity in this chapter is not explained by the gRNA:DNA mismatch rules identified by Hsu et al. (2013).
Heat map taken from Hsu et al (2013)[74] describes the relative SpCas9 cleavage efficiency for each gRNA:DNA mismatch at 15 screened targets. A whiter square indicates less editing and therefore a less tolerated mismatch. Outlines are drawn around the gRNA mismatches tested in Chapter 5. There is no obvious difference in the SpCas9 cleavage efficiency for the gRNAs identified in this chapter as being allele-specific (green outline) or not allele-specific (red outline).

binding but this was not investigated.

5.4.4 Therapeutic application of target sites

Both variants of SNPs rs6803468 and rs2410 can be targeted allele-specifically. All 4 gRNAs drove strong CRISPR/Cas9 gene disruption and CRISPRi but the subsequent impact on rhodopsin protein levels was not assessed, as rhodopsin is not natively expressed in the Y79 and HEK293T cell lines[127,196,209]. Attempts were made to activate expression of *RHO* in these cell lines by transfecting them with CRX and Nrl, transcription factors required for rod cell development. CRX is a transcription factor involved in the expression of photoreceptor specific genes. It is expressed in a range of retinal tissue so the endogenous expression of CRX in Y79 cells was expected[135–137,196]. CRX activation of *RHO* in Y79 cells has been confirmed via multiple mechanisms: expression of a luciferase plasmid driven by the human *RHO* promoter, induction of active chromosome loops on the *RHO* gene indicating transcriptional activation, and presence of endogenous *RHO* mRNA[196,210,211]. Experiments in this chapter were unable to replicate these results, with no *RHO* mRNA or protein detected. Peng et al. (2007), reported 30-50 % transfection efficiency of Y79 cells, much higher than the efficiencies achieved in this experiment which could be a limiting factor[196]. The Y79 cell line used here was found to be sensitive to changes in handling, with plate type, transfection protocol, and time since passaging all influencing their transfection rate. It is also possible that the western blot protocol was not optimised for detection of RHO protein as RHO was undetectable throughout experimental conditions and there was no positive control.

Endogenous activation of *RHO* has not been reported in HEK293T cells, but activation of a luciferase reporter plasmid driven by a bovine proximal *RHO* promoter has been reported[197,198]. Transfection of HEK293Ts with CRX and NRL in this chapter was able to drive a hRHOp reporter construct at low levels but again, this was not sufficient to detect *RHO* mRNA or protein. The promoters present on these reporter constructs are the proximal *RHO* promoters, beginning at position -225 and -796 relative to

the transcriptional start site of bovine and human *RHO*, respectively[212]. The human *RHO* gene has an enhancer at -2155 to -2027 that is absent from these proximal promoters, and may be preventing activation of genomic *RHO*. The octamer-binding protein NonO/p54^{nrb} binds to the *RHO* enhancer in the presence of CRX and Nrl and significantly increases *RHO* expression[213]. While NonO is expressed in all adult tissue, retinal cells express a unique, alternatively spliced form of NonO[214]. It is possible this isoform is absent in the transfected HEK293T cell line, preventing strong transcription of genomic *RHO.* Validation of these *RHO* target sites will require a cell line expressing *RHO,* preferably in the native genomic context. Creating transgenic lines of Y79 or HEK293T cells with strong CRX or NRL expression may be sufficient to activate endogenous *RHO* levels and avoid the issue of low transfection efficiencies.

SNP rs6803468 is in intron 2, and SNP rs2410 is after the stop codon in exon 5. Indels at these sites are unlikely to impact rhodopsin protein levels as they are outside the coding sequence. Small indels in introns are usually lost from the mRNA sequence during splicing, and indels in the final exon do not trigger the nonsense-mediated mRNA decay pathway[1,48]. dSaCas9.KRAB binding at these sites, however, may block transcriptional elongation and reduce the level of *RHO* mRNA and protein that is produced. Although the sites are outside the ideal CRISPRi region, repression at sites distal from the transcriptional start site is possible[58,59,62,63]. Notably, Chung et al. (2019) targeted a site in *Fabp4* over 2600 bp downstream of the transcriptional start site and achieved 60 % gene silencing in vitro[62]. *RHO* has a high number of gain-of-function mutations and few loss-of-function mutations, suggesting that mutations in *RHO* are likely to negatively affect protein function[1]. As sites of variability, SNPs only become common in a population if they are not associated with a damaging phenotype. This may explain why there were no common SNPs (MAF over 0.1) in the *RHO* coding sequence.

The gRNAs tested in this chapter used the most efficient PAM site for SaCas9, NNGRRT. SaCas9 has exhibited some flexibility of the final base of its PAM site; PAM NNGRRN can be used but is associated with lower levels of editing[64]. Screening with this PAM site dramatically increases the number of gRNAs

targeting *RHO*, some of which have predicted efficiencies rivalling NNGRRT PAM sites. The most ideally placed SNPs were rs2269736 and rs7984, which are both in exon 1 at +50 and +73 relative to the transcriptional start site, respectively. With the NNGRRT PAM, one gRNA (hRHO+50) targeted rs2269736 but had low in vitro editing, and there were no gRNAs available to target rs7984. With the NNGRRN PAM site, there are an additional five gRNAs capable of targeting rs2269736 and two gRNAs targeting rs7984.

The SNPs explored in this chapter are present in the *RHO* gene or promoter (up to 1500 bp upstream of the transcriptional start site). CRISPRi is most effective when blocking regulatory regions of the gene. *RHO* has an enhancer region at -2155 to -2027 relative to the transcriptional start site. Screening this site identified one "common" SNP in this region with an MAF of 0.13 (rs58508862). This SNP was targetable with one NNGRRT gRNA and four NNGRRN gRNAs, which could be explored for CRISPRi repression of *RHO* in the future.

5.4.5 Conclusion

This chapter used bioinformatics screens to identify SaCas9 gRNAs in *RHO* that targeted non-pathogenic SNPs. In vitro analysis demonstrated high levels of CRISPR/Cas9 gene disruption and CRISPRi gene repression. Using a luciferase assay, two promising gRNAs were identified which drove allele-specific repression of *RHO* when targeting both the major and minor SNP variant. The impact of indels or dSaCas9.KRAB binding on the level of RHO protein at these sites needs to be investigated to determine whether they have potential therapeutic benefit to treat adRP patients. Utilising a wider NNGRRN PAM requirement of SaCas9, and targeting distal enhancer elements will increase the available gRNAs in regions likely to drive strong gene knock down. The distribution of any chosen SNPs would need to be compared to the adRP population to confirm similarity with global frequencies.

6 CRISPR/Cas9 gene disruption of rod cell-specific EGFP in vivo

6.1 Introduction

In vivo assessment of AAV vectors is a crucial step in the development of gene therapies to treat retinal diseases. While in vitro experiments allow optimisation of the construct – in this thesis in vitro assessment optimised construct configuration and screened gRNAs – in vivo studies provide the opportunity to study the therapy within the context of the target organ and a living organism. Mouse eyes have key structural differences compared to human eyes[215,216]. They do not have a fovea, and instead their cone cells are distributed throughout the retina. Their optic disc is also located centrally. Despite this, mice remain a useful model, with murine retinal layers broadly mimicking human retinal layers. In vivo experiments also allow issues such as delivery methods and immune reactions to be investigated.

The Nrl-EGFP mouse contains three copies of a transgene in which EGFP is driven by a 2.5 kB *Nrl* promoter[121]. As *Nrl* is rod cell-specific, EGFP is expressed exclusively in the rod cells of these mice from embryonic day 12. Knocking down EGFP in this mouse line acts as a proof of concept for targeting rod cell-specific genes, such as *RHO*. This mouse line has been used for previous CRISPR adRP research, in which protocols and constructs were first optimised targeting EGFP before disrupting the clinically relevant gene *Nrl*[39].

In this chapter, the 154 bp rod cell-specific hPDE6B promoter identified in Chapter 3 will be used to drive expression of SaCas9 or dSaCas9.KRAB in a single AAV gene therapy construct. The EGFP-targeting gRNA F10 identified in Chapter 4 is able to drive EGFP knock down in vitro using both CRISPR/Cas9 and CRISPRi, and will be used to target EGFP in the Nrl-EGFP mice. Following subretinal injection of the CRISPR/Cas9 or CRISPRi AAV, EGFP knock down will be measured with TIDE analysis,

qPCR, and mean grey value of fluorescence confocal scanning laser ophthalmoscopy (cSLO) images.

6.2 Materials and methods

6.2.1 Cloning hPDE6Bp.SaCas9 and hPDE6Bp.dSaCas9.KRAB plasmids

The general details of molecular cloning are given in 2.1.10. Cloning of gRNAs into the plasmids are detailed in 2.1.11. The short version of hPDE6Bp (shorthPDE6Bp, described in Chapter 3) was PCR amplified from HEK293-EGFP DNA using KOD polymerase. To ensure the sequence between the ITR and the start of the promoter is the same in this plasmid as in the SaCas9 plasmids validated in Chapter 4, the forward primer contains a 19 bp overhang consisting of an Xba*I* overhang and a 12 bp sequence of the region between the ITR and CMV promoter in SaCas9. The reverse primer contains a Nco*I* restriction site on the 5' overhang. Primer sequences are given in Appendix 9.1.1. The PCR product was run through a PCR purification kit (QIAGEN) and sent for Sanger sequencing. The SaCas9 and dSaCas9.KRAB plasmids contain the CMV promoter flanked by a Nco*I* and Xba*I* restriction site. The plasmids and the hPDE6Bp PCR product were digested with Nco*I* and Xba*I*. The plasmid products were run on an agarose gel and the backbone (not containing the CMV promoter) was gel extracted (QIAGEN). The backbone and digested hPDE6Bp were then ligated together.

6.2.2 AAV production

The production and SDS PAGE of AAV are detailed in 2.3.1 and 2.3.2, respectively. The details of the AAV capsids and contents are detailed in Table 2.6.

6.2.3 Cell line transfection and transduction

The general protocols for cell maintenance, transfection, and transduction are given in sections 2.2.1, 2.2.5, and 2.2.6, respectively. The specific seeding densities and plasmid transfection quantities used in this chapter are given in Table 6.1.

6.2.4 Subretinal injections

The subretinal injections were conducted as described in 2.4.2. Nrl-EGFP mice were injected at 5-6 weeks old with 1.5 µl of diluted virus. The AAV conditions were split as evenly as possible between male and female mice and within litters to control for inter-mouse variables. In the pilot experiment and the dose response experiment, one eye was injected with an F10 construct and the other eye was injected with its corresponding scram control. Statistical analyses were done as paired analyses, comparing the knock down or gene expression between the left and right eye (and therefore between gRNAs F10 and scram) of each mouse. In mice with only one acceptable injection, that eye was used for sectioning and IHC analysis. Any eyes with subretinal bleeding, AAV reflux, or moderate bleeding elsewhere (such as epiretinally), were excluded from analysis.

6.2.5 Retinal imaging with cSLO and OCT

The mice were anaesthetised as described in 2.4.1. 1 % Tropicamide and 2.5 % phenylephrine hydrochloride were applied to the eyes as drops in succession to dilute the pupils, and they were left on for 3 min each. The required eye was treated with a drop of 0.3 % hypromellose solution and a contact lens (3.2 mm diameter, 1.7 mm back optic zone radius, 0.4 mm central thickness and plano refractive power) was applied. The other eye was treated with a carbomer gel to prevent corneal drying. The mouse was placed on a custom platform on the chin rest of the Spectralis ophthalmic imaging platform (Heidelberg Engineering, 55° camera lens) and angled to ensure the pupil aligned with the camera. The automatic real-time functionality was used when acquiring images. This function takes and collates multiple images while tracking the eye, creating an average composite to

Table 6.1 Details of cell transduction experiments conducted in Chapter 6.

Figure	Cell line	Seeding density	Plasmid copy number transfected	Viral particles transduced
Figure 6.2	HEK293T	$5x10^5$ cells/well (12 well plate)	$1.05x10^{11}$	N/A
Figure 6.3B	Y79	$1.375x10^5$ cells/well (96 well plate)	N/A	$2.75x10^9$

compensate for any movement, such as those caused by the mouse breathing. The camera was focused on the retina, setting the focal depth at the point with the highest near infrared reflectance (believed to indicate the retinal pigment epithelial layer is in focus). The angle was adjusted to ensure the infrared reflectance brightness was consistent across the retina, indicating the camera is viewing the retina centrally. Images were captured using the near-infrared reflectance channel, the blue auto fluorescence channel, and the indocyanine green angiography channel for 790 nm autofluorescence. The blue auto fluorescence channels images EGFP expression using a 486 nm blue diode excitation laser and a 500 nm barrier filter, and the indocyanine green angiography channel uses a 790 nm diode laser. The images were taken at a range of brightness settings to ensure the same setting could be used consistently between samples without having image overexposure. The indocyanine green angiography channel was set to the highest exposure. OCT images were taken across the width of the retina at eight equally spaced radially oriented scans centred on the optic disc.

6.2.6 Mean grey value of cSLO images

To quantify EGFP expression in the retina, the mean grey value of the blue auto fluorescence channel image was calculated in the superior of the retina and the inferior of the retina. The image was opened in ImageJ and a macro was run which was developed within the research group. Firstly, the images are processed with a Gaussian blur to smooth the pixels, then a superior and inferior region of interest are selected which are semi-circle shapes avoiding the optic nerve (Figure 6.1). Then the mean grey value of the regions of interest are calculated. The macro is given in Appendix 9.8, and was provided by Dr Lewis Fry, a fellow DPhil student member of my research group.

6.2.7 Calculating photoreceptor layer thickness using OCT images

The photoreceptor layer thickness was measured using the callipers in the Spectralis software. The photoreceptor layer was measured from the top of the outer plexiform layer to the bottom of the

outer photoreceptor segment layer (Figure 6.8B-C). The photoreceptor layer thickness was measured 2500 µm from the optic nerve both superiorly and inferiorly. For each eye, three scans were measured: the scan that passes through the site of the subretinal injection bleb, and the scan either side of this.

6.2.8 Retinal sectioning

Where unspecified, retinas were harvested and fixed for sectioning as described in 2.4.3 and 2.5.1, respectively. In the "5 min fixation" samples, the incubation in 4 % formaldehyde was reduced from 30 min to 4 min. This 4 % formaldehyde step was skipped when the samples were required unfixed. If the samples were treated with superglue, the eyes were placed on a petri dish with the lens facing down. A pipette tip was used to transfer 2 µl superglue to the sclera and to spread it evenly. It was left for 2 min to dry then dissected as usual[217].

6.2.9 Immunohistochemistry (IHC)

Where unspecified, IHC was conducted as described in 2.5.2. Heat-mediated antigen retrieval was performed after the slides were initially washed in PBS. Tris-EDTA was heated to either 60 C or 100 C in a slide container and placed inside a water bath set to the same temperature. The slides were added and incubated for 20 min (at 100 C) or overnight (at 60 C). Following this, the cells were washed in PBS for 5 min 3 times then the IHC protocol continued from the permeabilisation in 0.2 % triton-X 100 step. Following IHC the slides were imaged by confocal microscopy as described in 2.5.3.

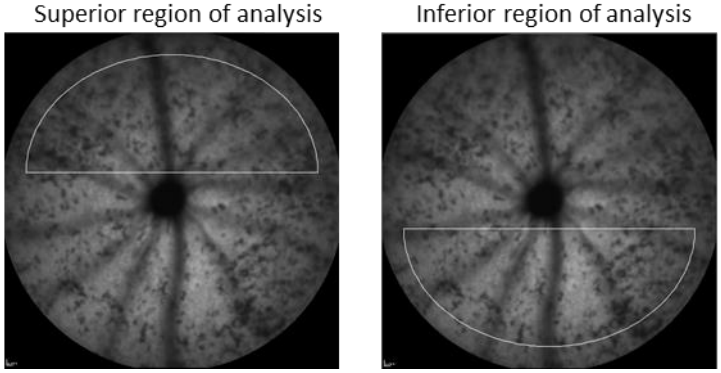

Figure 6.1 The superior and inferior regions of the cSLO images analysed for mean grey value calculations.

6.2.10 Extraction of DNA, RNA, small RNA and protein from a single sample using a modified Allprep extraction kit

DNA, RNA, small RNAs (RNAs between 18-200 bp), and protein were extracted from a sample using the Qiagen AllPrep kit with a modified protocol to allow extraction of small RNA molecules under 200 bp. The small RNA extraction procedure was taken from the Qiagen supplementary protocol RY38, but used the RNeasy spin columns in place of the RNeasy MinElute spin columns. This modified allprep protocol was used when extraction of gRNAs was required. DNA and RNA were extracted following the kit's instructions. Small RNAs were then extracted from the flow-through as follows:

1. Centrifuge the flow-through from the RNA extraction at full speed for 10 min.
2. Transfer the supernatant to a new tube. Discard the tube containing the pellet.
3. Add 1 volume of 100% ethanol. Pipette mix.
4. Transfer up to 700 µl of sample to the RNeasy spin column used for RNA extraction. Centrifuge at 8000g for 15 s.
5. Transfer the flow through to a new 2 ml collection tube. Set this aside for protein extraction.
6. Repeat steps 4 and 5 until all the solution has passed through the column
7. Place the spin column in a new 2 ml collection tube. 500 µl RPE added to the column. Centrifuge at 8000g for 15 s.
8. Discard flow through. 500 µl 80% ethanol added to the spin column. Centrifuged at 8000g for 2 min.
9. Discard flow through. Transfer the spin column to a new collection tube. Centrifuge at full speed for 5 min with the lid open.
10. Transfer the spin column to a 1.5 ml collection tube. Add 14 µl RNase-free water to the column. Centrifuge at full speed for 1 min.
11. Reapply the flow-through to the column. Centrifuge at full speed for 1 min. Store at -20 C.

Protein extraction was then conducted following the kit's instructions using the flow through from

step 5. 5 % SDS was used as a final protein buffer instead of buffer ALO.

6.2.11 Protein extraction from mouse retina

The neural retina was thawed on ice. 50 µl RIPA buffer (Thermo) was added to the retina, it was lysed using a hand-held homogeniser, and then the samples were incubated on ice for 30 min. Samples were centrifuged at 10 000 G at 4 C for 20 min then the protein-containing supernatant was transferred to a new tube.

6.2.12 TIDE analysis

TIDE analysis was conducted as described in 2.1.2 with the primers listed in Appendix 9.1.3.

6.2.13 Subcloning analysis

Subcloning analysis was conducted as described in 5.2.3, with the primers detailed in Appendix 9.1.3. As the amplified region could be sequenced by Sanger sequencing from either direction, the orientation of the insert was not determined by digestion prior to sequencing. The “T7 promoter” primer was used for sequencing in every case.

6.2.14 qPCR

RNA was extracted from Y79 cells and retinas using a modified version of the AllPrep extraction kit (detailed in 6.2.10), or using the RNeasy Mini Kit (Qiagen), and cDNA synthesis was performed using the SuperScript III First-Strand Synthesis Kit (Invitrogen) with the modified protocol for gRNA (see 2.1.4). qPCR was conducted using Taqman probes (see 2.1.5). EGFP, SaCas9, dSaCas9, dSaCas9-KRAB and gRNA levels were expressed relative to human or mouse beta-actin levels.

6.2.15 Western blot

Protein was extracted from samples using either the Allprep extraction kit detailed in 6.2.10, or following the protocol described in 6.2.11. Western blot was conducted as described in 2.1.8 with the anti-SaCas9 antibody and an anti-mouse beta actin antibody (see Table 2.2). For positive control samples and untransfected samples, protein from HEK293-EGFP cells previously transfected with CMV.dSaCas9.KRAB or CMV.SaCas9.F10, or untransfected from Figure 4.7 were used.

6.3 Results

6.3.1 PDE6B promoter drives SaCas9 and dSaCas9.KRAB AAV constructs in the retina

In order to assess construct functionality and EGFP knock down, in vivo studies required extraction of mRNA, gRNA, and protein to confirm construct transgene expression and measure knock down, and DNA to perform TIDE analysis. To reduce the number of mice used, a protocol was created to allow extraction of all molecules from a single retina. The AllPrep DNA/RNA/Protein kit (Qiagen) extracts DNA, RNA, and protein from a single sample, but RNAs under 200 bp in length, which includes gRNAs, cannot be captured and are lost. An additional small RNA extraction step was modified from a Qiagen supplementary protocol and added to the Allprep protocol. To confirm gRNAs were successfully captured, the modified allprep extraction was first performed on HEK293T cells transfected with the ubiquitously expressing SaCas9 and dSaCas9.KRAB plasmids (see Chapter 4). qPCR confirmed the presence of Cas9 and gRNA transcripts in the Cas9-transfected samples and not the untransfected samples (Figure 6.2). As seen in Chapter 4, Cas9 and gRNA transcript levels were higher in SaCas9-transfected cells than dSaCas9.KRAB-transfected cells (see 4.3.6).

The PDE6B promoter identified in Chapter 3 was cloned into the SaCas9 and dSaCas9.KRAB plasmids,

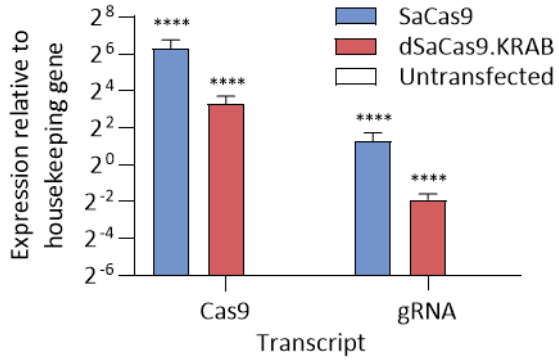

Figure 6.2 Modified Allprep extraction protocol allows extraction of both mRNA and gRNA.
qPCR detects successfully-extracted Cas9 and gRNA transcripts in HEK293T cells transfected with Cas9 plasmids. mRNA and small RNAs were extracted using the modified Allprep extraction protocol, n=3. Two-way ANVOA conducted with factors of gene and plasmid (SaCas9, dSaCas9.KRAB, or untransfected). Effect of gene $F(1, 12)=48.23$ $p<0.0001$, effect of plasmid $F(2, 12)=243.7$ $p<0.0001$, effect of interaction $F(2, 12)=1060$, $p=0.3768$. Multiple comparisons compared expression between SaCas9 or dSaCas9.KRAB with the untransfected control for each gene. SaCas9 Cas9 vs Untransfected Cas9 $p<0.0001$, dSaCas9.KRAB Cas9 vs Untransfected Cas9 $p<0.0001$, SaCas9 gRNA vs Untransfected gRNA $p<0.0001$, dSaCas9.KRAB gRNA vs Untransfected gRNA $p<0.0001$.

driving Cas9 expression. The scrambled gRNA (known henceforth as scram) was driven by the U6 promoter as in previous experiments (see 4.2.7 for gRNA description). These plasmids were used to produce AAV2/8(Y733F) (named AAV.SaCas9.scram and AAV.dSaCas9.KRAB.scram). SDS-PAGE showed the viral preps contained all three expected viral capsid proteins VP1, VP2, and VP3, at 87 kDa, 73 kDa, and 62 kDa, respectively in the concentrated AAV sample (Figure 6.3A). The wash sample of AAV.dSaCas9.KRAB.scram contained faint viral protein bands but these could not be seen in the wash sample of AAV.SaCas9.scram. There were no additional contaminating bands. Following transduction into Y79 cells (which express PDE6B, see Chapter 3), Cas9 and gRNA transcripts were detected, confirming the AAVs are functional (Figure 6.3B). Protein extraction was performed but there was insufficient protein for a western blot.

AAV.SaCas9.scram, AAV.dSaCas9.KRAB.scram, and AAV8.hPDE6Bp.DsRed (see Chapter 3) were subretinally injected into Nrl-EGFP mice at 10^9 genome copies per eye and the retinas harvested 4 weeks post-injection. Cas9 transcripts were detected only in retinas transduced with AAV.SaCas9.scram and AAV.dSaCas9.KRAB.scram, and DsRed transcripts were only detected in retinas transduced with AAV8.hPDE6Bp.DsRed ($p<0.0001$ for all) (Figure 6.4A). Unexpectedly, gRNA transcripts were detected in retinas treated with all three AAV, although there was significantly more gRNA present in the AAV.SaCas9.scram and AAV.dSaCas9.KRAB.scram conditions ($p<0.0001$ for all). This suggests that the gRNA taqman probes may be binding non-specifically to some transcripts

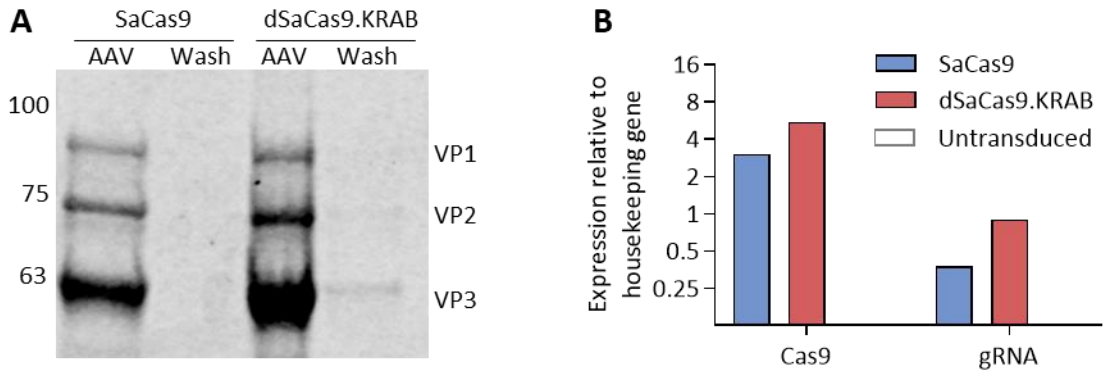

Figure 6.3 Production of scrambled AAV.
A) *SDS-PAGE of AAV.SaCas9.scram (SaCas9) and AAV.dSaCas9.KRAB.scram (dSaCas9.KRAB) viruses showing the three viral capsid proteins VP1, VP2, and VP3.* ***B)*** *qPCR detecting Cas9 and gRNA transcripts in Y79 cells transduced with AAV.SaCas9.scram or AAV.dSaCas9.KRAB.scram. Expression is relative to human beta-actin.*

present in mice, or to the introduced AAV8.hPDE6Bp.DsRed sequence. There were high levels of contamination in this qPCR, with Ct values of 30-35 detected for all three genes in the qPCR no template control. To confirm significant expression of the genes, the statistics were compared to the qPCR no template control as there was no sham-injected condition in this experiment. Despite significant expression of Cas9 transcript, no Cas9 protein could be detected in an AAV.dSaCas9.KRAB.scram sample by western blot (Figure 6.4B).

Transduced retinas were sectioned, and stained using an anti-SaCas9 antibody that has previously been used to detect SaCas9 and dSaCas9.KRAB by western blot and immunocytochemistry (see Figure 4.4, Figure 4.8, Figure 4.9). The secondary antibody was tested at a range of dilutions, from 1/250 to 1/1000 but no expression of SaCas9 was detected (Figure 6.5A). The antibody information sheet recommended performing a heat mediated antigen retrieval step prior to staining, as fixation of tissue with formalin can mask the antibody's epitope and prevent successful staining. Heat mediated antigen retrieval was tested at both 100 C for 20 min and at 60 C overnight, incubating the slides in Tris-EDTA. This caused severe damage to the retinal sections, with the majority of them lost from the slides (Figure 6.5B). The remaining sections lost their retinal pigment epithelial layer and the neural retina was highly folded. The heat treatment caused loss of the native EGFP expression, and SaCas9 remained undetectable. To remove the requirement for heat mediated antigen retrieval, retinas were then processed unfixed or with a fixation time reduced to 5 min. Native EGFP expression was again undetectable in these samples. With no fixation, or reduced fixation, the retinas struggled to hold their shape during sectioning and as a result, the layers of the retina were indistinct from one another, and there was widespread loss of cells. Applying superglue around the outside of an unfixed retina partially improved the sectioning, with DAPI staining showing a more layered-like structure. In this AAV.dSaCas9.KRAB.scram-treated retinal sample, dSaCas9.KRAB was detected with the anti-SaCas9 antibody but the loss of retinal structure made it difficult to understand the level or localisation of expression.

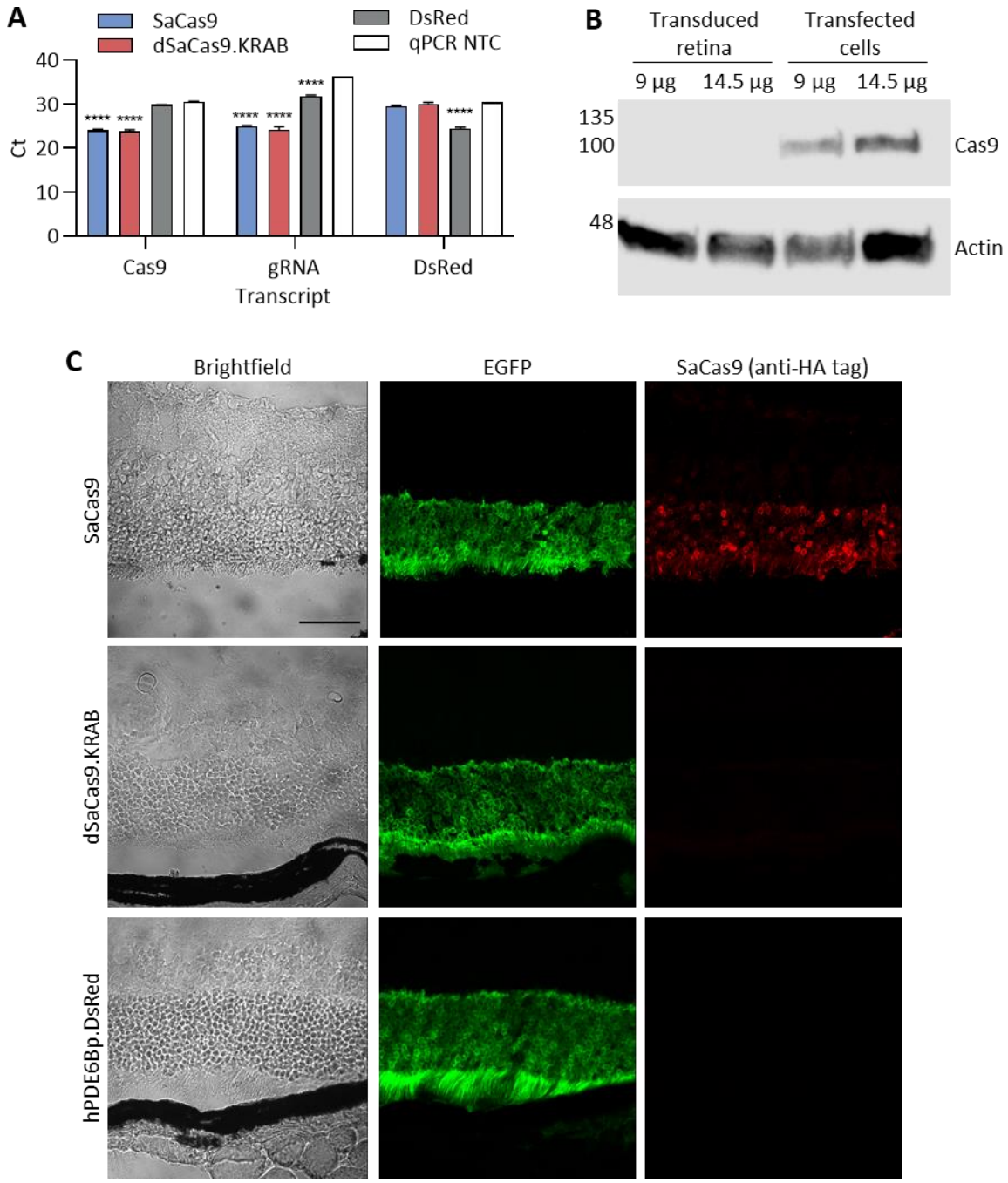

Figure 6.4 Transgene expression following delivery of AAV.SaCas9.scram (SaCas9), AAV.dSaCas9.KRAB.scram (dSaCas9.KRAB) or hPDE6Bp.DsRed (DsRed).

A) *Cas9, gRNA, and DsRed transcripts are detected in transduced retinas. Ct values using Cas9, gRNA, and DsRed probes, n=3 (a lower Ct value indicates greater presence of gene transcripts). NTC is the qPCR no template control. Two-way ANOVA conducted with factors Gene and AAV. Effect of Gene $F(2, 22)=56.07$ $p<0.0001$, effect of AAV $F(3, 22)=333.4$ $p<0.0001$, effect of interaction $F(6, 22)=162.4$ $p<0.0001$. Multiple comparisons compared Ct values for each gene. SaCas9 Cas9 vs qPCR NTC Cas9 $p<0.0001$, dSaCas9.KRAB Cas9 vs qPCR NTC Cas9 $p<0.0001$, SaCas9 gRNA vs qPCR NTC gRNA $p<0.0001$, dSaCas9.KRAB gRNA vs qPCR NTC gRNA $p<0.0001$, DsRed gRNA vs qPCR NTC gRNA $p<0.0001$, SaCas9 gRNA vs DsRed gRNA $p<0.0001$, dSaCas9.KRAB gRNA vs DsRed gRNA $p<0.0001$, DsRed DsRed vs qPCR NTC DsRed $p<0.001$.* ***B)*** *Western blot failed to detect SaCas9 (124 kDa) in transduced retinas. Human beta-actin (also binds to mouse beta-actin)(42 kDa) is a loading control. Protein samples from dSaCas9.KRAB-injected retinas and CMV.dSaCas9.KRAB plasmids-transfected cells loaded at 9 µg and 14.5 µg total protein.* ***C)*** *SaCas9 is detected in SaCas9-transduced retinas with IHC using an anti-HA tag antibody that is absent from the dSaCas9.KRAB and hPDE6Bp.DsRed AAV. Scale bar is 50 µm.*

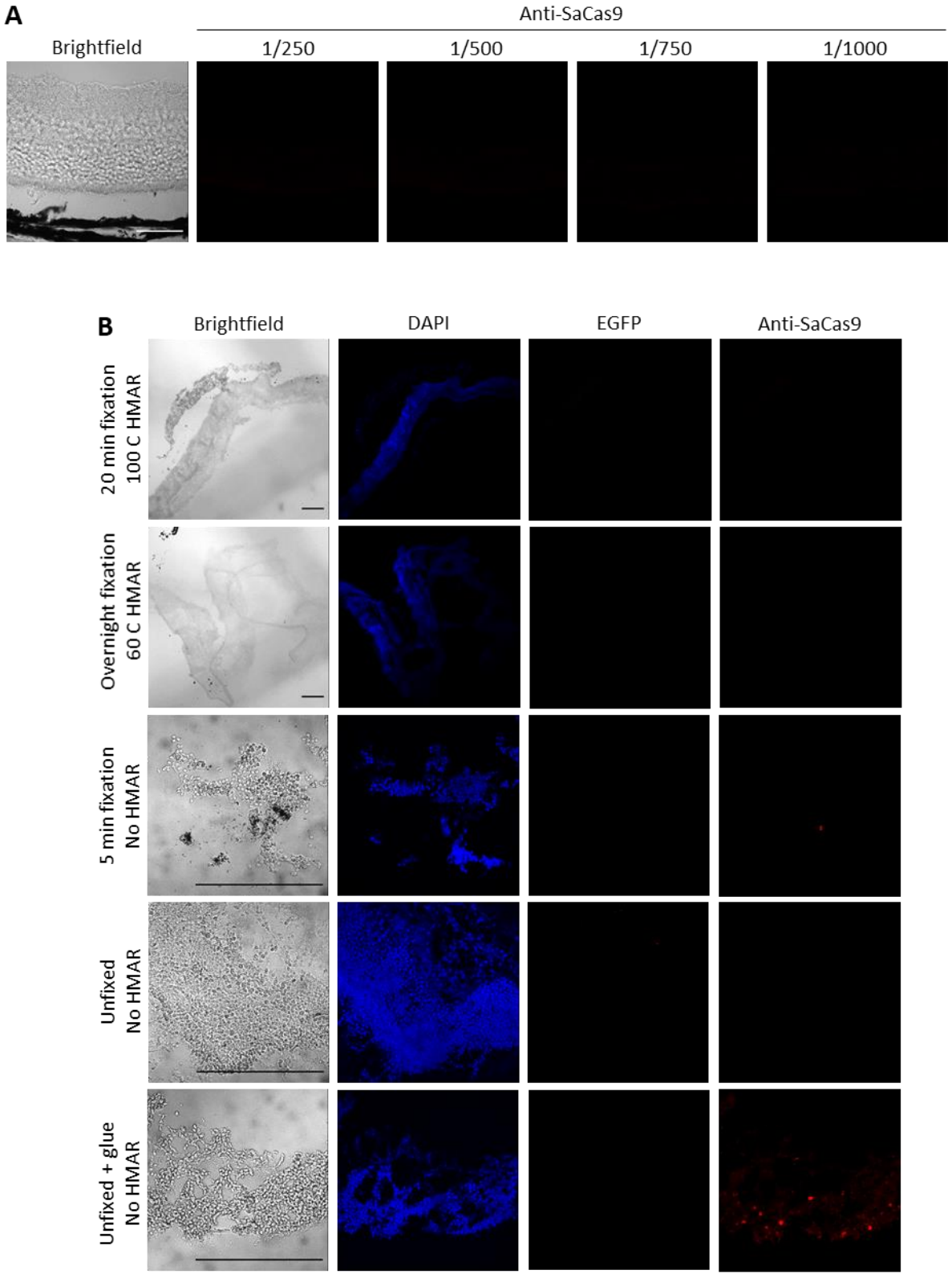

Figure 6.5 IHC optimisation of an anti-SaCas9 antibody.
A) *SaCas9-transduced retinal sections stained with a range of secondary antibody dilutions from 1/250 to 1/1000.* ***B)*** *Testing different methods of retinal tissue fixation and heat mediated antigen retrieval (HMAR) protocols. Scale bars represent 50 µm.*

The SaCas9 sequence contains a HA-tag that can be targeted with an anti-HA-tag antibody. Fixed sections stained with the anti-HA-tag antibody detected the presence of SaCas9 in the photoreceptor layer, with strong expression in the nucleus of the cells (Figure 6.4C). Unfortunately, this HA tag was inadvertently removed from the dSaCas9.KRAB sequence during cloning so this antibody did not bind in dSaCas9.KRAB or hPDE6Bp.DsRed transduced retinas.

Whole-retina images revealed extensive loss of photoreceptor cells in the AAV.SaCas9.scram and AAV.dSaCas9.KRAB.scram-injected eyes (2 eyes of each were examined). This can be seen in both the brightfield images, with loss of the photoreceptor layer emanating from the injection site, and in the EGFP channel, where the loss of rod cells is clear (Figure 6.6A). Later experiments using OCT visually confirmed that the thinning is limited to the photoreceptor layer (Figure 6.8C). SaCas9-expression was detected by immunohistochemistry (using the anti-HA tag antibody) around the area of photoreceptor loss, in a gradient diffusing away from the injection site as expected (Figure 6.6B). In the hPDE6Bp.DsRed-injected retinas there was thinning of the photoreceptor layer near the injection site, but the loss of cells was not as extreme (Figure 6.6A). This implied that the Cas9 AAV may be toxic at this dose, but more replicates were required to understand this effect.

6.3.2 SaCas9 disrupts EGFP in the retina

SaCas9 and dSaCas9.KRAB AAV were generated carrying either the scrambled gRNA or the EGFP-targeting gRNA F10 described in Chapter 4 (referred to henceforth as AAV.SaCas9.F10 and AAV.dSaCas9.KRAB.F10) (Figure 6.7), and using hPDE6Bp to drive Cas9 expression. Mice were subretinally injected with a scram construct in one eye and the F10 construct in the opposite eye for paired analysis, at 10^9 viral genomes per eye. The retinas were harvested at 2 weeks, 3 weeks, and 4 weeks post-injection. Only 1-3 samples were taken for each AAV at week 4 so these were not included in the statistical analysis.

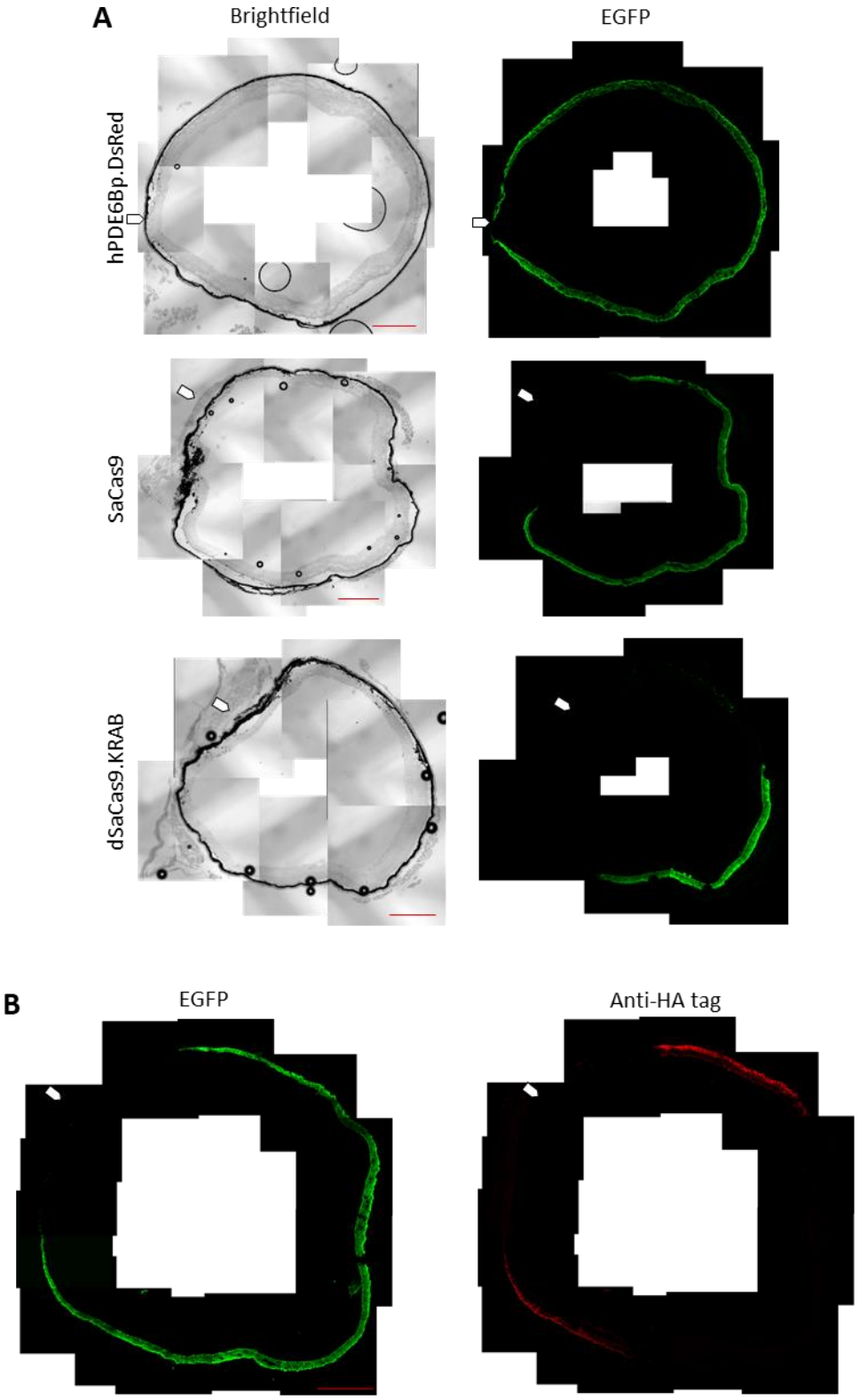

Figure 6.6 Whole retinal images of Nrl-EGFP mice subretinally injected with Cas9 AAV carrying scrambled gRNA.
A) *AAV.SaCas9.scram (SaCas9) and AAV.dSaCas9.KRAB.scram (dSaCas9.KRAB)-injected eyes have widespread loss of photoreceptors, while hPDE6Bp.DsRed injected eyes have thinning of the photoreceptor layer near the injection site.* ***B)*** *AAV.SaCas9.scram-injected retina stained for the HA tag present on SaCas9. Scale bars in red represent 500 µm. The approximate site of injection is indicated with an arrow.*

To investigate photoreceptor loss, the thickness of the photoreceptor layer was measured at each time point using optical coherence tomography (OCT) at both the superior of the eye, where the injection took place, and the inferior of the eye which is the furthest from the injection site (Figure 6.8). The superior photoreceptor layer thickness was significantly reduced (compared to the inferior retinal thickness) by week 2 with AAV.SaCas9.F10 and by week 3 with AAV.SaCas9.scram and AAV.dSaCas9.KRAB.scram ($p=0.0104$, $p<0.0001$, $p=0.0017$). AAV.dSaCas9.KRAB.F10 on the other hand had no significant reduction in superior photoreceptor layer thickness. The photoreceptor loss was not consistent between AAV, with greater loss in both scram AAV. The scram-injected eyes may therefore have fewer EGFP-expressing cells than their F10-injected counterparts, which may mask EGFP knock down. The superior photoreceptor layer thickness decreased between weeks 2 and 3 for AAV.SaCas9.scram and AAV.SaCas9.F10. As degeneration worsens with time since injection and the response is inconsistent between AAV, it was possible that the loss of the photoreceptor layer was due to batch AAV toxicity (possibly caused by the AAV purity varying between batches). Figure 6.8A highlights in orange the samples harvested at week 3 (which were imaged at week 2 and week 3). Although the samples were randomly allocated to their harvesting date, in the AAV.SaCas9.scram condition 5 of the 6 most degenerate retinas from week 2 were harvested at week 3, which may be skewing the week 3 data. If the AAV batch were the sole cause of the photoreceptor degeneration, cell loss would be expected to be more consistent within AAV treatments. Photoreceptor loss within the AAV.SaCas9.scram-, AAV.SaCas9.F10-, and AAV.dSaCas9.KRAB.scram-treated groups ranged from

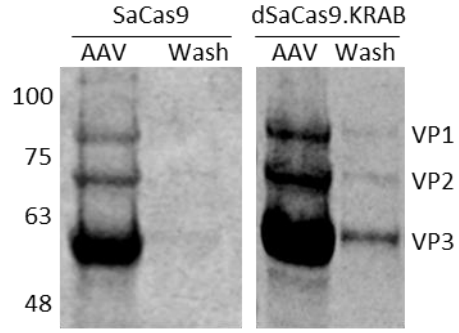

Figure 6.7 Production of F10 AAV.
SDS-PAGE of AAV.SaCas9.F10 and AAV.dSaCas9.KRAB.F10 showing the three viral capsid proteins, VP1, VP2, and VP3.

no degeneration to over 70 % loss of photoreceptor layer thickness.

Following allprep extraction of the neural retinas, Cas9 mRNA was detected across all samples by qPCR, but the Cas9 levels were consistent across the time points examined (Figure 6.9C). There was a significant effect of Cas9 type (p=0.0111) and the interaction between Cas9 and gRNA (p=0.0119) on the level of Cas9 expression, with higher Cas9 visible in the SaCas9.F10-treated retinas than the other retinas. As the initial western blot for SaCas9 in the previous experiment did not produce a band

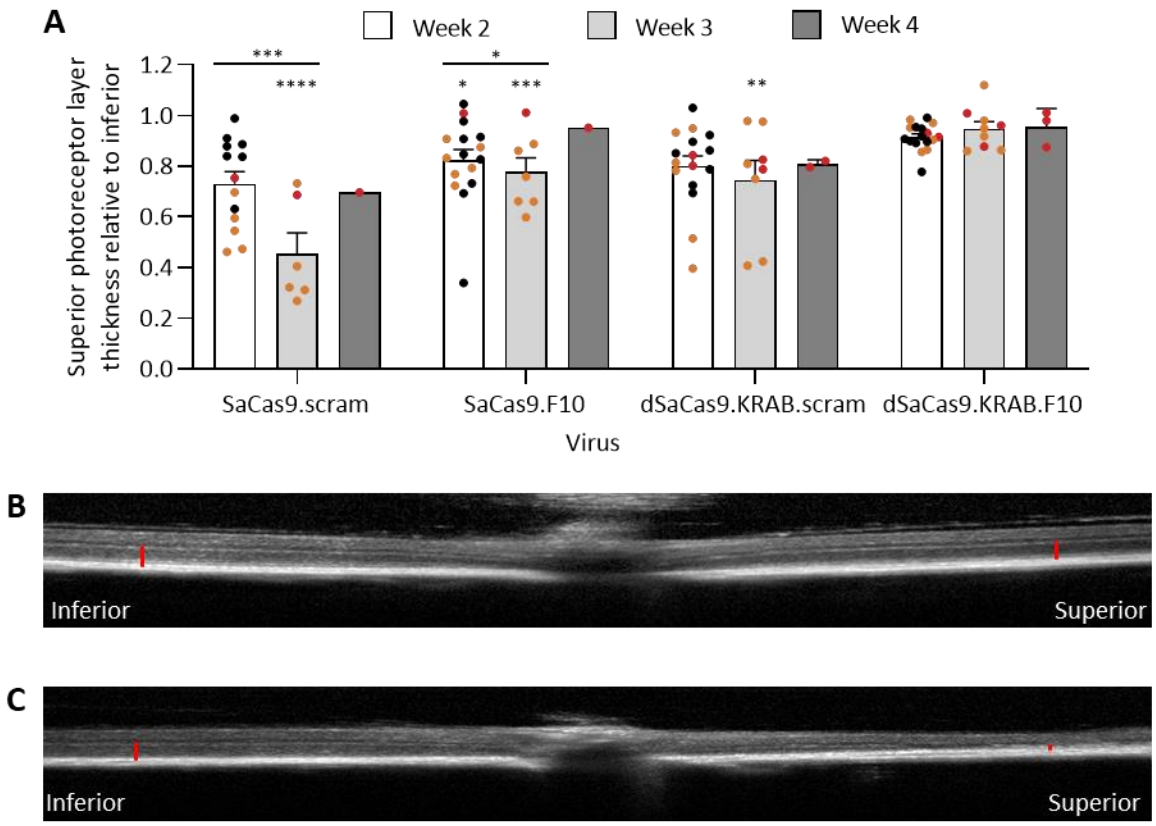

Figure 6.8 Photoreceptor layer degeneration in AAV.Cas9-injected eyes.
A) *Superior photoreceptor layer thickness relative to inferior photoreceptor layer thickness, measured by OCT. Black circles indicate samples imaged and harvested at week 2, orange circles indicate samples imaged at week 2 and 3, and harvested at week 3, red circles indicate samples imaged at week 2, 3, and week 4 and harvested at week 4. Two-way ANOVA compared the superior and inferior photoreceptor layer thickness at the harvesting time point with factors of treatment condition and retinal area. Effect of treatment condition F(1, 110)=82.76 p<0.0001, effect of retinal area F(7, 110)=9.976 p<0.0001, effect of interaction F(7, 110)=4.144 p=0.0004. SaCas9.scram week 3 superior vs inferior p<0.0001, SaCas9.F10 week 3 superior vs inferior p=0.0104, SaCas9.F10 week 3 superior vs inferior p=0.0093, dSaCas9.scram week 3 superior vs inferior p=0.0017. Two-way ANOVA compared the relative superior photoreceptor layer thickness between week 2 and 3 for the samples harvested at week 3 and week 4, with factors of week and AAV. The repeat measures for each retina were paired. Effect of week F(1, 25)=15.52 p=0.0006, effect of AAV F(3, 25)-9.142 p=0.0003, effect of interaction F(3, 25)=7.344 p=0.0011. SaCas9.scram week 2 vs week 3 p=0.0001, SaCas9.F10 week 2 vs week 3 p=0.0451.* ***B-C)*** *Example OCT images of injected retinas. Red line indicates the photoreceptor layer measured.* ***B)*** *Retina without superior degeneration.* ***C)*** *Retina with high superior degeneration.*

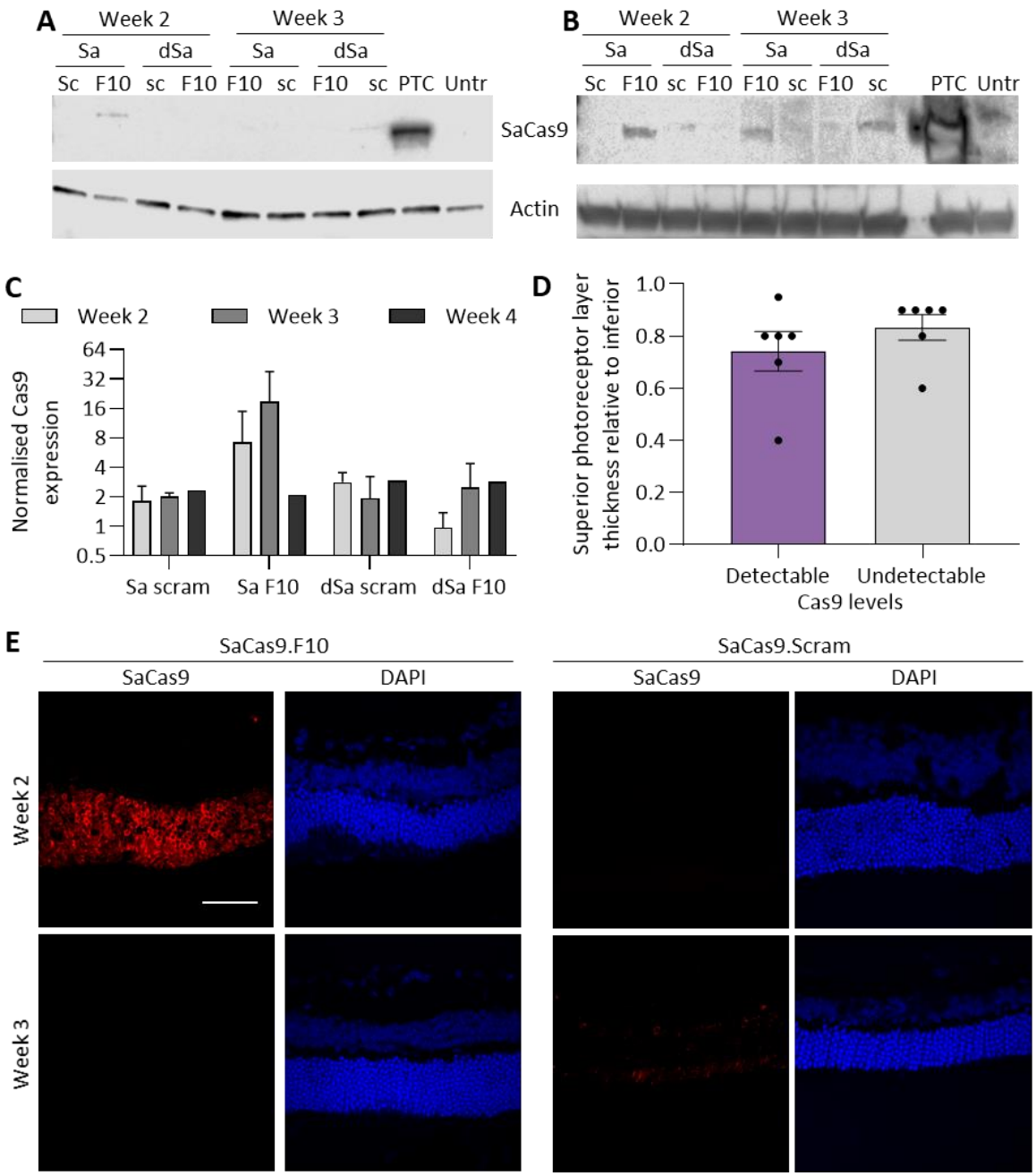

Figure 6.9 SaCas9 expression in transduced retinas.

A-B) *Western blot staining detects SaCas9 and dSaCas9.KRAB (124 kDa for SaCas9, 134 kDa for dSaCas9.KRAB, anti-SaCas9 antibody) in some retinal samples. Human beta actin (42 kDa, also reacts with mouse beta actin) is a loading control. Protein extracted from retinas transduced with AAV.SaCas9 (Sa), AAV.dSaCas9.KRAB (dSa) with the scram (sc) gRNA or F10 gRNA. Positive control (PTC) is protein extracted from HEK293-EGFP cells transfected with SaCas9.F10 plasmid and untransfected (Untr) is protein extracted from untransfected HEK293-EGFP cells.* ***A)*** *10 µg total protein loaded.* ***B)*** *100 µg total protein loaded.* ***C)*** *Cas9 expression normalised to mouse beta-actin, detected by qPCR, n=4. Three-way ANOVA conducted with samples from week 2 and week 3 with factors of Cas9, week, and gRNA. Eyes from the same mouse were paired. Effects of Cas9 ($F(1, 12)=8.982$ $p=0.0111$, effect of week $F(1, 12)=1.772$ $p=0.2079$, effect of gRNA $F(1, 12)=1.829$ $p=0.2012$, effect of Cas9 x week $F(1, 12)=0.8459$ $p=0.3758$, effect of Cas9 x gRNA $F(1, 12)=8.773$ $p=0.0119$, effect of gRNA x week $F(1, 12)=2.812$ $p=0.1194$, effect of Cas9 x gRNA x week $F(1, 12)=0.1417$ $p=0.7312$. Multiple comparisons compared the Cas9 expression between weeks 2 and 3 for each AAV.* ***D)*** *The relative superior photoreceptor layer thickness of the retinas at the date of harvest was comparable between samples with detectable SaCas9 protein using IHC or western blot and samples with undetectable SaCas9 protein, n=6. Unpaired t-test $t(10)=1.013$ $p=0.3347$.* ***E)*** *AAV.SaCas9.F10 and AAV.SaCas9.scram-transduced retinal sections stained with anti-HA tag antibody (binds to SaCas9), and DAPI (stains the nuclei). Scale bar represents 50 µm.*

(Figure 6.4B), one retina from each condition underwent protein extraction exclusively (rather than Allprep extraction) to harvest as much protein as possible. A western blot was conducted for Cas9 using 10 µg and 100 µg total protein (Figure 6.9A, and Figure 6.9B, respectively). Faint Cas9 bands were detected inconsistently, with a band seen in both the SaCas9.F10 samples, and AAV.dSaCas9.KRAB.scram week 3 sample. Detection of Cas9 within the retinal tissue was also inconsistent across samples (Figure 6.9E). Strong retinal expression was seen with AAV.SaCas9.F10 in a week 2 sample, but none was present in the examined week 3 sample. With AAV.SaCas9.scram, weak expression was seen at week 3 but none at week 2. The samples were then classified by Cas9 protein detectability to see if stronger Cas9 expression was linked to photoreceptor degradation. Samples with detectable Cas9 protein by western blot or IHC have comparable photoreceptor layer thickness to samples with no detectable Cas9 protein by these methods (Figure 6.9D).

Disruption of the EGFP DNA sequence was detected by TIDE analysis in the samples treated with AAV.SaCas9.F10 and harvested 3 weeks post-injection (Figure 6.10C). This disruption was low, measuring only 4.1 % compared to 1.8 % with AAV.SaCas9.scram ($p=0.0084$), and there was no significant disruption 2 weeks post-injection. The impact of this editing was assessed at an mRNA level with qPCR and at a protein level, comparing the mean grey value of retinal confocal scanning laser ophthalmoscopy (cSLO) images. qPCR detected a significant 55.3 % reduction in EGFP mRNA at week 2 and week 3 with AAV.SaCas9.F10 ($p=0.0303$ and $p=0.0322$, respectively) but no significant reduction with AAV.dSaCas9.KRAB.F10 (Figure 6.10B). The cSLO retinal images were taken using a 486 nm laser which excites and detects EGFP expression. Mean grey value of cSLO images detected no reduction in EGFP at any of the time points (Figure 6.10A, D). AAV.dSaCas9.KRAB.F10 showed high variability between replicates, with a 46.8 % reduction in mean grey value and a 176.9 % increase in mean grey value measured within the week 3 replicates (n=4).

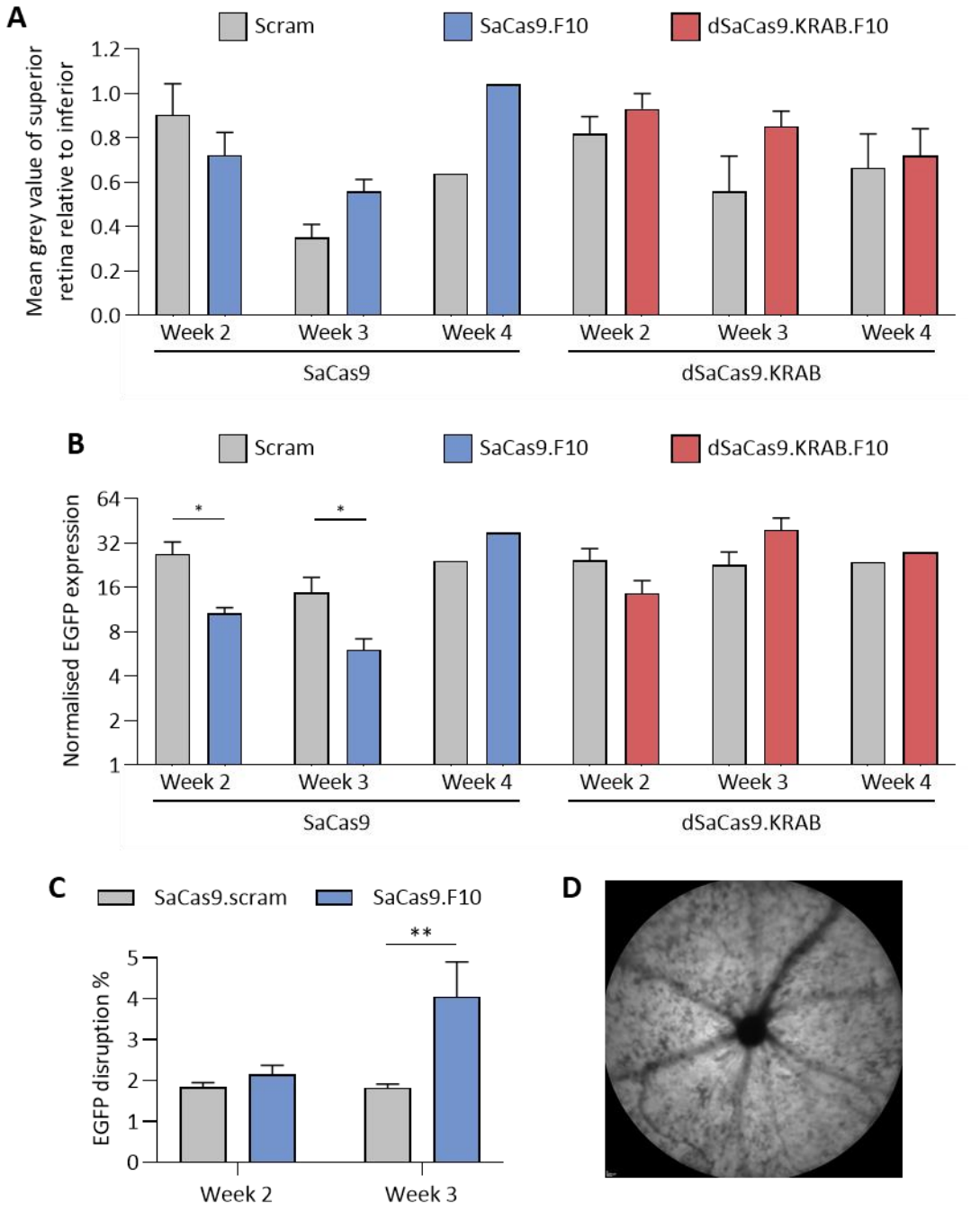

Figure 6.10 EGFP knock down following subretinal injection of SaCas9 and dSaCas9.KRAB AAV with scram or F10 gRNA.

A) *Mean grey value of fluorescence cSLO retinal images is unaffected, n=4. Three-way ANOVA conducted with factors of Cas9, week, and gRNA. Eyes from the same mouse were paired. Effect of Cas9 F(1, 10)=6.574 p=0.0185, effect of week F(1, 20)=18.86 p=0.0003, effect of gRNA F(1, 20)=1.704 p=0.2066, effect of Cas9 x week F(1, 20)=2.428 p=0.1349, effect of Cas9 x gRNA F(1, 20)=1.328 p=0.2627, effect of gRNA x week F(1, 20)=2.987 p=0.0994, effect of Cas9 x week x gRNA F(1, 20)=0.4010 p=0.5337. Multiple comparisons compared gRNA scram and F10 for each condition.* ***B)*** *EGFP transcript level is reduced in AAV.SaCas9.F10-treated retinas at 2 weeks and 3 weeks post-injection (detected by qPCR), n=4. Three-way ANOVA conducted with factors of Cas9, week, and gRNA. Eyes from the same mouse were paired. Effects of Cas9 (F(1, 12)=10.11 p=0.0079, effect of week F9, 12)=0.9292 p=0.3541, effect of gRNA F(1, 12)=0.01203 p=0.9145, effect of Cas9 x week F(1, 12)=37.89 p<0.0001, effect of Cas9 x gRNA (f1, 12)=0.007917 p=0.9306, effect of gRNA x week F(1, 12)=3.532 p=0.0847, effect of Cas9 x gRNA x week F(1, 12)=65.03 p<0.0001. Multiple comparisons compared gRNA scram and F10 for each condition. SaCas9 week 2 scram vs SaCas9 week 2 F10 p=0.0303, SaCas9 week 3 scram vs SaCas9 week 3 F10 p=0.0322.* ***C)*** *TIDE analysis measured disruption of the EGFP gene with AAV.SaCas9.F10*

and 3 weeks post injection, n=4. Eyes from the same mouse were paired. One-way ANOVA compared the disruption between SaCas9.scram and SaCas9.F10 at each time point, with factors of time point and virus. Effect of time point F(1, 12)=4.405 p=0.0577, effect of virus F(1, 12)=7.988 p=0.0153, effect of interaction F(1, 12)=4.643 p=0.0522. SaCas9.scram week 3 vs SaCas9.F10 week 3 p=0.0084. ***D)*** *Example cSLO image taken with the fluorescence channel used for mean grey value analysis.*

6.3.3 SaCas9 AAV dose response

Retinal sections and OCT measurements of photoreceptor layer thickness highlighted that injection of the CRISPR constructs is associated with loss of the photoreceptor layer of the retina, which could be due to toxicity of the AAV. To investigate this further, AAV.SaCas9.scram and AAV.SaCas9.F10 were contra-laterally injected into Nrl-EGFP mice at three doses: 10^8, $5x10^8$ or 10^9 viral genomes per retina. Before injection, each virus was independently titred three times and an average taken to increase the accuracy of the estimated titres. This changed the estimated titre of the AAV, from $1.10x10^{12}$ to $2.29x10^{12}$ genome copies per ml for AAV.SaCas9.scram and from $1.47x10^{12}$ to $7.81x10^{12}$ genome copies per ml for AAV.SaCas9.F10.

Following subretinal injection there was no difference in photoreceptor layer thickness between the AAV or doses (Figure 6.11A). In all conditions, the majority of the replicates had a relative superior photoreceptor layer thickness of over 0.7, with one or two samples associated with higher levels of photoreceptor layer loss. There was no strong correlation in photoreceptor layer thickness between the left and right eye of each mouse, suggesting the photoreceptor loss is not due to mouse-specific factors, such as pre-existing immunity to Cas9 (Figure 6.11B). Injection quality also did not determine the loss of photoreceptors, as both injections with no blood, and those with mild blood, had comparable photoreceptor layer thicknesses (Figure 6.11C). Injections causing blood were only accepted for analysis if the blood did not occur subretinally, and the blood introduction was deemed mild. During cSLO imaging, an image was acquired using the indocyanine green angiography channel, which uses a 790 nm laser that is believed to excite melanolipofuscin molecules in the retinal pigment epithelium. The 790 nm autofluorescence damage was qualitatively characterised as no damage, mild damage, moderate damage, or high damage (Figure 6.11E). Photoreceptor layer thickness decreased

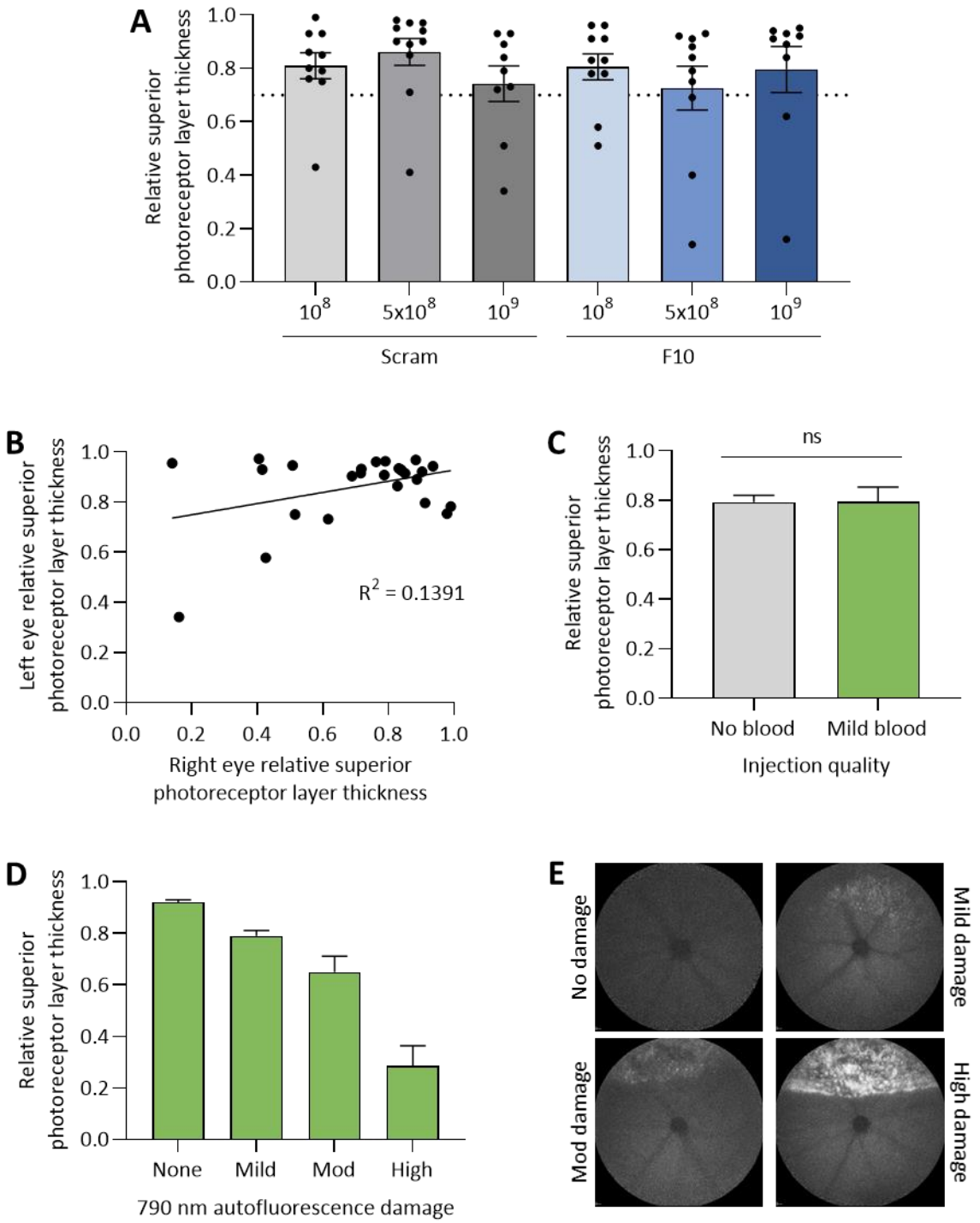

Figure 6.11 Photoreceptor damage following AAV dose response.
Superior photoreceptor layer thickness is expressed relative to the inferior photoreceptor layer thickness. ***A)*** *Superior photoreceptor thickness is consistent following subretinal injection of AAV.SaCas9.scram (Scram) or AAV.SaCas9.F10 (F10) at 10^8, $5x10^8$, or 10^9 genome copies per eye. One-way ANOVA conducted F(5, 53)=0.6057 p=0.6958. n=9-11.* ***B)*** *There is poor correlation between the superior photoreceptor thickness of the left and right eye of each mouse. Simple linear regression R^2=0.1391 p=0.0606.* ***C)*** *Superior photoreceptor thickness is not associated with the presence of subretinal blood. T-test compared the relative superior photoreceptor layer thickness between eyes with no blood and mild blood following subretinal injection, n=54 for no blood, n=5 for mild blood. F=2.367, p=0.9908, ns indicates not significant.* ***D)*** *790 nm autofluorescence images were qualitatively categorized into levels of damage (mod stands for moderate) and the superior photoreceptor thickness compared with a one-way ANOVA F(3, 54)=60.44 p<0.0001, n=28, 18, 8, 4 for conditions none, mild, mod, and high, respectively.* ***E)*** *Example 790 nm autofluorescence images of each categorized level of damage.*

as the 790 nm autofluorescence damage classification increased ($p<0.0001$) (Figure 6.11D).

Increasing dose was associated with an increase in Cas9 expression detected by qPCR ($p=0.0143$), with a 4.4-fold increase in Cas9 mRNA between AAV.SaCas9.scram at 10^8 and 10^9 viral genomes per retina ($p=0.0283$) (Figure 6.12A). This pattern can also be seen in retinal sections, with the fewest SaCas9-positive cells seen at 10^8 and the most SaCas9-positive cells seen at 10^9 genome copies per eye for both AAV (Figure 6.13). SaCas9 could not be detected by western blot when 20 µg of total protein was loaded (Figure 6.12B).

Contrary to the previous experiment, there was no detectable disruption of the EGFP gene by TIDE analysis at any dose, and no detectable knock down of EGFP by qPCR (Figure 6.12F, E). Subcloning was attempted on two AAV.SaCas9.F10 10^9 injected retinas but due to a low cloning efficiency, few colonies were usable. Interestingly, 2/4 clones for one retina showed editing, with a 1 bp mismatch, and a 3 bp insertion present at the predicted cut site (Figure 6.12G). The other retina had no edited reads in the 8 clones examined. Despite the low incidence of editing detected, the gRNA (i.e. scram or F10) had a significant effect on superior retinal fluorescence (measured by mean grey value of fluorescence cSLO images, Two-way ANOVA $p=0.0025$), with a 36.5% reduction in superior retinal fluorescence between AAV.SaCas9.scram and AAV.SaCas9.F10 at $5x10^8$ viral genomes per retina ($p=0.0248$, Figure 6.12C-D).

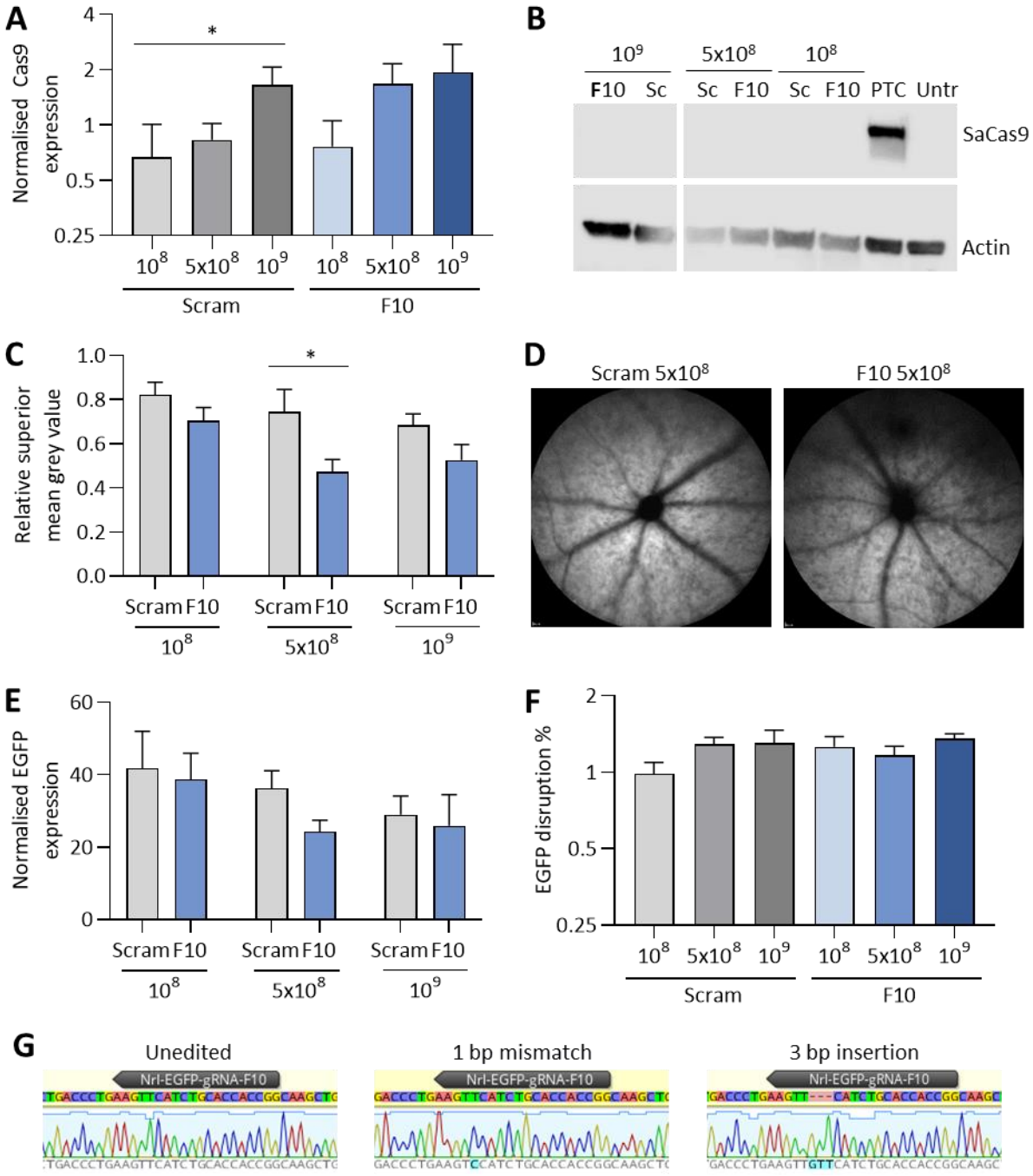

Figure 6.12 Cas9 expression and EGFP knock down following AAV dose response.
Eyes were subretinally injected with AAV.SaCas9.scram (Scram) or AAV.SaCas9.F10 (F10) at 10^9, $5x10^8$, or 10^8 genome copies per eye, n=11 for $5x10^8$, n=10 for 10^8 and 10^9. ***A)*** *Cas9 expression increased with AAV dose. qPCR detecting Cas9 expression normalised to mouse beta-actin. Two-way ANOVA with factors of gRNA and dose. Effect of gRNA F(1, 38)=1.100 p=0.3008, effect of dose F(2, 38)=4.757 p=0.0143, effect of gRNA x dose F(2, 38)=0.4876 p=0.6179. Multiple comparisons compared Cas9 expression at each dose for each AAV. Scram 10^8 vs scram 10^9 p=0.0283.* ***B)*** *Western blot is unable to detect SaCas9 (124 kDa) in transduced retinal samples. Human beta-actin (also binds to mouse beta-actin, 42 kDa) is a loading control. Positive control (PTC) is protein extracted from HEK293-EGFP cells transfected with SaCas9.F10 plasmid and untransfected (Untr) is protein extracted from untransfected HEK293-EGFP cells. 20 µg total protein loaded.* ***C)*** *Relative superior mean grey value of retinal EGFP image is significantly reduced in F10-treated retinas compared to scram-treated retinas at $5x10^8$. Two-way ANOVA with factors of gRNA and dose. Effect of gRNA F(1, 22)=11.68 p=0.0025, effect of dose F(2, 22)=0.0491, effect of gRNA x dose F(2, 22)=0.7709 p=0.4747. Multiple comparisons compared scram and F10 for each dose, Scram $5x10^8$ vs F10 $5x10^8$ p=0.0248.* ***D)*** *Example cSLO images of paired eyes injected*

with 5x10^8 AAV particles showing superior EGFP loss in the F10 and not the scram eyes. Neither eye had significant superior photoreceptor loss. ***E)*** *qPCR does not detect EGFP knock down. Expression normalised to mouse beta-actin. Two-way ANOVA with factors of gRNA and dose. Effect of gRNA F(1, 19)=1.615 p=0.2191, effect of dose F(2, 19)=1.507 p=0.2466, effect of gRNA x dose F(2, 19)=0.5768 p=0.5712. Multiple comparisons compared scram and F10 for each dose.* ***F)*** *TIDE analysis measured no disruption of the EGFP gene. One-way ANOVA compared the disruption between Scram and F10 at each dose, with factors of dose and gRNA. Effect of gRNA F(1, 38)=0.5862 p=0.4486, effect of dose F(2, 38)=1.745 p=0.1883, effect of gRNA x dose F(2.38)=1.704 p=0.1955.* ***G)*** *Sanger sequencing traces following subcloning analysis show DNA editing in a retina injected with F10 at 10^9.*

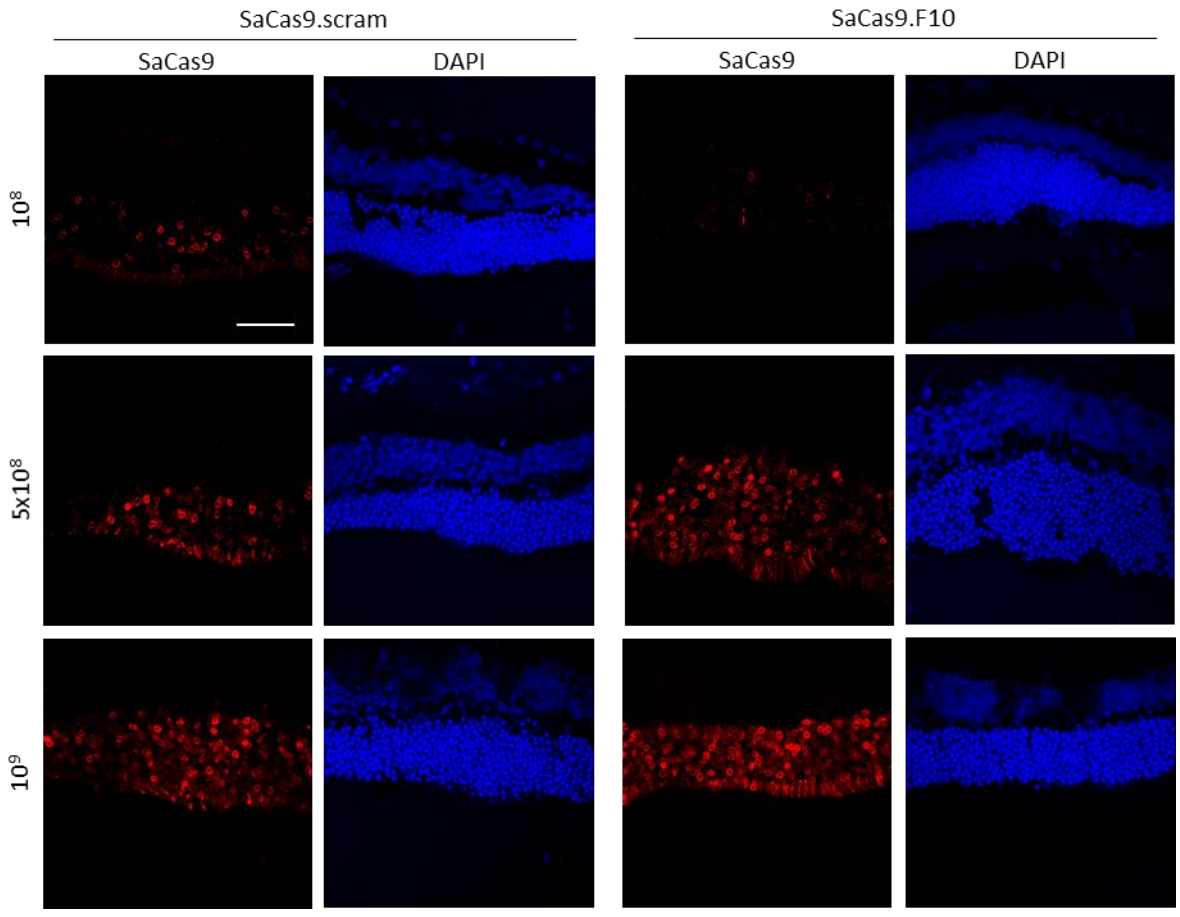

Figure 6.13 Retinal SaCas9 staining increases with AAV dose.
Anti-HA tag antibody binds to SaCas9, and DAPI stains cell nuclei. Scale bar represents 50 µm.

6.4 Discussion

This chapter assessed the ability of the single AAV CRISPR/Cas9 and CRISPRi constructs developed throughout this thesis to suppress expression of a rod cell-specific gene in vivo. CRISPR/Cas9 induced indels into the EGFP sequence, resulting in significant knock down of EGFP mRNA and fluorescence. CRISPRi, on the other hand, was unable to significantly repress EGFP, despite comparable transgene expression. These experiments revealed how the single CRISPR/Cas9 and CRISPRi systems performed within a retina and revealed some challenges associated with these techniques.

6.4.1 Expression of CRISPR transgene

Following subretinal injection of SaCas9 or dSaCas9.KRAB AAVs, the two CRISPR components – Cas9 and gRNA – were detected in the retinal samples, indicating successful transduction. The development of the Allprep extraction protocol allowed TIDE analysis, subcloning, qPCR, and western blot to be conducted on the same retinal sample. Although co-extraction of some molecules, such as DNA and mRNA are possible with the commercial kit, extraction of all four from a single retina has not been previously described. Extraction of multiple molecules typically relies on harvesting separate samples, and therefore the development of this Allprep protocol significantly reduces the number of animals used[165,206,218].

Transcriptional interference between the Cas9 and gRNA components has been highlighted as a potential issue with the dSaCas9.KRAB plasmid construct in Chapter 4. While the level of expression was consistent between SaCas9 and dSaCas9.KRAB AAV, comparisons between the expression levels achieved in vitro and in vivo were not possible due to contamination of the SaCas9 and gRNA taqman primers in the in vivo experiments. This artificially inflates the transcript level relative to the uncontaminated actin control. There was also detection of gRNA in the retinas injected with the control DsRed AAV, suggesting there is non-specific binding of the gRNA primers either in the DsRed

AAV transgene or in the mouse genome. Given both the non-specific binding of the gRNA primers and the primer contamination, future experiments should optimise new qPCR primers.

Detection of SaCas9 protein by western blot had limited success, producing faint bands. Western blots detecting transgenes following AAV subretinal injection have been demonstrated in a range of gene augmentation studies[219–221]. These studies used both cell specific and ubiquitous promoters, and a range of doses from $2.7x10^{10}$ to $1.44x10^{12}$ genome copies per eye, which are all greater than the highest 10^9 dose used in this experiment. Some show strong bands while in others the bands are faint, as seen in this chapter. AAV-driven Cas9 expression in the retina is typically confirmed by IHC or FACS analysis, and to the authors knowledge, retinal Cas9 expression has not been previously confirmed by western blot[38–41,110,218]. Comparison of IHC images between studies is difficult as there are many factors influencing the brightness of a fluorophore in a given image (including sectioning thickness, image depth, and staining protocol among others). The transgene levels are also directly influenced by the strength of the promoter as well as the efficiency of viral infection. Despite this, similar expression was seen in a 2017 paper by Yu et al, who injected the Nrl-EGFP mice with SpCas9 AAV driven by a photoreceptor-specific promoter[39], and saw 11.95% EGFP disruption.

Unfortunately, dSaCas9.KRAB does not contain the HA tags used to detect SaCas9 by IHC. Attempts were made to detect dSaCas9.KRAB with an anti-SaCas9 antibody. This detected low levels of dSaCas9.KRAB if the retinas were processed unfixed but the lack of fixation resulted in poor retinal morphology, and loss of the native EGFP signal due to leakage out the cell membrane[222]. Therefore, the in situ expression profile of dSaCas9.KRAB could not be determined. Levels of Cas9 and gRNA transcript were comparable between the SaCas9 and dSaCas9.KRAB AAV, and dSaCas9.KRAB protein was detected in one sample by western blot, so it is likely that the dSaCas9.KRAB and SaCas9 protein levels are similar but this is unconfirmed.

SaCas9 expression increased with AAV dose: antibody response increased with dose, and a 10-fold increase in dose produced a 4-fold increase in SaCas9 mRNA. It is not surprising that the AAV dose and

SaCas9 transcript levels do not increase linearly, as there are multiple factors influencing the levels of SaCas9 transcript. For example, every AAV is unlikely to transduce a cell successfully, each SaCas9 gene will not be associated with a single SaCas9 transcript, and multiple AAV may enter a single cell, causing the transcriptional machinery to be overwhelmed, and therefore creating a ceiling effect. Analysis of the number of AAV transgenes in the retinal cells was not conducted and this analysis would have provided more insight into the relationship between dose, transduction, and transgene expression[165,218]. In the initial in vivo experiment, detection of SaCas9 by western blot and IHC was more successful in SaCas9.F10-injected eyes than other eyes. qPCR revealed these retinas had higher levels of SaCas9 mRNA. The SaCas9.F10 and SaCas9.scram AAV were subsequently re-titred, and estimated to be 5.3-fold, and 2.1-fold more concentrated than initially believed. If accurate, this may explain why SaCas9.F10 had greater levels of SaCas9 mRNA and protein, as it was initially injected at $5.3x10^9$ genome copies per eye (whereas SaCas9.scram was injected at $2.1x10^9$ genome copies per eye).

6.4.2 Retinal damage

Severe loss of the photoreceptor layer following subretinal injection of AAV.SaCas9 or AAV.dSaCas9.KRAB constructs has been seen throughout this chapter. It was detectable at 2 weeks post injection, increasing by week 3 post injection. Some retinal thinning was observed at the injection site in eyes treated with the control DsRed AAV but this was in line with expected damage following subretinal injection[223,224]. The severe photoreceptor cell loss was associated with increased autofluorescence using a 790 nm diode laser. Light at this wavelength is thought to excite melanolipofuscin granules that accumulate in the retinal pigment epithelial layer. In healthy retinas, melanolipofuscin is generated from retinal pigment epithelial cells phagocytosing photoreceptor outer segments. If the photoreceptors were damaged due to the subretinal injection it is possible this triggered phagocytosis by the retinal pigment epithelium, resulting in increased melanolipofuscin

accumulation, and therefore increasing autofluorescence in these retinas[221,225–227].

The photoreceptor loss was initially suspected to be caused by toxicity linked to the AAV, although a previous study subretinally injected Nrl-EGFP mice with $5x10^9$ genome copies of an AAV carrying SpCas9 and saw no impact on retinal responses by electroretinogram[39]. A 2019 study also injected up to 10^{10} genome copies of a single SaCas9 AAV into the HuCEP290 mouse and did not report any toxicity[228]. Despite the four AAV having similar sequences (differing only by the presence of the KRAB repressor, or the gRNA sequence), there were inconsistencies in cell death when initially injected at 10^9 genome copies per retina. If 10^9 genome copies per retina was close to the toxicity limit of the construct, it is possible that variable AAV titre accuracies may have resulted in some AAV being injected at a toxic dose, and some AAV being injected at a tolerable dose, accounting for the inconsistencies. Following re-titering in triplicate, AAV.SaCas9.scram and AAV.SaCas9.F10 were determined to be 2.1-fold and 5.3-fold more concentrated than initially believed. Following a series of dose response injections between 10^8 and 10^9 genome copies per retina using this new estimated titre, the photoreceptor loss was consistent between doses, accounting for 9.7-22.2 % of injected retinas. If the second titre is taken as accurate, this indicates that AAV.SaCas9.scram and AAV.SaCas9.F10 were initially injected at $2.1x10^9$ and $5.3x10^9$ genome copies per retina. While an increase from 10^9 to $5.3x10^9$ genome copies per eye may confer the difference between a tolerable and toxic dose, such a dramatic change in toxicity between 10^9 and $2.1x10^9$ genome copies per eye for AAV.SaCas9.scram would not be expected. There was also no difference in cell death between samples with detectable and undetectable Cas9 protein levels. Together, these results suggest transgene or AAV toxicity does not fully explain the photoreceptor death seen in this experiment.

Staphylococcus aureus is a common pathogen of humans, and a mouse-adapted strain has been identified that is reported to colonise up to 21 % of specified-pathogen-free laboratory mice sold by commercial vendors[229]. As a result, colonized mice have antibodies against a range of *Staphylococcus aureus* proteins (SaCas9 was not investigated in this study). It is possible that anti-SaCas9 antibodies

could be recruited into the retina following AAV injection, potentially resulting in the destruction of cells expressing SaCas9. While the blood-ocular barrier reduces immune cell recruitment into the retina, barrier breakdown can occur, and post-operative inflammation has been reported following subretinal injection in humans[101–103]. The photoreceptor loss between the left and right eye of each mouse was compared to see if some mice were more susceptible to photoreceptor loss following the Cas9 injection, therefore introducing the possibility that the systemic immune system could be involved. No correlation was identified but it is possible that blood-ocular barrier breakdown, and therefore immune cell introduction, is not consistent between eyes. Due to concerns surrounding adaptive immune responses to Cas9 proteins from common human pathogens, some Cas9 proteins from bacteria that do not colonise human cells have been explored, such as GeoCas9 from *Geobacillus stearothermophilus*.

The introduction of blood into the subretinal space is associated with toxicity and loss of photoreceptors[230]. Any retinas with subretinal blood visible immediately following injection were excluded from the study and no bleeds were observed in the days following treatment. Some injections produced mild ocular bleeds that were included in analysis. These were also determined to be unrelated to the loss of photoreceptors seen in some of the eyes. It is possible, however, that unobserved subretinal bleeds occurred after the mouse was removed from the microscope. These would not be expected to be common, and could account for the random nature of the cell death in the dose response study. If injection quality was related to the photoreceptor layer death, improving operator skill may explain the inconsistencies between experiments as the later experiments (when repetition likely improved injection skill) have fewer eyes with damage.

Unfortunately, aside from the first round of injections with AAV.SaCas9.scram and AAV.dSaCas9.KRAB.scram, subsequent experiments did not include any non-Cas9 control AAV, which would have been useful in determining the likely cause of the photoreceptor death. Inclusion of an uninjected, PBS-injected, and AAV8.hPDE6Bp.DsRed at a range of matching doses would have allowed

the impact of injection, transgene toxicity, and AAV particle toxicity to be investigated more thoroughly. Future work should also aim to include higher doses of AAV to identify doses of definitive toxicity.

6.4.3 In vivo knock down compared to other studies

The single CRISPR/Cas9 AAV was able to significantly knock down EGFP, producing 4.1 % indels, and 55.3 % and 36.5 % reduction in EGFP mRNA and fluorescence, respectively, in various experiments in this chapter. CRISPR/Cas9 has driven significant retinal gene disruption in a number of studies with varying methodologies[38,39,41,70,188,218,228,231]**.** Two studies have delivered an all-in-one AAV.SaCas9 in the retina with contrasting success. Chung et al. (2020) delivered SaCas9 as a single AAV and SpCas9 as a dual AAV targeting VEGFA into wild type mice. Both constructs had similar transduction efficiencies, with Cas9 detected in all layers of the retina. Despite this, they measured 2.1 % gene editing and no protein knock down with SaCas9, but 22.5 % editing, and 27 % protein knock down with SpCas9[218]. Maeder et al (2019) also used a single AAV strategy in the Leber Congenital Amaurosis mouse model HuCEP290[228], delivering SaCas9 and two gRNAs targeting the pathogenic mutation in CEP290. They achieved up to 94 % editing[232]. There are important methodological differences between the experiments presented in this thesis and these two key papers (Table 6.2). Both this thesis and Maeder et al (2019), targeted photoreceptors and detected CRISPR editing, with Maeder et al (2019) using a photoreceptor-specific promoter but aiming to edit cone cells. Chung et al. (2020) on the other hand, unsuccessfully targeted the retinal pigment epithelium. The method of measuring knock down has been shown to influence the estimated knock down rate throughout this thesis (See 7.2.2), and this varied between studies. Maeder et al. (2019) analysed only the successfully transduced cells, resulting in a high editing rate, whereas in this thesis, the entire neural retina was analysed. As most of these cells do not express Cas9 (either because the AAV did not transduce the cells or the hPDE6Bp is not active in them), this dilutes the estimated editing rate.

Table 6.2 Key experimental features of studies using a single AAV to deliver SaCas9 CRISPR/Cas9 gene editing in the retina.

Paper	Target gene	Target cell	Promoter	Mouse age	Mouse line	Vector dose gc/retina	Harvesting timepoint	Editing rate	DNA analysis method
Thesis	EGFP	Rod cells	hPDE6Bp (rod cell-specific)	6 weeks	Nrl-EGFP	10^8-10^9	2-4 weeks post injection	4.1 % editing 53 % mRNA reduction	DNA extracted from neural retina. TIDE analysis.
Maeder et al. (2019)[215]	CEP290	Cone cells	hGRK1 (photoreceptor -specific)	6-12 weeks	HuCEP290	10^8 -10^{10}	3 days to 9 months post injection	94 % editing	DNA extracted from GFP positive cells (transduced). UDiTas sequencing.
Chung et al. (2020)[229]	VEGFA	RPE	CMV (ubiquitous)	6-8 weeks	C57BL/6J	$4x10^{11}$	6 weeks post injection	2.1% editing	DNA extracted from RPE-choroid. Deep sequencing.

CRISPR/Cas9-mediated EGFP disruption in this Nrl-EGFP mouse line was previously demonstrated in a 2017 study[39]. Yu et al. subretinally injected two AAV into 2-week-old Nrl-EGFP mice: the first AAV expressed SpCas9, and the second AAV expressed the reporter gene TdTomato and an EGFP-targeting gRNA. Both SpCas9 and TdTomato were driven by the human rhodopsin kinase promoter, limiting expression to the photoreceptors. 2.5 months after subretinal injection, 11.95 % indel formation and 30 % reduction in EGFP-expressing cells were measured in the TdTomato-positive cell population. They calculated high levels of overall transduction, with 66.6 % of cells expressing TdTomato.

CRISPRi using AAV.dSaCas9.KRAB was unsuccessful in vivo and was unable to knock down EGFP in this chapter. CRISPRi EGFP knock down in this mouse line has previously been achieved by Moreno et al. (2018)[188]. They subretinally injected a dual AAV delivering split *Streptococcus pyogenes* Cas9 and a gRNA targeting the *Nrl* promoter, into the Nrl-EGFP mouse line. This reduced *Nrl* expression by 50 %, which was associated with reduced EGFP in the treated areas on sectioned retinas. AAV.dSaCas9.KRAB has been used successfully in vivo in other research. Thakore et al (2018) delivered dSaCas9.KRAB and *Pcsk9*-targeting gRNA in separate AAVs and injected them into the tail vein of a wild type mouse[165]. 6 weeks post-injection, a roughly 50 % reduction in *Pcsk9* mRNA in the liver and an 80 % reduction in Pcsk9 serum protein levels were recorded.

6.4.4 Measuring EGFP knock down

Significant in vivo CRISPR/Cas9-driven EGFP disruption was measured by TIDE analysis, subcloning, qPCR, and fluorescence SLO but the outcome was inconsistent between experiments and between techniques. As found by previous studies, the knock down in vivo was lower than that the knock down in vitro[165,188,233]. In the initial EGFP-targeting experiment, TIDE analysis detected EGFP disruption of 4.1 % at week 3 but none at week 2. Despite this, a 55.3 % reduction in EGFP transcript was detected by qPCR at both week 2 and week 3 post injection. In the dose response experiment, no samples had significant EGFP disruption by TIDE analysis but there was a significant reduction in retinal

fluorescence using AAV.SaCas9.F10 at $5x10^8$ genome copies per retina. While EGFP expression is produced exclusively in the target rod cells, the EGFP gene is present in all cells in the retina, and therefore EGFP disruption measured by TIDE analysis would be expected to be lower than measures of EGFP knock down. Interestingly, subcloning analysis identified edited reads in 2 out of 12 analysed clones (from two retinas) injected at 10^9 genome copies per retina despite TIDE detecting no editing. Inconsistency of editing rates and knock down between techniques has been documented in other retinal CRISPR experiments[41,234]. Following plasmid electroporation, Giannelli et al (2018) measured 28 %, 77 %, and 88 % editing rates in transduced cells using the T7E1 assay, TIDE analysis, and subcloning, respectively[41]. Following dual AAV transduction in the Nrl-EGFP mouse line, Yu et al. (2017) measured indels at 12 % but a 30 % reduction in EGFP-expressing cells[39]. In vivo CRISPRi studies have also reported discrepancies between knock down techniques. Thakore et al. (2018) targeted *Psck9* in the liver using a dual AAV-delivered dSaCas9.KRAB. They recorded a 50 % reduction in mRNA levels but 80 % reduction in protein levels[165].

The techniques used to measure EGFP expression were qPCR and mean grey value of fluorescence cSLO images. Both these measurements are reduced if the number of total rod cells are reduced. The photoreceptor loss seen in these experiments can therefore appear as EGFP knock down. This is a particular issue when measuring fluorescence by cSLO images as removal of the rod cells removes the fluorescence. The inconsistency of the photoreceptor loss throughout the replicates in the initial cohort, and the high levels of cell death in the AAV.SaCas9.scram condition may explain why there was significant knock down by qPCR but not by mean grey value of fluorescence cSLO images. Furthermore, accurate retinal imaging is a complex process which requires development of high levels of skill. The fluorescence is influenced by the angle of the camera relative to the retina, and the pupil area among other factors[227]. As the superior retinal mean grey value is normalised relative to the inferior retina, this controls for many eye-specific factors, such as the pupil area. The angle of the camera, however, can influence the measured fluorescence in different regions of the retina, even if they have comparable levels of EGFP activity. While attempts were made to ensure correct imaging

of the retina, variations in imaging quality between samples may mask a treatment effect.

Given the significant knock down measured by qPCR and fluorescence cSLO, the low levels of EGFP disruption by TIDE analysis were surprising. AAV-driven retinal gene disruption with CRISPR/Cas9 has been used to target a range of genes, with in vivo disruption rates frequently measuring 10-40 %[39,110,218]. In most retinal CRISPR studies, a selection method is used to ensure only the transduced cells are analysed. This is typically fluorescence-activated cell sorting, selecting cells expressing a transgenic marker or reporter gene. The effectiveness of cell selection was highlighted by Giannelli et al[41]. They intravitreally-injected mice with two AAV: one containing SpCas9, and the other containing gRNA and a GFP reporter. Even with selection of GFP-expressing cells, they only detected 9.6 % editing, but when selecting cells expressing high levels of GFP, the editing rate increased to 48.9 %.

6.4.5 Improving EGFP knock down - future research

DNA editing and gene knock down were detected in these in vivo experiments, and multiple strategies can be explored to try to improve the CRISPR editing rates. As the photoreceptor cell death observed here does not appear to be related to dose, higher doses may improve the CRISPR/Cas9 gene disruption and CRISPRi gene repression. Both published retinal studies using a single SaCas9 AAV tested higher doses than were explored in this thesis but did not see significant improvements. Chung et al. (2020) injected $4x10^{11}$ genome copies per eye (400 times more than the highest dose used in this chapter) of AAV.SaCas9, but saw no editing[218]. Maeder et al. (2019) tested doses of 10^9 and 10^{10} AAV particles per eye and found they had comparable editing rates of approximately 20 %[228].

Later time points may be associated with greater editing and knock down. AAV transgene expression following subretinal injection, and CRISPR/Cas9 gene disruption of exogenous genes, have been reported to increase over 4 weeks post injection[133,235]. Following these studies, the latest time point analysed in this chapter was 4 weeks. Significant knock down in this mouse model has been documented at 2.5 months and 23 days post injection using CRISPR/Cas9 and CRISPRi,

respectively[39,188]. Maeder et al. (2019) measured the indel rate for 9 months following subretinal injection of a single SaCas9 AAV into a mouse model of Leber Congenital Amaurosis[228]. At 10^{10} viral genomes per eye the editing rate peaked at approximately 2 weeks post injection, but with 10^{9} viral genomes per eye (the highest dose used in this thesis), editing rates did not peak until approximately 6 weeks post injection.

Most CRISPR/Cas9 gene editing studies in the retina have focused on using the most common Cas9 species, SpCas9. A key difference between the SaCas9 and SpCas9 strategies is the single vs dual AAV. A single AAV strategy is often preferred as it requires fewer AAV particles and therefore may reduce any potential AAV-related toxicity or immune reactions. Plasmid transcriptional interference has previously been highlighted in this thesis as a limiting factor for CRISPR rates (see Chapter 4). Expressing the SaCas9 and gRNA constructs from separate AAV may reduce transcriptional interference, and allow higher expression of both transgenes. Only two studies using SaCas9 in vivo have used a single AAV strategy, with most using a dual AAV strategy instead[69,165,218,228,233]. Future work should explore the differences in transgene expression and EGFP knock down between a single and dual SaCas9 AAV strategy in vivo.

This chapter explored a single gRNA, F10. This gRNA was selected as it demonstrated knock down with both CRISPR/Cas9 and CRISPRi in vitro, but despite this, the editing rates in the retina were low. As the target-binding regions are the optimal 21 bp length for SaCas9 activity, there are currently no known gRNA modifications to improve CRISPR activity[69]. Other promising gRNAs, such as F15 could be assessed, either individually or in combination with gRNA F10, to increase the likelihood of identifying successful gRNAs candidates in vivo.

Finally, introducing a method of analysing transduced regions would improve the estimation of gene editing efficiency. Although there is not sufficient space to include a selection marker within this single AAV strategy, the neural retina could be physically separated into superior and inferior fragments. These could then be processed individually to allow comparison between the more efficiently

transduced superior retina and the less efficiently transduced inferior retina. Magnetic activated cell sorting with CD73 has been shown to enrich rod cells in a neural retinal cell population[236–238]. By sorting the neural retina, this would reduce the proportion of cells in the analysed population that are unable to express SaCas9, and therefore reduce the dilution effect when measuring DNA editing. Alternatively, EGFP expression in retinal sections could be compared between highly- and poorly-transduced regions[39].

6.4.6 Conclusions

AAV.SaCas9 and AAV.dSaCas9.KRAB were associated with loss of photoreceptors in vivo. The causes are currently unknown and therefore further experiments are required to determine this and identify an optimal dose. Subretinally injected AAV.SaCas9 drives in vivo EGFP disruption. The DNA editing rates measured are low, but are associated with moderate levels of EGFP knock down. Unfortunately, AAV.dSaCas9.KRAB was unable to drive detectable CRISPRi repression of EGFP in vivo. There are many avenues to be explored to increase the level of measured knock down, including assessing only transduced regions, screening additional gRNAs, testing higher AAV doses, testing later harvesting dates, and exploring a dual AAV delivery strategy.

7 Discussion

CRISPR/Cas9 gene disruption and CRISPRi gene repression were first described in 2012 and 2013, respectively. Since its discovery, CRISPR gene editing has revolutionised the field of biology, with applications in the creation of models, the study of gene and protein function, and as potential gene therapies for the treatment of dominant diseases[53,60,239]. Toxic gain-of-function mutations in *RHO* are the most common cause of autosomal dominant retinitis pigmentosa (RHO-adRP), and removal of the mutant RHO protein has been shown to prevent photoreceptor degradation[38,240–243]. This thesis developed a single AAV CRISPR/Cas9 vector that was capable of driving rod cell-specific CRISPR gene disruption in vivo, and explored the possibility of targeting non-pathogenic RHO SNPs for a mutation-independent, allele-specific knock down of RHO.

7.1 hPDE6Bp – a short rod cell-specific promoter

Expressing an AAV gene therapy exclusively in the target cell population increases the safety profile of the treatment, confining the transgene expression and any off-target effects to the diseased cells[109,111]. For a single AAV CRISPR/Cas9 or CRISPRi treatment using SaCas9, a rod cell-specific promoter under 270 bp was required. A shortened 154 bp section of the human PDE6B promoter was isolated and screened with reporter constructs.

This promoter was active in the human retinoblastoma cell line Y79, in human retinal tissue cultured ex vivo, and was rod cell-specific when subretinally injected in mice. It was able to drive strong SaCas9 and dSaCas9.KRAB expression when packaged in a single AAV8(Y733F) construct, resulting in significant CRISPR/Cas9 gene disruption of the rod cell specific EGFP gene in the Nrl-EGFP mouse line.

All known DNA regulatory elements of the hPDE6B gene are included in this shortened promoter so it is expected to retain its native rod cell-specificity in human tissue. Confirming this experimentally would further increase the safety profile of these constructs[117,124]. Retinal specificity could be explored in retinal organoids, which contain rod-like cells which express PDE6B, or in human retinal tissue cultured ex vivo[134,152–154].

The short size of this promoter makes it of interest to other AAV-based strategies targeting rod cells, particularly due to the limited carrying capacity of AAV. Autosomal recessive and X-linked forms of retinitis pigmentosa are candidates for gene augmentation, and replacement gene expression cassettes are typically driven with rod cell-specific promoters[130,244,245]. Other strategies to treat retinitis pigmentosa involve delivering protective factors to the retina which have shown promise in vivo, reducing photoreceptor apoptosis[246–248]. These are often driven by ubiquitous promoter in pre-clinical studies but using a rod cell-specific promoter would limit expression to the target cell type. The shortened hPDE6B promoter has potential application in these therapies, and others targeting rod cells.

7.2 CRISPR gene editing rates

7.2.1 On-target activity

High levels of CRISPR/Cas9 gene disruption and CRISPRi gene repression were measured throughout this thesis. CRISPR/Cas9 gene disruption of endogenous EGFP, VEGFA, and RHO was demonstrated in vitro, with up to 73 % disruption (measured by subcloning) using a RHO-targeting gRNA. CRISPRi was also successful in vitro, repressing luciferase expression by 71 % using a RHO-targeting gRNA. Endogenous EGFP was also targeted with CRISPRi but this was less successful: the greatest reduction in EGFP fluorescence was 26 % in vitro.

In vivo, the single CRISPR/Cas9 AAV was able to knock down EGFP mRNA levels by 53.0 % but the single CRISPRi AAV did not significantly repress EGFP in this experiment. The reasons behind this lack of CRISPRi repression are currently unknown but should be explored in future research. When the mouse EGFP sequence was originally screened for gRNAs, none were predicted to have high binding efficiency, which is likely a limiting factor for CRISPRi rates. This was confirmed by low in vitro knock down of endogenous EGFP compared to CRISPR/Cas9 gene disruption. Throughout this thesis, the most optimal PAM site for SaCas9 – NNGRRT – was used, but significant SaCas9 activity has also been seen using the less stringent PAM NNGRRN[64]. Screening gRNAs with this PAM site may have identified candidates with higher rates of CRISPRi. Other transcriptional repressors have been identified which outperform the KRAB repressor but these are too large for a single AAV strategy. Swapping the KRAB repressor from *KOX1* (used in this thesis) for the KRAB repressor from the *ZIM3* gene may offer a simple method of improving the CRISPRi knock down, as this *ZIM3* KRAB repressor has been shown to outperform the *KOX1* KRAB repressor, and could still be packaged in a single AAV[186]. Inclusion of a previously validated endogenous control gRNA would clarify whether target site selection, or the construct design, was responsible for the low CRISPRi rates.

As discussed in section 6.4.5, there are many avenues of further research that can be explored for improving the CRISPR/Cas9 and CRISPRi gene editing rates in vivo. Other research using SaCas9 in the

retina have explored higher doses of AAV and later harvesting time points, without seeing any detrimental effects of toxicity[218,228]. Screening additional gRNAs with higher in vitro efficiencies would reveal the potential editing range with these constructs. Introducing methods for selection of transduced regions of the retina, or enrichment of the target rod cell population, would also improve the accuracy of the measured DNA editing.

7.2.2 Measuring CRISPR editing

Throughout this thesis the impact of CRISPR editing was measured at multiple levels. This was made possible in vivo due to the development of the modified allprep extraction protocol in Chapter 6, allowing gRNA, mRNA, DNA, and protein extraction from a single retina. Analyses revealed that knock down rates were not consistent between measurements, and highlighted the importance of selecting appropriate analyses. When CRISPR/Cas9 was used to disrupt EGFP, the indel rate was lower than the mRNA reduction and fluorescence reduction both in vitro and in vivo. TIDE is known to underestimate indel rate at roughly 10-20 %[180]. This accounts for the difference between measures of knock down in vitro but not in vivo, in which 4.1 % indels by TIDE analysis were associated with 55.3 % reduction in EGFP transcripts. In the Nrl-EGFP mice, the EGFP transgene is present in all retinal cells but it is only active in rod cells[121]. Due to the hPDE6B promoter, SaCas9 is only transcribed in rod cells. As all the neural retina cells were analysed collectively, the unedited EGFP copies in all non-rod cells may be diluting the estimated editing rate, accounting for the difference between indels and knock down.

Measuring the reduction in protein activity is dependent upon the half-life of the protein of interest. As the half-life of EGFP is approximately 26 hours, EGFP molecules present in the HEK293-EGFP cells before transfection were still contributing to fluorescence at the 48 hour harvesting time point[179]. This issue was absent from the in vivo study as imaging was conducted 2-4 weeks post injection. In vitro, the fluorescence was measured by both fluorescence spectroscopy of extracted protein, and mean grey value of fluorescence images. Despite both measuring fluorescence, the knock down measured

by fluorescence spectroscopy was over 15 % greater than with mean grey value. Although cells were grown as a monolayer, they had begun to overlap considerably by the time of harvest. Setting the laser power or exposure time too high can also result in overexposure. Both of these factors can mask fluorescence knock down using mean grey value.

CRISPR/Cas9 activity at a DNA level was measured by TIDE analysis or subcloning analysis at different points throughout this thesis. In vitro comparison revealed that TIDE estimates approximately 37 % lower editing than subcloning. This discrepancy was also present in vivo. In a dose response experiment, TIDE analysis detected no significant editing at any dose, despite a 36.5 % reduction in fluorescence using the medium dose. Two high dose samples were sent for subcloning analysis and, although this analysis could not be fully completed, indels were detected in 2 out of 12 total clones. To better estimate CRISPR/Cas9 editing rates in retinal DNA, selection for the target cell population or successfully transduced cells should be conducted, and subcloning analysis or deep sequencing should be used.

7.3 Targeting RHO for adRP

Knocking down the mutant rhodopsin protein is a commonly explored strategy for the treatment of RHO-adRP[42]. RHO-targeting strategies are either non-discriminatory, knocking down wild type and mutant *RHO* then introducing a treatment-resistant *RHO*, or they are allele-specific, selectively targeting the mutant *RHO*. Both strategies have demonstrated success, with clinical trials currently ongoing for both an allele-specific antisense oligonucleotide therapy (ClinicalTrials.gov: NCT04123626), and a short interfering RNA knock down and replace therapy[42,44–47]. Knock down and replace strategies can treat more patients as they are independent of the pathogenic mutation, but they must control cellular RHO protein as levels under 50 % and over 200 % are toxic to the retina[38,43]. A CRISPR/Cas9 system developed by EDITAS limits this risk by expressing RHO-targeting gRNAs and the RHO replacement gene in the same AAV, and Cas9 in another AAV[47]. This ensures RHO disruption only occurs in the cells that also express the replacement RHO. Overexpression remains a potential issue, however, as the replacement RHO can be expressed in cells that have not undergone CRISPR editing.

This thesis demonstrated that targeting non-pathogenic SNPs or indels in *RHO* was a viable strategy for achieving allele-specificity with CRISPRi. 14 candidate SNPs or indels were identified in *RHO*, 8 occurred in an SaCas9 gRNA binding region or PAM site, and 2 could be targeted allele-specifically. This strategy is more likely to be feasible with CRISPRi than CRISPR/Cas9 for two reasons. Firstly, CRISPR/Cas9 has greater tolerance of single base pair mismatches than CRISPRi and therefore the gRNAs identified with the CRISPRi luciferase assay may not be allele-specific with CRISPR/Cas9[49]. An enhanced-fidelity version of SaCas9 named efSaCas9 was created in 2020 with a single N260D amino acid change[249]. This species has 2- to 93- fold fewer off-target effects than SaCas9, and may therefore be more effective at discriminating between *RHO* alleles. Unfortunately, defSaCas9 had no greater specificity than dSaCas9, so it does not offer improvements with CRISPRi. Secondly, RHO is a highly conserved gene and as a result, the common, non-pathogenic SNPs and indels all occurred outside the

coding sequence[3]. Other than a SNP in exon one, these regions are unlikely to drive any reduction in rhodopsin protein with CRISPR/Cas9, as indels in introns will typically be lost during splicing[48]. CRISPRi, however, has driven gene repression targeting regulatory regions and introns[250,251].

Complete removal of mutant RHO is not required for the treatment of adRP, and therapeutic benefits have been achieved in vivo with lower editing levels. One study treated retinas of the P23H rat model of RHO-adRP with an allele-specific antisense oligonucleotide targeting the mutant *Rho* transgene. They detected a 40 % reduction in mutant *Rho* which was associated with an 18 % increase in outer nuclear layer thickness and improved ERG responses[252]. Another study treated the S334ter-3 rat model of RHO-adRP with a subretinal injection and electroporation of CRISPR plasmids targeting the mutant *Rho*[38]. 33 days after treatment there was 33-36 % disruption of mutant *Rho*, and the treated regions of the retina had a significant increase in the number of photoreceptor layers from 1 to 8.

This thesis was able to achieve a 53 % reduction in rod cell-expressed EGFP mRNA following treatment with an all-in-one CRISPR/Cas9 AAV. If similar knock down rates could be achieved with mutant *Rho*, it is likely this would drive some phenotypic rescue of a RHO-adRP model, as seen in other papers[38,252]. Targeting *RHO* SNPs with the allele-specific gRNAs in vitro produced high levels of CRISPR/Cas9 disruption and CRISPRi repression, between 38.5-73.2 % and 43.1-65.8 %, respectively. Unfortunately, the impacts of these edits on RHO protein could not be assessed, and as the target sites are intronic, they are unlikely to be effective with CRISPR/Cas9. The all-in-one CRISPRi AAV was unable to drive EGFP repression in vivo but the reason for this is unknown and requires further investigation (see 7.2.1).

As this strategy targets common SNPs in the human *RHO* sequence and regulatory regions, a suitable in vivo model would require the full-length human *RHO* sequence, driven by the *RHO* promoter. The transgenic P23H and NHR mice developed by Olsson et al (1992) may be suitable[253]. These contain a large transgenic insertion of either the mutant or wild type *RHO* allele (including its upstream and downstream regulatory elements) from a patient with RHO-adRP caused by the P23H mutation. The

wild type NHR mice have a normal retinal structure and electroretinogram responses, while the mutant P23H mice have loss of photoreceptors over time and diminished electroretinogram responses - replicating adRP human symptoms.

7.4 Considerations for clinical application

7.4.1 Off-target effects

Off-target effects with CRISPR/Cas9 and CRISPRi occur when Cas9 binds at unintended sites in the genome, which are partially homogenous to the gRNA target sequence[89]. They are a concern in translational research as disruption of critical genes can theoretically lead to cell dysfunction or the development of cancer[52,254–256]. CRISPRi typically has greater specificity than CRISPR/Cas9 but off-target effects with CRISPRi have been reported, and therefore remain a concern[49,58]. Off-target effects were not investigated in this thesis. This is not essential for the experiments targeting EGFP as they have no clinical application and instead serve as a proof-of-concept for targeting rod cell-specific genes in vivo. For the gRNAs targeting *RHO*, off-target effects will determine whether these are feasible treatments for adRP. In early CRISPR research, off-target sites were predicted by screening for genomic regions with sequence similarity to the gRNA binding site[89,257]. However, it was subsequently discovered that these screens fail to identify many off-target effects, and so next-generation sequencing techniques were developed to search for off-target activity in an unbiased way[258]. These include Digenome-seq, BLESS, and DISCOVER-seq, which search for indels, double-stranded breaks, or recruitment of DNA repair machinery in the genome, respectively[86,259,260]. As CRISPRi does not introduce breaks into the genome, off-target effects are investigated either with ChIP-seq, identifying areas of the genome where dCas9 binds (subsequent RNA analysis is then required at these sites), or by RNA-seq, identifying changes in the cells transcriptome relative to a reference database[69,81,88,261]. These techniques can be used to identify off-target effects of *RHO*-targeting gRNAs with CRISPR/Cas9 and CRISPRi. Off-target effects can vary between cell types so to best mimic the potential off-target effects in human rod cells, screening should be conducted in human retinal cells: either an immortalised retinal cell line such as Y79 cells, retinal organoids, or in human retinal tissue cultured ex vivo[89,134,152]. If off-target effects of *RHO* targeting gRNAs are a concern, the use of the enhanced-fidelity version of SaCas9, efSaCas9 may improve off-target effects with CRISPR/Cas9, but will not

improve CRISPRi off-target effects[249].

7.4.2 Unintended consequences

As well as off-target effects from CRISPR activity in unintended sites of the genome, there are additional side effects of CRISPR gene editing that are potential hurdles for clinical application. CRISPR/Cas9 gene editing causes a double stranded break in the genome, which triggers cellular repair mechanisms. This causes indels to be incorporated into the genome, the exact sequence of which is uncontrollable. Concerns have been raised that this could lead to the production of a toxic protein, causing cellular stress or death. Giannelli et al. (2018) investigated the impact of indels in the *RHO* coding sequence[41]. They identified the two most common indels following in vivo SaCas9-driven *RHO* disruption, and expressed them in the P19 mouse cell line. Encouragingly, neither sequence produced a protein or were toxic to the cell. Other papers have identified that exonic indels can cause the mutated exon to be skipped during splicing, leading to the formation of a truncated protein[262,263]. Truncated RHO proteins are known to be toxic, and three of the targetable *RHO* SNPs are in exons 1 and 5, which could result in truncated proteins if skipped[3,264,265]. Finally, integration of the AAV genome into the cut site has been repeatedly documented[206,207,266]. In this thesis, integration of plasmid components into the RHO sequence following CRISPR/Cas9 gene disruption in vitro occurred in 4.1 % of edits. This was not investigated in vivo but would be a useful avenue of further research. To progress RHO-targeting CRISPR/Cas9 therapies to the clinic, the impacts of CRISPR/Cas9 gene editing should be investigated thoroughly. Next generation sequencing of the target site would reveal common indels and AAV integrations, which could then be investigated for cellular toxicity. RNA-sequencing and western blot analysis would highlight any exon skipping and protein truncations. As with off-target effects, this analysis should be conducted in human retinal cells to mimic the target cells of the therapy. As CRISPRi does not induce double stranded breaks, unpredictable integrations are not a concern, making this therapy simpler, and potentially safer.

Following subretinal injection of both the CRISPR/Cas9 and CRISPRi AAV in this thesis, there was severe loss of photoreceptors in some mouse eyes. This result was unexpected and was not consistent between different AAV, experiments, or eyes of the same mouse. The photoreceptor loss was unrelated to the dose of CRISPR/Cas9 AAV so it is not likely to be a response to the gene therapy vector but due to a lack of sham injection controls, this could not be ruled out entirely. It should be noted, however, that there is a wealth of data from similar experiments using subretinal AAV in similar doses in mice which do not show any obvious toxic effect[97].

In order to understand potential detrimental effects of CRISPR gene therapy in pre-clinical studies, appropriate controls are essential. Throughout this thesis, a "scrambled" gRNA was used as a CRISPR negative control. Other than the gRNA coding sequence, these constructs were identical to the EGFP, or RHO-targeting constructs, and therefore controlled for the introduction of Cas9, gRNA, the plasmid or AAV presence, and the gene introduction methods. The scrambled gRNA sequence originates from the unmodified px601 plasmid. This plasmid contains ubiquitous SaCas9 and gRNA expression cassettes. In the unmodified version, the scrambled gRNA is composed of BsaI restriction sites that are used to clone in target-specific gRNA sequences. The scrambled gRNA has no targets in the mouse or human genome with 100 % homology but, as discussed previously, CRISPR editing can occur in regions with partial homology. This gRNA was used in multiple experimental approaches – targeting endogenous genes in vitro, targeting luciferase assay reporters in vitro, targeting endogenous genes in vivo – and there were no unexpected differences between the scrambled or target gRNAs in any assays (e.g. housekeeping gene expression levels were comparable, cell morphology was comparable, etc.). Screening scrambled-treated cells for CRISPR/Cas9 and CRISPRi activity would allow a deeper understand of the limits of this gRNA as a negative control. In the majority of studies, the genome-wide impacts of control gRNAs are not investigated[267–271]. The introduction of a double stranded DNA break has a mildly toxic effect on the cell, so some CRISPR screens recommend using a gRNA with a single "safe" binding site, expected to have no impact on phenotype, rather than a non-targeting gRNA[272,273].

7.5 Progress in retinal gene therapy

The eye is an organ that is ideal for gene therapy, and this is reflected in the remarkable progress in gene therapy treatments into inherited retinal diseases in recent years. In 2017, the gene therapy treatment Luxturna became the first gene therapy to gain US Food and Drug Administration approval, quickly followed by European Medicines Agency approval in 2018. This gene augmentation therapy uses AAV2 to deliver a working copy of the *RPE65* gene to patients with Leber Congenital Amaurosis type 2. While this is currently the only approved gene therapy treatment for retinal diseases, there are clinical trials underway for other types of Leber Congenital Amaurosis, choroideremia, retinitis pigmentosa, age-related macular degeneration, and diabetic retinopathy[274]. Two of these trials target mutant rhodopsin to treat RHO-adRP. ION357 is an antisense oligonucleotide developed by Ionis Pharmaceuticals that binds exclusively to the P23H mutation in mutant *RHO* mRNA. In vivo mouse and rat models demonstrated a 40 % reduction in mutant *RHO* exclusively, which increased outer nuclear layer thickness and the number of photoreceptors[42,44]. The phase 1/2 human clinical trial began in October 2019 and is expected to be complete by October 2021. The second trial, developed by IVERIC Bio, treats RHO-adRP using a knock down and replace strategy. This mutation independent strategy delivers an AAV2 drug called IC-100 which contains a short-interfering RNA molecule which targets *RHO* mRNA, alongside a resistant copy of the *RHO* coding sequence [42,275]. In vivo studies in a dog model of RHO-adRP reduced native *RHO* by 97 %, and produced resistant RHO protein at 30 % normal levels. In mouse RHO-adRP models this delayed photoreceptor loss and improved electroretinogram responses. This trial aims to start recruiting patients at the start of 2021[275]. In a similar mechanism to RNAi strategies (see 1.4 CRISPR), antisense oligonucleotides and short-interfering RNA molecules bind to target mRNA through sequence homology (in this case *RHO* mRNA), and reduce transcription of the mRNA through blocking protein access, or triggering degradation of the mRNA transcript[276].

The first in-human clinical trial using CRISPR/Cas9 is currently underway to treat the recessive retinal disease Leber Congenital Amaurosis 10 caused by the IVS26 mutation (Clinical trial number

NCT03872479)[83,277]. This mutation generates a cryptic splice site in an intron of *CEP290*, which produces a non-functional mRNA. The trial uses a single AAV5 to deliver SaCas9 driven by the rhodopsin kinase promoter, and two gRNAs driven by a U6 promoter. The gRNAs are targeted to either side of the pathogenic splice site mutation IVS26, removing the mutation and restoring normal splicing. Pre-clinical experiments were performed in both a knock-in mouse model of Leber congenital amaurosis 10 and wild type non-human primates[228]. Their constructs drove strong photoreceptor transduction in both organisms, transducing approximately 30 % of the murine retina. At their highest tested dose, they were able to achieve approximately 75-90 % editing in the mouse model, following selection of transduced cells. No phenotypic analysis was done to see the impact of these mutations on the retinal morphology, retinal response, or visual acuity, but editing in over 10 % of cones is believed to produce a clinical benefit in patients. The estimation completion date of the study is 2024, and the results are highly anticipated, as they will provide details on CRISPR efficiency rates and tolerability in the human retina.

7.6 Conclusion

When this DPhil project originated, CRISPR/Cas9 was a relatively new molecular system and throughout the duration of the project, research progressed rapidly. This thesis has contributed to this field by developing CRISPR/Cas9 and CRISPRi AAV vectors for rod cell-specific gene therapies. A novel, small, 154 bp rod cell-specific promoter was created and characterised. It drove transgene expression in multiple AAV, producing high SaCas9 and dSaCas9.KRAB expression in murine rod cells in vivo. CRISPR/Cas9 demonstrated strong disruption of rod cell-specific EGFP in the Nrl-EGFP mouse line. CRISPRi, however, was unable to significantly reduce EGFP expression in the same time frame. In vitro analysis with CRISPRi revealed that targeting non-pathogenic SNPs in RHO can drive allele-specific targeting and is a potentially useful strategy for a mutation-independent treatment of RHO-adRP. The generation of rod cell-specific, single transgene CRISPR/Cas9 and CRISPRi AAV vectors was a critical achievement and will enable further research in the rapidly advancing field of genome editing for the treatment of inherited retinal diseases.

8 References

1. Daiger SP, Bowne SJ, Sullivan LS. Genes and mutations causing autosomal dominant retinitis pigmentosa. *Cold Spring Harb Perspect Med*. 2015;5(10):a017129. doi:10.1101/cshperspect.a017129

2. Rosenfeld PJ, Cowley GS, McGee TL, Sandberg MA, Berson EL, Dryja TP. A Null mutation in the rhodopsin gene causes rod photoreceptor dysfunction and autosomal recessive retinitis pigmentosa. *Nat Genet*. 1992;1(3):209-213. doi:10.1038/ng0692-209

3. Athanasiou D, Aguila M, Bellingham J, et al. The molecular and cellular basis of rhodopsin retinitis pigmentosa reveals potential strategies for therapy. *Prog Retin Eye Res*. 2018;62:1-23. doi:10.1016/j.preteyeres.2017.10.002

4. Schillder PH, Tehovnik EJ. The Retina. In: *Vision and the Visual System*. ; 2015. doi:10.1093/acprof

5. Purves D, Augustine GJ, Fitzpatrick D, et al. Anatomical Distribution of Rods and Cones. In: *Neuroscience, 2nd Edition*. Sinauer Associates; 2001.

6. Furukawa T, Hurley JB, Kawamura S. *Vetebrate Photoreceptors*. Springer; 2014. doi:10.1016/S1350-9462(00)00014-8

7. Humphries MM, Rancourt D, Farrar GJ, et al. Retinopathy induced in mice by targeted disruption of the rhodopsin gene. *Nat Genet*. 1997;15(2):216-219. doi:10.1038/ng0297-216

8. Sugawara T, Hagiwara A, Hiramatsu A, Ogata K, Mitamura Y, Yamamoto S. Relationship between peripheral visual field loss and vision-related quality of life in patients with retinitis pigmentosa. *Eye*. 2010;24:535-539. doi:10.1038/eye.2009.176

9. Hahm BJ, Shin YW, Shim EJ, et al. Depression and the vision-related quality of life in patients with retinitis pigmentosa. *Br J Ophthalmol*. 2008;92(5):650-654. doi:10.1136/bjo.2007.127092

10. Jangra D, Ganesh A, Thackray R, et al. Psychosocial adjustment to visual loss in patients with retinitis pigmentosa. *Ophthalmic Genet*. 2007;28(1):25-30. doi:10.1080/13816810701201930

11. Garip G, Kamal A. Systematic review and meta-synthesis of coping with retinitis pigmentosa: Implications for improving quality of life. *BMC Ophthalmol*. 2019;19(1):181. doi:10.1186/s12886-019-1169-z

12. Hartong DT, Berson EL, Dryja TP. Retinitis pigmentosa. *Lancet*. 2006;368(9549):1795-1809. doi:10.1016/S0140-6736(06)69740-7

13. Verbakel SK, van Huet RAC, Boon CJF, et al. Non-syndromic retinitis pigmentosa. *Prog Retin Eye Res*. 2018;66:157-186. doi:10.1016/j.preteyeres.2018.03.005

14. Denniston AK, Murray PI. Oxford Handbook of Ophthalmology. 2018.

15. Athanasiou D, Aguila M, Bellingham J, et al. The molecular and cellular basis of rhodopsin retinitis pigmentosa reveals potential strategies for therapy. *Prog Retin Eye Res*. 2018;62:1-23. doi:10.1016/j.preteyeres.2017.10.002

16. Chang S, Vaccarella L, Olatunji S, Cebulla C, Christoforidis J. Diagnostic Challenges in Retinitis Pigmentosa: Genotypic Multiplicity and Phenotypic Variability. *Curr Genomics*. 2011;12(4):267-275. doi:10.2174/138920211795860116

17. Kaur J, Mencl S, Sahaboglu A, et al. Calpain and PARP Activation during Photoreceptor Cell Death in P23H and S334ter Rhodopsin Mutant Rats. Sharif N, ed. *PLoS One*. 2011;6(7):e22181. doi:10.1371/journal.pone.0022181

18. Viringipurampeer IA, Metcalfe AL, Bashar AE, et al. NLRP3 inflammasome activation drives bystander cone photoreceptor cell death in a P23H rhodopsin model of retinal degeneration. *Hum Mol Genet*. 2016;25(8):1501-1516. doi:10.1093/HMG

19. Murakami Y, Ikeda Y, Nakatake S, et al. Commentary Necrotic cone photoreceptor cell death in retinitis pigmentosa. *Cell Death Dis*. 2015;6:e2038. doi:10.1038/cddis.2015.385

20. Trichonas G, Murakami Y, Thanos A, et al. Receptor interacting protein kinases mediate retinal detachment-induced photoreceptor necrosis and compensate for inhibition of apoptosis. *Proc Natl Acad Sci U S A*. 2010;107(50):21695-21700. doi:10.1073/pnas.1009179107

21. Campochiaro PA, Mir TA. The mechanism of cone cell death in Retinitis Pigmentosa. *Prog Retin Eye Res*. 2018;62:24-37. doi:10.1016/j.preteyeres.2017.08.004

22. Comitato A, Di Salvo MT, Turchiano G, et al. Dominant and Recessive Mutations in Rhodopsin Activate Different Cell Death Pathways. *Hum Mol Genet*. 2016;25(13):2801-2812.

23. Hamel C. Retinitis pigmentosa. *Orphanet J Rare Dis*. 2006;1(1):40. doi:10.1186/1750-1172-1-40

24. Haggstrom M. Medical Gallery of Mikael Haggstrom 2014. WikiJournal of Miedicine. doi:10.15347

25. Mitamura Y, Mitamura-Aizawa S, Toshihiko N, Takashi K, Hiroshi E, Takeshit N. Diagnostic imaging in patients with retinitis pigmentosa. *J Med Investig*. 2012;59.

26. RetNet - Retinal Information Network. https://sph.uth.edu/retnet/home.htm. Accessed June 12, 2020.

27. Ali MU, Rahman MSU, Cao J, Yuan PX. Genetic characterization and disease mechanism of retinitis pigmentosa; current scenario. *3 Biotech*. 2017;7(4):1-20. doi:10.1007/s13205-017-0878-3

28. Wu Y, Guo Y, Yi J, et al. Heterozygous RHO p.R135W missense mutation in a large Han-Chinese family with retinitis pigmentosa and different refractive errors. *Biosci Rep*. 2019;39(7). doi:10.1042/BSR20182198

29. Katagiri S, Hayashi T, Akahori M, et al. RHO Mutations (p.W126L and p.A346P) in Two Japanese Families with Autosomal Dominant Retinitis Pigmentosa. *J Ophthalmol*. 2014. doi:10.1155/2014/210947

30. Li S, Xiao X, Wang P, Guo X, Zhang Q. Mutation spectrum and frequency of the RHO gene in 248 Chinese families with retinitis pigmentosa. *Biochem Biophys Res Commun*. 2010;401(1):42-47. doi:10.1016/j.bbrc.2010.09.004

31. Sullivan LS, Bowne SJ, Birch DG, et al. Prevalence of disease-causing mutations in families with autosomal dominant retinitis pigmentosa: A screen of known genes in 200 families. *Investig Ophthalmol Vis Sci*. 2006;47(7):3052-3064. doi:10.1167/iovs.05-1443

32. Mendes HF, Van Der Spuy J, Chapple JP, Cheetham ME. Mechanisms of cell death in rhodopsin retinitis pigmentosa: Implications for therapy. *Trends Mol Med*. 2005;11(4):177-185. doi:10.1016/j.molmed.2005.02.007

33. Zhang N, Kolesnikov A V., Jastrzebska B, et al. Autosomal recessive retinitis pigmentosa E150K

opsin mice exhibit photoreceptor disorganization. *J Clin Invest*. 2013;123(1):121-137. doi:10.1172/JCI66176

34. Simunovic MP, Shen W, Lin JY, Protti DA, Lisowski L, Gillies MC. Optogenetic approaches to vision restoration. *Exp Eye Res*. 2019;178:15-26. doi:10.1016/j.exer.2018.09.003

35. Terrell D, Comander J. Current Stem-Cell Approaches for the Treatment of Inherited Retinal Degenerations. *Semin Ophthalmol*. 2019;34(4):287-292. doi:10.1080/08820538.2019.1620808

36. Bloch E, Luo Y, da Cruz L. Advances in retinal prosthesis systems. *Ther Adv Ophthalmol*. 2019;11:251584141881750. doi:10.1177/2515841418817501

37. Latella MC, Di Salvo MT, Cocchiarella F, et al. In vivo Editing of the Human Mutant Rhodopsin Gene by Electroporation of Plasmid-based CRISPR/Cas9 in the Mouse Retina. *Mol Ther - Nucleic Acids*. 2016;5:e389. doi:10.1038/mtna.2016.92

38. Bakondi B, Lv W, Lu B, et al. In vivo CRISPR/Cas9 gene editing corrects retinal dystrophy in the S334ter-3 rat model of autosomal dominant retinitis pigmentosa. *Mol Ther*. 2016;24(3):556-563. doi:10.1038/mt.2015.220

39. Yu W, Mookherjee S, Chaitankar V, et al. Nrl knockdown by AAV-delivered CRISPR/Cas9 prevents retinal degeneration in mice. *Nat Commun*. 2017;8. doi:10.1038/ncomms14716

40. Li P, Kleinstiver BP, Leon MY, et al. Allele-Specific CRISPR-Cas9 Genome Editing of the Single-Base P23H Mutation for Rhodopsin-Associated Dominant Retinitis Pigmentosa. *Cris J*. 2018;1(1):55-64. doi:10.1089/crispr.2017.0009

41. Giannelli SG, Luoni M, Castoldi V, et al. Cas9/sgRNA selective targeting of the P23H Rhodopsin mutant allele for treating retinitis pigmentosa by intravitreal AAV9.PHP.B-based delivery. *Hum Mol Genet*. 2018;27(5):761-779. doi:10.1093/HMG

42. Meng D, Ragi SD, Tsang SH. Therapy in Rhodopsin-Mediated Autosomal Dominant Retinitis Pigmentosa. *Mol Ther*. 2020;28(10):2139-2149. doi:10.1016/j.ymthe.2020.08.012

43. Wilson JH, Wensel TG. The Nature of Dominant Mutations of Rhodopsin and Implications for Gene Therapy. In: *Molecular Neurobiology*. Vol 28. Humana Press; 2003:149-158. doi:10.1385/MN:28:2:149

44. Biasutto P, Adamson PS, Dulla K, Murray S, Monia B, McCaleb M. Allele specific knock-down of human P23H rhodopsin mRNA and prevention of retinal degeneration in humanized P23H rhodopsin knock-in mouse, following treatment with an intravitreal GAPmer antisense oligonucleotide (QR-1123) | IOVS | ARVO Journals. Investigative Ophthalmology and Visual Science. https://iovs.arvojournals.org/article.aspx?articleid=2744920. Published 2019. Accessed March 20, 2021.

45. Cideciyan A V., Sudharsan R, Dufour VL, et al. Mutation-independent rhodopsin gene therapy by knockdown and replacement with a single AAV vector. *Proc Natl Acad Sci U S A*. 2018;115(36):E8547-E8556. doi:10.1073/pnas.1805055115

46. Millington-Ward S, Chadderton N, O'Reilly M, et al. Suppression and replacement gene therapy for autosomal dominant disease in a murine model of dominant retinitis pigmentosa. *Mol Ther*. 2011;19(4):642-649. doi:10.1038/mt.2010.293

47. Dass A, Diner B, Nayak R, et al. *Dual AAV-Based "Knock-out-and-Replace" of RHO as a Therapeutic Approach to Treat RHO-Associated Autosomal Dominant Retinitis Pigmentosa (RHO AdRP) Acknowledgements Disclosures: Employees and Shareholders of Editas Medicine: A.*; 2020.

48. Peddle CF, Maclaren RE. The Application of CRISPR / Cas9 for the Treatment of Retinal Diseases. *Yale J Biol Med*. 2017;90(4):533-541.

49. Peddle CF, Fry LE, McClements ME, Maclaren RE. Crispr interference–potential application in retinal disease. *Int J Mol Sci*. 2020;21(7). doi:10.3390/ijms21072329

50. Carroll D. Genome engineering with zinc-finger nucleases. *Genetics*. 2011;188(4):773-782. doi:10.1534/genetics.111.131433

51. Gupta RM, Musunuru K. Expanding the genetic editing tool kit: ZFNs, TALENs, and CRISPR-Cas9. *J Clin Invest*. 2014;124(10):4154-4161. doi:10.1172/JCI72992

52. Hung SSC, McCaughey T, Swann O, Pébay A, Hewitt AW. Genome engineering in ophthalmology: Application of CRISPR/Cas to the treatment of eye disease. *Prog Retin Eye Res*. 2016;53:1-20. doi:10.1016/j.preteyeres.2016.05.001

53. Jinek M, Chylinski K, Fonfara I, Hauer M, Doudna JA, Charpentier E. A Programmable Dual-RNA – Guided DNA endonuclease in adaptive bacterial immunity. *Science (80-)*. 2012;337(August):816-822.

54. Cong L, Ran FA, Cox D, et al. Multiplex genome engineering using CRISPR/Cas systems. *Science (80-)*. 2013;339(6121):819-823. doi:10.1126/science.1231143

55. Mojica FJM, Díez-Villaseñor C, García-Martínez J, Almendros C. Short motif sequences determine the targets of the prokaryotic CRISPR defence system. *Microbiology*. 2009;155(3):733-740. doi:10.1099/mic.0.023960-0

56. Anders C, Niewoehner O, Duerst A, Jinek M. Structural basis of PAM-dependent target DNA recognition by the Cas9 endonuclease. *Nature*. 2014;513(7519):569-573. doi:10.1038/nature13579

57. Ran FA, Hsu PD, Lin CY, et al. Double nicking by RNA-guided CRISPR cas9 for enhanced genome editing specificity. *Cell*. 2013;154(6):1380-1389. doi:10.1016/j.cell.2013.08.021

58. Gilbert LA, Horlbeck MA, Adamson B, et al. Genome-Scale CRISPR-Mediated Control of Gene Repression and Activation. *Cell*. 2014;159(3):647-661. doi:10.1016/j.cell.2014.09.029

59. Radzisheuskaya A, Shlyueva D, Müller I, Helin K. Optimizing sgRNA position markedly improves the efficiency of CRISPR/dCas9-mediated transcriptional repression. *Nucleic Acids Res*. 2016;44(18). doi:10.1093/nar/gkw583

60. Qi LS, Larson MH, Gilbert LA, et al. Repurposing CRISPR as an RNA-guided platform for sequence-specific control of gene expression. *Cell*. 2013;152(5):1173-1183. doi:10.1016/j.cell.2013.02.022

61. Larson MH, Gilbert LA, Wang X, Lim WA, Weissman JS, Qi LS. CRISPR interference (CRISPRi) for sequence-specific control of gene expression. *Nat Protoc*. 2013;8(11):2180-2196. doi:10.1038/nprot.2013.132

62. Chung JY, Ul Ain Q, Song Y, Yong SB, Kim YH. Targeted delivery of CRISPR interference system against Fabp4 to white adipocytes ameliorates obesity, inflammation, hepatic steatosis, and insulin resistance. *Genome Res*. 2019;29(9):1442-1452. doi:10.1101/gr.246900.118

63. Yeo NC, Chavez A, Lance-Byrne A, et al. An enhanced CRISPR repressor for targeted mammalian gene regulation. *Nat Methods*. 2018;15(8):611-616. doi:10.1038/s41592-018-0048-5

64. Nishimasu H, Cong L, Yan WX, et al. Crystal Structure of Staphylococcus aureus Cas9. *Cell*. 2015;162(5):1113-1126. doi:10.1016/j.cell.2015.08.007

65. Gilbert LA, Larson MH, Morsut L, et al. CRISPR-mediated modular RNA-guided regulation of transcription in eukaryotes. *Cell*. 2013;154(2):442. doi:10.1016/j.cell.2013.06.044

66. Lawrence M, Daujat S, Schneider R. Lateral Thinking: How Histone Modifications Regulate Gene Expression. *Trends Genet*. 2016;32(1):42-56. doi:10.1016/j.tig.2015.10.007

67. Lupo A, Cesaro E, Montano G, Zurlo D, Izzo P, Costanzo P. KRAB-Zinc Finger Proteins: A Repressor Family Displaying Multiple Biological Functions. *Curr Genomics*. 2013;14(4):268-278. doi:10.2174/1389202911314999000 2

68. Karimi Z, Ahmadi A, Najafi A, Ranjbar R. Bacterial CRISPR Regions: General Features and their Potential for Epidemiological Molecular Typing Studies. *Open Microbiol J*. 2018;12(1):59-70. doi:10.2174/1874285801812010059

69. Ran FA, Cong L, Yan WX, et al. In vivo genome editing using Staphylococcus aureus Cas9. *Nature*. 2015;520(7546):186-191. doi:10.1038/nature14299

70. Kim E, Koo T, Park SW, et al. In vivo genome editing with a small Cas9 orthologue derived from Campylobacter jejuni. *Nat Commun*. 2017;8. doi:10.1038/ncomms14500

71. Knott GJ, Doudna JA. CRISPR-Cas guides the future of genetic engineering. *Science (80-)*. 2018;361(6405):866-869. doi:10.1126/science.aat5011

72. Evers B, Jastrzebski K, Heijmans JPM, Grernrum W, Beijersbergen RL, Bernards R. CRISPR knockout screening outperforms shRNA and CRISPRi in identifying essential genes. *Nat Biotechnol*. 2016;34(6):631-633. doi:10.1038/nbt.3536

73. Cong L, Ran FA, Cox D, et al. Multiplex Genome Engineering Using CRISPR/Cas Systems. *Science (80-)*. 2013;339(6121):819-823.

74. Hsu PD, Scott DA, Weinstein JA, et al. DNA targeting specificity of RNA-guided Cas9 nucleases. *Nat Biotechnol*. 2013;31(9):827-832. doi:10.1038/nbt.2647

75. Jiang W, Bikard D, Cox D, Zhang F, Marraffini LA. RNA-guided editing of bacterial genomes using CRISPR-Cas systems. *Nat Biotechnol*. 2013;31(3):233-239. doi:10.1038/nbt.2508

76. Fu Y, Foden JA, Khayter C, et al. High-frequency off-target mutagenesis induced by CRISPR-Cas nucleases in human cells. *Nat Biotechnol*. 2013;31(9):822-826. doi:10.1038/nbt.2623

77. Slaymaker IM, Gao L, Zetsche B, Scott DA, Yan WX, Zhang F. Rationally engineered Cas9 nucleases with improved specificity. *Science (80-)*. 2016;351(6268):84-88. doi:10.1126/science.aad5227

78. Kleinstiver BP, Pattanayak V, Prew MS, et al. High-fidelity CRISPR-Cas9 nucleases with no detectable genome-wide off-target effects. *Nature*. 2016;529(7587):490-495. doi:10.1038/nature16526

79. Ikeda A, Fujii W, Sugiura K, Naito K. High-fidelity endonuclease variant HypaCas9 facilitates accurate allele-specific gene modification in mouse zygotes. *Commun Biol*. 2019;2(1). doi:10.1038/s42003-019-0627-8

80. Casini A, Olivieri M, Petris G, et al. A highly specific SpCas9 variant is identified by in vivo screening in yeast. *Nat Biotechnol*. 2018;36(3):265-271. doi:10.1038/nbt.4066

81. Zheng Y, Shen W, Zhang J, et al. CRISPR interference-based specific and efficient gene inactivation in the brain. *Nat Neurosci*. 2018;21(6):894. doi:10.1038/s41593-018-0125-1

82. Courtney DG, Moore JE, Atkinson SD, et al. CRISPR/Cas9 DNA cleavage at SNP-derived PAM

enables both in vitro and in vivo KRT12 mutation-specific targeting. *Gene Ther*. 2016;23(1):108-112. doi:10.1038/gt.2015.82

83. Ledford H. CRISPR treatment inserted directly into the body for first time. *Nature*. 2020;579(7798):185. doi:10.1038/d41586-020-00655-8

84. Taylor P. First patient dosed in trial of Allergan/Editas' CRISPR blindness drug. Pharmaphorum. https://pharmaphorum.com/news/first-patient-dosed-in-trial-of-allergan-editas-crispr-blindness-drug/. Published 2020. Accessed July 17, 2020.

85. Zischewski J, Fischer R, Bortesi L. Detection of on-target and off-target mutations generated by CRISPR/Cas9 and other sequence-specific nucleases. *Biotechnol Adv*. 2017;35(1):95-104. doi:10.1016/j.biotechadv.2016.12.003

86. Kim D, Bae S, Park J, et al. Digenome-seq: Genome-wide profiling of CRISPR-Cas9 off-target effects in human cells. *Nat Methods*. 2015;12(3):237-243. doi:10.1038/nmeth.3284

87. Tsai SQ, Nguyen NT, Malagon-Lopez J, Topkar V V., Aryee MJ, Joung JK. CIRCLE-seq: A highly sensitive in vitro screen for genome-wide CRISPR-Cas9 nuclease off-targets. *Nat Methods*. 2017;14(6):607-614. doi:10.1038/nmeth.4278

88. Thakore PI, Song L, Safi A, et al. Highly Specific Epigenome Editing by CRISPR/Cas9 Repressors for Silencing of Distal Regulatory Elements. *Nat Methods*. 2015;12(12):1143-1149. doi:10.1038/nmeth.3630.Highly

89. Zhang XH, Tee LY, Wang XG, Huang QS, Yang SH. Off-target effects in CRISPR/Cas9-mediated genome engineering. *Mol Ther - Nucleic Acids*. 2015;4(11):e264. doi:10.1038/mtna.2015.37

90. Charlesworth CT, Deshpande PS, Dever DP, et al. Identification of preexisting adaptive immunity to Cas9 proteins in humans. *Nat Med*. 2019;25(2):249-254. doi:10.1038/s41591-018-0326-x

91. Simhadri VL, McGill J, McMahon S, Wang J, Jiang H, Sauna ZE. Prevalence of Pre-existing Antibodies to CRISPR-Associated Nuclease Cas9 in the USA Population. *Mol Ther - Methods Clin Dev*. 2018;10:105-112. doi:10.1016/j.omtm.2018.06.006

92. Wagner DL, Amini L, Wendering DJ, et al. High prevalence of Streptococcus pyogenes Cas9-reactive T cells within the adult human population. *Nat Med*. 2019;25(2):242-248. doi:10.1038/s41591-018-0204-6

93. Kim S, Koo T, Jee HG, et al. CRISPR RNAs trigger innate immune responses in human cells. *Genome Res*. 2018;28(3):367-373. doi:10.1101/gr.231936.117

94. Samulski RJ, Muzyczka N. AAV-Mediated Gene Therapy for Research and Therapeutic Purposes. *Annu Rev Virol*. 2014;1(1):427-451. doi:10.1146/annurev-virology-031413-085355

95. Naso MF, Tomkowicz B, Perry WL, Strohl WR. Adeno-Associated Virus (AAV) as a Vector for Gene Therapy. *BioDrugs*. 2017;31(4):317-334. doi:10.1007/s40259-017-0234-5

96. Rodrigues GA, Shalaev E, Karami TK, Cunningham J, Slater NKH, Rivers HM. Pharmaceutical Development of AAV-Based Gene Therapy Products for the Eye. *Pharm Res*. 2019;36(2). doi:10.1007/s11095-018-2554-7

97. Trapani I, Auricchio A. Seeing the Light after 25 Years of Retinal Gene Therapy. *Trends Mol Med*. 2018;24(8):669-681. doi:10.1016/j.molmed.2018.06.006

98. Chamberlain K, Riyad JM, Weber T. Expressing transgenes that exceed the packaging capacity of adeno-associated virus capsids. *Hum Gene Ther Methods*. 2016;27(1):1-12.

doi:10.1089/hgtb.2015.140

99. Dong B, Nakai H, Xiao W. Characterization of genome integrity for oversized recombinant AAV vector. *Mol Ther*. 2010;18(1):87-92. doi:10.1038/mt.2009.258

100. Chandler LC, Barnard AR, Caddy SL, et al. Enhancement of Adeno-Associated Virus-Mediated Gene Therapy Using Hydroxychloroquine in Murine and Human Tissues. *Mol Ther - Methods Clin Dev*. 2019;14. doi:10.1016/j.omtm.2019.05.012

101. Bainbridge JWB, Mehat MS, Sundaram V, et al. Long-term effect of gene therapy on Leber's congenital amaurosis. *N Engl J Med*. 2015;372(20):1887-1897. doi:10.1056/NEJMoa1414221

102. Guy J, Feuer WJ, Davis JL, et al. Gene Therapy for Leber Hereditary Optic Neuropathy: Low- and Medium-Dose Visual Results. *Ophthalmology*. 2017;124(11):1621-1634. doi:10.1016/j.ophtha.2017.05.016

103. Xue K, Jolly JK, Barnard AR, et al. Beneficial effects on vision in patients undergoing retinal gene therapy for choroideremia. *Nat Med*. 2018;24(10):1507-1512. doi:10.1038/s41591-018-0185-5

104. Vandenberghe LH, Bell P, Maguire AM, et al. Dosage thresholds for AAV2 and AAV8 photoreceptor gene therapy in monkey. *Sci Transl Med*. 2011;3(88):88ra54. doi:10.1126/scitranslmed.3002103

105. Grob S, Finn A, Papakostas T, Eliott D. Clinical trials in retinal dystrophies. *Middle East Afr J Ophthalmol*. 2016;23(1):49-59. doi:10.4103/0974-9233.173135

106. Benhar I, London A, Schwartz M. The privileged immunity of immune privileged organs: The case of the eye. *Front Immunol*. 2012;3(SEP). doi:10.3389/fimmu.2012.00296

107. Lipinski DM, Thake M, MacLaren RE. Clinical applications of retinal gene therapy. *Prog Retin Eye Res*. 2013;32(1):22-47. doi:10.1016/j.preteyeres.2012.09.001

108. Kumaran N, Michaelides M, Smith AJ, Ali RR, Bainbridge JWB. Retinal gene therapy. *Br Med Bull*. 2018;126:13-25. doi:10.1093/bmb/ldy005

109. Trapani I, Auricchio A. Has retinal gene therapy come of age? From bench to bedside and back to bench. *Hum Mol Genet*. 2019;28(R1):R108-R118. doi:10.1093/hmg/ddz130

110. Kim K, Park SW, Kim JH, et al. Genome surgery using Cas9 ribonucleoproteins for the treatment of age-related macular degeneration. *Genome Res*. 2017;27(3):419-426. doi:10.1101/gr.219089.116

111. Carroll D. Collateral damage: benchmarking off-target effects in genome editing. *Genome Biol*. 2019;20(1):114. doi:10.1186/s13059-019-1725-0

112. Willis IM, Moir RD. Signaling to and from the RNA Polymerase III Transcription and Processing Machinery. *Annu Rev Biochem*. 2018;87(1):75-100. doi:10.1146/annurev-biochem-062917-012624

113. Kim E, Koo T, Park SW, et al. In vivo genome editing with a small Cas9 orthologue derived from Campylobacter jejuni. *Nat Commun*. 2017;8. doi:10.1038/ncomms14500

114. Lau CH, Ho JWT, Lo PK, Tin C. Targeted Transgene Activation in the Brain Tissue by Systemic Delivery of Engineered AAV1 Expressing CRISPRa. *Mol Ther - Nucleic Acids*. 2019;16:637-649. doi:10.1016/j.omtn.2019.04.015

115. Botta S, Marrocco E, de Prisco N, et al. Rhodopsin targeted transcriptional silencing by DNA-

binding. *Elife*. 2016;5(MARCH2016). doi:10.7554/eLife.12242

116. Allocca M, Mussolino C, Garcia-Hoyos M, et al. Novel Adeno-Associated Virus Serotypes Efficiently Transduce Murine Photoreceptors. *J Virol*. 2007;81(20):11372-11380. doi:10.1128/jvi.01327-07

117. Lerner LE, Gribanova YE, Ji M, Knox BE, Farber DB. Nrl and Sp nuclear proteins mediate transcription of rod-specific cGMP-phosphodiesterase β-subunit gene: Involvement of multiple response elements. *J Biol Chem*. 2001;276(37):34999-35007. doi:10.1074/jbc.M103301200

118. Han J, Dinculescu A, Dai X, Du W, Clay Smith W, Pang J. Review: The history and role of naturally occurring mouse models with Pde6b mutations. *Mol Vis*. 2013;19(December):2579-2589.

119. Muradov H, Boyd KK, Artemyev NO. Rod phosphodiesterase-6 PDE6A and PDE6B subunits are enzymatically equivalent. *J Biol Chem*. 2010;285(51):39828-39834. doi:10.1074/jbc.M110.170068

120. Brightman DS, Razafsky D, Potter C, Hodzic D, Chen S. Nrl-Cre transgenic mouse mediates loxP recombination in developing rod photoreceptors. *Genesis*. 2016;54(3):129-135. doi:10.1002/dvg.22918

121. Akimoto M, Cheng H, Zhu D, et al. Targeting of GFP to newborn rods by Nrl promoter and temporal expression profiling of flow-sorted photoreceptors. *Proc Natl Acad Sci U S A*. 2006;103(10):3890-3895. doi:10.1073/pnas.0508214103

122. Lee J, Myers CA, Williams N, Abdelaziz M, Corbo JC. Quantitative fine-tuning of photoreceptor cis-regulatory elements through affinity modulation of transcription factor binding sites. *Gene Ther*. 2010;17(11):1390-1399. doi:10.1038/gt.2010.77

123. Cheng H. Photoreceptor-specific nuclear receptor NR2E3 functions as a transcriptional activator in rod photoreceptors. *Hum Mol Genet*. 2004;13(15):1563-1575. doi:10.1093/hmg/ddh173

124. Di Polo A, Lerner LE, Farber DB. Transcriptional activation of the human rod cGMP-phosphodiesterase β-subunit gene is mediated by an upstream AP-1 element. *Nucleic Acids Res*. 1997;25(19):3863-3867. doi:10.1093/nar/25.19.3863

125. Image J Macros. https://imagej.nih.gov/ij/macros/. Accessed June 11, 2019.

126. Orlans HO, Edwards TL, Silva SR De, Patrício MI, Maclaren RE. Human Retinal Explant Culture for Ex Vivo Validation of AAV Gene Therapy. In: *Retinal Gene Therapy*. ; 2018:289-303.

127. Di Polo A, Farber DB. Rod photoreceptor-specfic gene expression in human retinoblastoma cells. *Cell Biol*. 1995;92:4016-4020.

128. Petrs-Silva H, Dinculescu A, Li Q, et al. High-efficiency transduction of the mouse retina by tyrosine-mutant AAV serotype vectors. *Mol Ther*. 2009;17(3):463-471. doi:10.1038/mt.2008.269

129. Pang JJ, Dai X, Boye SE, et al. Long-term retinal function and structure rescue using capsid mutant AAV8 vector in the rd10 mouse, a model of recessive retinitis pigmentosa. *Mol Ther*. 2011;19(2):234-242. doi:10.1038/mt.2010.273

130. Koch S, Sothilingam V, Garcia garrido M, et al. Gene therapy restores vision and delays degeneration in the CNGB1-/- mouse model of retinitis pigmentosa. *Hum Mol Genet*. 2012;21(20):4486-4496. doi:10.1093/hmg/dds290

131. Zhong H, Eblimit A, Moayedi Y, et al. AAV8(Y733F)-mediated gene therapy in a Spata7 knockout

mouse model of Leber congenital amaurosis and retinitis pigmentosa. *Gene Ther*. 2015;22(8):619-627. doi:10.1038/gt.2015.42

132. Strobel B, Miller FD, Rist W, Lamla T. Comparative Analysis of Cesium Chloride- and Iodixanol-Based Purification of Recombinant Adeno-Associated Viral Vectors for Preclinical Applications. *Hum Gene Ther Methods*. 2015;26(4):147. doi:10.1089/HGTB.2015.051

133. Patrício MI, Barnard AR, Orlans HO, McClements ME, MacLaren RE. Inclusion of the Woodchuck Hepatitis Virus Posttranscriptional Regulatory Element Enhances AAV2-Driven Transduction of Mouse and Human Retina. *Mol Ther - Nucleic Acids*. 2017;6:198-208. doi:10.1016/j.omtn.2016.12.006

134. Orlans HO, Edwards TL, Silva SR De, Patrício MI, Maclaren RE. Human Retinal Explant Culture for Ex Vivo Validation of AAV Gene Therapy. In: *Retinal Gene Therapy*. ; 2017:289-303.

135. Uhlen M, Fagerberg L, Hallstrom BM, et al. Tissue-based map of the human proteome. *Science (80-)*. 2015;347(6220):1260419-1260419. doi:10.1126/science.1260419

136. Thul PJ, Akesson L, Wiking M, et al. A subcellular map of the human proteome. *Science (80-)*. 2017;356(6340). doi:10.1126/science.aal3321

137. Danielsson F, Wiking M, Mahdessian D, et al. RNA deep sequencing as a tool for selection of cell lines for systematic subcellular localization of all human proteins. *J Proteome Res*. 2013;12(1):299-307. doi:10.1021/pr3009308

138. Chelly J, Concordet JP, Kaplan JC, Kahn A. Illegitimate transcription: Transcription of any gene in any cell type. *Proc Natl Acad Sci U S A*. 1989;86(8):2617-2621. doi:10.1073/pnas.86.8.2617

139. Carter M, Shieh J. Cell Culture Techniques. In: *Guide to Research Techniques in Neuroscience*. Elsevier; 2015:295-310. doi:10.1016/B978-0-12-800511-8.00014-9

140. Dunn KW, Kamocka MM, McDonald JH. A practical guide to evaluating colocalization in biological microscopy. *Am J Physiol - Cell Physiol*. 2011;300(4):C723. doi:10.1152/ajpcell.00462.2010

141. Khani SC, Pawlyk BS, Bulgakov O V., et al. AAV-mediated expression targeting of rod and cone photoreceptors with a human rhodopsin kinase promoter. *Investig Ophthalmol Vis Sci*. 2007;48(9):3954-3961. doi:10.1167/iovs.07-0257

142. Wu Z, Asokan A, Samulski RJ. Adeno-associated Virus Serotypes: Vector Toolkit for Human Gene Therapy. *Mol Ther*. 2006;14(3):316-327. doi:10.1016/j.ymthe.2006.05.009

143. Pipe S, Leebeek FWG, Ferreira V, Sawyer EK, Pasi J. Clinical Considerations for Capsid Choice in the Development of Liver-Targeted AAV-Based Gene Transfer. *Mol Ther - Methods Clin Dev*. 2019;15:170-178. doi:10.1016/j.omtm.2019.08.015

144. Gao GP, Alvira MR, Wang L, Calcedo R, Johnston J, Wilson JM. Novel adeno-associated viruses from rhesus monkeys as vectors for human gene therapy. *Proc Natl Acad Sci U S A*. 2002;99(18):11854-11859. doi:10.1073/pnas.182412299

145. Katz MG, Fargnoli AS, Weber T, Hajjar RJ, Bridges CR. Use of Adeno-Associated Virus Vector for Cardiac Gene Delivery in Large-Animal Surgical Models of Heart Failure. *Hum Gene Ther Clin Dev*. 2017;28(3):157-164. doi:10.1089/humc.2017.070

146. Liu Y, Chen SJ, Li SY, et al. Long-Term safety of human retinal progenitor cell transplantation in retinitis pigmentosa patients. *Stem Cell Res Ther*. 2017;8(1). doi:10.1186/s13287-017-0661-8

147. Tudurí E, Glavas MM, Asadi A, et al. AAV GCG-EGFP, a new tool to identify glucagon-secreting

α-cells. *Sci Rep*. 2019;9(1):1-11. doi:10.1038/s41598-019-46735-2

148. Ong T, Pennesi ME, Birch DG, Lam BL, Tsang SH. Adeno-Associated Viral Gene Therapy for Inherited Retinal Disease. *Pharm Res*. 2019;36(2):34. doi:10.1007/s11095-018-2564-5

149. Seitz IP, Michalakis S, Wilhelm B, et al. Superior retinal gene transfer and biodistribution profile of subretinal versus intravitreal delivery of AAV8 in nonhuman primates. *Investig Ophthalmol Vis Sci*. 2017;58(13):5792-5801. doi:10.1167/iovs.17-22473

150. Vinores SA. Breakdown of the blood-retinal barrier. In: *Encyclopedia of the Eye*. Elsevier; 2010:216-222. doi:10.1016/B978-0-12-374203-2.00137-8

151. McCarty DM. Self-complementary AAV vectors; advances and applications. *Mol Ther*. 2008;16(10):1648-1656. doi:10.1038/mt.2008.171

152. Regent F, Chen HY, Kelley RA, Qu Z, Swaroop A, Li T. A simple and efficient method for generating human retinal organoids. *Mol Vis*. 2020;26:97-105. http://www.molvis.org/molvis/v26/97. Accessed January 17, 2021.

153. Eiraku M, Takata N, Ishibashi H, et al. Self-organizing optic-cup morphogenesis in three-dimensional culture. *Nature*. 2011;472(7341):51-58. doi:10.1038/nature09941

154. Meyer JS, Howden SE, Wallace KA, et al. Optic vesicle-like structures derived from human pluripotent stem cells facilitate a customized approach to retinal disease treatment. *Stem Cells*. 2011;29(8):1206-1218. doi:10.1002/stem.674

155. Jin ZB, Okamoto S, Osakada F, et al. Modeling retinal degeneration using patient-specific induced pluripotent stem cells. *PLoS One*. 2011;6(2). doi:10.1371/journal.pone.0017084

156. Curtin JA, Dane AP, Swanson A, Alexander IE, Ginn SL. Bidirectional promoter interference between two widely used internal heterologous promoters in a late-generation lentiviral construct. *Gene Ther*. 2008;15(5):384-390. doi:10.1038/sj.gt.3303105

157. Park SK, Hwang BJ, Kee Y. Promoter cross-talk affects the inducible expression of intronic shRNAs from the tetracycline response element. *Genes and Genomics*. 2019;41(4):483-490. doi:10.1007/s13258-019-00784-z

158. Semple-Rowland SL, Coggin WE, Geesey M, et al. Expression characteristics of dual-promoter lentiviral vectors targeting retinal photoreceptors and müller cells. *Mol Vis*. 2010;16:916-934.

159. Nie L, Thakur M Das, Wang Y, Su Q, Zhao Y, Feng Y. Regulation of U6 Promoter Activity by Transcriptional Interference in Viral Vector-Based RNAi. *Genomics, Proteomics Bioinforma*. 2010;8(3):170-179. doi:10.1016/S1672-0229(10)60019-8

160. Ferrari FK, Samulski T, Shenk T, Samulski RJ. Second-strand synthesis is a rate-limiting step for efficient transduction by recombinant adeno-associated virus vectors. *J Virol*. 1996;70(5):3227-3234. doi:10.1128/jvi.70.5.3227-3234.1996

161. Nieuwenhuis B, Haenzi B, Hilton S, et al. Optimization of adeno-associated viral vector-mediated transduction of the corticospinal tract: comparison of four promoters. *Gene Ther*. 2020;28(1):56-74. doi:10.1038/s41434-020-0169-1

162. Rodriguez-Estevez L, Asokan P, Borrás T. Transduction optimization of AAV vectors for human gene therapy of glaucoma and their reversed cell entry characteristics. *Gene Ther*. 2020;27(3-4):127-142. doi:10.1038/s41434-019-0105-4

163. Li A, Lee CM, Hurley AE, et al. A Self-Deleting AAV-CRISPR System for In Vivo Genome Editing. *Mol Ther - Methods Clin Dev*. 2019;12:111-122. doi:10.1016/j.omtm.2018.11.009

164. Suzuki K, Tsunekawa Y, Hernandez-Benitez R, et al. In vivo genome editing via CRISPR/Cas9 mediated homology-independent targeted integration. *Nature*. 2016;540(7631):144-149. doi:10.1038/nature20565

165. Thakore PI, Kwon JB, Nelson CE, et al. RNA-guided transcriptional silencing in vivo with S. aureus CRISPR-Cas9 repressors. *Nat Commun*. (2018):1-9. doi:10.1038/s41467-018-04048-4

166. Lupo A, Cesaro E, Montano G, Zurlo D, Izzo P, Costanzo P. KRAB-Zinc Finger Proteins: A Repressor Family Displaying Multiple Biological Functions. *Curr Genomics*. 2013;14(4):268-278. doi:10.2174/1389202911314999000 2

167. Doench JG, Hartenian E, Graham DB, et al. Rational design of highly active sgRNAs for CRISPR-Cas9-mediated gene inactivation. *Nat Biotechnol*. 2014;32(12):1262-1267. doi:10.1038/nbt.3026

168. Doench JG, Fusi N, Sullender M, et al. Optimized sgRNA design to maximize activity and minimize off-target effects of CRISPR-Cas9. *Nat Biotechnol*. 2016;34(2):184-191. doi:10.1038/nbt.3437

169. Sanson KR, Hanna RE, Hegde M, et al. Optimized libraries for CRISPR-Cas9 genetic screens with multiple modalities. *Nat Commun*. 2018;9(1):1-15. doi:10.1038/s41467-018-07901-8

170. Friedland AE, Baral R, Singhal P, et al. Characterization of Staphylococcus aureus Cas9: A smaller Cas9 for all-in-one adeno-associated virus delivery and paired nickase applications. *Genome Biol*. 2015;16(1):1-10. doi:10.1186/s13059-015-0817-8

171. Levy JM, Yeh WH, Pendse N, et al. Cytosine and adenine base editing of the brain, liver, retina, heart and skeletal muscle of mice via adeno-associated viruses. *Nat Biomed Eng*. 2020;4(1):97-110. doi:10.1038/s41551-019-0501-5

172. Stepanenko AA, Dmitrenko V V. HEK293 in cell biology and cancer research: Phenotype, karyotype, tumorigenicity, and stress-induced genome-phenotype evolution. *Gene*. 2015;569(2):182-190. doi:10.1016/j.gene.2015.05.065

173. Kleinstiver BP, Prew MS, Tsai SQ, et al. Engineered CRISPR-Cas9 nucleases with altered PAM specificities. *Nature*. 2015;523(7561):481-485. doi:10.1038/nature14592

174. Lin M-T, Mosier SL, Thiess M, et al. Clinical Validation of KRAS, BRAF, and EGFR Mutation Detection Using Next-Generation Sequencing. *Am J Clin Pathol*. 2014;141(6):856-866. doi:10.1309/AJCPMWGWGO34EGOD

175. Davidson CJ, Zeringer E, Champion KJ, et al. Improving the limit of detection for Sanger sequencing: A comparison of methodologies for *KRAS* variant detection. *Biotechniques*. 2012;53(3):182-188. doi:10.2144/000113913

176. Tsiatis AC, Norris-Kirby A, Rich RG, et al. Comparison of Sanger sequencing, pyrosequencing, and melting curve analysis for the detection of KRAS mutations: Diagnostic and clinical implications. *J Mol Diagnostics*. 2010;12(4):425-432. doi:10.2353/jmoldx.2010.090188

177. Desfarges S, Ciuffi A. Retroviral integration site selection. *Viruses*. 2010;2(1):111-130. doi:10.3390/v2010111

178. Uusi-Mäkelä MIE, Barker HR, Bäuerlein CA, Häkkinen T, Nykter M, Rämet M. Chromatin accessibility is associated with CRISPR-Cas9 efficiency in the zebrafish (Danio rerio). Riley BB, ed. *PLoS One*. 2018;13(4):e0196238. doi:10.1371/journal.pone.0196238

179. Corish P, Tyler-Smith C. Attenuation of green fluorescent protein half-life in mammalian cells. *Protein Eng*. 1999;12(12):1035-1040. doi:10.1093/protein/12.12.1035

180. Sentmanat MF, Peters ST, Florian CP, Connelly JP, Pruett-Miller SM. A Survey of Validation Strategies for CRISPR-Cas9 Editing. *Sci Rep*. 2018;8(1):888. doi:10.1038/s41598-018-19441-8

181. Jin J, Xu Y, Huo L, et al. An improved strategy for CRISPR/Cas9 gene knockout and subsequent wildtype and mutant gene rescue. He B, ed. *PLoS One*. 2020;15(2):e0228910. doi:10.1371/journal.pone.0228910

182. Tuladhar R, Yeu Y, Tyler Piazza J, et al. CRISPR-Cas9-based mutagenesis frequently provokes on-target mRNA misregulation. *Nat Commun*. 2019;10(1):1-10. doi:10.1038/s41467-019-12028-5

183. Liu S, Wei X, Dong X, Xu L, Liu J, Jiang B. Structural plasticity of green fluorescent protein to amino acid deletions and fluorescence rescue by folding-enhancing mutations. *BMC Biochem*. 2015;16(1):17. doi:10.1186/s12858-015-0046-5

184. Rodríguez-Mejía J-L, Roldán-Salgado A, Osuna J, Merino E, Gaytán P. A Codon Deletion at the Beginning of Green Fluorescent Protein Genes Enhances Protein Expression. *J Mol Microbiol Biotechnol*. 2017;27(1):1-10. doi:10.1159/000448786

185. Nishimasu H, Ran FA, Hsu PD, et al. Crystal structure of Cas9 in complex with guide RNA and target DNA. *Cell*. 2014;156(5):935-949. doi:10.1016/j.cell.2014.02.001

186. Alerasool N, Segal D, Lee H, Taipale M. An efficient KRAB domain for CRISPRi applications in human cells. *Nat Methods*. 2020;17(11):1093-1096. doi:10.1038/s41592-020-0966-x

187. Fry LE, Peddle CF, Stevanovic M, Barnard AR, McClements ME, MacLaren RE. Promoter Orientation within an AAV-CRISPR Vector Affects Cas9 Expression and Gene Editing Efficiency. *Cris J*. 2020;3(4):276-283. doi:10.1089/crispr.2020.0021

188. Moreno AM, Fu X, Zhu J, et al. In Situ Gene Therapy via AAV-CRISPR-Cas9-Mediated Targeted Gene Regulation. *Mol Ther*. 2018;26(7):1818-1827. doi:10.1016/j.ymthe.2018.04.017

189. Mao H, James T, Schwein A, et al. AAV delivery of wild-type rhodopsin preserves retinal function in a mouse model of autosomal dominant retinitis pigmentosa. *Hum Gene Ther*. 2011;22(5):567-575. doi:10.1089/hum.2010.140

190. Wu J, Tang B, Tang Y. Allele-specific genome targeting in the development of precision medicine. *Theranostics*. 2020;10(7):3118-3137. doi:10.7150/thno.43298

191. Smith C, Abalde-Atristain L, He C, et al. Efficient and allele-specific genome editing of disease loci in human iPSCs. *Mol Ther*. 2015;23(3):570-577. doi:10.1038/mt.2014.226

192. Yu J, Xiang X, Huang J, et al. Haplotyping by CRISPR-mediated DNA circularization (CRISPR-hapC) broadens allele-specific gene editing. *Nucleic Acids Res*. 2020;48(5):E25. doi:10.1093/nar/gkz1233

193. Christie KA, Courtney DG, Dedionisio LA, et al. Towards personalised allele-specific CRISPR gene editing to treat autosomal dominant disorders. *Sci Rep*. 2017;7(1):1-11. doi:10.1038/s41598-017-16279-4

194. He Q, Chen M, Lin X, Chen Z. Allele-specific PCR with a novel data processing method based on difference value for single nucleotide polymorphism genotyping of ALDH2 gene. *Talanta*. 2020;220:121432. doi:10.1016/j.talanta.2020.121432

195. Altschul SF, Gish W, Miller W, Myers EW, Lipman DJ. Basic local alignment search tool. *J Mol Biol*. 1990;215(3):403-410. doi:10.1016/S0022-2836(05)80360-2

196. Peng GH, Chen S. Crx activates opsin transcription by recruiting HAT-containing co-activators

and promoting histone acetylation. *Hum Mol Genet*. 2007;16(20):2433-2452. doi:10.1093/hmg/ddm200

197. Peng GH, Chen S. Chromatin immunoprecipitation identifies photoreceptor transcription factor targets in mouse models of retinal degeneration: New findings and challenges. *Vis Neurosci*. 2005;22(5):575-586. doi:10.1017/S0952523805225063

198. Mollema NJ, Yuan Y, Jelcick AS, et al. Nuclear Receptor Rev-erb Alpha (Nr1d1) Functions in Concert with Nr2e3 to Regulate Transcriptional Networks in the Retina. Nollen E, ed. *PLoS One*. 2011;6(3):e17494. doi:10.1371/journal.pone.0017494

199. Altshuler DL, Durbin RM, Abecasis GR, et al. A map of human genome variation from population-scale sequencing. *Nature*. 2010;467(7319):1061-1073. doi:10.1038/nature09534

200. Auton A, Abecasis GR, Altshuler DM, et al. A global reference for human genetic variation. *Nature*. 2015;526(7571):68-74. doi:10.1038/nature15393

201. Al-Ali M, Osman W, Tay GK, Alsafar HS. A 1000 Arab genome project to study the Emirati population. *J Hum Genet*. 2018;63(4):533-536. doi:10.1038/s10038-017-0402-y

202. Belsare S, Levy-Sakin M, Mostovoy Y, et al. Evaluating the quality of the 1000 genomes project data. *BMC Genomics*. 2019;20(1). doi:10.1186/s12864-019-5957-x

203. Zischewski J, Fischer R, Bortesi L. Detection of on-target and off-target mutations generated by CRISPR/Cas9 and other sequence-specific nucleases. *Biotechnol Adv*. 2017;35(1):95-104. doi:10.1016/j.biotechadv.2016.12.003

204. Brinkman EK, Chen T, Amendola M, Van Steensel B. Easy quantitative assessment of genome editing by sequence trace decomposition. *Nucleic Acids Res*. 2014;42(22):e168. doi:10.1093/nar/gku936

205. Hanlon KS, Kleinstiver BP, Garcia SP, et al. High levels of AAV vector integration into CRISPR-induced DNA breaks. *Nat Commun*. 2019;10(1):1-11. doi:10.1038/s41467-019-12449-2

206. Nelson CE, Wu Y, Gemberling MP, et al. Long-term evaluation of AAV-CRISPR genome editing for Duchenne muscular dystrophy. *Nat Med*. 2019;25(3):427-432. doi:10.1038/s41591-019-0344-3

207. McCullough KT, Boye SL, Fajardo D, et al. Somatic Gene Editing of GUCY2D by AAV-CRISPR/Cas9 Alters Retinal Structure and Function in Mouse and Macaque. *Hum Gene Ther*. 2019;30(5):571-589. doi:10.1089/hum.2018.193

208. Mladenova V, Mladenov E, Russev G. Organization of Plasmid DNA into Nucleosome-Like Structures after Transfection in Eukaryotic Cells. *Biotechnol Biotechnol Equip*. 2009;23(1). doi:10.1080/13102818.2009.10817609

209. Peng GH, Chen S. Chromatin immunoprecipitation identifies photoreceptor transcription factor targets in mouse models of retinal degeneration: New findings and challenges. *Vis Neurosci*. 2005;22(5):575-586. doi:10.1017/S0952523805225063

210. Satoh S, Tang K, Iida A, et al. Development/Plasticity/Repair The Spatial Patterning of Mouse Cone Opsin Expression Is Regulated by Bone Morphogenetic Protein Signaling through Downstream Effector COUP-TF Nuclear Receptors. *J Ne*. 2009;29(40):12401-12411. doi:10.1523/JNEUROSCI.0951-09.2009

211. Peng G-H, Chen S. Active opsin loci adopt intrachromosomal loops that depend on the photoreceptor transcription factor network. *PNAS*. 2011;108(43):17821-17826. doi:10.1073/pnas.1109209108

212. Kumar R, Chen S, Scheurer D, et al. The bZIP transcription factor Nrl stimulates rhodopsin promoter activity in primary retinal cell cultures. *J Biol Chem*. 1996;271(47):29612-29618. doi:10.1074/jbc.271.47.29612

213. Yadav SP, Hao H, Yang H-J, et al. The transcription-splicing protein NonO/p54 nrb and three NonO-interacting proteins bind to distal enhancer region and augment rhodopsin expression. *Hum Gene Ther Methods*. 2014;23(8):2132-2144. doi:10.1093/hmg/ddt609

214. Yang YS, Hanke JH, Carayannopoulos L, Craft CM, Capra JD, Tucker PW. NonO, a non-POU-domain-containing, octamer-binding protein, is the mammalian homolog of Drosophila nonAdiss. *Mol Cell Biol*. 1993;13(9):5593-5603. doi:10.1128/mcb.13.9.5593

215. Jeon CJ, Strettoi E, Masland RH. The major cell populations of the mouse retina. *J Neurosci*. 1998;18(21):8936-8946. doi:10.1523/jneurosci.18-21-08936.1998

216. Ortiń-Martínez A, Nadal-Nicolás FM, Jimeńez-López M, et al. Number and distribution of mouse retinal cone photoreceptors: Differences between an albino (Swiss) and a pigmented (C57/BL6) strain. *PLoS One*. 2014;9(7). doi:10.1371/journal.pone.0102392

217. Li L, Lin Y, Yang F, Zou T, Yang J, Zhang H. An improved method for preparation of mouse retinal cryosections. *Eur J Histochem*. 2020;64(3):1-5. doi:10.4081/ejh.2020.3154

218. Chung SH, Mollhoff IN, Nguyen U, et al. Factors Impacting Efficacy of AAV-Mediated CRISPR-Based Genome Editing for Treatment of Choroidal Neovascularization. *Mol Ther - Methods Clin Dev*. 2020;17:409-417. doi:10.1016/j.omtm.2020.01.006

219. Vasireddy V, Mills JA, Gaddameedi R, et al. AAV-Mediated Gene Therapy for Choroideremia: Preclinical Studies in Personalized Models. *PLoS One*. 2013;8(5):61396. doi:10.1371/journal.pone.0061396

220. Deng WT, Dinculescu A, Li Q, et al. Tyrosine-mutant AAV8 delivery of human MERTK provides long-term retinal preservation in RCS rats. *Invest Ophthalmol Vis Sci*. 2012;53(4):1895-1904. doi:10.1167/iovs.11-8831

221. McClements ME, Barnard AR, Singh MS, et al. An AAV Dual Vector Strategy Ameliorates the Stargardt Phenotype in Adult Abca4-/- Mice. *Hum Gene Ther*. 2019;30(5):590-600. doi:10.1089/hum.2018.156

222. Scandella V, Paolicelli RC, Knobloch M. A novel protocol to detect green fluorescent protein in unfixed, snap-frozen tissue. *Sci Rep*. 2020;10(1):14642. doi:10.1038/s41598-020-71493-x

223. Qi Y, Dai X, Zhang H, et al. Trans-Corneal Subretinal Injection in Mice and Its Effect on the Function and Morphology of the Retina. Ljubimov A V., ed. *PLoS One*. 2015;10(8):e0136523. doi:10.1371/journal.pone.0136523

224. Mühlfriedel R, Michalakis S, Garrido MG, Biel M, Seeliger MW. Optimized Technique for Subretinal Injections in Mice. In: *Methods in Molecular Biology*. Vol 935. Humana Press, Totowa, NJ; 2012:343-349. doi:10.1007/978-1-62703-080-9_24

225. Charbel Issa P, Barnard AR, Singh MS, et al. Fundus autofluorescence in the Abca4-/- mouse model of stargardt disease-correlation with accumulation of A2E, retinal function, and histology. *Investig Ophthalmol Vis Sci*. 2013;54(8):5602-5612. doi:10.1167/iovs.13-11688

226. Fischer J, Otto T, Delori F, Pace L, Staurenghi G. Scanning Laser Ophthalmoscopy (SLO). In: *High Resolution Imaging in Microscopy and Ophthalmology*. Cham: Springer International Publishing; 2019:35-57. doi:10.1007/978-3-030-16638-0_2

227. Issa PC, Singh MS, Lipinski DM, et al. Optimization of in vivo confocal autofluorescence imaging

of the ocular fundus in mice and its application to models of human retinal degeneration. *Investig Ophthalmol Vis Sci*. 2012;53(2):1066-1075. doi:10.1167/iovs.11-8767

228. Maeder ML, Stefanidakis M, Wilson CJ, et al. Development of a gene-editing approach to restore vision loss in Leber congenital amaurosis type 10. *Nat Med*. 2019;25(2):229-233. doi:10.1038/s41591-018-0327-9

229. Schulz D, Grumann D, Trübe P, et al. Laboratory mice are frequently colonized with Staphylococcus aureus and mount a systemic immune response-note of caution for in vivo infection experiments. *Front Cell Infect Microbiol*. 2017;7(MAY):152. doi:10.3389/fcimb.2017.00152

230. Hochman MA, Seery CM, Zarbin MA. Pathophysiology and management of subretinal hemorrhage. *Surv Ophthalmol*. 1997;42(3):195-213. doi:10.1016/S0039-6257(97)00089-1

231. Li P, Kleinstiver BP, Leon MY, et al. Allele-Specific CRISPR-Cas9 Genome Editing of the Single-Base P23H Mutation for Rhodopsin-Associated Dominant Retinitis Pigmentosa. *Cris J*. 2018;1(1):55-64. doi:10.1089/crispr.2017.0009

232. Giannoukos G, Ciulla DM, Marco E, et al. UDiTaS™, A genome editing detection method for indels and genome rearrangements. *BMC Genomics*. 2018;19(1). doi:10.1186/s12864-018-4561-9

233. Nelson CE, Hakim CH, Ousterout DG, et al. In vivo genome editing improves muscle function in a mouse model of Duchenne muscular dystrophy. *Science (80-)*. 2016;351(6271):403-407. doi:10.1126/science.aad5143

234. Yu W, Wu Z. In Vivo applications of CRISPR-based genome editing in the retina. *Front Cell Dev Biol*. 2018;6(MAY). doi:10.3389/fcell.2018.00053

235. Li F, Hung SSC, Mohd Khalid MKN, et al. Utility of self-destructing CRISPR/Cas constructs for targeted gene editing in the retina. *Hum Gene Ther*. 2019;30(11):1349-1360. doi:10.1089/hum.2019.021

236. Eberle D, Kurth T, Santos-Ferreira T, Wilson J, Corbeil D, Ader M. Outer Segment Formation of Transplanted Photoreceptor Precursor Cells. *PLoS One*. 2012;7(9). doi:10.1371/journal.pone.0046305

237. Eberle D, Santos-Ferreira T, Grahl S, Ader M. Subretinal transplantation of MACS purified photoreceptor precursor cells into the adult mouse retina. *J Vis Exp*. 2014;(84). doi:10.3791/50932

238. Eberle D, Schubert S, Postel K, Corbeil D, Ader M. Increased integration of transplanted CD73-positive photoreceptor precursors into adult mouse retina. *Investig Ophthalmol Vis Sci*. 2011;52(9):6462-6471. doi:10.1167/iovs.11-7399

239. Pickar-Oliver A, Gersbach CA. The next generation of CRISPR–Cas technologies and applications. *Nat Rev Mol Cell Biol*. 2019;20(8):490-507. doi:10.1038/s41580-019-0131-5

240. LaVail MM, Yasumura D, Matthes MT, et al. Ribozyme rescue of photoreceptor cells in P23H transgenic rats: Long-term survival and late-stage therapy. *Proc Natl Acad Sci U S A*. 2000;97(21):11488-11493. doi:10.1073/pnas.210319397

241. Chadderton N, Millington-Ward S, Palfi A, et al. Improved retinal function in a mouse model of dominant retinitis pigmentosa following AAV-delivered gene therapy. *Mol Ther*. 2009;17(4):593-599. doi:10.1038/mt.2008.301

242. O'Reilly M, Palfi A, Chadderton N, et al. RNA interference-mediated suppression and

replacement of human rhodopsin in vivo. *Am J Hum Genet*. 2007;81(1):127-135. doi:10.1086/519025

243. Botta S, Marrocco E, de Prisco N, et al. Rhodopsin targeted transcriptional silencing by DNA-binding. *Elife*. 2016;5(MARCH2016). doi:10.7554/eLife.12242

244. Fischer MD, McClements ME, Martinez-Fernandez de la Camara C, et al. Codon-Optimized RPGR Improves Stability and Efficacy of AAV8 Gene Therapy in Two Mouse Models of X-Linked Retinitis Pigmentosa. *Mol Ther*. 2017;25(8):1854-1865. doi:10.1016/j.ymthe.2017.05.005

245. Cehajic-Kapetanovic J, Xue K, Martinez-Fernandez de la Camara C, et al. Initial results from a first-in-human gene therapy trial on X-linked retinitis pigmentosa caused by mutations in RPGR. *Nat Med*. 2020;26(3):354-359. doi:10.1038/s41591-020-0763-1

246. Gorbatyuk MS, Knox T, LaVail MM, et al. Restoration of visual function in P23H rhodopsin transgenic rats by gene delivery of BiP/Grp78. *Proc Natl Acad Sci U S A*. 2010;107(13):5961-5966. doi:10.1073/pnas.0911991107

247. Leonard KC, Petrin D, Coupland SG, et al. XIAP Protection of Photoreceptors in Animal Models of Retinitis Pigmentosa. Lewin A, ed. *PLoS One*. 2007;2(3):e314. doi:10.1371/journal.pone.0000314

248. Buch PK, MacLaren RE, Durán Y, et al. In Contrast to AAV-Mediated Cntf Expression, AAV-Mediated Gdnf Expression Enhances Gene Replacement Therapy in Rodent Models of Retinal Degeneration. *Mol Ther*. 2006;14(5):700-709. doi:10.1016/j.ymthe.2006.05.019

249. Xie H, Ge X, Yang F, et al. High-fidelity SaCas9 identified by directional screening in human cells. *PLoS Biol*. 2020;18(7). doi:10.1371/journal.pbio.3000747

250. Matharu N, Rattanasopha S, Tamura S, et al. CRISPR-mediated activation of a promoter or enhancer rescues obesity caused by haploinsufficiency. *Science (80-)*. 2019;363(6424). doi:10.1126/science.aau0629

251. Tanenbaum ME, Gilbert LA, Qi LS, Weissman JS, Vale RD. A protein-tagging system for signal amplification in gene expression and fluorescence imaging. *Cell*. 2014;159(3):635-646. doi:10.1016/j.cell.2014.09.039

252. Murray SF, Jazayeri A, Matthes MT, et al. Allele-specific inhibition of rhodopsin with an antisense oligonucleotide slows photoreceptor cell degeneration. *Investig Ophthalmol Vis Sci*. 2015;56(11):6362-6375. doi:10.1167/iovs.15-16400

253. Olsson JE, Gordon JW, Pawlyk BS, et al. Transgenic mice with a rhodopsin mutation (Pro23His): A mouse model of autosomal dominant retinitis pigmentosa. *Neuron*. 1992;9(5):815-830. doi:10.1016/0896-6273(92)90236-7

254. Tsai SQ, Zheng Z, Nguyen NT, et al. GUIDE-seq enables genome-wide profiling of off-target cleavage by CRISPR-Cas nucleases. *Nat Biotechnol*. 2015;33(2):187-198. doi:10.1038/nbt.3117

255. Yin J, Liu M, Liu Y, et al. Optimizing genome editing strategy by primer-extension-mediated sequencing. *Cell Discov*. 2019;5(1):18. doi:10.1038/s41421-019-0088-8

256. Anderson KR, Haeussler M, Watanabe C, et al. CRISPR off-target analysis in genetically engineered rats and mice. *Nat Methods*. 2018;15(7):512-514. doi:10.1038/s41592-018-0011-5

257. Woo Cho S, Kim S, Min Kim J, Kim J-S. Targeted genome engineering in human cells with the Cas9 RNA-guided endonuclease. *Nat Biotechnol*. 2013;31(3):230-232. doi:10.1038/nbt.2507

258. Manghwar H, Li B, Ding X, et al. CRISPR/Cas Systems in Genome Editing: Methodologies and

Tools for sgRNA Design, Off-Target Evaluation, and Strategies to Mitigate Off-Target Effects. *Adv Sci*. 2020;7(6). doi:10.1002/advs.201902312

259. Crosetto N, Mitra A, Silva MJ, et al. Nucleotide-resolution DNA double-strand break mapping by next-generation sequencing. *Nat Methods*. 2013;10(4):361-365. doi:10.1038/nmeth.2408

260. Wienert B, Wyman SK, Richardson CD, et al. Unbiased detection of CRISPR off-targets in vivo using DISCOVER-Seq. *Science (80-)*. 2019;364(6437):286-289. doi:10.1126/science.aav9023

261. Mundade R, Ozer HG, Wei H, Prabhu L, Lu T. Role of ChIP-seq in the discovery of transcription factor binding sites, differential gene regulation mechanism, epigenetic marks and beyond. *Cell Cycle*. 2014;13(18):2847-2852. doi:10.4161/15384101.2014.949201

262. Lalonde S, Stone OA, Lessard S, et al. Frameshift indels introduced by genome editing can lead to in-frame exon skipping. *PLoS One*. 2017;12(6). doi:10.1371/journal.pone.0178700

263. Kapahnke M, Banning A, Tikkanen R. Random Splicing of Several Exons Caused by a Single Base Change in the Target Exon of CRISPR/Cas9 Mediated Gene Knockout. *Cells*. 2016;5(4):45. doi:10.3390/cells5040045

264. Lee ES, Flannery JG. Transport of truncated rhodopsin and its effects on rod function and degeneration. *Investig Ophthalmol Vis Sci*. 2007;48(6):2868-2876. doi:10.1167/iovs.06-0035

265. Chen YF, Wang IJ, Lin LLK, Chen MS. Examining rhodopsin retention in endoplasmic reticulum and intracellular localization in vitro and in vivo by using truncated rhodopsin fragments. *J Cell Biochem*. 2011;112(2):520-530. doi:10.1002/jcb.22942

266. Hanlon KS, Kleinstiver BP, Garcia SP, et al. High levels of AAV vector integration into CRISPR-induced DNA breaks. *Nat Commun*. 2019;10(1):1-11. doi:10.1038/s41467-019-12449-2

267. Kearns NA, Genga RMJ, Enuameh MS, Garber M, Wolfe SA, Maehr R. Cas9 effector-mediated regulation of transcription and differentiation in human pluripotent stem cells. *Dev*. 2014;141(1):219-223. doi:10.1242/dev.103341

268. Mimee M, Tucker AC, Voigt CA, Lu TK. Programming a Human Commensal Bacterium, Bacteroides thetaiotaomicron, to Sense and Respond to Stimuli in the Murine Gut Microbiota. *Cell Syst*. 2015;1(1):62-71. doi:10.1016/j.cels.2015.06.001

269. Moore R, Spinhirne A, Lai MJ, et al. CRISPR-based self-cleaving mechanism for controllable gene delivery in human cells. *Nucleic Acids Res*. 2015;43(2):1297-1303. doi:10.1093/nar/gku1326

270. Stolfi A, Gandhi S, Salek F, Christiaen L. Tissue-specific genome editing in ciona embryos by CRISPR/Cas9. *Dev*. 2014;141(21):4115-4120. doi:10.1242/dev.114488

271. Tran MTN, Khalid MKNM, Pébay A, et al. Screening of CRISPR/Cas base editors to target the AMD high-risk Y402H complement factor H variant. *Mol Vis*. 2019;25(October 2018):174-182.

272. Chen CH, Xiao T, Xu H, et al. Improved design and analysis of CRISPR knockout screens. *Bioinformatics*. 2018;34(23):4095-4101. doi:10.1093/bioinformatics/bty450

273. Hanna RE, Doench JG. Design and analysis of CRISPR–Cas experiments. *Nat Biotechnol*. 2020;38(7):813-823. doi:10.1038/s41587-020-0490-7

274. Home - ClinicalTrials.gov. https://www.clinicaltrials.gov/ct2/home. Accessed March 20, 2021.

275. Cideciyan A V., Sudharsan R, Dufour VL, et al. Mutation-independent rhodopsin gene therapy by knockdown and replacement with a single AAV vector. *Proc Natl Acad Sci U S A*. 2018;115(36):E8547-E8556. doi:10.1073/pnas.1805055115

276. Bobbin ML, Rossi JJ. RNA Interference (RNAi)-Based Therapeutics: Delivering on the Promise? *Annu Rev Pharmacol Toxicol*. 2016;56(1):103-122. doi:10.1146/annurev-pharmtox-010715-103633

277. First CRISPR therapy dosed. *Nat Biotechnol*. 2020;38(4):382. doi:10.1038/s41587-020-0493-4

9 Appendix

9.1 Primers

9.1.1 PCR primers

Chapter	Product	Primer name	Primer sequence	Primer overhang 5'	Annealing temperature	Specialised conditions
PDE6Bp validation	shorthPDE6Bp with cloning overhangs	PDE6B_F2c	GTCTGAGGAGAGGGAGCGCA	ATGGTACC	62C	+5% DMSO
		PDE6B_R1c	TGCCTGTCCCTGGAGACGCT	CCATGCGCACCTTGAAGCGCA TGAACTCCTTGATGACGTCCTC GGAGGAGGCCATGGCGGT		
	longhPDE6Bp with cloning overhangs	PDE6B_F1c	CTCCCAGCCTTCATTCCACA	ATGGTACC	62C	+5% DMSO
		PDE6B_R1c	TGCCTGTCCCTGGAGACGCT	CCATGCGCACCTTGAAGCGCA TGAACTCCTTGATGACGTCCT CGGAGGAGGCCATGGCGGT		
	Promoterless.DsRed	PromlessDsRed_F1	GAACCCAGAGTCATCCACCG	None	65C	+5% DMSO, extension time 70s
		PromlessDsRed_R1	GATCTCGAGAGCTTGGCGTA	None		
Construct design	Nrl-EGFP transgene upstream	Nrl-EGFP-F6	GTGTCCTCTGGGCTCTGTG	None	65C	None
		Nrl-EGFP-R5	CTTGTACAGCTCGTCCATGC	None		
	HEK293-EGFP transgene upstream	CMV_F5	GGCACCAAAATCAACGGGAC	None	55C	None
		Nrl-EGFP-R4	GTCTTGTAGTTGCCGTCGTC	None		
	HEK293-EGFP transgene central	EGFP_F4	GAGCAAAGACCCCAACGAGA	None	65C	None
		BSR_R1	GCTCAAGATGCCCCTGTTCT	None		
	HEK293-EGFP transgene downstream	EGFP_F1	CGAGGAGCTGTTCACCGG	None	60C	None
		Nrl-EGFP-R5	CTTGTACAGCTCGTCCATGC	None		
Nrl-EGFP in vivo	hPDE6Bp with cloning overhangs	PDE6B_F2D	GTCTGAGGAGAGGGAGCGCA	ACTCTAGACTCGAGGCGTTG	60C	None
		PDE6B_R2	TGGCTGCCTGTCCCTGGAGACGCT	GCCCATGG		

9.1.2 Sequencing primers

Chapter	DNA to be sequenced	Primer name	Primer sequence
hPDE6Bp validation	DsRed reporter plasmids	dsRed(hRHOp1)FW	TCCACCGCCATGGCCTCCTCCGA
		DsRed2SEQFW3	CCAAGAAGCCCGTGCAGC
		PolyA(DsRed2)FW	GTTCCTGTAGGACCTGCGCTGATCAGCCTCG
		pDsRed SEQ FW f(RC)	CGTCGGAGGGGAAGTTCAC
		rhodsred_R1	GGCTGTGAGGTTGTGGAGAC
		pscAAVMCS SEQFW7	TGCAGCTGGCACGACAGGT
		pscAAVMCS SEQFW3	GGCCCGCATGCGTCGACA
		px601_F11	CCGCTCATGAGACAATAACCC
		px601_F12	TCTGACAACGATCGGAGGAC
		px601_F14	GAGCGCAGATACCAAATACTGT
Materials and methods	AAV Helper Plasmid	pAD_F1	GCGCATTCAGCAGGCCG
		pAD_F2	GACGCTCAAGTCAGAG
		pAD_F3	CTGACGCTCAGTGGAAC
		pAD_F4	CTCCGATCGTTGTC
		pAD_F5	GACAGCTTATCATCG
		pAD_F5a	TTCGCTACTTGGAGCCACT
		pAD_F6a	CTTGGTTATGCCGGTACTGC
		pAD_F7	TGACCGAGGAGCTGT
		pAD_F8	TACAATGGCCGGACT
		pAD_F9	ATGACACTACGACCA
		pAD_F10	CAGTTACTGTGCTGA
		pAD_F11	TCTTGGGCAATGTATG
		pAD_F12	TAGGAACCATAGCCTTG
		pAD_F13	GTACTGCTATCGGTG
		pAD_F14	GCAAGGAGGTGCTGCTG
		pAD_F15	CAAGCGAGGAGCTCAC
		pAD_F16	GATCGCAGAGACCTG
		pAD_F17	GTCTGACACCTCTTCG
		pAD_F18	AGACCGTCACCGCTCA
		pAD_F19	ATCTCCGGGTCAGCA
		pAD_F20	TGGGCTCGCATGTGCCGT
		pAD_F21	CGGATGAGGCGGCGTATC
		pAD_F22	CAGAGGTGACCTACAAGC
		pAD_F23	CGACTTCAAGATATC

		pAD_F24	GCTACGGCGCAGGAGTG
		pAD_F25	CGGCATCACCTGGATGTC
		pAD_R	ACAGTCAGCCTTACCAGTA
		pAD_Ra	TCAAACATGTCTGCGGGT
	AAV8(Y733F) RepCap	Cap2 FW1	ATGGCTGCCGATGGTTA
		Cap8 FW1	TGGCTGCCGATGGTTATCT
		Cap8 FW2	TTCCAGACCCTCAACCTCTCG
		Cap8 FW3	ACGGCTACCTAACACTCA
		Cap8 FW4	ATCCTGGCATCGCTATGGCA
		Cap8 FW5	ACTACAAATCTACAAGTGTGGA
		Cap8 RC1	CAGGTTTCAGCGCCCACCAC
		Rep2 Fw1	AGAAGCTGCAGCGCGA
		Rep2 Fw2	TGCGGCCTCCAACTCGCGGT
		Rep2 FW3	GCCGTCTGGATCATGACT
		Rep2 RC1	CTCCCATTCCTTCTC
		Rep2 RC2	ACGTGCATGTGGAAGTA
		RepCap FW1	CGTCTATCAGGGCGAT
		RepCap FW2	ACCTGTCGTGCCAGCTGC
		RepCap FW3	ACTATCGTCTTGAGTCCA
		RepCap FW4	ATCTGGCCCCAGTGCTGCA
		RepCap FW5	AGGATCTTACCGCTGTTGA
		RepCap RC1	TGTGATGGATATCTGCAGAAT
Construct design	SaCas9, dSaCas9, dSaCas9.KRAB plasmids	px601_F1	CCAAGTCTCCACCCCATTGA
		px601_F2	TGAAGAAAGACGGCGAAGTG
		px601_F4	GGACGCCCAGAAAATGATCA
		px601_F6	AAGCTGCTGATGTACCACCA
		px601_F7	TGAACAACGACCTGCTGAAC
		px601_F8	GTAGGTGTCATTCTATTCTGGGG
		px601_R2	CCATAAGGTCATGTACTGGGC
		px601_R4	TTGTGCACGCCTCTTCTCTT
		px601_R7	CCCTTGGCCAGATTCAGGAT
		px601_R9	GCCTGGTTGCTGATCTTCTTC
	Nrl-EGFP transgene	Nrl-EGFP-F2	ATGATGGGACCAACTGCTCA
		Nrl-EGFP-F11	GAGAAGGAGGGATGGAGGGA
		Nrl-EGFP-F17	CAAAGACCCCAACGAGAAGC
		Nrl-EGFP-F18	CCAACAAGCTGGCTGAGGAT
		Nrl-EGFP-R5	CTTGTACAGCTCGTCCATGC
		Nrl-EGFP-R6	GGCGGATCTTGAAGTTCACC

		Nrl-EGFP-R13	GGCTGTCAGTATGAATTGGCC
		Nrl-EGFP-R15	GGTATTCCCTGCCTGTTGG
		Nrl-EGFP-R17	CCTCAGCTTCCTCTCACCTT
		Nrl-EGFP-R18	GCATCCTCACATTTCAGCCC
		Nrl-EGFP-R22	TGGTGTCGTCCCTGTATTCA
	HEK293-EGFP transgene	EGFP_F2	CACATGAAGCAGCACGACTT
		EGFP_F4	GAGCAAAGACCCCAACGAGA
		EGFP_R2	GAAGCACTGCACGCCGTAG
		Nrl-EGFP-R6	GGCGGATCTTGAAGTTCACC
Targeting RHO	RHO	SNP genotyping done using TIDE primers and subcloning	
	Sequencing pGEM-T Easy Vector for subcloning	T7 promoter	TAATACGACTCACTATAGGG
		M13 rev (-29)	CAGGAAACAGCTATGACC
	Sequencing gRNA target inserted into PsiCheck2	PCseqRV2	GTGCTTCTCGGAATCATAG

9.1.3 TIDE and subcloning primers

gRNA	Primer	Primer sequence	Annealing temperature	Sequencing primer
F9	CMV_F3	TCATATGCCAAGTACGCCCC	65C	EGFP_R2
	EGFP_R2	GAAGCACTGCACGCCGTAG		
F10	CMV_F4	CCATGGTGATGCGGTTTTGG	65C	Nrl-EGFP-R4
	Nrl-EGFP-R4	GTCTTGTAGTTGCCGTCGTC		
F11/No PAM	EGFP_F1	CGAGGAGCTGTTCACCGG	65C	EGFP_F1
	EGFP_R1	GTCCATGCCGAGAGTGATCC		
F12	EGFP_F2	CACATGAAGCAGCACGACTT	65C	EGFP_F2
	EGFP_R3	GCAGCGTATCCACATAGCGT		
F13	EGFP_F1	CGAGGAGCTGTTCACCGG	65C	EGFP_R1
	EGFP_R1	GTCCATGCCGAGAGTGATCC		
F14	EGFP_F1	CGAGGAGCTGTTCACCGG	65C	EGFP_R3
	EGFP_R3	GCAGCGTATCCACATAGCGT		
F15	EGFP_F1	CGAGGAGCTGTTCACCGG	65C	EGFP_R3
	EGFP_R3	GCAGCGTATCCACATAGCGT		
hRHO+28	hRHO_F5	TTAGGCCCTCAGTTTCTGCA	60C	hRHO_F5
	hRHO+466R	GGAGAAGGGAGAAGGCCTCT		
hRHO+2300	hRHO+2097F	CTTAGGCAGTGGGGTCTGTG	60C	hRHO+2097F
	hRHO+2699R	GAGTGGGACCCAGTTCCAAG		
VEGFA_val	VEGFA_F1	GGCTCCAACAGGTCCTCTTC	60C	VEGFA_R1
	VEGFA_R1	CACCAAGGTTCACAGCCTGA		
hRHO-677	hRHO-1268F	TTTTCCCCCAGTCATCTGCC	60C	hRHO-559R
	hRHO-559R	GAAACGGAAGCTGCAGGTTG		
hRHO+50	hRHO-244F	CTTGGCCCCTCTTAGAAGCC	60C	hRHO-244F
	hRHO+466R	GGAGAAGGGAGAAGGCCTCT		
hRHO+1841	hRHO_F17	TGTCCCTTTCACTGTTAGGAATG	60C	N/A
	hRHO+2226R	CGAAGCGGAAGTTGCTCATG		
hRHO+1844	hRHO_F17	TGTCCCTTTCACTGTTAGGAATG	60C	N/A
	hRHO+2226R	CGAAGCGGAAGTTGCTCATG		
hRHO+2781	hRHO+2524F	TCCTGAGCCCCATGTCAAAC	65C	hRHO+2524F
	hRHO+3194R	CCCTCAGGCTCTGCATTTGA		
hRHO+4447 +4452	hRHO+4169F	CAGTCTTGGGTCAGCAGTCC	60C	hRHO+4169F
	hRHO+4882R	TTCCGGAACTGGAAGGCAAG		
hRHO+5317	hRHO+5038F	GTCTCCCATCCCCTACACCT	60C	N/A
	hRHO+5730R	CCCCATCATCTGAATGCCCA		

hRHO+5991 +6009	hRHO+5730F	TGGGCATTCAGATGATGGGG	65C	hRHO+5730F
	hRHO+6454R	CAACAAAACCCACCACCGTT		

9.1.4 Site-directed mutagenesis primers

Chapter	DNA product	DNA template	Primer name	Primer sequence	Extension time
PDE6Bp validation	hRHOp.BamHI.DsRed	hRHOp.DsRed	PDE6bSDM_F1	GGTCAGAACCCAGAG**G** **G**ATCCACCGCCATGGC	4 min 42 s
			PDE6bSDM_R1	GCCATGGCGGTGGAT**C** **C**CTCTGGGTTCTGACC	
Construct design	CMV.SaCas9.D10A.bGHpA.U6.gRNA	CMV.SaCas9.bGHpA.U6.gRNA	dSaCas9SDM1_F1	ATCCTGGGCCTGG CCATCGGCATCACC	7 min 24 s
			dSaCas9SDM1_R1	GGTGATGCCGATG GCCAGGCCCAGGAT	
	CMV.dSaCas9.bGHpA.U6.gRNA	CMV.SaCas9.D10A.bGHpA.U6.gRNA	dSaCas9SDM2_F1	GGTGCTCGTGAAG CAGGAAGAAGCCA GCAAGAAGGG	7 min 24 s
			dSaCas9SDM2_R1	CCCTTCTTGCTGGCT TCTTCCTGCTTCACG AGCACC	

9.2 Nrl-EGFP transgene

Transgene present in Nrl-EGFP mice. Grey highlighted sequence is the Nrl promoter, Green highlighted sequence in the EGFP gene

ATGATGGGACCAACTGCTCACTGGCTAGGCTCTCCAAGGCAGCAAACCAAAGCAAAGCGCTTTCCGATTAAGT
CAATTACTTCAGGTATGTATTGGAGCAATTATGTTAGTGTTAGTCGGTTTTTGTTATTGTGACAAAGTGCCCGA
GAAAGATCAAAGGAGGGGAGCCTTCTTTGGGCTAATGGCTTCAGTTTCAGCTGATGGTTGTGGGTGTCCTATT
GCTTTGGTCCAAAATCTAACATCACGATGGAAAATGTATAGTGAAGAAGTAAAGAGAGAAAAGAGAGAGGA
AGAGGGGGAAGTGGAGGTGGGGGAGAAGGAGGGATGGAGGGACACAGACAAAATGCACCAATGAACTAA
GGAGAAGATACACCATTCAAACGCATGTTTTTTCTAGTTAGGCCAATTCATACTGACAGCCAATTCAGTATGGA
TTCTTCAGCTGGTTAGTTATGGATAAGTTTAACCTCTAATAATATCTCAGTGAAAACTAGCTTTTAAAATATACC
GGAACCATAGCAGTGATAGAAAACTAATGTAGGGTGGACACACACACACACACACACACACAAACACACACT
TTGAGACTGGGTTGAAGGTAGGCATCTGTGGACCAGTGGGTCTCAAACATTAGTGTGTTTCAGAGCTGTTGG
AAGGGTTTATTAAACAGCAGCTGTCTATAACCTACTTACTGAGTTTCTGGTTCTGTGAGTTTGAGGTAAAGCAA
AAGAATTTGTTTCTTCAAGTTCCCAAGGGGTGATTTCTTAAGACTGTGGAAGCCATTGTTCCAACAGGCAGGG
AATACCCTTTAACTTCTGGAGTTTCTTTTATCACAGCACCTATTTAAACAGCTTCAGGCAGGTTTAAACATCTCC
TTGGCTAAGTCCTACTATCCCTGCTTCGGCCCCTACTAGGGGGTGACAGCTCTAAGAGGCGTTAGGCGATTAG
GCTGAAAATGTAGGTCACACCCCAGCCGTCTGGGAATGAGCGAGAGAGGAGAAGAGGGACTGAGACACCGC
ACGGKGAAAAGGTGAGAGGAAGCTGAGGGCTCATGAGGGCATTCACAGAAGTGTGGTGGTGATTGGATTTC
AGCTTCTTTTAGTCTCCAGATGAAAGACCAGAGTTGGGATCTCCGCTTTTTCTATCTCTTCTCTCCAGCTGGGCT
GCTTGTCTTCGGGATGGGCTATTAAGAGCGAGTTTCTTCATGGAAGCTCATGGCTTATCTTTCTAATACAGTGA
CTCTGTGAGGAATAAGACGAGTCAGGGTGAAGGTAGGGCAGGGGCTGAAATGTGAGGATGCTTGAAAAGA
AGCAGCAGCCCCAACAAGCTGGCTGAGGATGGGCTGGGAACGCGTATATGTCTCCTTGACACGGAGTCTTAA
AAGAGGTTTTGGGTAGTATGTCTGGACTCTTACCACTCTAAGCTTTGAGTGATTGGGCTGAGAATTGTGTTTCC
ATGGAGGGGTGGTGTTTGGGGTCAACATGGCTCTCTATATTGGAAACCAAGCTCACAACATAAGCAAGGTCT
GATATAGGAAGCTTCTCTGGGGAAGATGCCGTTTGTTTTTTTCCTTTTTGGAGAACTGATAGCACCTGTCTTTC
ACTGGCTTCTGAGTCCCTGCCCCAGGCCAATGAGATATGCAAATAAGCCCTTCATCTTATTGGATGAGGCTCG
AGGACCACAGATGATCTCAGGGAACCAGTCCTTTAAGAGTGTCCTCTGGGCTCTGTGCCCACAGCCCCCTTGT
TCTGAATACAGGGACGACACCAGCCCCTGCTCTATGGAGTATTTAGCCTCCAGGGAAGCTGTGCCTTTCTGGT
TCTGACAGTGACTACGTCATCTCTGCCATTACATCGGATCCACCGGTCGCCACCATGGTGAGCAAGGGCGAGG
AGCTGTTCACCGGGGTGGTGCCCATCCTGGTCGAGCTGGACGGCGACGTAAACGGCCACAAGTTCAGCGTGT
CCGGCGAGGGCGAGGGCGATGCCACCTACGGCAAGCTGACCCTGAAGTTCATCTGCACCACCGGCAAGCTGC
CCGTGCCCTGGCCCACCCTCGTGACCACCCTGACCTACGGCGTGCAGTGCTTCAGCCGCTACCCCGACCACAT
GAAGCAGCACGACTTCTTCAAGTCCGCCATGCCCGAAGGCTACGTCCAGGAGCGCACCATCTTCTTCAAGGAC
GACGGCAACTACAAGACCCGCGCCGAGGTGAAGTTCGAGGGCGACACCCTGGTGAACCGCATCGAGCTGAA
GGGCATCGACTTCAAGGAGGACGGCAACATCCTGGGGCACAAGCTGGAGTACAACTACAACAGCCACAACGT
CTATATCATGGCCGACAAGCAGAAGAACGGCATCAAGGTGAACTTCAAGATCCGCCACAACATCGAGGACGG
CAGCGTGCAGCTCGCCGACCACTACCAGCAGAACACCCCCATCGGCGACGGCCCCGTGCTGCTGCCCGACAA
CCACTACCTGAGCACCCAGTCCGCCCTGAGCAAAGACCCCAACGAGAAGCGCGATCACATGGTCCTGCTGGA
GTTCGTGACCGCCGCCGGGATCACTCTCGGCATGGACGAGCTGTACAAGTAA

9.3 SaCas9 gRNAs targeting EGFP

All possible SaCas9 gRNAs in the confirmed Nrl-EGFP sequence targeting EGFP with the PAM NNGRRT.

Positions are the predicted cut site relative to the EGFP start codon.

Position	Strand	Sequence	PAM	Specificity Score	Efficiency Score
-9	-1	TGCTCACCATGGTGGCGACCG	GTGGAT	92.8	29.3
+27	1	CAAGGGCGAGGAGCTGTTCAC	CGGGGT	86.5	15.3
+50	-1	TACGTCGCCGTCCAGCTCGAC	CAGGAT	97.3	7.0
+137	-1	GCCGGTGGTGCAGATGAACTT	CAGGGT	82.0	19.3
+185	-1	GCCGTAGGTCAGGGTGGTCAC	GAGGGT	85.1	7.0
+197	-1	GAAGCACTGCACGCCGTAGGT	CAGGGT	97.2	21.2
+231	-1	AGTCGTGCTGCTTCATGTGGT	CGGGGT	81.2	12.2
+332	-1	GCCCTCGAACTTCACCTCGGC	GCGGGT	93.2	3.9
+362	-1	CTTCAGCTCGATGCGGTTCAC	CAGGGT	95.6	9.3
+416	-1	GTTGTACTCCAGCTTGTGCCC	CAGGAT	79.4	15.9
+422	1	GCAACATCCTGGGGCACAAGC	TGGAGT	80.2	8.7
+509	-1	GCTGCCGTCCTCGATGTTGTG	GCGGAT	92.5	18.1
+566	-1	CAGCACGGGGCCGTCGCCGAT	GGGGGT	99.1	4.9
+617	-1	GGGGTCTTTGCTCAGGGCGGA	CTGGGT	85.8	13.0
+639	-1	CCATGTGATCGCGCTTCTCGT	TGGGGT	98.4	15.4
+662	1	AGCGCGATCACATGGTCCTGC	TGGAGT	89.3	11.4
+681	1	GCTGGAGTTCGTGACCGCCGC	CGGGAT	98.8	5.9
+698	-1	CTTGTACAGCTCGTCCATGCC	GAGAGT	91.8	9.8

9.4 HEK293-EGFP cell transgene sequence

EGFP transgene sequence of the HEK293-EGFP cell line. Grey highlighted sequence is the CMV promoter, green highlighted sequence is EGFP.

GGCACCAAAATCAACGGGACTTTCCAAAATGTCGTAACAACTCCGCCCCATTGACGCAAATGGGCGGTAGGC
GTGTACGGTGGGAGGTCTATATAAGCAGAGCTCGTTTAGTGAACCGTCAGATCGCCTGGAGACGCCATCCAC
GCTGTTTTGACCTCCATAGAAGACACCGACTCTAGAGGATCCACTAGTCCAGTGTGGTGGAATTCTGCAGATA
TCAACAAGTTTGTACAAAAAAGCAGGCTCCACCATGGTGAGCAAGGGCGAGGAGCTGTTCACCGGGGTGGT
GCCCATCCTGGTCGAGCTGGACGGCGACGTAAACGGCCACAAGTTCAGCGTGTCCGGCGAGGGCGAGGGCG
ATGCCACCTACGGCAAGCTGACCCTGAAGTTCATCTGCACCACCGGCAAGCTGCCCGTGCCCTGGCCCACCCT
CGTGACCACCTTCACCTACGGCGTGCAGTGCTTCGCCCGCTACCCCGACCACATGAAGCAGCACGACTTCTTCA
AGTCCGCCATGCCCGAAGGCTACGTCCAGGAGCGCACCATCTTCTTCAAGGACGACGGCAACTACAAGACCC
GCGCCGAGGTGAAGTTCGAGGGCGACACCCTGGTGAACCGCATCGAGCTGAAGGGCATCGACTTCAAGGAG
GACGGCAACATCCTGGGGCACAAGCTGGAGTACAACTACAACAGCCACAAGGTCTATATCACCGCCGACAAG
CAGAAGAACGGCATCAAGGTGAACTTCAAGACCCGCCACAACATCGAGGACGGCAGCGTGCAGCTCGCCGAC
CACTACCAGCAGAACACCCCCATCGGCGACGGCCCCGTGCTGCTGCCCGACAACCACTACCTGAGCACCCAGT
CCGCCCTGAGCAAAGACCCCAACGAGAAGCGCGATCACATGGTCCTGCTGGAGTTCGTGACCGCCGCCGGGA
TCACTCTCGGCATGGACGAGCTGTACAAGTAAACCCAGCTTTCTTGTACAAAGTGGTTGATATCCAGCACAGT
GGCGGCCGCTCGAGTCTAGAGGGCCCGCGGTTCGAAGGTAAGCCTATCCCTAACCCTCTCCTCGGTCTCGATT
CTACGCGTACCGGTTAGTAATGATCGACAATCAACCTCTGGATTACAAAATTTGTGAAAGATTGACTGGTATTC
TTAACTATGTTGCTCCTTTTACGCTATGTGGATACGCTGCTTTAATGCCTTTGTATCATGCTATTGCTTCCCGTAT
GGCTTTCATTTTCTCCTCCTTGTATAAATCCTGGTTGCTGTCTCTTTATGAGGAGTTGTGGCCCGTTGTCAGGCA
ACGTGGCGTGGTGTGCACTGTGTTTGCTGACGCAACCCCCACTGGTTGGGGCATTGCCACCACCTGTCAGCTC
CTTTCCGGGACTTTCGCTTTCCCCCTCCCTATTGCCACGGCGGAACTCATCGCCGCCTGCCTTGCCCGCTGCTGG
ACAGGGGCTCGGCTGTTGGGCACTGACAATTCCGTGGTGTTGTCGGGGAAGCTGACGTCCTTTCCATGGCTG
CTCGCCTGTGTTGCCACCTGGATTCTGCGCGGGACGTCCTTCTGCTACGTCCCTTCGGCCCTCAATCCAGCGGA
CCTTCCTTCCCGCGGCCTGCTGCCGGCTCTGCGGCCTCTTCCGCGTCTTCGCCTTCGCC

9.5 RHO SNPs

All SNPs in the RHO sequence with a global MAF over .01

SNP ID	Mutation	Chromosomal location	Global MAF	Global MAF
rs2625954	TACATGGCATT[C/T]GAGGCCCTC	3:129527571	T=0.4714/2361 C=0.4482/14215	0.4714
rs2625955	CAACCTCACAG[A/C]CACCCTGGA	3:129527956	C=0.4728/2368 A=0.4856/14140	0.4728
rs2269736	CTCAGGCCTTC[A/C/G]CAGCATTCTTG	3:129528683	A=0.1697/850	0.1697
rs7984	TGGGAGCAGCC[A/G]CGGGTCAGCCA	3:129528708	A=0.4716/2362	0.4716
rs2855552	CTCAGGGAATC[G/T]CTGGCCATTGT	3:129530082	G=0.1006/504	0.1006
rs200054443	ACTCTGCCCCA[/CATTAGGATG]CATTCTTCTGC	3:129530483	-=0.1524/763	0.1524
rs570795323	CACACACACAC[/ACACACACACACACACAA]ACACACACACA	3:129530549	ACACACACACACACACAA=0.1615/809	0.1615
rs6803468	GTGGCCCCTTG[G/T]AACTGGGTCCC	3:129531436	T=0.098442/493	0.0984
rs2855557	AAGTCAGAAGG[A/T]CCCAAGTCGGG	3:129533079	A=0.4778/2393	0.4778
rs2071092	GCCCTGGCCCT[A/G]ACTCAAGCCTC	3:129533585	A=0.1150/576	0.1150
rs796098464	AGGCTCCTTAA[-/T]TTTTTTTTTTT	3:129533858	-=0.4828/2418	0.4828
rs2410	CCACGTTCCCC[A/G]AGGCCAGCGG	3:129533950	G=0.2656/1330	0.2656
rs2855558	CCAAGTTCCCA[A/G]TGAGGGTGAGA	3:129534630	A=0.4790/2399	0.4790
rs60645924	GAGGGTGAGAT[C/T]GGGCCTGGGGT	3:129534643	C=0.1096/549	0.1096

9.6 RHO SNPs and gRNAs

Key: **Exon** SNP gRNA Start codon Overlap of 2 gRNAs Stop codon

GCTGCGACTGAACTGTCCCTACTGTTATTCGCTCTTCTATTTGTTTGTGGTCCCTGTGCCCCCTCACCCCACAAAAACACTG
GCTTCTTGTGAGCAGGAGCTTGCTCTTTCGTGTACCCTGTGTGTCCCCAAGGACCAAGCACCTTGTCTGGGCCACAGTAGG
TGCTCAATACACATGTTGGCTGGACAGTGGTCACTGAGCGGCCGCACGTCGGGCACTCTCAGCACTTGCACAGGCCGCCC
CAGACACCCCACTTCATTCCTGGGAGGTGTCATCATGTTGCTTGGACGACGGGGAGAGGGGGACCTGCCAGTGTTGGCCT
CCATTTTCCCCCAGTCATCTGCCCCCAAGGCTCTGACTACTTTCTTTCTCACGGTACATCCTGCTATTCTGGAATCGGCCCTC
GTGGGGCCACCTGGTACATGGCATTTGAGGCCCTCGTGGCTGATTAGGCCTCCCCCAACAGTGCCCTGTCTGCTGCCTCCA
GGGCCAGCCTCCCCTTCAGACTGGAGTCCCCTGAAGGGTTCTGCCCCTCCCCTGCTCTGGTAGCCCCCTCCATCCTCCCTCC
CTCCACTCCATCTTTGGGGGCATTTGAGTCACCTTTCTACACCAGTGATCTGCCCAAGCCACTGCTCACTTTCCTCTGGATA
AAGCCAGGTTCCCCGGCCTAGCGTTCAAGACCCATTACAACTGCCCCCAGCCCAGATCTTCCCCACCTAGCCACCTGGCAA
ACTGCTCCTTCTCTCAAAGGCCCAAACATGGCCTCCCAGACTGCAACCCCCAGGCAGTCAGGCCCTGTCTCCACAACCTCA
CAGCCACCCTGGACGGAATCTGCTTCTTCCCACATTTGAGTCCTCCTCAGCCCCTGAGCTCCTCTGGGCAGGGCTGTTTCTT
TCCATCTTTGTATTCCCAGGGGCCTGCAAATAAATGTTTAATGAACGAACAAGAGAGTGAATTCCAATTCCATGCAACAAG
GATTGGGCTCCTGGGCCCTAGGCTATGTGTCTGGCACCAGAAACGGAAGCTGCAGGTTGCAGCCCCTGCCCTCATGGAGC
TCCTCCTGTCAGAGGAGTGTGGGGACTGGATGACTCCAGAGGTAACTTGTGGGGGAACGAACAGGTAAGGGGCTGTGT
GACGAGATGAGAGACTGGGAGAATAAACCAGAAAGTCTCTAGCTGTCCAGAGGACATAGCACAGAGGCCCATGGTCCCT
ATTTCAAACCCAGGCCACCAGACTGAGCTGGGACCTTGGGACAGACAAGTCATGCAGAAGTTAGGGGACCTTCTCCTCCC
TTTTCCTGGATCCTGAGTACCTCTCCTCCCTGACCTCAGGCTTCCTCCTAGTGTCACCTTGGCCCCTCTTAGAAGCCAATTAG
GCCCTCAGTTTCTGCAGCGGGGATTAATATGATTATGAACACCCCCAATCTCCCAGATGCTGATTCAGCCAGGAGCTTAGG
AGGGGGAGGTCACTTTATAAGGGTCTGGGGGGGTCAGAACCCA**GAGTCATCCAGCTGGAGCCCTGAGTGGCTGAGCTC**
AGGCCTTCGCAGCATTCTTGGGTGGGAGCAGCCACGGGTCAGCCACAAGGGCCACAGCCATGAATGGCACAGAAGGC
CCTAACTTCTACGTGCCCTTCTCCAATGCGACGGGTGTGGTACGCAGCCCCTTCGAGTACCCACAGTACTACCTGGCTGA
GCCATGGCAGTTCTCCATGCTGGCCGCCTACATGTTTCTGCTGATCGTGCTGGGCTTCCCCATCAACTTCCTCACGCTCTA
CGTCACCGTCCAGCACAAGAAGCTGCGCACGCCTCTCAACTACATCCTGCTCAACCTAGCCGTGGCTGACCTCTTCATGG
TCCTAGGTGGCTTCACCAGCACCCTCTACACCTCTCTGCATGGATACTTCGTCTTCGGGCCCACAGGATGCAATTTGGAG
GGCTTCTTTGCCACCCTGGGCGGTATGAGCCGGGTGTGGGTGGGGGTGTGCAGGAGCCCGGGAGCATGGAGGGGTCTGG
GAGAGTCCCGGGCTTGGCGGTGGTGGCTGAGAGGCCTTCTCCCTTCTCCTGTCCTGTCAATGTTATCCAAAGCCCTCATAT
ATTCAGTCAACAAACACCATTCATGGTGATAGCCGGGCTGCTGTTTGTGCAGGGCTGGCACTGAACACTGCCTTGATCTTA
TTTGGAGCAATATGCGCTTGTCTAATTTCACAGCAAGAAAACTGAGCTGAGGCTCAAAGAAGTCAAGCGCCCTGCTGGGG
CGTCACACAGGGACGGGTGCAGAGTTGAGTTGGAAGCCCGCATCTATCTCGGGCCATGTTTGCAGCACCAAGCCTCTGTT
TCCCTTGGAGCAGCTGTGCTGAGTCAGACCCAGGCTGGGCACTGAGGGAGAGCTGGGCAAGCCAGACCCCTCCTCTCTG
GGGGCCCAAGCTCAGGGTGGGAAGTGGATTTTCCATTCTCCAGTCATTGGGTCTTCCCTGTGCTGGGCAATGGGCTCGGT
CCCCTCTGGCATCCTCTGCCTCCCCTCTCAGCCCCTGTCCTCAGGTGCCCCTCCAGCCTCCCTGCCGCGTTCCAAGTCTCCTG
GTGTTGAGAACCGCAAGCAGCCGCTCTGAAGCAGTTCCTTTTTGCTTTAGAATAATGTCTTGCATTTAACAGGAAAACAGA
TGGGGTGCTGCAGGGATAACAGATCCCACTTAACAGAGAGGAAAACTGAGGCAGGGAGAGGGGAAGAGACTCATTTAG
GGATGTGGCCAGGCAGCAACAAGAGCCTAGGTCTCCTGGCTGTGATCCAGGAATATCTCTGCTGAGATGCAGGAGGAGA
CGCTAGAAGCAGCCATTGCAAAGCTGGGTGACGGGGAGAGCTTACCGCCAGCCACAAGCGTCTCTCTGCCAGCCTTGCCC
TGTCTCCCCCATGTCCAGGCTGCTGCCTCGGTCCCATTCTCAGGGAATCTCTGGCCATTGTTGGGTGTTTGTTGCATTCAAT
AATCACAGATCACTCAGTTCTGGCCAGAAGGTGGGTGTGCCACTTACGGGTGGTTGTTCTCTGCAGGGTCAGTCCCAGTT
TACAAATATTGTCCCTTTCACTGTTAGGAATGTCCCAGTTTGGTTGATTAACTATATGGCCACTCTCCCTATGGAACTTCAT
GGGGTGGTGAGCAGGACAGATGTCTGAATTCCATCATTTCCTTCTTCTTCCTCTGGGCAAAACATTGCACATTGCTTCATG
GCTCCTAGGAGAGGCCCCCACATGTCCGGGTTATTTCATTTCCCGAGAAGGGAGAGGGAGGAAGGACTGCCAATTCTGG
GTTTCCACCACCTCTGCATTCCTTCCCAACACAAGGAACTCTGCCCCACATTAGGATGCATTCTTCTGCTAAACACACACACAC
ACACACACACACACAACACACACACACACACACACACACACACACACACACAAAACTCCCTACCGGGTTCCCAGTTCAATCCT
GACCCCCTGATCTGATTCGTGTCCCTTATGGGCCCAGAGCGCTAAGCAAATAACTTCCCCCATTCCCTGGAATTTCTTTGCC
CAGCTCTCCTCAGCGTGTGGTCCCTCTGCCCCTTCCCCCTCCTCCCAGCACCAAGCTCTCTCCTTCCCCAAGGCCTCCTCAAA
TCCCTCTCCCACTCCTGGTTGCCTTCCTAGCTACCCTCTCCCTGTCTAGGGGGGAGTGCACCCTCCTTAGGCAGTGGGGTCT
GTGCTGACCGCCTGCTGACTGCCTTGCAG**GTGAAATTGCCCTGTGGTCCTTGGTGGTCCTGGCCATCGAGCGGTACGTG**
GTGGTGTGTAAGCCCATGAGCAACTTCCGCTTCGGGGAGAACCATGCCATCATGGGCGTTGCCTTCACCTGGGTCATGG
CGCTGGCCTGCGCCGCACCCCCACTCGCCGGCTGGTCCAGGTAATGGCACTGAGCAGAAGGGAAGAAGCTCCGGGGGC
TCTTTGTAGGGTCCTCCAGTCAGGACTCAAACCCAGTAGTGTCTGGTTCCAGGCACTGACCTTGTATGTCTCCTGGCCCAA
ATGCCCACTCAGGGTAGGGGTGTAGGGCAGAAGAAGAAACAGACTCTAATGTTGCTACAAGGGCTGGTCCCATCTCCTG
AGCCCCATGTCAAACAGAATCCAAGACATCCCAACCCTTCACCTTGGCTGTGCCCCTAATCCTCAACTAAGCTAGGCGCAA

ATTCCAATCCTCTTTGGTCTAGTACCCCGGGGGCAGCCCCCTCTAACCTTGGGCCTCAGCAGCAGGGGAGGCCACACCTTC
CTAGTGCAGGTGGCCATATTGTGGCCCCTTGGAACTGGGTCCCACTCAGCCTCTAGGCGATTGTCTCCTAATGGGGCTGA
GATGAGACACAGTGGGGACAGTGGTTTGGACAATAGGACTGGTGACTCTGGTCCCCAGAGGCCTCATGTCCCTCTGTCTC
CAGAAAATTCCCACTCTCACTTCCCTTTCCTCCTCAGTCTTGCTAGGGTCCATTTCTTACCCCTTGCTGAATTTGAGCCCACC
CCCTGGACTTTTTCCCCATCTTCTCCAATCTGGCCTAGTTCTATCCTCTGGAAGCAGAGCCGCTGGACGCTCTGGGTTTCCT
GAGGCCCGTCCACTGTCACCAATATCAGGAACCATTGCCACGTCCTAATGACGTGCGCTGGAAGCCTCTAGTTTCCAGAA
GCTGCACAAAGATCCCTTAGATACTCTGTGTGTCCATCTTTGGCCTGGAAAATACTCTCACCCTGGGGCTAGGAAGACCTC
GGTTTGTACAAACTTCCTCAAATGCAGAGCCTGAGGGCTCTCCCCACCTCCTCACCAACCCTCTGCGTGGCATAGCCCTAG
CCTCAGCGGGCAGTGGATGCTGGGGCTGGGCATGCAGGGAGAGGCTGGGTGGTGTCATCTGGTAACGCAGCCACCAAA
CAATGAAGCGACACTGATTCCACAAGGTGCATCTGCATCCCCATCTGATCCATTCCATCCTGTCACCCAGCCATGCAGACG
TTTATGATCCCCTTTTCCAGGGAGGGAATGTGAAGCCCC`AGAAAGGGCCAGCGCTCGGCAGCCACCTTGGCTGTTCCCAA
GTCCCTCACAGGCAGGGTCTCCCTACCTGCCTGTCCTCAG**GTACATCCCCGAGGGCCTGCAGTGCTCGTGTGGAATCGAC**
TACTACACGCTCAAGCCGGAGGTCAACAACGAGTCTTTTGTCATCTACATGTTCGTGGTCCACTTCACCATCCCCATGATT
ATCATCTTTTTCTGCTATGGGCAGCTCGTCTTCACCGTCAAGGAGGTACGGGCCGGGGGGTGGGCGGCCTCACGGCTCT
GAGGGTCCAGCCCCCAGCATGCATCTGCGGCTCCTGCTCCCTGGAGGAGCCATGGTCTGGACCCGGGTCCCGTGTCCTGC
AG**GCCGCTGCCCAGCAGCAGGAGTCAGCCACCACACAGAAGGCAGAGAAGGAGGTCACCCGCATGGTCATCATCATG**
GTCATCGCTTTCCTGATCTGCTGGGTGCCCTACGCCAGCGTGGCATTCTACATCTTCACCCACCAGGGCTCCAACTTCGGT
CCCATCTTCATGACCATCCCAGCGTTCTTTGCCAAGAGCGCCGCCATCTACAACCCTGTCATCTATATCATGATGAACAAG
CAGGTGCCTACTGCGGGTGGGAGGGCCCCAGTGCCCCAGGCCACAGGCGCTGCCTGCCAAGGACAAGCTACTTCCCAGG
GCAGGGGAGGGGGCTCCATCAGGGTTACTGGCAGCAGTCTTGGGTCAGCAGTCCCAATGGGGAGTGTGTGAGAAATGC
AGATTCCTGGCCCCACTCAGAACTGCTGAATCTCAGGGTGGGCCCAGGAACCTGCATTTCCAGCAAGCCCTCCACAGGTG
GCTCAGATGCTCACTCAGGTGGGAGAAGCTCCAGTCAGCTAGTTCTGGAAGCCCAATGTCAAAGTCAGAAGGACCCAAG
TCGGGAATGGGATGGGCCAGTCTCCATAAAGCTGAATAAGGAGCTAAAAAGTCTTATTCTGAGGGGTAAAGGGGTAAAG
GGTTCCTCGGAGAGGTACCTCCGAGGGGTAAACAGTTGGGTAAACAGTCTCTGAAGTCAGCTCTGCCATTTTCTAGCTGT
ATGGCCCTGGGCAAGTCAATTTCCTTCTCTGTGCTTTGGTTTCCTCATCCATAGAAAGGTAGAAAGGGCAAAACACCAAAC
TCTTGGATTACAAGAGATAATTTACAGAACACCCTTGGCACACAGAGGGCACCATGAAATGTCACGGGTGACACAGCCCC
CTTGTGCTCAGTCCCTGGCATCTCTAGGGGTGAGGAGCGTCTGCCTAGCAGGTTCCCTCCAGGAAGCTGGATTTGAGTGG
ATGGGGCGCTGGAATCGTGAGGGGCAGAAGCAGGCAAAGGGTCGGGGCGAACCTCACTAACGTGCCAGTTCCAAGCAC
ACTGTGGGCAGCCCTGGCCCTGACTCAAGCCTCTTGCCTTCCAG**TTCCGGAACTGCATGCTCACCACCATCTGCTGCGGCA**
AGAACCCACTGGGTGACGATGAGGCCTCTGCTACCGTGTCCAAGACGGAGACGAGCCAGGTGGCCCCGGCCTAAGACC
TGCCTAGGACTCTGTGGCCGACTATAGGCGTCTCCCATCCCCTACACCTTCCCCCAGCCACAGCCATCCCACCAGGAGCA
GCGCCTGTGCAGAATGAACGAAGTCACATAGGCTCCTTAATTTTTTTTTTTTTTTTAAGAAATAATTAATGAGGCTCCTCA
CTCACCTGGGACAGCCTGAGAAGGGACATCCACCAAGACCTACTGATCTGGAGTCCCACGTTCCCCAAGGCCAGCGGG
ATGTGTGCCCCTCCTCCTCCCAACTCATCTTTCAGGAACACGAGGATTCTTGCTTTCTGGAAAAGTGTCCCAGCTTAGGG
ATAAGTGTCTAGCACAGAATGGGGCACACAGTAGGTGCTTAATAAATGCTGGATGGATGCAGGAAGGAATGGAGGAA
TGAATGGGAAGGGAGAACATATCTATCCTCTCAGACCCTCGCAGCAGCAGCAACTCATACTTGGCTAATGATATGGAGC
AGTTGTTTTTCCCTCCCTGGGCCTCACTTTCTTCTCCTATAAAATGGAAATCCCAGATCCCTGGTCCTGCCGACACGCAGC
TACTGAGAAGACCAAAAGAGGTGTGTGTGTGTCTATGTGTGTGTTTCAGCACTTTGTAAATAGCAAGAAGCTGTACAG
ATTCTAGTTAATGTTGTGAATAACATCAATTAATGTAACTAGTTAATTACTATGATTATCACCTCCTGATAGTGAACATTT
TGAGATTGGGCATTCAGATGATGGGGGTTTCACCCAACCTTGGGGCAGGTTTTTAAAAATTAGCTAGGCATCAAGGCCA
GACCAGGGCTGGGGGTTGGGCTGTAGGCAGGGACAGTCACAGGAATGCAGAATGCAGTCATCAGACCTGAAAAAAC
AACACTGGGGGAGGGGGACGGTGAAGGCCAAGTTCCCAATGAGGGTGAGATTGGGCCTGGGGTCTCACCCCTAGTGT
GGGGCCCCAGGTCCCGTGCCTCCCCTTCCCAATGTGGCCTATGGAGAGACAGGCCTTTCTCTCAGCCTCTGGAAGCCACC
TGCTCTTTTGCTCTAGCACCTGGGTCCCAGCATCTAGAGCATGGAGCCTCTAGAAGCCATGCTCACCCGCCCACATTTAA
TTAACAGCTGAGTCCCTGATGTCATCCTTATCTCGAAGAGCTTAGAAACAAAGAGTGGGAAATTCCACTGGGCCTACCT
TCCTTGGGGATGTTCATGGGCCCCAGTTTCCAGTTTCCCTTGCCAGACAAGCCCATCTTCAGCAGTTGCTAGTCCATTCTC
CATTCTGGAGAATCTGCTCCAAAAAGCTGGCCACATCTCTGAGGTGTCAGAATTAAGCTGCCTCAGTAACTGCTCCCCCT
TCTCCATATAAGCAAAGCCAGAAGCTCTAGCTTTACCCAGCTCTGCCTGGAGACTAAGGCAAATTGGGCCATTAAAAGC
TCAGCTCCTATGTTGGTATTAACGGTGGTGGGTTTTGTTGCTTTCACACTCTATCCACAGGATAGATTGAAACTGCCAGCT
TCCACCTGATCCCTGACCCTGGGATGGCTGGATTGAGCAATGAGCAGAGCCAAGCAGCACAGAGTCCCCTGGGGCTAGA
GGTGGAGGAGGCAGTCCTGGGAATGGGAAAAACCCCAACTTTGGGGTCATAGAGGCACAGGTAACCCATAAAACTGCA
AACAAGCTTTGTCACCTCTCAGAGCTTCCTTATCTGCAAAAAAGAATCTTAAAACTGACCTTGGCTGGGCACAGTGGCTCA
CACCTCTAATCCCAGCACTTTGGGAGGCCAAGGTGGGCAGATCACGAGGTCAGGAGTTTGAGACCAGCCTGACCAACAC
GGTGAAACCCTGTCTCTACTAAAAATACAAAAATCAGCTGGGCATGGTGGCGCGTGCCTGTAATCCCAGCTATTCAGTGG
GCTGAGGCAGGAGAATCGCTTGAACCTGGGAGGTGGAGGTTGCAGTGAGCCGAGATTGCGCCACTGCACTCCAGCCTGA
GCAACAGAGGGACAGTCTGTCTCCAAACAAAACAAAACAAACAAACAAACAAACAAACAAA

9.7 RHO gRNA target regions cloned into the Psicheck2 vector

gRNA	gRNA sequence	gRNA target
RHO-677_C	CAACCTCACAGCCACCCTGGA	CAGGCCCTGTCTCCACAACCTCACAGCCACCCTGGACGGA ATCTGCTTCT
RHO-677_A	CAACCTCACAGACACCCTGGA	CAGGCCCTGTCTCCACAACCTCACAGACACCCTGGACGGA ATCTGCTTCT
RHO+50_G	GCTCAGGCCTTCGCAGCATTC	GCCCTGAGTGGCTGAGCTCAGGCCTTCGCAGCATTCTTGG GTGGGAGCAG
RHO+50_A	GCTCAGGCCTTCACAGCATTC	GCCCTGAGTGGCTGAGCTCAGGCCTTCACAGCATTCTTGG GTGGGAGCAG
RHO+1841_ins	AGAATGCATCCTAATGTGGGG	CAACAAGGAACTCTGCCCCACATTAGGATGCATTCTTCTGC TAAACACAC
RHO+1841_del	AGAATGTGGGGCAGAGTTCCT	CATTCCTTCCCAACAAGGAACTCTGCCCCACATTCTTCTGCT AAACACAC
RHO+1844_ins	ACAAGGAACTCTGCCCCACAT	CTGCATTCCTTCCCAACAAGGAACTCTGCCCCACATTAGGA TGCATTCTT
RHO+2781_G	CCATATTGTGGCCCCTTGGAA	TCCTAGTGCAGGTGGCCATATTGTGGCCCCTTGGAACTGG GTCCCACTCA
RHO+2781_T	CCATATTGTGGCCCCTTGTAA	TCCTAGTGCAGGTGGCCATATTGTGGCCCCTTGTAACTGG GTCCCACTCA
RHO+4447_A	AAAGTCAGAAGGACCCAAGTC	TGGAAGCCCAATGTCAAAGTCAGAAGGACCCAAGTCGGG AATGGGATGGG
RHO+4447_T	AAAGTCAGAAGGTCCCAAGTC	TGGAAGCCCAATGTCAAAGTCAGAAGGTCCCAAGTCGGG AATGGGATGGG
RHO+4452_A	CAGAAGGACCCAAGTCGGGAA	GCCCAATGTCAAAGTCAGAAGGACCCAAGTCGGGAATGG GATGGGCCAGT
RHO+4452_T	CAGAAGGTCCCAAGTCGGGAA	GCCCAATGTCAAAGTCAGAAGGTCCCAAGTCGGGAATGG GATGGGCCAGT
RHO+5317_A	TCCCACGTTCCCCAAGGCCAG	CCTACTGATCTGGAGTCCCACGTTCCCCAAGGCCAGCGGG ATGTGTGCCC
RHO+5317_G	TCCCACGTTCCCCGAGGCCAG	CCTACTGATCTGGAGTCCCACGTTCCCCGAGGCCAGCGGG ATGTGTGCCC
RHO+5991_A	GGTGAAGGCCAAGTTCCCAAT	CTGGGGGAGGGGGACGGTGAAGGCCAAGTTCCCAATGAG GGTGAGATTGG
RHO+5991_G	GGTGAAGGCCAAGTTCCCAGT	CTGGGGGAGGGGGACGGTGAAGGCCAAGTTCCCAGTGAG GGTGAGATTGG
RHO+6009_T	CAATGAGGGTGAGATTGGGCC	TGAAGGCCAAGTTCCCAATGAGGGTGAGATTGGGCCTGG GGTCTCACCCC
RHO+6009_C	CAATGAGGGTGAGATCGGGCC	TGAAGGCCAAGTTCCCAATGAGGGTGAGATCGGGCCTGG GGTCTCACCCC

9.8 cSLO mean grey value macro

The imageJ macro used to measure mean grey value of the superior and inferior retina on cSLO images taken using the blue auto fluorescence channel.

```
function processFolder_supMGV(input) {
list = getFileList(input);
	for (i = 0; i <list.length; i++) {
		if(endsWith(list[i], ".tif"))
			processFile_supMGV(input, list[i]);
			}
}
function processFile_supMGV(input, file) {
		print("Measuring Superior MGV: " + input + file);
		open(input+list[i]);
		run("Gaussian Blur...", "sigma=3");
		run("Specify...", "width=1336 height=1080 x=100 y=100 oval"); {
			if (selectionType!=1)
			   exit("Elliptical selection required");
			getBoundingRect(x, y, width, height);
			midy = y + height/2;
			getSelectionCoordinates(sx, sy);
			for (i=0; i<sy.length; i++) {
			   if (sy[i]>midy) sy[i] = midy;
			}
			makeSelection(3, sx, sy);
		 }
		run("Measure");
		close();
			}
function processFolder_infMGV(input) {
list = getFileList(input);
```

```
	for (i = 0; i <list.length; i++) {
		if(endsWith(list[i], ".tif"))
			processFile_infMGV(input, list[i]);
			}
}
function processFile_infMGV(input, file) {
		print("Measuring Inferior MGV: " + input + file);
		open(input+list[i]);
		run("Gaussian Blur...", "sigma=3");
		run("Specify...", "width=1336 height=1080 x=100 y=356 oval");
			{
			    if (selectionType!=1)
			       exit("Elliptical selection required");
			    getBoundingRect(x, y, width, height);
			    midy = y + height/2;
			    getSelectionCoordinates(sx, sy);
			    for (i=0; i<sy.length; i++) {
			       if (sy[i]<midy) sy[i] = midy;
			    }
			    makeSelection(3, sx, sy);
			 }
		run("Measure");
		close();
			}
function processFolder_bandMGV(input) {
list = getFileList(input);
	for (i = 0; i <list.length; i++) {
		if(endsWith(list[i], ".tif"))
			processFile_bandMGV(input, list[i]);
			}
}
function processFile_bandMGV(input, file) {
```

```
print("Measuring Band MGV: " + input + file);
open(input+list[i]);
run("Gaussian Blur...", "sigma=3");
run("Specify...", "width=600 height=600 x=468 y=468 oval constrain");
run("Make Band...", "band=2.65");
run("Measure");
close();
        }
```

9.9 Plasmid transgene sequences

9.9.1 hRHOp.DsRed

Grey sequence is ITRs, blue sequence is hRHOp, pink sequence is DsRed, yellow sequence is bGHpA.

GGCCACTCCCTCTCTGCGCGCTCGCTCGCTCACTGAGGCCGGGCGACCAAAGGTCGCCCGACGCCCGGGCTTT
GCCCGGGCGGCCTCAGTGAGCGAGCGAGCGCGCAGAGAGGGAGTGGCCAACTCCATCACTAGGGGTTCCTG
GAGGGGTGGAGTCGTGACCTAGGTACCCAGATCTTCCCCACCTAGCCACCTGGCAAACTGCTCCTTCTCTCAA
AGGCCCAAACATGGCCTCCCAGACTGCAACCCCCAGGCAGTCAGGCCCTGTCTCCACAACCTCACAGCCACCC
TGGACGGAATCTGCTTCTTCCCACATTTGAGTCCTCCTCAGCCCCTGAGCTCCTCTGGGCAGGGCTGTTTCTTTC
CATCTTTGTATTCCCAGGGGCCTGCAAATAAATGTTTAATGAACGAACAAGAGAGTGAATTCCAATTCCATGC
AACAAGGATTGGGCTCCTGGGCCCTAGGCTATGTGTCTGGCACCAGAAACGGAAGCTGCAGGTTGCAGCCCC
TGCCCTCATGGAGCTCCTCCTGTCAGAGGAGTGTGGGGACTGGATGACTCCAGAGGTAACTTGTGGGGGAAC
GAACAGGTAAGGGGCTGTGTGACGAGATGAGAGACTGGGAGAATAAACCAGAAAGTCTCTAGCTGTCCAGA
GGACATAGCACAGAGGCCCATGGTCCCTATTTCAAACCCAGGCCACCAGACTGAGCTGGGACCTTGGGACAG
ACAAGTCATGCAGAAGTTAGGGGACCTTCTCCTCCCTTTTCCTGGATCCTGAGTACCTCTCCTCCCTGACCTCA
GGCTTCCTCCTAGTGTCACCTTGGCCCCTCTTAGAAGCCAATTAGGCCCTCAGTTTCTGCAGCGGGGATTAATA
TGATTATGAACACCCCCAATCTCCCAGATGCTGATTCAGCCAGGAGCTTAGGAGGGGGAGGTCACTTTATAAG
GGTCTGGGGGGGTCAGAACCCAGAGTCATCCACCGCCATGGCCTCCTCCGAGGACGTCATCAAGGAGTTCAT
GCGCTTCAAGGTGCGCATGGAGGGCTCCGTGAACGGCCACGAGTTCGAGATCGAGGGCGAGGGCGAGGGC
CGCCCCTACGAGGGCACCCAGACCGCCAAGCTGAAGGTGACCAAGGGCGGCCCCCTGCCCTTCGCCTGGGAC
ATCCTGTCCCCCCAGTTCCAGTACGGCTCCAAGGTGTACGTGAAGCACCCCGCCGACATCCCCGACTACAAGA
AGCTGTCCTTCCCCGAGGGCTTCAAGTGGGAGCGCGTGATGAACTTCGAGGACGGCGGCGTGGTGACCGTG
ACCCAGGACTCCTCCCTGCAGGACGGCTCCTTCATCTACAAGGTGAAGTTCATCGGCGTGAACTTCCCCTCCGA
CGGCCCCGTAATGCAGAAGAAGACTATGGGCTGGGAGGCCTCCACCGAGCGCCTGTACCCCCGCGACGGCGT
GCTGAAGGGCGAGATCCACAAGGCCCTGAAGCTGAAGGACGGCGGCCACTACCTGGTGGAGTTCAAGTCCA
TCTACATGGCCAAGAAGCCCGTGCAGCTGCCCGGCTACTACTACGTGGACTCCAAGCTGGACATCACCTCCCA
CAACGAGGACTACACCATCGTGGAGCAGTACGAGCGCGCCGAGGGCCGCCACCACCTGTTCCTGTAGGACCT
GCGCTGATCAGCCTCGACTGTGCCTTCTAGTTGCCAGCCATCTGTTGTTTGCCCCTCCCCCGTGCCTTCCTTGAC
CCTGGAAGGTGCCACTCCCACTGTCCTTTCCTAATAAAATGAGGAAATTGCATCGCATTGTCTGAGTAGGTGTC
ATTCTATTCTGGGGGGTGGGGTGGGGCAGGACAGCAAGGGGGAGGATTGGGAAGACAATAGCAGGCATGC
TGGGGATGCGGTGGGCTCTATGGCTTCTGAGGCGGAAAGAACCAGCTGGGGACTAGTCCACTCCCTCTCTGC
GCGCTCGCTCGCTCACTGAGGCCGGGCGACCAAAGGTCGCCCGACGCCCGGGCTTTGCCCGGGCGGCCTCAG
TGAGCGAGCGAGCGCGCAGAGAGGGA

9.9.2 shorthPDE6Bp.DsRed

Grey sequence is ITRs, blue sequence is shorthPDE6Bp, red sequence is DsRed, yellow sequence is bGHpA.

GGCCACTCCCTCTCTGCGCGCTCGCTCGCTCACTGAGGCCGGGCGACCAAAGGTCGCCCGACGCCCGGGCTTT
GCCCGGGCGGCCTCAGTGAGCGAGCGAGCGCGCAGAGAGGGAGTGGCCAACTCCATCACTAGGGGTTCCTG
GAGGGGTGGAGTCGTGACCTAGGTACCGTCTGAGGAGAGGGAGCGCAGGCCCCCATTTGTAGGAGTGAGTC
AGCTGACCCGCCCCCGGGGTTCCTAATCTCACTAAGAAAGACTTTGCTGATGACAGGGTTTCCTGGGAGTCCA
TGCGTGCCTGGAGCAGCAGCGTCTCCAGGGACAGGCAACCGCCATGGCCTCCTCCGAGGACGTCATCAAGGA

GTTCATGCGCTTCAAGGTGCGCATGGAGGGCTCCGTGAACGGCCACGAGTTCGAGATCGAGGGCGAGGGCG
AGGGCCGCCCCTACGAGGGCACCCAGACCGCCAAGCTGAAGGTGACCAAGGGCGGCCCCCTGCCCTTCGCCT
GGGACATCCTGTCCCCCCAGTTCCAGTACGGCTCCAAGGTGTACGTGAAGCACCCCGCCGACATCCCCGACTA
CAAGAAGCTGTCCTTCCCCGAGGGCTTCAAGTGGGAGCGCGTGATGAACTTCGAGGACGGCGGCGTGGTGA
CCGTGACCCAGGACTCCTCCCTGCAGGACGGCTCCTTCATCTACAAGGTGAAGTTCATCGGCGTGAACTTCCCC
TCCGACGGCCCCGTAATGCAGAAGAAGACTATGGGCTGGGAGGCCTCCACCGAGCGCCTGTACCCCCGCGAC
GGCGTGCTGAAGGGCGAGATCCACAAGGCCCTGAAGCTGAAGGACGGCGGCCACTACCTGGTGGAGTTCAA
GTCCATCTACATGGCCAAGAAGCCCGTGCAGCTGCCCGGCTACTACTACGTGGACTCCAAGCTGGACATCACC
TCCCACAACGAGGACTACACCATCGTGGAGCAGTACGAGCGCGCCGAGGGCCGCCACCACCTGTTCCTGTAG
GACCTGCGCTGATCAGCCTCGACTGTGCCTTCTAGTTGCCAGCCATCTGTTGTTTGCCCCTCCCCCGTGCCTTCC
TTGACCCTGGAAGGTGCCACTCCCACTGTCCTTTCCTAATAAAATGAGGAAATTGCATCGCATTGTCTGAGTAG
GTGTCATTCTATTCTGGGGGGTGGGGTGGGGCAGGACAGCAAGGGGGAGGATTGGGAAGACAATAGCAGG
CATGCTGGGGATGCGGTGGGCTCTATGGCTTCTGAGGCGGAAAGAACCAGCTGGGGACTAGTCCACTCCCTC
TCTGCGCGCTCGCTCGCTCACTGAGGCCGGGCGACCAAAGGTCGCCCGACGCCCGGGCTTTGCCCGGGCGGC
CTCAGTGAGCGAGCGAGCGCGCAGAGAGGGA

9.9.3 longhPDE6Bp.DsRed

Grey sequence is ITRs, blue sequence is longhPDE6Bp, red sequence is DsRed, yellow sequence is bGHpA.

GGCCACTCCCTCTCTGCGCGCTCGCTCGCTCACTGAGGCCGGGCGACCAAAGGTCGCCCGACGCCCGGGCTTT
GCCCGGGCGGCCTCAGTGAGCGAGCGAGCGCGCAGAGAGGGAGTGGCCAACTCCATCACTAGGGGTTCCTG
GAGGGGTGGAGTCGTGACCTAGGTACCCTCCCAGCCTTCATTCCACAGGGTCTGGTTTTCCTGGAAGGTGGG
AAGTCCCAGGGTCTGAGGAGAGGGAGCGCAGGCCCCCATTTGTAGGAGTGAGTCAGCTGACCCGCCCCCGG
GGTTCCTAATCTCACTAAGAAAGACTTTGCTGATGACAGGGTTTCCTGGGAGTCCATGCGTGCCTGGAGCAGC
AGCGTCTCCAGGGACAGGCAACCGCCATGGCCTCCTCCGAGGACGTCATCAAGGAGTTCATGCGCTTCAAGG
TGCGCATGGAGGGCTCCGTGAACGGCCACGAGTTCGAGATCGAGGGCGAGGGCGAGGGCCGCCCCTACGAG
GGCACCCAGACCGCCAAGCTGAAGGTGACCAAGGGCGGCCCCCTGCCCTTCGCCTGGGACATCCTGTCCCCCC
AGTTCCAGTACGGCTCCAAGGTGTACGTGAAGCACCCCGCCGACATCCCCGACTACAAGAAGCTGTCCTTCCC
CGAGGGCTTCAAGTGGGAGCGCGTGATGAACTTCGAGGACGGCGGCGTGGTGACCGTGACCCAGGACTCCT
CCCTGCAGGACGGCTCCTTCATCTACAAGGTGAAGTTCATCGGCGTGAACTTCCCCTCCGACGGCCCCGTAAT
GCAGAAGAAGACTATGGGCTGGGAGGCCTCCACCGAGCGCCTGTACCCCCGCGACGGCGTGCTGAAGGGCG
AGATCCACAAGGCCCTGAAGCTGAAGGACGGCGGCCACTACCTGGTGGAGTTCAAGTCCATCTACATGGCCA
AGAAGCCCGTGCAGCTGCCCGGCTACTACTACGTGGACTCCAAGCTGGACATCACCTCCCACAACGAGGACTA
CACCATCGTGGAGCAGTACGAGCGCGCCGAGGGCCGCCACCACCTGTTCCTGTAGGACCTGCGCTGATCAGC
CTCGACTGTGCCTTCTAGTTGCCAGCCATCTGTTGTTTGCCCCTCCCCCGTGCCTTCCTTGACCCTGGAAGGTGC
CACTCCCACTGTCCTTTCCTAATAAAATGAGGAAATTGCATCGCATTGTCTGAGTAGGTGTCATTCTATTCTGG
GGGGTGGGGTGGGGCAGGACAGCAAGGGGGAGGATTGGGAAGACAATAGCAGGCATGCTGGGGATGCGG
TGGGCTCTATGGCTTCTGAGGCGGAAAGAACCAGCTGGGGACTAGTCCACTCCCTCTCTGCGCGCTCGCTCGC
TCACTGAGGCCGGGCGACCAAAGGTCGCCCGACGCCCGGGCTTTGCCCGGGCGGCCTCAGTGAGCGAGCGA
GCGCGCAGAGAGGGA

9.9.4 hRHOp.DsRed

Grey sequence is ITRs, blue sequence is hRHOp, red sequence is DsRed, yellow sequence is bGHpA.

GGCCACTCCCTCTCTGCGCGCTCGCTCGCTCACTGAGGCCGGGCGACCAAAGGTCGCCCGACGCCCGGGCTTT
GCCCGGGCGGCCTCAGTGAGCGAGCGAGCGCGCAGAGAGGGAGTGGCCAACTCCATCACTAGGGGTTCCTG
GAGGGGTGGAGTCGTGACCTAGGTACCCAGATCTTCCCCACCTAGCCACCTGGCAAACTGCTCCTTCTCTCAA
AGGCCCAAACATGGCCTCCCAGACTGCAACCCCCAGGCAGTCAGGCCCTGTCTCCACAACCTCACAGCCACCC
TGGACGGAATCTGCTTCTTCCCACATTTGAGTCCTCCTCAGCCCCTGAGCTCCTCTGGGCAGGGCTGTTTCTTTC
CATCTTTGTATTCCCAGGGGCCTGCAAATAAATGTTTAATGAACGAACAAGAGAGTGAATTCCAATTCCATGC
AACAAGGATTGGGCTCCTGGGCCCTAGGCTATGTGTCTGGCACCAGAAACGGAAGCTGCAGGTTGCAGCCCC
TGCCCTCATGGAGCTCCTCCTGTCAGAGGAGTGTGGGGACTGGATGACTCCAGAGGTAACTTGTGGGGGAAC
GAACAGGTAAGGGGCTGTGTGACGAGATGAGAGACTGGGAGAATAAACCAGAAAGTCTCTAGCTGTCCAGA
GGACATAGCACAGAGGCCCATGGTCCCTATTTCAAACCCAGGCCACCAGACTGAGCTGGGACCTTGGGACAG
ACAAGTCATGCAGAAGTTAGGGGACCTTCTCCTCCCTTTTCCTGGATCCTGAGTACCTCTCCTCCCTGACCTCA
GGCTTCCTCCTAGTGTCACCTTGGCCCCTCTTAGAAGCCAATTAGGCCCTCAGTTTCTGCAGCGGGGATTAATA
TGATTATGAACACCCCCAATCTCCCAGATGCTGATTCAGCCAGGAGCTTAGGAGGGGGAGGTCACTTTATAAG
GGTCTGGGGGGGTCAGAACCCAGAGTCATCCACCGCCATGGCCTCCTCCGAGGACGTCATCAAGGAGTTCAT
GCGCTTCAAGGTGCGCATGGAGGGCTCCGTGAACGGCCACGAGTTCGAGATCGAGGGCGAGGGCGAGGGC
CGCCCCTACGAGGGCACCCAGACCGCCAAGCTGAAGGTGACCAAGGGCGGCCCCCTGCCCTTCGCCTGGGAC
ATCCTGTCCCCCCAGTTCCAGTACGGCTCCAAGGTGTACGTGAAGCACCCCGCCGACATCCCCGACTACAAGA
AGCTGTCCTTCCCCGAGGGCTTCAAGTGGGAGCGCGTGATGAACTTCGAGGACGGCGGCGTGGTGACCGTG
ACCCAGGACTCCTCCCTGCAGGACGGCTCCTTCATCTACAAGGTGAAGTTCATCGGCGTGAACTTCCCCTCCGA
CGGCCCCGTAATGCAGAAGAAGACTATGGGCTGGGAGGCCTCCACCGAGCGCCTGTACCCCCGCGACGGCGT
GCTGAAGGGCGAGATCCACAAGGCCCTGAAGCTGAAGGACGGCGGCCACTACCTGGTGGAGTTCAAGTCCA
TCTACATGGCCAAGAAGCCCGTGCAGCTGCCCGGCTACTACTACGTGGACTCCAAGCTGGACATCACCTCCCA
CAACGAGGACTACACCATCGTGGAGCAGTACGAGCGCGCCGAGGGCCGCCACCACCTGTTCCTGTAGGACCT
GCGCTGATCAGCCTCGACTGTGCCTTCTAGTTGCCAGCCATCTGTTGTTTGCCCCTCCCCCGTGCCTTCCTTGAC
CCTGGAAGGTGCCACTCCCACTGTCCTTTCCTAATAAAATGAGGAAATTGCATCGCATTGTCTGAGTAGGTGTC
ATTCTATTCTGGGGGGTGGGGTGGGGCAGGACAGCAAGGGGGAGGATTGGGAAGACAATAGCAGGCATGC
TGGGGATGCGGTGGGCTCTATGGCTTCTGAGGCGGAAAGAACCAGCTGGGGACTAGTCCACTCCCTCTCTGC
GCGCTCGCTCGCTCACTGAGGCCGGGCGACCAAAGGTCGCCCGACGCCCGGGCTTTGCCCGGGCGGCCTCAG
TGAGCGAGCGAGCGCGCAGAGAGGGA

9.9.5 CAG.DsRed

Grey sequence is ITRs, blue sequence is CAG, red sequence is DsRed, yellow sequence is bGHpA.

CCATTGACGTCAATAATGACGTATGTTCCCATAGTAACGCCAATAGGGACTTTCCATTGACGTCAATGGGTGG
AGTATTTACGGTAAACTGCCCACTTGGCAGTACATCAAGTGTATCATATGCCAAGTACGCCCCCTATTGACGTC
AATGACGGTAAATGGCCCGCCTGGCATTATGCCCAGTACATGACCTTATGGGACTTTCCTACTTGGCAGTACAT
CTACGTATTAGTCATCGCTATTACCATGGTCGAGGTGAGCCCCACGTTCTGCTTCACTCTCCCCATCTCCCCCCC
CTCCCCACCCCCAATTTTGTATTTATTTATTTTTTAATTATTTTGTGCAGCGATGGGGGCGGGGGGGGGGGGG
GGGCGCGCGCCAGGCGGGGCGGGGCGGGGCGAGGGGCGGGGCGGGGCGAGGCGGAGAGGTGCGGCGGC
AGCCAATCAGAGCGGCGCGCTCCGAAAGTTTCCTTTTATGGCGAGGCGGCGGCGGCGGCGGCCCTATAAAAA
GCGAAGCGCGCGGCGGGCGGGAGTCGCTGCGCGCTGCCTTCGCCCCGTGCCCCGCTCCGCCGCCGCCTCGCG
CCGCCCGCCCCGGCTCTGACTGACCGCGTTACTCCCACAGGTGAGCGGGCGGGACGGCCCTTCTCCTCCGGGC
TGTAATTAGCGCTTGGTTTAATGACGGCTTGTTTCTTTTCTGTGGCTGCGTGAAAGCCTTGAGGGGCTCCGGG

AGGGCCCTTTGTGCGGGGGGAGCGGCTCGGGGCTGTCCGCGGGGGGACGGCTGCCTTCGGGGGGGACGGG
GCAGGGCGGGGTTCGGCTTCTGGCGTGTGACCGGCGGCTCTAGAGCCTCTGCTAACCATGTTCATGCCTTCTT
CTTTTTCCTACAGCTCCTGGGCAACGTGCTGGTTATTGTGCTGTCTCATCATTTTGGCAAAGAATTGGATCCACC
GCCATGGCCTCCTCCGAGGACGTCATCAAGGAGTTCATGCGCTTCAAGGTGCGCATGGAGGGCTCCGTGAAC
GGCCACGAGTTCGAGATCGAGGGCGAGGGCGAGGGCCGCCCCTACGAGGGCACCCAGACCGCCAAGCTGAA
GGTGACCAAGGGCGGCCCCCTGCCCTTCGCCTGGGACATCCTGTCCCCCCAGTTCCAGTACGGCTCCAAGGTG
TACGTGAAGCACCCCGCCGACATCCCCGACTACAAGAAGCTGTCCTTCCCCGAGGGCTTCAAGTGGGAGCGC
GTGATGAACTTCGAGGACGGCGGCGTGGTGACCGTGACCCAGGACTCCTCCCTGCAGGACGGCTCCTTCATCT
ACAAGGTGAAGTTCATCGGCGTGAACTTCCCCTCCGACGGCCCCGTAATGCAGAAGAAGACTATGGGCTGGG
AGGCCTCCACCGAGCGCCTGTACCCCCGCGACGGCGTGCTGAAGGGCGAGATCCACAAGGCCCTGAAGCTGA
AGGACGGCGGCCACTACCTGGTGGAGTTCAAGTCCATCTACATGGCCAAGAAGCCCGTGCAGCTGCCCGGCT
ACTACTACGTGGACTCCAAGCTGGACATCACCTCCCACAACGAGGACTACACCATCGTGGAGCAGTACGAGC
GCGCCGAGGGCCGCCACCACCTGTTCCTGTAGGACCTGCGCTGATCAGCCTCGACTGTGCCTTCTAGTTGCCA
GCCATCTGTTGTTTGCCCCTCCCCCGTGCCTTCCTTGACCCTGGAAGGTGCCACTCCCACTGTCCTTTCCTAATA
AAATGAGGAAATTGCATCGCATTGTCTGAGTAGGTGTCATTCTATTCTGGGGGGTGGGGTGGGGCAGGACAG
CAAGGGGGAGGATTGGGAAGACAATAGCAGGCATGCTGGGGATGCGGTGGGCTCTATGGCTTCTGAGGCG
GAAAGAACCAGCTGGGGACTAGTCCACTCCCTCTCTGCGCGCTCGCTCGCTCACTGAGGCCGGGCGACCAAA
GGTCGCCCGACGCCCGGGCTTTGCCCGGGCGGCCTCAGTGAGCGAGCGAGCGCGCAGAGAGGGA

9.9.6 Promoterless.DsRed

Grey sequence is ITRs, red sequence is DsRed, yellow sequence is bGHpA.

GAACCCAGAGTCATCCACCGCCATGGCCTCCTCCGAGGACGTCATCAAGGAGTTCATGCGCTTCAAGGTGCGC
ATGGAGGGCTCCGTGAACGGCCACGAGTTCGAGATCGAGGGCGAGGGCGAGGGCCGCCCCTACGAGGGCA
CCCAGACCGCCAAGCTGAAGGTGACCAAGGGCGGCCCCCTGCCCTTCGCCTGGGACATCCTGTCCCCCCAGTT
CCAGTACGGCTCCAAGGTGTACGTGAAGCACCCCGCCGACATCCCCGACTACAAGAAGCTGTCCTTCCCCGAG
GGCTTCAAGTGGGAGCGCGTGATGAACTTCGAGGACGGCGGCGTGGTGACCGTGACCCAGGACTCCTCCCTG
CAGGACGGCTCCTTCATCTACAAGGTGAAGTTCATCGGCGTGAACTTCCCCTCCGACGGCCCCGTAATGCAGA
AGAAGACTATGGGCTGGGAGGCCTCCACCGAGCGCCTGTACCCCCGCGACGGCGTGCTGAAGGGCGAGATC
CACAAGGCCCTGAAGCTGAAGGACGGCGGCCACTACCTGGTGGAGTTCAAGTCCATCTACATGGCCAAGAAG
CCCGTGCAGCTGCCCGGCTACTACTACGTGGACTCCAAGCTGGACATCACCTCCCACAACGAGGACTACACCA
TCGTGGAGCAGTACGAGCGCGCCGAGGGCCGCCACCACCTGTTCCTGTAGGACCTGCGCTGATCAGCCTCGA
CTGTGCCTTCTAGTTGCCAGCCATCTGTTGTTTGCCCCTCCCCCGTGCCTTCCTTGACCCTGGAAGGTGCCACTC
CCACTGTCCTTTCCTAATAAAATGAGGAAATTGCATCGCATTGTCTGAGTAGGTGTCATTCTATTCTGGGGGGT
GGGGTGGGGCAGGACAGCAAGGGGGAGGATTGGGAAGACAATAGCAGGCATGCTGGGGATGCGGTGGGC
TCTATGGCTTCTGAGGCGGAAAGAACCAGCTGGGGACTAGTCCACTCCCTCTCTGCGCGCTCGCTCGCTCACT
GAGGCCGGGCGACCAAAGGTCGCCCGACGCCCGGGCTTTGCCCGGGCGGCCTCAGTGAGCGAGCGAGCGCG
CAGAGAGGGACAGA

9.9.7 CAG.GFP.WPRE

Grey sequence is ITRs, blue sequence is CAG, green sequence is GFP, purple sequence is WPRE, yellow sequence is bGHpA.

CACATACGATTTAGGTGACACTATAGAATACACGGAATTAATTCTAGCTGCGCGCTCGCTCGCTCACTGAGGC

CGCCCGGGCAAAGCCCGGGCGTCGGGCGACCTTTGGTCGCCCGGCCTCAGTGAGCGAGCGAGCGCGCAGAG
AGGGAGTGGCCAACTCCATCACTAGGGGTTCCTTGTAGTTAATGATTAACCCGCCATGCTACTTATCTACGTAG
CCATGCTCTAGGTACCCATTGACGTCAATAATGACGTATGTTCCCATAGTAACGCCAATAGGGACTTTCCATTG
ACGTCAATGGGTGGAGTATTTACGGTAAACTGCCCACTTGGCAGTACATCAAGTGTATCATATGCCAAGTACG
CCCCCTATTGACGTCAATGACGGTAAATGGCCCGCCTGGCATTATGCCCAGTACATGACCTTATGGGACTTTCC
TACTTGGCAGTACATCTACGTATTAGTCATCGCTATTACCATGGTCGAGGTGAGCCCCACGTTCTGCTTCACTC
TCCCCATCTCCCCCCCCTCCCCACCCCCAATTTTGTATTTATTTATTTTTTAATTATTTTGTGCAGCGATGGGGGC
GGGGGGGGGGGGGGGGCGCGCGCCAGGCGGGGCGGGGCGGGGCGAGGGGCGGGGCGGGGCGAGGCGG
AGAGGTGCGGCGGCAGCCAATCAGAGCGGCGCGCTCCGAAAGTTTCCTTTTATGGCGAGGCGGCGGCGGCG
GCGGCCCTATAAAAAGCGAAGCGCGCGGCGGGCGGGAGTCGCTGCGCGCTGCCTTCGCCCCGTGCCCCGCTC
CGCCGCCGCCTCGCGCCGCCCGCCCCGGCTCTGACTGACCGCGTTACTCCCACAGGTGAGCGGGCGGGACGG
CCCTTCTCCTCCGGGCTGTAATTAGCGCTTGGTTTAATGACGGCTTGTTTCTTTTCTGTGGCTGCGTGAAAGCCT
TGAGGGGCTCCGGGAGGGCCCTTTGTGCGGGGGGAGCGGCTCGGGGCTGTCCGCGGGGGGACGGCTGCCT
TCGGGGGGGACGGGGCAGGGCGGGGTTCGGCTTCTGGCGTGTGACCGGCGGCTCTAGAGCCTCTGCTAACC
ATGTTCATGCCTTCTTCTTTTTCCTACAGCTCCTGGGCAACGTGCTGGTTATTGTGCTGTCTCATCATTTTGGCA
AAGAATTGGATCCTAGCTTGATATCGAATTCCTGCAGCCCGGCGGCACCATGAGCAAGGGCGAGGAACTGTT
CACTGGCGTGGTCCCAATTCTCGTGGAACTGGATGGCGATGTGAATGGGCACAAATTTTCTGTCAGCGGAGA
GGGTGAAGGTGATGCCACATACGGAAAGCTCACCCTGAAATTCATCTGCACCACTGGAAAGCTCCCTGTGCCA
TGGCCAACACTGGTCACTACCCTGACCTATGGCGTGCAGTGCTTTTCCAGATACCCAGACCATATGAAGCAGC
ATGACTTTTTCAAGAGCGCCATGCCCGAGGGCTATGTGCAGGAGAGAACCATCTTTTTCAAAGATGACGGGA
ACTACAAGACCCGCGCTGAAGTCAAGTTCGAAGGTGACACCCTGGTGAATAGAATCGAGCTGAAGGGCATTG
ACTTTAAGGAGGATGGAAACATTCTCGGCCACAAGCTGGAATACAACTATAACTCCCACAATGTGTACATCAT
GGCCGACAAGCAAAAGAATGGCATCAAGGTCAACTTCAAGATCAGACACAACATTGAGGATGGATCCGTGCA
GCTGGCCGACCATTATCAACAGAACACTCCAATCGGCGACGGCCCTGTGCTCCTCCCAGACAACCATTACCTGT
CCACCCAGTCTGCCCTGTCTAAAGATCCCAACGAAAAGAGAGACCACATGGTCCTGCTGGAGTTTGTGACCGC
TGCTGGGATCACACATGGCATGGACGAGCTGTACAAGTGAAAGCTTATCGATAATCAACCTCTGGATTACAAA
ATTTGTGAAAGATTGACTGGTATTCTTAACTATGTTGCTCCTTTTACGCTATGTGGATACGCTGCTTTAATGCCT
TTGTATCATGCTATTGCTTCCCGTATGGCTTTCATTTTCTCCTCCTTGTATAAATCCTGGTTGCTGTCTCTTTATG
AGGAGTTGTGGCCCGTTGTCAGGCAACGTGGCGTGGTGTGCACTGTGTTTGCTGACGCAACCCCCACTGGTT
GGGGCATTGCCACCACCTGTCAGCTCCTTTCCGGGACTTTCGCTTTCCCCCTCCCTATTGCCACGGCGGAACTC
ATCGCCGCCTGCCTTGCCCGCTGCTGGACAGGGGCTCGGCTGTTGGGCACTGACAATTCCGTGGTGTTGTCGG
GGAAATCATCGTCCTTTCCTTGGCTGCTCGCCTGTGTTGCCACCTGGATTCTGCGCGGGACGTCCTTCTGCTAC
GTCCCTTCGGCCCTCAATCCAGCGGACCTTCCTTCCCGCGGCCTGCTGCCGGCTCTGCGGCCTCTTCCGCGTCT
TCGCCTTCGCCCTCAGACGAGTCGGATCTCCCTTTGGGCCGCCTCCCCGCATCGATACCGTCGACTCGCTGATC
AGCCTCGACTGTGCCTTCTAGTTGCCAGCCATCTGTTGTTTGCCCCTCCCCCGTGCCTTCCTTGACCCTGGAAGG
TGCCACTCCCACTGTCCTTTCCTAATAAAATGAGGAAATTGCATCGCATTGTCTGAGTAGGTGTCATTCTATTCT
GGGGGGTGGGGTGGGGCAGGACAGCAAGGGGGAGGATTGGGAAGACAATAGCAGGCATGCTGGGGATGC
GGTGGGCTCTATGGCTTCTGAGGCGGAAAGAACCAGCTGGGGCTCGACTAGAGCATGGCTACGTAGATAAGT
AGCATGGCGGGTTAATCATTAACTACAAGGAACCCCTAGTGATGGAGTTGGCCACTCCCTCTCTGCGCGCTCG
CTCGCTCACTGAGGCCGGGCGACCAAAGGTCGCCCGACGCCCGGGCGGCCTCAGTGAGCGAGCGAGCGCGC
AGAGCTTTTTGCAAAAGCCTA

9.9.8 SaCas9

Grey sequence is ITRs, blue sequence is CMV, green sequence is SaCas9, yellow sequence is bGHpA, pink sequence is U6, orange sequence is gRNA scaffold.

CCTGCAGGCAGCTGCGCGCTCGCTCGCTCACTGAGGCCGCCCGGGCGTCGGGCGACCTTTGGTCGCCCGGCC

TCAGTGAGCGAGCGAGCGCGCAGAGAGGGAGTGGCCAACTCCATCACTAGGGGTTCCTGCGGCCTCTAGACT
CGAGGCGTTGACATTGATTATTGACTAGTTATTAATAGTAATCAATTACGGGGTCATTAGTTCATAGCCCATAT
ATGGAGTTCCGCGTTACATAACTTACGGTAAATGGCCCGCCTGGCTGACCGCCCAACGACCCCCGCCCATTGA
CGTCAATAATGACGTATGTTCCCATAGTAACGCCAATAGGGACTTTCCATTGACGTCAATGGGTGGAGTATTT
ACGGTAAACTGCCCACTTGGCAGTACATCAAGTGTATCATATGCCAAGTACGCCCCCTATTGACGTCAATGAC
GGTAAATGGCCCGCCTGGCATTATGCCCAGTACATGACCTTATGGGACTTTCCTACTTGGCAGTACATCTACGT
ATTAGTCATCGCTATTACCATGGTGATGCGGTTTTGGCAGTACATCAATGGGCGTGGATAGCGGTTTGACTCA
CGGGGATTTCCAAGTCTCCACCCCATTGACGTCAATGGGAGTTTGTTTTGGCACCAAAATCAACGGGACTTTCC
AAAATGTCGTAACAACTCCGCCCCATTGACGCAAATGGGCGGTAGGCGTGTACGGTGGGAGGTCTATATAAG
CAGAGCTCTCTGGCTAACTACCGGTGCCACCATGGCCCCAAAGAAGAAGCGGAAGGTCGGTATCCACGGAGT
CCCAGCAGCCAAGCGGAACTACATCCTGGGCCTGGACATCGGCATCACCAGCGTGGGCTACGGCATCATCGA
CTACGAGACACGGGACGTGATCGATGCCGGCGTGCGGCTGTTCAAAGAGGCCAACGTGGAAAACAACGAGG
GCAGGCGGAGCAAGAGAGGCGCCAGAAGGCTGAAGCGGCGGAGGCGGCATAGAATCCAGAGAGTGAAGA
AGCTGCTGTTCGACTACAACCTGCTGACCGACCACAGCGAGCTGAGCGGCATCAACCCCTACGAGGCCAGAG
TGAAGGGCCTGAGCCAGAAGCTGAGCGAGGAAGAGTTCTCTGCCGCCCTGCTGCACCTGGCCAAGAGAAGA
GGCGTGCACAACGTGAACGAGGTGGAAGAGGACACCGGCAACGAGCTGTCCACCAAAGAGCAGATCAGCCG
GAACAGCAAGGCCCTGGAAGAGAAATACGTGGCCGAACTGCAGCTGGAACGGCTGAAGAAAGACGGCGAA
GTGCGGGGCAGCATCAACAGATTCAAGACCAGCGACTACGTGAAAGAAGCCAAACAGCTGCTGAAGGTGCA
GAAGGCCTACCACCAGCTGGACCAGAGCTTCATCGACACCTACATCGACCTGCTGGAAACCCGGCGGACCTAC
TATGAGGGACCTGGCGAGGGCAGCCCCTTCGGCTGGAAGGACATCAAAGAATGGTACGAGATGCTGATGGG
CCACTGCACCTACTTCCCCGAGGAACTGCGGAGCGTGAAGTACGCCTACAACGCCGACCTGTACAACGCCCTG
AACGACCTGAACAATCTCGTGATCACCAGGGACGAGAACGAGAAGCTGGAATATTACGAGAAGTTCCAGATC
ATCGAGAACGTGTTCAAGCAGAAGAAGAAGCCCACCCTGAAGCAGATCGCCAAAGAAATCCTCGTGAACGAA
GAGGATATTAAGGGCTACAGAGTGACCAGCACCGGCAAGCCCGAGTTCACCAACCTGAAGGTGTACCACGAC
ATCAAGGACATTACCGCCCGGAAAGAGATTATTGAGAACGCCGAGCTGCTGGATCAGATTGCCAAGATCCTG
ACCATCTACCAGAGCAGCGAGGACATCCAGGAAGAACTGACCAATCTGAACTCCGAGCTGACCCAGGAAGAG
ATCGAGCAGATCTCTAATCTGAAGGGCTATACCGGCACCCACAACCTGAGCCTGAAGGCCATCAACCTGATCC
TGGACGAGCTGTGGCACACCAACGACAACCAGATCGCTATCTTCAACCGGCTGAAGCTGGTGCCCAAGAAGG
TGGACCTGTCCCAGCAGAAAGAGATCCCCACCACCCTGGTGGACGACTTCATCCTGAGCCCCGTCGTGAAGAG
AAGCTTCATCCAGAGCATCAAAGTGATCAACGCCATCATCAAGAAGTACGGCCTGCCCAACGACATCATTATC
GAGCTGGCCCGCGAGAAGAACTCCAAGGACGCCCAGAAAATGATCAACGAGATGCAGAAGCGGAACCGGCA
GACCAACGAGCGGATCGAGGAAATCATCCGGACCACCGGCAAAGAGAACGCCAAGTACCTGATCGAGAAGA
TCAAGCTGCACGACATGCAGGAAGGCAAGTGCCTGTACAGCCTGGAAGCCATCCCTCTGGAAGATCTGCTGA
ACAACCCCTTCAACTATGAGGTGGACCACATCATCCCCAGAAGCGTGTCCTTCGACAACAGCTTCAACAACAA
GGTGCTCGTGAAGCAGGAAGAAAACAGCAAGAAGGGCAACCGGACCCCATTCCAGTACCTGAGCAGCAGCG
ACAGCAAGATCAGCTACGAAACCTTCAAGAAGCACATCCTGAATCTGGCCAAGGGCAAGGGCAGAATCAGCA
AGACCAAGAAAGAGTATCTGCTGGAAGAACGGGACATCAACAGGTTCTCCGTGCAGAAAGACTTCATCAACC
GGAACCTGGTGGATACCAGATACGCCACCAGAGGCCTGATGAACCTGCTGCGGAGCTACTTCAGAGTGAACA
ACCTGGACGTGAAAGTGAAGTCCATCAATGGCGGCTTCACCAGCTTTCTGCGGCGGAAGTGGAAGTTTAAGA
AAGAGCGGAACAAGGGGTACAAGCACCACGCCGAGGACGCCCTGATCATTGCCAACGCCGATTTCATCTTCA
AAGAGTGGAAGAAACTGGACAAGGCCAAAAAAGTGATGGAAAACCAGATGTTCGAGGAAAAGCAGGCCGA
GAGCATGCCCGAGATCGAAACCGAGCAGGAGTACAAAGAGATCTTCATCACCCCCCACCAGATCAAGCACAT
TAAGGACTTCAAGGACTACAAGTACAGCCACCGGGTGGACAAGAAGCCTAATAGAGAGCTGATTAACGACAC
CCTGTACTCCACCCGGAAGGACGACAAGGGCAACACCCTGATCGTGAACAATCTGAACGGCCTGTACGACAA
GGACAATGACAAGCTGAAAAAGCTGATCAACAAGAGCCCCGAAAAGCTGCTGATGTACCACCACGACCCCCA
GACCTACCAGAAACTGAAGCTGATTATGGAACAGTACGGCGACGAGAAGAATCCCCTGTACAAGTACTACGA
GGAAACCGGGAACTACCTGACCAAGTACTCCAAAAAGGACAACGGCCCCGTGATCAAGAAGATTAAGTATTA
CGGCAACAAACTGAACGCCCATCTGGACATCACCGACGACTACCCCAACAGCAGAAACAAGGTCGTGAAGCT
GTCCCTGAAGCCCTACAGATTCGACGTGTACCTGGACAATGGCGTGTACAAGTTCGTGACCGTGAAGAATCTG
GATGTGATCAAAAAAGAAAACTACTACGAAGTGAATAGCAAGTGCTATGAGGAAGCTAAGAAGCTGAAGAA
GATCAGCAACCAGGCCGAGTTTATCGCCTCCTTCTACAACAACGATCTGATCAAGATCAACGGCGAGCTGTAT

AGAGTGATCGGCGTGAACAACGACCTGCTGAACCGGATCGAAGTGAACATGATCGACATCACCTACCGCGAG
TACCTGGAAAACATGAACGACAAGAGGCCCCCCAGGATCATTAAGACAATCGCCTCCAAGACCCAGAGCATT
AAGAAGTACAGCACAGACATTCTGGGCAACCTGTATGAAGTGAAATCTAAGAAGCACCCTCAGATCATCAAA
AAGGGCAAAAGGCCGGCGGCCACGAAAAAGGCCGGCCAGGCAAAAAAGAAAAAGGGATCCTACCCATACG
ATGTTCCAGATTACGCTTACCCATACGATGTTCCAGATTACGCTTACCCATACGATGTTCCAGATTACGCTTAAG
AATTCCTAGAGCTCGCTGATCAGCCTCGACTGTGCCTTCTAGTTGCCAGCCATCTGTTGTTTGCCCCTCCCCCGT
GCCTTCCTTGACCCTGGAAGGTGCCACTCCCACTGTCCTTTCCTAATAAAATGAGGAAATTGCATCGCATTGTC
TGAGTAGGTGTCATTCTATTCTGGGGGGTGGGGTGGGGCAGGACAGCAAGGGGGAGGATTGGGAAGAGAA
TAGCAGGCATGCTGGGGAGGTACCGAGGGCCTATTTCCCATGATTCCTTCATATTTGCATATACGATACAAGG
CTGTTAGAGAGATAATTGGAATTAATTTGACTGTAAACACAAAGATATTAGTACAAAATACGTGACGTAGAAA
GTAATAATTTCTTGGGTAGTTTGCAGTTTTAAAATTATGTTTTAAAATGGACTATCATATGCTTACCGTAACTTG
AAAGTATTTCGATTTCTTGGCTTTATATATCTTGTGGAAAGGACGAAACACCGGAGACCACGGCAGGTCTCAG
TTTTAGTACTCTGGAAACAGAATCTACTAAAACAAGGCAAAATGCCGTGTTTATCTCGTCAACTTGTTGGCGAG
ATTTTTGCGGCCGCAGGAACCCCTAGTGATGGAGTTGGCCACTCCCTCTCTGCGCGCTCGCTCGCTCACTGAG
GCCGGGCGACCAAAGGTCGCCCGACGCCCGGGCTTTGCCCGGGCGGCCTCAGTGAGCGAGCGAGCGCGCAG
CTGCCTGCAGG

9.9.9 dSaCas9

Grey sequence is ITRs, blue sequence is CMV, green sequence is dSaCas9, yellow sequence is bGHpA,

pink sequence is U6, orange sequence is gRNA scaffold.

CCTGCAGGCAGCTGCGCGCTCGCTCGCTCACTGAGGCCGCCCGGGCGTCGGGCGACCTTTGGTCGCCCGGCC
TCAGTGAGCGAGCGAGCGCGCAGAGAGGGAGTGGCCAACTCCATCACTAGGGGTTCCTGCGGCCTCTAGACT
CGAGGCGTTGACATTGATTATTGACTAGTTATTAATAGTAATCAATTACGGGGTCATTAGTTCATAGCCCATAT
ATGGAGTTCCGCGTTACATAACTTACGGTAAATGGCCCGCCTGGCTGACCGCCCAACGACCCCCGCCCATTGA
CGTCAATAATGACGTATGTTCCCATAGTAACGCCAATAGGGACTTTCCATTGACGTCAATGGGTGGAGTATTT
ACGGTAAACTGCCCACTTGGCAGTACATCAAGTGTATCATATGCCAAGTACGCCCCCTATTGACGTCAATGAC
GGTAAATGGCCCGCCTGGCATTATGCCCAGTACATGACCTTATGGGACTTTCCTACTTGGCAGTACATCTACGT
ATTAGTCATCGCTATTACCATGGTGATGCGGTTTTGGCAGTACATCAATGGGCGTGGATAGCGGTTTGACTCA
CGGGGATTTCCAAGTCTCCACCCCATTGACGTCAATGGGAGTTTGTTTTGGCACCAAAATCAACGGGACTTTCC
AAAATGTCGTAACAACTCCGCCCCATTGACGCAAATGGGCGGTAGGCGTGTACGGTGGGAGGTCTATATAAG
CAGAGCTCTCTGGCTAACTACCGGTGCCACCATGGCCCCAAAGAAGAAGCGGAAGGTCGGTATCCACGGAGT
CCCAGCAGCCAAGCGGAACTACATCCTGGGCCTGGCCATCGGCATCACCAGCGTGGGCTACGGCATCATCGA
CTACGAGACACGGGACGTGATCGATGCCGGCGTGCGGCTGTTCAAAGAGGCCAACGTGGAAAACAACGAGG
GCAGGCGGAGCAAGAGAGGCGCCAGAAGGCTGAAGCGGCGGAGGCGGCATAGAATCCAGAGAGTGAAGA
AGCTGCTGTTCGACTACAACCTGCTGACCGACCACAGCGAGCTGAGCGGCATCAACCCCTACGAGGCCAGAG
TGAAGGGCCTGAGCCAGAAGCTGAGCGAGGAAGAGTTCTCTGCCGCCCTGCTGCACCTGGCCAAGAGAAGA
GGCGTGCACAACGTGAACGAGGTGGAAGAGGACACCGGCAACGAGCTGTCCACCAAAGAGCAGATCAGCCG
GAACAGCAAGGCCCTGGAAGAGAAATACGTGGCCGAACTGCAGCTGGAACGGCTGAAGAAAGACGGCGAA
GTGCGGGGCAGCATCAACAGATTCAAGACCAGCGACTACGTGAAAGAAGCCAAACAGCTGCTGAAGGTGCA
GAAGGCCTACCACCAGCTGGACCAGAGCTTCATCGACACCTACATCGACCTGCTGGAAACCCGGCGGACCTAC
TATGAGGGACCTGGCGAGGGCAGCCCCTTCGGCTGGAAGGACATCAAAGAATGGTACGAGATGCTGATGGG
CCACTGCACCTACTTCCCCGAGGAACTGCGGAGCGTGAAGTACGCCTACAACGCCGACCTGTACAACGCCCTG
AACGACCTGAACAATCTCGTGATCACCAGGGACGAGAACGAGAAGCTGGAATATTACGAGAAGTTCCAGATC
ATCGAGAACGTGTTCAAGCAGAAGAAGAAGCCCACCCTGAAGCAGATCGCCAAAGAAATCCTCGTGAACGAA
GAGGATATTAAGGGCTACAGAGTGACCAGCACCGGCAAGCCCGAGTTCACCAACCTGAAGGTGTACCACGAC
ATCAAGGACATTACCGCCCGGAAAGAGATTATTGAGAACGCCGAGCTGCTGGATCAGATTGCCAAGATCCTG

ACCATCTACCAGAGCAGCGAGGACATCCAGGAAGAACTGACCAATCTGAACTCCGAGCTGACCCAGGAAGAG
ATCGAGCAGATCTCTAATCTGAAGGGCTATACCGGCACCCACAACCTGAGCCTGAAGGCCATCAACCTGATCC
TGGACGAGCTGTGGCACACCAACGACAACCAGATCGCTATCTTCAACCGGCTGAAGCTGGTGCCCAAGAAGG
TGGACCTGTCCCAGCAGAAAGAGATCCCCACCACCCTGGTGGACGACTTCATCCTGAGCCCCGTCGTGAAGAG
AAGCTTCATCCAGAGCATCAAAGTGATCAACGCCATCATCAAGAAGTACGGCCTGCCCAACGACATCATTATC
GAGCTGGCCCGCGAGAAGAACTCCAAGGACGCCCAGAAAATGATCAACGAGATGCAGAAGCGGAACCGGCA
GACCAACGAGCGGATCGAGGAAATCATCCGGACCACCGGCAAAGAGAACGCCAAGTACCTGATCGAGAAGA
TCAAGCTGCACGACATGCAGGAAGGCAAGTGCCTGTACAGCCTGGAAGCCATCCCTCTGGAAGATCTGCTGA
ACAACCCCTTCAACTATGAGGTGGACCACATCATCCCCAGAAGCGTGTCCTTCGACAACAGCTTCAACAACAA
GGTGCTCGTGAAGCAGGAAGAAGCCAGCAAGAAGGGCAACCGGACCCCATTCCAGTACCTGAGCAGCAGCG
ACAGCAAGATCAGCTACGAAACCTTCAAGAAGCACATCCTGAATCTGGCCAAGGGCAAGGGCAGAATCAGCA
AGACCAAGAAAGAGTATCTGCTGGAAGAACGGGACATCAACAGGTTCTCCGTGCAGAAAGACTTCATCAACC
GGAACCTGGTGGATACCAGATACGCCACCAGAGGCCTGATGAACCTGCTGCGGAGCTACTTCAGAGTGAACA
ACCTGGACGTGAAAGTGAAGTCCATCAATGGCGGCTTCACCAGCTTTCTGCGGCGGAAGTGGAAGTTTAAGA
AAGAGCGGAACAAGGGGTACAAGCACCACGCCGAGGACGCCCTGATCATTGCCAACGCCGATTTCATCTTCA
AAGAGTGGAAGAAACTGGACAAGGCCAAAAAAGTGATGGAAAACCAGATGTTCGAGGAAAAGCAGGCCGA
GAGCATGCCCGAGATCGAAACCGAGCAGGAGTACAAAGAGATCTTCATCACCCCCCACCAGATCAAGCACAT
TAAGGACTTCAAGGACTACAAGTACAGCCACCGGGTGGACAAGAAGCCTAATAGAGAGCTGATTAACGACAC
CCTGTACTCCACCCGGAAGGACGACAAGGGCAACACCCTGATCGTGAACAATCTGAACGGCCTGTACGACAA
GGACAATGACAAGCTGAAAAAGCTGATCAACAAGAGCCCCGAAAAGCTGCTGATGTACCACCACGACCCCCA
GACCTACCAGAAACTGAAGCTGATTATGGAACAGTACGGCGACGAGAAGAATCCCCTGTACAAGTACTACGA
GGAAACCGGGAACTACCTGACCAAGTACTCCAAAAAGGACAACGGCCCCGTGATCAAGAAGATTAAGTATTA
CGGCAACAAACTGAACGCCCATCTGGACATCACCGACGACTACCCCAACAGCAGAAACAAGGTCGTGAAGCT
GTCCCTGAAGCCCTACAGATTCGACGTGTACCTGGACAATGGCGTGTACAAGTTCGTGACCGTGAAGAATCTG
GATGTGATCAAAAAAGAAAACTACTACGAAGTGAATAGCAAGTGCTATGAGGAAGCTAAGAAGCTGAAGAA
GATCAGCAACCAGGCCGAGTTTATCGCCTCCTTCTACAACAACGATCTGATCAAGATCAACGGCGAGCTGTAT
AGAGTGATCGGCGTGAACAACGACCTGCTGAACCGGATCGAAGTGAACATGATCGACATCACCTACCGCGAG
TACCTGGAAAACATGAACGACAAGAGGCCCCCCAGGATCATTAAGACAATCGCCTCCAAGACCCAGAGCATT
AAGAAGTACAGCACAGACATTCTGGGCAACCTGTATGAAGTGAAATCTAAGAAGCACCCTCAGATCATCAAA
AAGGGCAAAAGGCCGGCGGCCACGAAAAAGGCCGGCCAGGCAAAAAAGAAAAAGGGATCCTACCCATACG
ATGTTCCAGATTACGCTTACCCATACGATGTTCCAGATTACGCTTACCCATACGATGTTCCAGATTACGCTTAAG
AATTCCTAGAGCTCGCTGATCAGCCTCGACTGTGCCTTCTAGTTGCCAGCCATCTGTTGTTTGCCCCTCCCCCGT
GCCTTCCTTGACCCTGGAAGGTGCCACTCCCACTGTCCTTTCCTAATAAAATGAGGAAATTGCATCGCATTGTC
TGAGTAGGTGTCATTCTATTCTGGGGGGTGGGGTGGGGCAGGACAGCAAGGGGGAGGATTGGGAAGAGAA
TAGCAGGCATGCTGGGGAGGTACCGAGGGCCTATTTCCCATGATTCCTTCATATTTGCATATACGATACAAGG
CTGTTAGAGAGATAATTGGAATTAATTTGACTGTAAACACAAAGATATTAGTACAAAATACGTGACGTAGAAA
GTAATAATTTCTTGGGTAGTTTGCAGTTTTAAAATTATGTTTTAAAATGGACTATCATATGCTTACCGTAACTTG
AAAGTATTTCGATTTCTTGGCTTTATATATCTTGTGGAAAGGACGAAACACCGGAGACCACGGCAGGTCTCAG
TTTTAGTACTCTGGAAACAGAATCTACTAAAACAAGGCAAAATGCCGTGTTTATCTCGTCAACTTGTTGGCGAG
ATTTTTGCGGCCGCAGGAACCCCTAGTGATGGAGTTGGCCACTCCCTCTCTGCGCGCTCGCTCGCTCACTGAG
GCCGGGCGACCAAAGGTCGCCCGACGCCCGGGCTTTGCCCGGGCGGCCTCAGTGAGCGAGCGAGCGCGCAG
CTGCCTGCAGG

9.9.10 dSaCas9.KRAB

Grey sequence is ITRs, blue sequence is CMV, green sequence is dSaCas9.KRAB, yellow sequence is bGHpA, pink sequence is U6, orange sequence is gRNA scaffold.

CCTGCAGGCAGCTGCGCGCTCGCTCGCTCACTGAGGCCGCCCGGGCGTCGGGCGACCTTTGGTCGCCCGGCC
TCAGTGAGCGAGCGAGCGCGCAGAGAGGGAGTGGCCAACTCCATCACTAGGGGTTCCTGCGGCCTCTAGACT
CGAGGCGTTGACATTGATTATTGACTAGTTATTAATAGTAATCAATTACGGGGTCATTAGTTCATAGCCCATAT
ATGGAGTTCCGCGTTACATAACTTACGGTAAATGGCCCGCCTGGCTGACCGCCCAACGACCCCCGCCCATTGA
CGTCAATAATGACGTATGTTCCCATAGTAACGCCAATAGGGACTTTCCATTGACGTCAATGGGTGGAGTATTT
ACGGTAAACTGCCCACTTGGCAGTACATCAAGTGTATCATATGCCAAGTACGCCCCCTATTGACGTCAATGAC
GGTAAATGGCCCGCCTGGCATTATGCCCAGTACATGACCTTATGGGACTTTCCTACTTGGCAGTACATCTACGT
ATTAGTCATCGCTATTACCATGGTGATGCGGTTTTGGCAGTACATCAATGGGCGTGGATAGCGGTTTGACTCA
CGGGGATTTCCAAGTCTCCACCCCATTGACGTCAATGGGAGTTTGTTTTGGCACCAAAATCAACGGGACTTTCC
AAAATGTCGTAACAACTCCGCCCCATTGACGCAAATGGGCGGTAGGCGTGTACGGTGGGAGGTCTATATAAG
CAGAGCTCTCTGGCTAACTACCGGTGCCACCATGGCCCCAAAGAAGAAGCGGAAGGTCGGTATCCACGGAGT
CCCAGCAGCCAAGCGGAACTACATCCTGGGCCTGGCCATCGGCATCACCAGCGTGGGCTACGGCATCATCGA
CTACGAGACACGGGACGTGATCGATGCCGGCGTGCGGCTGTTCAAAGAGGCCAACGTGGAAAACAACGAGG
GCAGGCGGAGCAAGAGAGGCGCCAGAAGGCTGAAGCGGCGGAGGCGGCATAGAATCCAGAGAGTGAAGA
AGCTGCTGTTCGACTACAACCTGCTGACCGACCACAGCGAGCTGAGCGGCATCAACCCCTACGAGGCCAGAG
TGAAGGGCCTGAGCCAGAAGCTGAGCGAGGAAGAGTTCTCTGCCGCCCTGCTGCACCTGGCCAAGAGAAGA
GGCGTGCACAACGTGAACGAGGTGGAAGAGGACACCGGCAACGAGCTGTCCACCAAAGAGCAGATCAGCCG
GAACAGCAAGGCCCTGGAAGAGAAATACGTGGCCGAACTGCAGCTGGAACGGCTGAAGAAAGACGGCGAA
GTGCGGGGCAGCATCAACAGATTCAAGACCAGCGACTACGTGAAAGAAGCCAAACAGCTGCTGAAGGTGCA
GAAGGCCTACCACCAGCTGGACCAGAGCTTCATCGACACCTACATCGACCTGCTGGAAACCCGGCGGACCTAC
TATGAGGGACCTGGCGAGGGCAGCCCCTTCGGCTGGAAGGACATCAAAGAATGGTACGAGATGCTGATGGG
CCACTGCACCTACTTCCCCGAGGAACTGCGGAGCGTGAAGTACGCCTACAACGCCGACCTGTACAACGCCCTG
AACGACCTGAACAATCTCGTGATCACCAGGGACGAGAACGAGAAGCTGGAATATTACGAGAAGTTCCAGATC
ATCGAGAACGTGTTCAAGCAGAAGAAGAAGCCCACCCTGAAGCAGATCGCCAAAGAAATCCTCGTGAACGAA
GAGGATATTAAGGGCTACAGAGTGACCAGCACCGGCAAGCCCGAGTTCACCAACCTGAAGGTGTACCACGAC
ATCAAGGACATTACCGCCCGGAAAGAGATTATTGAGAACGCCGAGCTGCTGGATCAGATTGCCAAGATCCTG
ACCATCTACCAGAGCAGCGAGGACATCCAGGAAGAACTGACCAATCTGAACTCCGAGCTGACCCAGGAAGAG
ATCGAGCAGATCTCTAATCTGAAGGGCTATACCGGCACCCACAACCTGAGCCTGAAGGCCATCAACCTGATCC
TGGACGAGCTGTGGCACACCAACGACAACCAGATCGCTATCTTCAACCGGCTGAAGCTGGTGCCCAAGAAGG
TGGACCTGTCCCAGCAGAAAGAGATCCCCACCACCCTGGTGGACGACTTCATCCTGAGCCCCGTCGTGAAGAG
AAGCTTCATCCAGAGCATCAAAGTGATCAACGCCATCATCAAGAAGTACGGCCTGCCCAACGACATCATTATC
GAGCTGGCCCGCGAGAAGAACTCCAAGGACGCCCAGAAAATGATCAACGAGATGCAGAAGCGGAACCGGCA
GACCAACGAGCGGATCGAGGAAATCATCCGGACCACCGGCAAAGAGAACGCCAAGTACCTGATCGAGAAGA
TCAAGCTGCACGACATGCAGGAAGGCAAGTGCCTGTACAGCCTGGAAGCCATCCCTCTGGAAGATCTGCTGA
ACAACCCCTTCAACTATGAGGTGGACCACATCATCCCCAGAAGCGTGTCCTTCGACAACAGCTTCAACAACAA
GGTGCTCGTGAAGCAGGAAGAAGCCAGCAAGAAGGGCAACCGGACCCCATTCCAGTACCTGAGCAGCAGCG
ACAGCAAGATCAGCTACGAAACCTTCAAGAAGCACATCCTGAATCTGGCCAAGGGCAAGGGCAGAATCAGCA
AGACCAAGAAAGAGTATCTGCTGGAAGAACGGGACATCAACAGGTTCTCCGTGCAGAAAGACTTCATCAACC
GGAACCTGGTGGATACCAGATACGCCACCAGAGGCCTGATGAACCTGCTGCGGAGCTACTTCAGAGTGAACA
ACCTGGACGTGAAAGTGAAGTCCATCAATGGCGGCTTCACCAGCTTTCTGCGGCGGAAGTGGAAGTTTAAGA
AAGAGCGGAACAAGGGGTACAAGCACCACGCCGAGGACGCCCTGATCATTGCCAACGCCGATTTCATCTTCA
AAGAGTGGAAGAAACTGGACAAGGCCAAAAAAGTGATGGAAAACCAGATGTTCGAGGAAAAGCAGGCCGA
GAGCATGCCCGAGATCGAAACCGAGCAGGAGTACAAAGAGATCTTCATCACCCCCCACCAGATCAAGCACAT
TAAGGACTTCAAGGACTACAAGTACAGCCACCGGGTGGACAAGAAGCCTAATAGAGAGCTGATTAACGACAC
CCTGTACTCCACCCGGAAGGACGACAAGGGCAACACCCTGATCGTGAACAATCTGAACGGCCTGTACGACAA
GGACAATGACAAGCTGAAAAAGCTGATCAACAAGAGCCCCGAAAAGCTGCTGATGTACCACCACGACCCCCA
GACCTACCAGAAACTGAAGCTGATTATGGAACAGTACGGCGACGAGAAGAATCCCCTGTACAAGTACTACGA
GGAAACCGGGAACTACCTGACCAAGTACTCCAAAAAGGACAACGGCCCCGTGATCAAGAAGATTAAGTATTA
CGGCAACAAACTGAACGCCCATCTGGACATCACCGACGACTACCCCAACAGCAGAAACAAGGTCGTGAAGCT
GTCCCTGAAGCCCTACAGATTCGACGTGTACCTGGACAATGGCGTGTACAAGTTCGTGACCGTGAAGAATCTG
GATGTGATCAAAAAAGAAAACTACTACGAAGTGAATAGCAAGTGCTATGAGGAAGCTAAGAAGCTGAAGAA

GATCAGCAACCAGGCCGAGTTTATCGCCTCCTTCTACAACAACGATCTGATCAAGATCAACGGCGAGCTGTAT
AGAGTGATCGGCGTGAACAACGACCTGCTGAACCGGATCGAAGTGAACATGATCGACATCACCTACCGCGAG
TACCTGGAAAACATGAACGACAAGAGGCCCCCCAGGATCATTAAGACAATCGCCTCCAAGACCCAGAGCATT
AAGAAGTACAGCACAGACATTCTGGGCAACCTGTATGAAGTGAAATCTAAGAAGCACCCTCAGATCATCAAA
AAGGGCAAAAGGCCGGCGGCCACGAAAAAGGCCGGCCAGGCAAAAAAGAAAAAGGGATCCGATGCTAAGT
CACTGACTGCCTGGTCCCGGACACTGGTGACCTTCAAGGATGTGTTTGTGGACTTCACCAGGGAGGAGTGGA
AGCTGCTGGACACTGCTCAGCAGATCCTGTACAGAAATGTGATGCTGGAGAACTATAAGAACCTGGTTTCCTT
GGGTTATCAGCTTACTAAGCCAGATGTGATCCTCCGGTTGGAGAAGGGAGAAGAGCCCTGGCTGGTGGAGA
GAGAAATTCACCAAGAGACACATCCTGATTCAGAGACTGCATTTGAAATCAAATCATCAGTTCCGAAAAAGAA
ACGCAAAGTTTAAGAATTCCTAGAGCTCGCTGATCAGCCTCGACTGTGCCTTCTAGTTGCCAGCCATCTGTTGT
TTGCCCCTCCCCCGTGCCTTCCTTGACCCTGGAAGGTGCCACTCCCACTGTCCTTTCCTAATAAAATGAGGAAAT
TGCATCGCATTGTCTGAGTAGGTGTCATTCTATTCTGGGGGGTGGGGTGGGGCAGGACAGCAAGGGGGAGG
ATTGGGAAGAGAATAGCAGGCATGCTGGGGAGGTACCGAGGGCCTATTTCCCATGATTCCTTCATATTTGCAT
ATACGATACAAGGCTGTTAGAGAGATAATTGGAATTAATTTGACTGTAAACACAAAGATATTAGTACAAAATA
CGTGACGTAGAAAGTAATAATTTCTTGGGTAGTTTGCAGTTTTAAAATTATGTTTTAAAATGGACTATCATATG
CTTACCGTAACTTGAAAGTATTTCGATTTCTTGGCTTTATATATCTTGTGGAAAGGACGAAACACCGGAGACCA
CGGCAGGTCTCAGTTTTAGTACTCTGGAAACAGAATCTACTAAAACAAGGCAAAATGCCGTGTTTATCTCGTC
AACTTGTTGGCGAGATTTTTGCGGCCGCAGGAACCCCTAGTGATGGAGTTGGCCACTCCCTCTCTGCGCGCTC
GCTCGCTCACTGAGGCCGGGCGACCAAAGGTCGCCCGACGCCCGGGCTTTGCCCGGGCGGCCTCAGTGAGCG
AGCGAGCGCGCAGCTGCCTGCAGG

9.9.11 AAV2/8(Y733F) RepCap

Blue sequence is p5 promoter, green sequence is AAV2 Rep genes, orange sequence is AAV8 Y733F Cap genes.

CGCAGGGTCTCCATTTTGAAGCGGGAGGTTTGAACGCGCAGCCGCCATGCCGGGGTTTTACGAGATTGTGAT
TAAGGTCCCCAGCGACCTTGACGAGCATCTGCCCGGCATTTCTGACAGCTTTGTGAACTGGGTGGCCGAGAAG
GAATGGGAGTTGCCGCCAGATTCTGACATGGATCTGAATCTGATTGAGCAGGCACCCCTGACCGTGGCCGAG
AAGCTGCAGCGCGACTTTCTGACGGAATGGCGCCGTGTGAGTAAGGCCCCGGAGGCTCTTTTCTTTGTGCAAT
TTGAGAAGGGAGAGAGCTACTTCCACATGCACGTGCTCGTGGAAACCACCGGGGTGAAATCCATGGTTTTGG
GACGTTTCCTGAGTCAGATTCGCGAAAAACTGATTCAGAGAATTTACCGCGGGATCGAGCCGACTTTGCCAAA
CTGGTTCGCGGTCACAAAGACCAGAAATGGCGCCGGAGGCGGGAACAAGGTGGTGGATGAGTGCTACATCC
CCAATTACTTGCTCCCCAAAACCCAGCCTGAGCTCCAGTGGGCGTGGACTAATATGGAACAGTATTTAAGCGC
CTGTTTGAATCTCACGGAGCGTAAACGGTTGGTGGCGCAGCATCTGACGCACGTGTCGCAGACGCAGGAGCA
GAACAAAGAGAATCAGAATCCCAATTCTGATGCGCCGGTGATCAGATCAAAAACTTCAGCCAGGTACATGGA
GCTGGTCGGGTGGCTCGTGGACAAGGGGATTACCTCGGAGAAGCAGTGGATCCAGGAGGACCAGGCCTCAT
ACATCTCCTTCAATGCGGCCTCCAACTCGCGGTCCCAAATCAAGGCTGCCTTGGACAATGCGGGAAAGATTAT
GAGCCTGACTAAAACCGCCCCCGACTACCTGGTGGGCCAGCAGCCCGTGGAGGACATTTCCAGCAATCGGAT
TTATAAAATTTTGGAACTAAACGGGTACGATCCCCAATATGCGGCTTCCGTCTTTCTGGGATGGGCCACGAAA
AAGTTCGGCAAGAGGAACACCATCTGGCTGTTTGGGCCTGCAACTACCGGGAAGACCAACATCGCGGAGGCC
ATAGCCCACACTGTGCCCTTCTACGGGTGCGTAAACTGGACCAATGAGAACTTTCCCTTCAACGACTGTGTCGA
CAAGATGGTGATCTGGTGGGAGGAGGGGAAGATGACCGCCAAGGTCGTGGAGTCGGCCAAAGCCATTCTCG
GAGGAAGCAAGGTGCGCGTGGACCAGAAATGCAAGTCCTCGGCCCAGATAGACCCGACTCCCGTGATCGTCA
CCTCCAACACCAACATGTGCGCCGTGATTGACGGGAACTCAACGACCTTCGAACACCAGCAGCCGTTGCAAGA
CCGGATGTTCAAATTTGAACTCACCCGCCGTCTGGATCATGACTTTGGGAAGGTCACCAAGCAGGAAGTCAAA
GACTTTTTCCGGTGGGCAAAGGATCACGTGGTTGAGGTGGAGCATGAATTCTACGTCAAAAAGGGTGGAGCC
AAGAAAAGACCCGCCCCCAGTGACGCAGATATAAGTGAGCCCAAACGGGTGCGCGAGTCAGTTGCGCAGCC

ATCGACGTCAGACGCGGAAGCTTCGATCAACTACGCAGACAGGTACCAAAACAAATGTTCTCGTCACGTGGG
CATGAATCTGATGCTGTTTCCCTGCAGACAATGCGAGAGAATGAATCAGAATTCAAATATCTGCTTCACTCACG
GACAGAAAGACTGTTTAGAGTGCTTTCCCGTGTCAGAATCTCAACCCGTTTCTGTCGTCAAAAAGGCGTATCA
GAAACTGTGCTACATTCATCATATCATGGGAAAGGTGCCAGACGCTTGCACTGCCTGCGATCTGGTCAATGTG
GATTTGGATGACTGCATCTTTGAACAATAAATGATTTAAATCAGGTATGGCTGCCGATGGTTATCTTCCAGATT
GGCTCGAGGACAACCTCTCTGAGGGCATTCGCGAGTGGTGGGCGCTGAAACCTGGAGCCCCGAAGCCCAAA
GCCAACCAGCAAAAGCAGGACGACGGCCGGGGTCTGGTGCTTCCTGGCTACAAGTACCTCGGACCCTTCAAC
GGACTCGACAAGGGGGAGCCCGTCAACGCGGCGGACGCAGCGGCCCTCGAGCACGACAAGGCCTACGACCA
GCAGCTGCAGGCGGGTGACAATCCGTACCTGCGGTATAACCACGCCGACGCCGAGTTTCAGGAGCGTCTGCA
AGAAGATACGTCTTTTGGGGGCAACCTCGGGCGAGCAGTCTTCCAGGCCAAGAAGCGGGTTCTCGAACCTCT
CGGTCTGGTTGAGGAAGGCGCTAAGACGGCTCCTGGAAAGAAGAGACCGGTAGAGCCATCACCCCAGCGTT
CTCCAGACTCCTCTACGGGCATCGGCAAGAAAGGCCAACAGCCCGCCAGAAAAAGACTCAATTTTGGTCAGAC
TGGCGACTCAGAGTCAGTTCCAGACCCTCAACCTCTCGGAGAACCTCCAGCAGCGCCCTCTGGTGTGGGACCT
AATACAATGGCTGCAGGCGGTGGCGCACCAATGGCAGACAATAACGAAGGCGCCGACGGAGTGGGTAGTTC
CTCGGGAAATTGGCATTGCGATTCCACATGGCTGGGCGACAGAGTCATCACCACCAGCACCCGAACCTGGGC
CCTGCCCACCTACAACAACCACCTCTACAAGCAAATCTCCAACGGGACATCGGGAGGAGCCACCAACGACAAC
ACCTACTTCGGCTACAGCACCCCCTGGGGGTATTTTGACTTTAACAGATTCCACTGCCACTTTTCACCACGTGAC
TGGCAGCGACTCATCAACAACAACTGGGGATTCCGGCCCAAGAGACTCAGCTTCAAGCTCTTCAACATCCAGG
TCAAGGAGGTCACGCAGAATGAAGGCACCAAGACCATCGCCAATAACCTCACCAGCACCATCCAGGTGTTTAC
GGACTCGGAGTACCAGCTGCCGTACGTTCTCGGCTCTGCCCACCAGGGCTGCCTGCCTCCGTTCCCGGCGGAC
GTGTTCATGATTCCCCAGTACGGCTACCTAACACTCAACAACGGTAGTCAGGCCGTGGGACGCTCCTCCTTCTA
CTGCCTGGAATACTTTCCTTCGCAGATGCTGAGAACCGGCAACAACTTCCAGTTTACTTACACCTTCGAGGACG
TGCCTTTCCACAGCAGCTACGCCCACAGCCAGAGCTTGGACCGGCTGATGAATCCTCTGATTGACCAGTACCT
GTACTACTTGTCTCGGACTCAAACAACAGGAGGCACGGCAAATACGCAGACTCTGGGCTTCAGCCAAGGTGG
GCCTAATACAATGGCCAATCAGGCAAAGAACTGGCTGCCAGGACCCTGTTACCGCCAACAACGCGTCTCAACG
ACAACCGGGCAAAACAACAATAGCAACTTTGCCTGGACTGCTGGGACCAAATACCATCTGAATGGAAGAAAT
TCATTGGCTAATCCTGGCATCGCTATGGCAACACACAAAGACGACGAGGAGCGTTTTTTTCCCAGTAACGGGA
TCCTGATTTTTGGCAAACAAAATGCTGCCAGAGACAATGCGGATTACAGCGATGTCATGCTCACCAGCGAGGA
AGAAATCAAAACCACTAACCCTGTGGCTACAGAGGAATACGGTATCGTGGCAGATAACTTGCAGCAGCAAAA
CACGGCTCCTCAAATTGGAACTGTCAACAGCCAGGGGGCCTTACCCGGTATGGTCTGGCAGAACCGGGACGT
GTACCTGCAGGGTCCCATCTGGGCCAAGATTCCTCACACGGACGGCAACTTCCACCCGTCTCCGCTGATGGGC
GGCTTTGGCCTGAAACATCCTCCGCCTCAGATCCTGATCAAGAACACGCCTGTACCTGCGGATCCTCCGACCAC
CTTCAACCAGTCAAAGCTGAACTCTTTCATCACGCAATACAGCACCGGACAGGTCAGCGTGGAAATTGAATGG
GAGCTGCAGAAGGAAAACAGCAAGCGCTGGAACCCCGAGATCCAGTACACCTCCAACTACTACAAATCTACA
AGTGTGGACTTTGCTGTTAATACAGAAGGCGTGTACTCTGAACCCCGCCCCATTGGCACCCGTTACCTCACCCG
TAATCTGTAATTGCCTGTTAATCAATAAACCGGTTGATTCGTTTCAGTTGAACTTTGGTCTCTGCGAAGGGCGA
ATTCGTTTAAACCTGCAGGACTAGAGGTCCTGTATTAGAGGTCACGTGAGTGTTTTGCGACATTTTGCGACAC
CATGTGGTCACGCTGGGTATTTAAGCCCGAGTGAGCACGCAGGGTCTCCATTTTGAAGCGGGAGGTTTGAAC
GCGCAGCCGCC

9.10 Review: The Application of CRISPR/Cas9 for the Treatment of Retinal Diseases

YALE JOURNAL OF BIOLOGY AND MEDICINE 90 (2017), pp.533-541.

REVIEW YJBM

The Application of CRISPR/Cas9 for the Treatment of Retinal Diseases

Caroline F. Peddle[a,*] and Robert E. MacLaren[a,b]

[a]*Nuffield Laboratory of Ophthalmology, Department of Clinical Neurosciences, University of Oxford, Oxford, UK;* [b]*Oxford Eye Hospital, Oxford, UK*

The CRISPR/Cas9 system of genome editing has revolutionized molecular biology, offering a simple, and relatively inexpensive method of creating precise DNA edits. It has potential application in gene therapy treatment of retinal diseases providing targeted disruption, alteration, or transcriptional regulation of pathogenic genes. *In vivo* studies have demonstrated therapeutic benefit for a variety of diseases. Despite this, there are many challenges to clinical use of CRISPR/Cas9, including editing efficiency, off-target effects, and disease heterogeneity. This review details the mechanisms of the CRISPR/Cas9 system and the treatment strategies that can be applied to retinal diseases. It gives an overview of *in vivo* studies published to date and discusses the challenges and potential solutions to the wide-scale clinical use of CRISPR/Cas9 as a therapeutic intervention.

INTRODUCTION

Inherited retinal diseases are an important cause of blindness and are estimated to affect 2 million people worldwide [1]. Despite this there is no available treatment for the majority of patients. Gene therapy could potentially offer a cure. By introducing, silencing, or editing genes involved in the pathogenesis of these diseases, progression can be halted or even reversed [2]. The eye has been at the forefront of gene therapy as it has several useful qualities. Firstly, the eye is immune-privileged meaning a higher tolerance of introduced antigens [3]. Secondly, the presence of the blood retina barrier reduces the likelihood that viral vectors introduced into the eye during gene therapy will migrate to other areas [4]. This lowers the risk associated with potential off-target effects of treatment. Thirdly, the target site for gene therapy is easily accessible via current ophthalmic techniques and only requires local anaesthetics. This access means that the amount of virus required for retinal transduction is minimal compared to systemic targets such as the liver [5].

Retinal gene therapy has traditionally involved gene replacement, a technique known as gene augmentation

*To whom all correspondence should be addressed: Caroline F. Peddle, NDCN, Level 6, West Wing, John Radcliffe Hospital, Oxford, United Kingdom, OX3 9DU, Email: enquiries@eye.ox.ac.uk.

†Abbreviations: ZNFs, zinc finger nucleases; TALENs, transcription activator-like effector nucleases; crRNA, CRISPR RNA; tracrRNA, trans-activating crRNA; Cas9, CRISPR-associated protein 9; PAM, protospacer adjacent motif; sgRNA, single guide RNA; NHEJ, non-homology end joining; HDR, homology-directed repair; Indels, insertions or deletions; dCas9, inactive Cas9; CRISPRi, CRISPR interference; CRISPRa, CRISPR activation; IVS26 mutations, intronic mutation in intron 26 of *CEP290*; AAV, adeno-associated virus; LCA10, Leber Congenital Amaurosis type 10; ONL, outer nuclear layer; AMD, age-related macular degeneration; RP, retinitis pigmentosa; CNV, choroidal neovascularisation; iPSC, induced pluripotent stem cells.

Keywords: CRISPR, Cas9, sgRNA, gene therapy, gene editing, retinal disease, NHEJ, HDR

Author Contributions: CFP: Conception and design of review, research, and analysis of materials, drafting manuscript, critical revision of manuscript. REM: Review conception and design, critical review of manuscript.

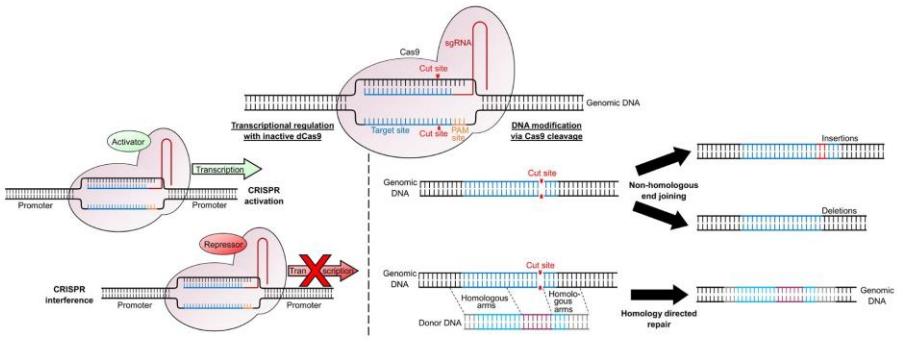

Figure 1. Applications of CRISPR/Cas9 for transcriptional regulation and genomic modification. Following Cas9 binding, cleavage of both DNA strands allows DNA modification. In the absence of any homologous sequences, the cell will undergo non-homologous end joining, resulting in small insertions or deletions around the cut site. If donor DNA is supplied which has homologous arms matching the genomic DNA it will be incorporated into the genome via homology directed repair. Catalytically inactive dCas9 can be targeted to a promoter to alter transcriptional regulation. Fusing a transcriptional activator to dCas9 will upregulate gene expression (termed CRISPR activation) while fusing a transcriptional repressor to dCas9 will downregulate gene expression (termed CRISPR interference).

[6,7]. The targeted diseases are caused by a lack of wild type function of a gene, and therefore supplying the missing gene may revert the pathology towards a normal phenotype, particularly when applied before the onset of cell death. While gene augmentation offers a promising outcome for patients with loss-of-function mutations, it cannot be used to treat dominant gain-of-function mutations. In these cases, the pathogenic mutation will need to be silenced or corrected for normal cell function to return. This presents a greater challenge than gene augmentation because the introduction of molecular inhibition into a host cell brings the possibility of off-target effects. Prior to the CRISPR/Cas9 system, gene editing at the DNA level was directed by zinc finger nucleases (ZFNs†) or transcription activator-like effector nucleases (TALENs). These techniques both have their disadvantages, with ZFNs having a low on-target efficiency and difficulty locating a potential target site [8,9], and TALENs being very large and therefore difficult to deliver to the cell [10]. The discovery of the CRISPR/Cas9 system has been revolutionary as it is simple to design and implement. Gene editing requires only three components: the presence of a short sequence, roughly 3 to 8 bp (the PAM site) adjacent to the target site, the endonuclease protein Cas9, and a customized piece of RNA which directs Cas9 to the target site for DNA cleavage [11-13].

CRISPR/CAS9 MECHANISM

CRISPR/Cas9 is a naturally occurring system that has evolved in bacteria and archaea as a method of evading viral infection. The microorganisms store copies of short sections of viral DNA in their genome which are transcribed into RNA called CRISPR RNA (crRNA). The crRNA forms a complex with a second piece of RNA, the trans-activating crRNA (tracrRNA), and CRISPR-associated protein 9 (Cas9), which are all encoded in the bacterial genome. If this complex encounters viral (bacteriophage) DNA which is complementary to the crRNA sequence it will bind to it. Cas9 is an endonuclease which cleaves double-stranded DNA, slicing through the viral DNA and preventing transcription [11,13].

Researchers soon realized that this system could be used for targeted gene editing in the genome of a chosen cell. By supplying a cell with Cas9, tracrRNA, and a crRNA specific to the target, Cas9 will cleave the region of interest. Since this discovery, the crRNA and tracrRNA have been artificially engineered into one single guide RNA (sgRNA) which can be customized to the target [13]. The final component required for CRISPR/Cas9-mediated gene editing is the presence of a protospacer adjacent motif (PAM) site adjacent to the target region [14]. A PAM site is a short DNA sequence (usually between 3 to 8 bp in length) that Cas9 binds to, inducing the double-stranded break approximately 3 bp upstream of the PAM [13]. These sites are naturally present on viral DNA and the exact sequence of the PAM is dependent on the species the Cas9 is isolated from. The most commonly

Table 1. *In vivo* experiments utilizing CRISPR/Cas9 for therapeutic interventions for retinal diseases.

Reference	Disease	Gene Target	Methodology	Results	Cas9 species
Ruan *et al.* 2017 [25]	LCA10	Removal of intron 25 of CEP290	Subretinal injection of dual AAVs into mice	Successful gene editing in 7.5% to 26.4% of reads between treated eyes	SpCas9
Kim *et al.* 2017 [33]	Wet age-related macular degeneration	Disruption of *Hif1a*	Subretinal injection of single AAV into CNV-induced mice	20±4% reduction in CNV	CjCas9
Courtney *et al.* 2016 [22]	Meesman's epithelial corneal dystrophy	Allele-specific disruption of *KRT12*-L132P	Intrasomal injection of Cas9-GFP and gRNA in *KRT12*-L132P mice	*KRT12*-L132P disruption in 38% of isolated clones	SpCas9
Suzuki *et al.* 2016 [32]	Retinitis pigmentosa	Insertion of missing *Mertk* exon 2	Subretinal injection of dual AAVs into Royal College of Surgeons rat model	Increased *Mertk* mRNA and protein levels. Improved ONL preservation and ERG response	SpCas9
Latella *et al.* 2016 [19]	Retinitis pigmentosa	Removal of 24 bp region of *Rho* at the P23H locus	Subretinal injection and electroporation of plasmid in $Rho^{-/-}P23H^{Tg}$ mice	16% of reads contained the desired 24 bp deletion	SpCas9
Yu *et al.* 2017 [37]	Retinitis pigmentosa	Disruption of *Nrl*	Subretinal injection of dual AAVs into Rhodopsin KO, Rd10, RHO-P347S mice	Delayed loss of rod function and prolonged cone survival	SpCas9
Zhu *et al.* 2017 [38]	Retinitis pigmentosa	Disruption of *Nrl* or *Nr2e3*	Subretinal injection of dual AAV into Rd10 and Rd1 mice	Significant rescue and restoration of both rod and cone function	SpCas9
Bakondi *et al.* 2016 [23]	Retinitis pigmentosa	Allele-specific disruption of Rho^{S334}	Subretinal injection and electroporation of plasmid in S334ter-3 rats	Increased retinal preservation and 35% increased VA	Human codon optimized SpCas9 (hCas9)

used Cas9 to date has been SpCas9 from *Streptococcus pyogenes*, which requires a PAM of 5'-NGG-3', where N is any nucleotide [15]. A number of bioinformatic programs are available which screen DNA sequences for PAM sites. Once a suitable PAM is selected, the sgRNA is designed to contain a region homologous to the sequence immediately upstream of the PAM (typically 18 to 25 bp long). By supplying a cell with the specific sgRNA and an active Cas9 protein, a double-stranded break will be induced at the site.

When a double-stranded break occurs in a host genome the cell will attempt to repair it using one of two processes: Non-Homologous End Joining (NHEJ) or Homology-Directed Repair (HDR) (Figure 1). In the absence of any homologous (identical complementary) DNA sequence, the cell will undergo NHEJ. Since there is no DNA template for repair, this process is somewhat random and hence extremely error prone, resulting in small insertions or deletions (indels) at the cleavage site. If these indels result in a frame-shift mutation in an exonic region, this can disrupt the gene, creating a non-functional protein. The HDR pathway allows researchers to perform precise edits of host DNA. Following a double-stranded break, any DNA molecules with a high level of homology to the target region will be substituted into the genome. By supplying a donor DNA molecule containing the desired mutation between two regions of homology to the target site (homologous arms), this increases the chances of the HDR pathway being used and the mutation being incorporated into the cell.

A third use of the CRISPR/Cas9 system involves introducing an artificially-engineered inactive version of Cas9 (dCas9) to alter the expression level of a gene at a transcriptional level, a technique called CRISPR

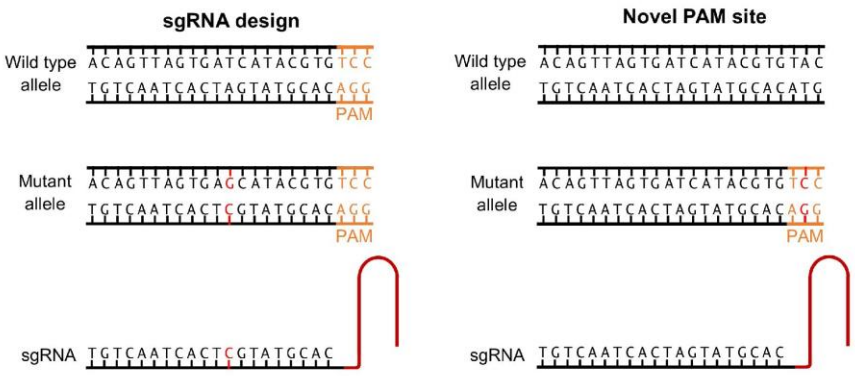

Figure 2. Allele-specific Cas9 targeting via sgRNA design or novel PAM sites. Cas9 can be targeted to the mutant allele by designing the sgRNA to the region containing the mutation. The discrepancy between the sgRNA sequence and wild type may be sufficient to prevent binding. If the target mutation generates a novel PAM site this will allow Cas9 binding on the mutant but not the wild type strand.

interference (CRISPRi). dCas9 retains the ability to bind to DNA via the sgRNA and PAM site, but has no cleavage activity. By targeting dCas9 to regulatory elements of the target gene it can sterically inhibit transcriptional machinery such as transcription factors or RNA Polymerase, decreasing transcription of the gene [16]. This effect can be enhanced by fusing dCas9 with a transcriptional inhibitor, such as Krüppel associated box [17]. Alternatively, fusing dCas9 with a transcriptional activator can upregulate expression via CRISPR activation (CRISPRa) [18] (Figure 1).

TREATMENT STRATEGIES

As knowledge of the CRISPR/Cas9 system increases, different applications of the technique are being developed. Many of these have already been applied *in vivo* for the treatment of retinal diseases, demonstrating its potential in gene therapy (Table 1).

Silencing/Targeting the Pathogenic Mutation

The most common use of CRISPR/Cas9 in the treatment of eye diseases is the direct silencing of dominant negative pathogenic mutations via the NHEJ pathway. If the target gene mutation has a dominant negative effect (*e.g.* Rhodopsin), then disrupting the mutant allele will restore wild type functionality of the gene. In contrast, if the target gene is haploinsufficient (*i.e.* two wild type alleles are needed to prevent the disease phenotype *e.g.* PAX6), or the CRISPR/Cas9 strategy is not allele-specific (knocking out both the wild type and mutant copy of the gene), then additional wild type copies of the gene can be reintroduced to the cells via gene augmentation [19].

Allele-specific CRISPR/Cas9 binding can be achieved in two ways: sgRNA design or novel PAM sites (Figure 2). While the specificity of Cas9 is variable (see Off-target Effects), many papers have reported that a one bp difference in the DNA target sequence is sufficient to drive allele-specific cleavage. This allows just the mutant allele to be targeted by designing the sgRNA to the region containing the mutation [20,21]. Alternatively, some mutations will generate a novel PAM site that is not present on the wild type allele, ensuring the Cas9 only binds to the target strand. While it may seem unlikely that a novel PAM site will be generated, the wide range of Cas9 species and associated PAM sites available (see Table 2) makes this possible, with one researcher reporting that of 76 known missense mutations associated within four retinal dystrophy genes, 36 percent produced a novel PAM site for SpCas9 [22]. Both Courtney *et al.* (2016) and Bakondi *et al.* (2016) used novel PAM sites to target allele-specific disruption of their mutant gene in the treatment of Meesman's epithelial corneal dystrophy and retinitis pigmentosa (RP), respectively [22,23]. Courtney *et al.* (2016) reported successful *in vivo* mutant gene disruption in 5 of 13 clones (though this is too low to be therapeutically viable), while Bakondi *et al.* (2016) reported target cleavage efficiencies of 33 percent and 36 percent in two CRISPR-edited rats, corresponding with a partial phenotypic rescue. Neither paper reported a reduction in the wild type allele expression, demonstrating that allele-specific knock down is possible

Table 2. Cas9 species and their associated PAM site sequences.

Species	Cas9	PAM site	Reference
Streptococcus pyogenes	SpCas9	NGG	Anders *et al.* 2014 [15]
Synthetically modified	SpCas9 VQR	NGAN or NGNG	Kleinstiver *et al.* 2015 [55]
Synthetically modified	SpCas9 EQR	NGAG	Kleinstiver *et al.* 2015 [55]
Synthetically modified	SpCas9 VRER	NGCG	Kleinstiver *et al.* 2015 [55]
Staphylococcus aureus	SaCas9	NNGRRT	Ran *et al.* 2015 [60]
Campylobacter jejuni	CjCas9	NNNNACAC	Kim *et al.* 2017 [33]
Neisseria meningitidis	NmCas9	NNNNGATT	Hou *et al.* 2013 [61]
Streptococcus thermophilus	St1Cas9	NNAGAAW	Müller *et al.* 2016 [62]
Streptococcus thermophilus	St3Cas9	NGGNG	Müller *et al.* 2016 [62]

using CRISPR/Cas9.

Another method of silencing pathogenic mutations is the removal of sections of DNA using a pair of sgRNAs which bind to either side of the target region. Following excision, the genomic DNA is repaired using the NHEJ pathway [24]. Ruan *et al.* (2017) proposed this method as a treatment for Leber Congenital Amaurosis type 10 (LCA10) caused by an intronic mutation in intron 26 of *CEP290* (IVS26 mutation) [25]. This mutation generates a premature stop codon in half of all transcripts due to aberrant splicing, resulting in reduced CEP290 activity [26]. This would normally be a viable candidate for gene augmentation but *CEP290* has a large 7440 bp open reading frame which exceeds adeno-associated viral (AAV) packaging capacity, and *CEP290* over-expression is cytotoxic to photoreceptors [27]. While there is no mouse model of human IVS26, mouse *Cep290* intron 25 is homologous to human *CEP290* intron 26 and was successfully removed from wild type mice retinal cells *in vivo* in 7.5 percent to 26.4 percent of reads. Since this region has no role in coding but simply directs splicing there is no need for a gRNA template for repair [25]. This dual sgRNA approach has also been used to excise a small 24 bp region surrounding the *RHO* P23H mutation with the aim to treat RP via gene silencing and augmentation [19].

Insertion of DNA

As well as inactivation of pathogenic mutations, CRISPR/Cas9 provides the opportunity to insert DNA at a specific locus to restore wild type functioning of a gene. Though this traditionally utilizes the HDR pathway [28-31], Suzuki *et al.* (2017) demonstrated a modified method of gene insertion via the NHEJ pathway, named Homology-Independent Targeting Integration [32]. Using this strategy, they successfully inserted the missing exon 2 into intron 1 of *Mertk* in the Royal College of Surgeons rat model of RP. This resulted in increased levels of *Mertk* mRNA and protein levels than the untreated animals, corresponding with improved outer nuclear layer (ONL) thickness and ERG responses indicating a partial rescue of the phenotype.

Treating Disease Symptoms

Retinal diseases with complex genetic and environmental risk factors may be unsuitable for traditional gene therapy approaches. In these cases, genetic modification may be used to reduce the severity of the disease by targeting genes involved in its pathogenesis. This approach was taken by Kim *et al.* (2017) for the treatment of wet age-related macular degeneration (AMD) [33]. In wet AMD, choroidal neovascularisation (CNV) leads to deterioration of central vision [34]. Kim *et al.* (2017) used CRISPR/Cas9 to disrupt *Hif1a* (crucial to the development of CNV [35]) in wild type mice who later underwent laser-induced CNV. The AAV-*Hif1a* treated eyes demonstrated a 20±4 percent reduction in area of CNV compared to the uninjected control, with no deleterious effects on cone function, demonstrating its potential as a therapeutic intervention.

Cellular Reprogramming

Therapeutic cellular reprogramming involves converting cells which are sensitive to a mutation to a functionally related cell type that is less affected by the mutation in the hopes of reducing the disease severity. This technique has potential in the treatment of retinal dystrophies due to the high levels of heterogeneity existing between diseases. RP, for example, is characterized by loss of rod cells leading to secondary cone cell death, but to date there have been over 3000 causative mutations in over 60 genes identified for this disease. This makes it difficult to develop gene therapy strategies to treat large cohorts of patients [36]. Two papers published within two months of each other sought to utilize CRISPR/Cas9 to induce cellular reprogramming of mutationally-sensitive

rod cells to cone cells within four models of RP [37,38]. *Nrl* and *Nr2e3* are transcription factors involved in the differentiation and regulation of rod cells. Absence of either of these transcription factors is known to cause rod cells to develop a cone cell fate [39,40]. CRISPR/Cas9 caused targeted gene disruption of either *Nrl* or *Nr2e3* via subretinal injection of mice between P7 and P14. Both researchers observed a downregulation of rod-specific genes and an up-regulation of some cone-specific genes. This occurred alongside significant rescue of photoreceptor functioning. Zhu *et al.* (2017) reported significantly improved cone and rod function with preserved ONL, and Yu *et al.* (2017) reported some functional cone and rod activity at 4 months of age, a month after rod death is usually complete in their tested mouse lines. Both authors conclude that cellular reprogramming of rods to cones is a promising area of further study for retinal disease treatment.

Stem Cells

The use of gene modification has promise as an early intervention strategy to prevent retinal degeneration, but for patients with advanced disease progression it offers little hope of a cure. CRISPR/Cas9 has the potential to correct pathogenic mutations in patient's own induced pluripotent stem cells (iPSCs). These can be differentiated into the required cell type and re-implanted into the eye. This route has the potential to be tailored to rare mutations found in small populations or individuals. Bassuk *et al.* (2016) demonstrated this in iPSCs derived from two brothers carrying a novel *RPGR* mutation [41]. iPSCs were differentiated from fibroblasts and the HDR pathway used to correct the c.3070G>T mutation in 13 percent of cells, a higher rate than previous CRISPR/Cas9 iPSC correction studies [42]. The use of retinal grafts to integrate stem cell-derived cells has demonstrated cell survival, safety, and efficacy in clinical trials, offering a potential therapeutic route for CRISPR/Cas9-corrrected iPSC therapies [43,44].

CHALLENGES TO CLINICAL APPLICATION

Efficiency of Gene Editing

While *in vitro* gene editing for retinal diseases using CRISPR/Cas9 often reports high rates of gene disruption *in vitro* (up to 82 percent [19]), the rates of successful gene editing *in vivo* are lower (up to 33 percent [19]). This success rate is highly variable between studies and may be dependent upon the type of Cas9 used [25,33], the design of the sgRNA, the target cell type, the delivery method, and the *in vivo* model amongst other factors [37,38]. One study using AAV-delivered CRISPR/Cas9 found a 50 percent *in vitro* deletion rate in neuro-2a cells which was reduced to 7.5 percent to 26.4 percent in treated retinas *in vivo* [25]. Though these rates are quite low, some diseases would not require complete silencing of the mutant gene. Meesmann's epithelial corneal dystrophy, for example, can be alleviated with a 50 percent reduction in mutant allele expression levels [22]. Other studies suggest that only a partial gene correction can result in a significant therapeutic impact [45]. Regardless of the rate of the CRISPR/Cas9 gene editing, *in vivo* studies are reporting improvements in disease phenotypes, which could have significant impacts on a patient's quality of life [32,33,37,38].

Off-target Effects

As with any genetic modification technique, there are concerns regarding the off-target effects of CRISPR/Cas9. Non-specific gene editing could remove essential genes or disrupt tumor suppressing genes causing cancers [10]. It is therefore vital that any genetic modification methods are specific and off-target effects are predictable. As Cas9 binding is dependent upon both the presence of a PAM site and upstream homology to the sgRNA sequence, bioinformatic programs can be used to predict off-target effects. Encouragingly, some papers reported that a one nucleotide discrepancy in the sgRNA binding region prevents indel formation [20,21] and most studies demonstrate no off-target effects at the most probable sites. In studies employing whole genome screening, off-target effects are rare (up to several hundred), with some studies reporting only one off-target effect within the entire genome [46-50].

Despite this, off-target effects have been varied across studies, with some papers reporting DNA editing with a 5-bp discrepancy between the sgRNA and target region [12,51]. The effect of base pair mismatch between the sgRNA and the target have been showed to be highly influenced by the distance between the mismatch and the PAM site, with PAM-distal mismatches being more tolerated than PAM-proximal mismatches [11-13,52]. There have also been incidents of reduced gene expression in a site with sgRNA homology but no PAM site [22]. The cleavage sites can also vary between *in vitro* and *in vivo* studies [53], making it difficult to accurately predict off-target effects.

Two artificial Cas9 molecules have been created with the aim of reducing off-target effects: nickases and high-fidelity Cas9 (SpCas9-HF1). Nickases are modified Cas9 molecules which can only cleave one strand of DNA. To induce a double-stranded break into the DNA for gene modification, one nickase must bind to either strand of DNA (each guided by an sgRNA) in close proximity. The use of nickases can reduce off-target effects by 50 to 1500 times compared to SpCas9 at the same site, and has been successfully used to disrupt genes in mouse embryos [54].

SpCas9-HF1 is a modified SpCas9 that has four altered amino acids [55]. These result in decreased non-specific binding and have been reported to have no detectable off-target effects while efficiency remains comparable to the wild-type SpCas9.

It has been proposed that reducing the temporal expression of Cas9 will reduce the off-target effects, and so the use of a self-limiting Cas9 construct has been explored. In a self-limiting Cas9, the Cas9 expression system carries at least one copy of the sgRNA target site. The sgRNA will guide the Cas9 to both the genomic target site and the Cas9 vector, inactivating it and halting Cas9 transcription. This has been shown to successfully reduce Cas9 expression to negligible levels while maintaining targeted gene editing *in vitro* [25]. While limiting transgene expression may have advantages from a regulatory approach, its usefulness is debated, with some papers reporting that long-term Cas9 expression is not associated with an increased risk of off-target effects [33].

Heterogeneity of Disease

Despite retinal dystrophies having many characteristics which make them a useful target for gene therapy, the heterogeneity of these diseases remain a challenge for widescale treatment therapies. Many diseases have hundreds of identified causative mutations (over 100 variants in over 20 loci for LCA [56,57]), with some mutations specific to singular families or even individuals [36,41].

Cellular reprogramming, targeting of disease symptoms, and iPSC-derived retinal grafts (described in more detail in Treatment Strategies), have been suggested as potential solutions to this problem. Cellular reprogramming and targeting disease symptoms via CRISPR/Cas9 can be applied to patients without an identified causative mutation, but these are still in early stages of research [37,38]. Stem cell derived retinal grafts, alternatively, have been used in multiple clinical trials and have demonstrated efficacy and safety [43,44]. Using patients own iPSC would allow the pathogenic mutation to be corrected *in vitro* before differentiation into photoreceptors. This would allow rare mutations to be targeted on a case-by-case basis and detailed screening of on and off-target effects to be conducted before transplantation into the eye.

Rates of HDR in the Eye

Precise gene correction with CRISPR/Cas9 relies on the HDR pathway. While HDR occurs most frequently in the late S and G2 stages of the cell cycle phase, retinal cells are post-mitotic, and therefore the HDR rate is low. Some studies have concluded these HDR rates are currently too low to have a therapeutic value.

The use of small molecules to suppress the NHEJ pathway and force cells to repair the double-stranded break with HDR has demonstrated efficacy in increasing the rates of HDR. SCR7 is an inhibitor of DNA ligase and has been shown to increase rates of HDR by 5-fold and 19-fold in separate *in vitro* studies [31,58]. It was subsequently used to enhance CRISPR/Cas9 editing of the HSV-1 viral genome and found to increase HDR rates by over 10-fold [59].

In 2016, a new CRISPR/Cas9 technique was described: Homology-Independent Targeted Integration. This allows precise gene knock-in without the HDR pathway. In this, the DNA insert is flanked by Cas9 cleavage sites. Following cleavage of both the genomic DNA target site and the DNA insert, the insert will be ligated into the genomic target site via NHEJ. The DNA insert is designed in such a way that integration in the reverse orientation will generate a CRISPR/Cas9 cleavage site allowing it to be removed by Cas9 again until it is integrated in the correct orientation. This was found to have higher knock-in efficiency than HDR both *in vitro* in HEK293 cells and *in vivo*, where it was used to correct a rat model of RP [32].

CONCLUSION

CRISPR/Cas9 is an exciting area of study which is revolutionizing all aspects of genetics, from basic biology to potential medical interventions. Due to its favorable characteristics and track record in gene therapy, retinal diseases are likely to be one of the earliest targets of CRISPR/Cas9 mediated therapy. *In vivo* studies demonstrate a promising future for CRISPR/Cas9 therapies, with rescue effects seen across a range of diseases. Its versatility lends itself to a variety of approaches to tackle these debilitating diseases. Despite all this, there is still a long way to go. HDR rates are currently below the therapeutic range, although there are avenues around this being explored. Reduction of off-target effects remains a priority as if CRISPR/Cas9 is to have a future in gene therapy, its off-target effects must be predictable and minimized.

REFERENCES

1. Berger W, Kloeckener-Gruissem B, Neidhardt J. The molecular basis of human retinal and vitreoretinal diseases. Prog Retin Eye Res. 2010;29(5):335-75.
2. McClements ME, MacLaren RE. Gene therapy for retinal disease. Translational Research. 2013;161(4):241-54.
3. Benhar I, London A, Schwartz M. The privileged immunity of immune privileged organs: the case of the eye. Front Immunol. 2012;3:296.
4. Zhou R, Caspi RR. Ocular immune privilege. F1000 Biol

Rep. 2010;2.
5. Lipinski DM, Thake M, MacLaren RE. Clinical applications of retinal gene therapy. Prog Retin Eye Res. 2013;32:22-47.
6. Boye SE, Boye SL, Lewin AS, Hauswirth WW. A comprehensive review of retinal gene therapy. Mol Ther. 2013;21(3):509-19.
7. Grob SR, Finn A, Papakostas TD, Eliott D. Clinical Trials in Retinal Dystrophies. Middle East Afr J Ophthalmol. 2016;23(1):49-59.
8. Carroll D. Genome engineering with zinc-finger nucleases. Genetics. 2011;188(4):773-82.
9. Gupta RM, Musunuru K. Expanding the genetic editing tool kit: ZFNs, TALENs, and CRISPR-Cas9. J Clin Invest. 2014;124(10):4154-61.
10. Hung SS, McCaughey T, Swann O, Pebay A, Hewitt AW. Genome engineering in ophthalmology: Application of CRISPR/Cas to the treatment of eye disease. Prog Retin Eye Res. 2016;53:1-20.
11. Cong L, Ran FA, Cox D, Lin S, Barretto R, Habib N, et al. Multiplex genome engineering using CRISPR/Cas systems. Science. 2013;339(6121):819-23.
12. Hsu PD, Scott DA, Weinstein JA, Ran FA, Konermann S, Agarwala V, et al. DNA targeting specificity of RNA-guided Cas9 nucleases. Nat Biotechnol. 2013;31(9):827-32.
13. Jinek M, Chylinski K, Fonfara I, Hauer M, Doudna JA, Charpentier E. A programmable dual-RNA-guided DNA endonuclease in adaptive bacterial immunity. Science. 2012;337(6096):816-21.
14. Mojica FJ, Diez-Villasenor C, Garcia-Martinez J, Almendros C. Short motif sequences determine the targets of the prokaryotic CRISPR defence system. Microbiology. 2009;155(Pt 3):733-40.
15. Anders C, Niewoehner O, Duerst A, Jinek M. Structural basis of PAM-dependent target DNA recognition by the Cas9 endonuclease. Nature. 2014;513(7519):569-73.
16. Qi LS, Larson MH, Gilbert LA, Doudna JA, Weissman JS, Arkin AP, et al. Repurposing CRISPR as an RNA-guided platform for sequence-specific control of gene expression. Cell. 2013;152(5):1173-83.
17. Gilbert LA, Larson MH, Morsut L, Liu Z, Brar GA, Torres SE, et al. CRISPR-mediated modular RNA-guided regulation of transcription in eukaryotes. Cell. 2013;154(2):442-51.
18. Bikard D, Jiang W, Samai P, Hochschild A, Zhang F, Marraffini LA. Programmable repression and activation of bacterial gene expression using an engineered CRISPR-Cas system. Nucleic Acids Research. 2013;41(15):7429-37.
19. Latella MC, Di Salvo MT, Cocchiarella F, Benati D, Grisendi G, Comitato A, et al. In vivo Editing of the Human Mutant Rhodopsin Gene by Electroporation of Plasmid-based CRISPR/Cas9 in the Mouse Retina. Mol Ther Nucleic Acids. 2016;5(11):e389.
20. Smith C, Abalde-Atristain L, He C, Brodsky BR, Braunstein EM, Chaudhari P, et al. Efficient and allele-specific genome editing of disease loci in human iPSCs. Mol Ther. 2015;23(3):570-7.
21. Yoshimi K, Kaneko T, Voigt B, Mashimo T. Allele-specific genome editing and correction of disease-associated phenotypes in rats using the CRISPR-Cas platform. Nat Commun. 2014;5:4240.
22. Courtney DG, Moore JE, Atkinson SD, Maurizi E, Allen EH, Pedrioli DM, et al. CRISPR/Cas9 DNA cleavage at SNP-derived PAM enables both in vitro and in vivo KRT12 mutation-specific targeting. Gene Ther. 2016;23(1):108-12.
23. Bakondi B, Lv W, Lu B, Jones MK, Tsai Y, Kim KJ, et al. In Vivo CRISPR/Cas9 Gene Editing Corrects Retinal Dystrophy in the S334ter-3 Rat Model of Autosomal Dominant Retinitis Pigmentosa. Mol Ther. 2016;24(3):556-63.
24. Brandl C, Ortiz O, Rottig B, Wefers B, Wurst W, Kuhn R. Creation of targeted genomic deletions using TALEN or CRISPR/Cas nuclease pairs in one-cell mouse embryos. FEBS Open Bio. 2015;5:26-35.
25. Ruan GX, Barry E, Yu D, Lukason M, Cheng SH, Scaria A. CRISPR/Cas9-Mediated Genome Editing as a Therapeutic Approach for Leber Congenital Amaurosis 10. Mol Ther. 2017;25(2):331-41.
26. den Hollander AI, Koenekoop RK, Yzer S, Lopez I, Arends ML, Voesenek KE, et al. Mutations in the CEP290 (NPHP6) gene are a frequent cause of Leber congenital amaurosis. Am J Hum Genet. 2006;79(3):556-61.
27. Tan E, Wang Q, Quiambao AB, Xu X, Qtaishat NM, Peachey NS, et al. The relationship between opsin overexpression and photoreceptor degeneration. Invest Ophthalmol Vis Sci. 2001;42(3):589-600.
28. Wang B, Li K, Wang A, Reiser M, Saunders T, Lockey RF, et al. Highly efficient CRISPR/HDR-mediated knock-in for mouse embryonic stem cells and zygotes. Biotechniques. 2015;59(4):201-2, 4, 6-8.
29. Zhang JP, Li XL, Li GH, Chen W, Arakaki C, Botimer GD, et al. Efficient precise knockin with a double cut HDR donor after CRISPR/Cas9-mediated double-stranded DNA cleavage. Genome Biol. 2017;18(1):35.
30. Paquet D, Kwart D, Chen A, Sproul A, Jacob S, Teo S, et al. Efficient introduction of specific homozygous and heterozygous mutations using CRISPR/Cas9. Nature. 2016;533(7601):125-9.
31. Chu VT, Weber T, Wefers B, Wurst W, Sander S, Rajewsky K, et al. Increasing the efficiency of homology-directed repair for CRISPR-Cas9-induced precise gene editing in mammalian cells. Nat Biotechnol. 2015;33(5):543-8.
32. Suzuki K, Tsunekawa Y, Hernandez-Benitez R, Wu J, Zhu J, Kim EJ, et al. In vivo genome editing via CRISPR/Cas9 mediated homology-independent targeted integration. Nature. 2016;540(7631):144-9.
33. Kim E, Koo T, Park SW, Kim D, Kim K, Cho HY, et al. In vivo genome editing with a small Cas9 orthologue derived from Campylobacter jejuni. Nat Commun. 2017;8:14500.
34. Bhutto I, Lutty G. Understanding age-related macular degeneration (AMD): relationships between the photoreceptor/retinal pigment epithelium/Bruch's membrane/choriocapillaris complex. Mol Aspects Med. 2012;33(4):295-317.
35. Andre H, Tunik S, Aronsson M, Kvanta A. Hypoxia-Inducible Factor-1alpha Is Associated With Sprouting Angiogenesis in the Murine Laser-Induced Choroidal Neovascularization Model. Invest Ophthalmol Vis Sci. 2015;56(11):6591-604.
36. Daiger SP, Sullivan LS, Bowne SJ. Genes and mutations causing retinitis pigmentosa. Clin Genet. 2013;84(2):132-41.

37. Yu W, Mookherjee S, Chaitankar V, Hiriyanna S, Kim JW, Brooks M, et al. Nrl knockdown by AAV-delivered CRISPR/Cas9 prevents retinal degeneration in mice. Nat Commun. 2017;8:14716.
38. Zhu J, Ming C, Fu X, Duan Y, Hoang DA, Rutgard J, et al. Gene and mutation independent therapy via CRISPR-Cas9 mediated cellular reprogramming in rod photoreceptors. Cell Res. 2017;27(6):830-3.
39. Montana CL, Kolesnikov AV, Shen SQ, Myers CA, Kefalov VJ, Corbo JC. Reprogramming of adult rod photoreceptors prevents retinal degeneration. Proc Natl Acad Sci U S A. 2013;110(5):1732-7.
40. Cheng H, Khanna H, Oh EC, Hicks D, Mitton KP, Swaroop A. Photoreceptor-specific nuclear receptor NR2E3 functions as a transcriptional activator in rod photoreceptors. Hum Mol Genet. 2004;13(15):1563-75.
41. Bassuk AG, Zheng A, Li Y, Tsang SH, Mahajan VB. Precision Medicine: Genetic Repair of Retinitis Pigmentosa in Patient-Derived Stem Cells. Sci Rep. 2016;6:19969.
42. Yang L, Guell M, Byrne S, Yang JL, De Los Angeles A, Mali P, et al. Optimization of scarless human stem cell genome editing. Nucleic Acids Res. 2013;41(19):9049-61.
43. Schwartz SD, Regillo CD, Lam BL, Eliott D, Rosenfeld PJ, Gregori NZ, et al. Human embryonic stem cell-derived retinal pigment epithelium in patients with age-related macular degeneration and Stargardt's macular dystrophy: follow-up of two open-label phase 1/2 studies. Lancet. 2015;385(9967):509-16.
44. Shirai H, Mandai M. Retinal regeneration by transplantation of retinal tissue derived from human embryonic or induced pluripotent stem cells. Inflammation and Regeneration. 2016;36(1):2.
45. Wu X, Scott DA, Kriz AJ, Chiu AC, Hsu PD, Dadon DB, et al. Genome-wide binding of the CRISPR endonuclease Cas9 in mammalian cells. Nat Biotechnol. 2014;32(7):670-6.
46. Iyer V, Shen B, Zhang W, Hodgkins A, Keane T, Huang X, et al. Off-target mutations are rare in Cas9-modified mice. Nat Methods. 2015;12(6):479.
47. Veres A, Gosis BS, Ding Q, Collins R, Ragavendran A, Brand H, et al. Low incidence of off-target mutations in individual CRISPR-Cas9 and TALEN targeted human stem cell clones detected by whole-genome sequencing. Cell Stem Cell. 2014;15(1):27-30.
48. Tsai SQ, Zheng Z, Nguyen NT, Liebers M, Topkar VV, Thapar V, et al. GUIDE-seq enables genome-wide profiling of off-target cleavage by CRISPR-Cas nucleases. Nat Biotechnol. 2015;33(2):187-97.
49. Tsai SQ, Nguyen NT, Malagon-Lopez J, Topkar VV, Aryee MJ, Joung JK. CIRCLE-seq: a highly sensitive in vitro screen for genome-wide CRISPR-Cas9 nuclease off-targets. Nat Methods. 2017;14(6):607-14.
50. Kim D, Bae S, Park J, Kim E, Kim S, Yu HR, et al. Digenome-seq: genome-wide profiling of CRISPR-Cas9 off-target effects in human cells. Nat Methods. 2015;12(3):237-43, 1 p following 43.
51. Fu Y, Foden JA, Khayter C, Maeder ML, Reyon D, Joung JK, et al. High-frequency off-target mutagenesis induced by CRISPR-Cas nucleases in human cells. Nat Biotechnol. 2013;31(9):822-6.
52. Jiang W, Bikard D, Cox D, Zhang F, Marraffini LA. RNA-guided editing of bacterial genomes using CRISPR-Cas systems. Nat Biotechnol. 2013;31(3):233-9.
53. DiCarlo JE, Sengillo JD, Justus S, Cabral T, Tsang SH, Mahajan VB. CRISPR-Cas Genome Surgery in Ophthalmology. Transl Vis Sci Technol. 2017;6(3):13.
54. Ran FA, Hsu PD, Lin CY, Gootenberg JS, Konermann S, Trevino AE, et al. Double nicking by RNA-guided CRISPR Cas9 for enhanced genome editing specificity. Cell. 2013;154(6):1380-9.
55. Kleinstiver BP, Prew MS, Tsai SQ, et al. Engineered CRISPR-Cas9 nucleases with altered PAM specificities. Nature. 2015;523(7561):481-485.
56. den Hollander AI. Omics in Ophthalmology: Advances in Genomics and Precision Medicine for Leber Congenital Amaurosis and Age-Related Macular Degeneration. Invest Ophthalmol Vis Sci. 2016;57(3):1378-87.
57. Hung SS, Chrysostomou V, Li F, Lim JK, Wang JH, Powell JE, et al. AAV-Mediated CRISPR/Cas Gene Editing of Retinal Cells In Vivo. Invest Ophthalmol Vis Sci. 2016;57(7):3470-6.
58. Maruyama T, Dougan SK, Truttmann MC, Bilate AM, Ingram JR, Ploegh HL. Increasing the efficiency of precise genome editing with CRISPR-Cas9 by inhibition of nonhomologous end joining. Nat Biotechnol. 2015;33(5):538-42.
59. Lin C, Li H, Hao M, Xiong D, Luo Y, Huang C, et al. Increasing the Efficiency of CRISPR/Cas9-mediated Precise Genome Editing of HSV-1 Virus in Human Cells. Sci Rep. 2016;6:34531.
60. Ran FA, Cong L, Yan WX, Scott DA, Gootenberg JS, Kriz AJ, et al. In vivo genome editing using Staphylococcus aureus Cas9. Nature. 2015;520(7546):186-91.
61. Hou Z, Zhang Y, Propson NE, Howden SE, Chu LF, Sontheimer EJ, et al. Efficient genome engineering in human pluripotent stem cells using Cas9 from Neisseria meningitidis. Proc Natl Acad Sci U S A. 2013;110(39):15644-9.
62. Muller M, Lee CM, Gasiunas G, Davis TH, Cradick TJ, Siksnys V, et al. Streptococcus thermophilus CRISPR-Cas9 Systems Enable Specific Editing of the Human Genome. Mol Ther. 2016;24(3):636-44.

9.11 Review: CRISPR Interference – Potential Application in Retinal Disease

International Journal of *Molecular Sciences*

MDPI

Review

CRISPR Interference–Potential Application in Retinal Disease

Caroline F. Peddle [1,*], Lewis E. Fry [1,2], Michelle E. McClements [1] and Robert E. MacLaren [1,2]

[1] Nuffield Laboratory of Ophthalmology, Nuffield Department of Clinical Neurosciences & NIHR Oxford Biomedical Research Centre, University of Oxford, Oxford OX3 9DU, UK; lewis.fry@ndcn.ox.ac.uk (L.E.F.); michelle.mcclements@eye.ox.ac.uk (M.E.M.); maclaren@eye.ox.ac.uk (R.E.M.)

[2] Oxford Eye Hospital, Oxford University Hospitals NHS Foundation Trust, Oxford OX3 9DU, UK

* Correspondence: caroline.peddle@ndcn.ox.ac.uk

Received: 20 January 2020; Accepted: 25 March 2020; Published: 27 March 2020

check for updates

Abstract: The treatment of dominantly inherited retinal diseases requires silencing of the pathogenic allele. RNA interference to suppress gene expression suffers from wide-spread off-target effects, while CRISPR-mediated gene disruption creates permanent changes in the genome. CRISPR interference uses a catalytically inactive 'dead' Cas9 directed by a guide RNA to block transcription of chosen genes without disrupting the DNA. It is highly specific and potentially reversible, increasing its safety profile as a therapy. Pre-clinical studies have demonstrated the versatility of CRISPR interference for gene silencing both in vivo and in ex vivo modification of iPSCs for transplantation. Applying CRISPR interference techniques for the treatment of autosomal dominant inherited retinal diseases is promising but there are few in vivo studies to date. This review details how CRISPR interference might be used to treat retinal diseases and addresses potential challenges for clinical translation.

Keywords: CRISPR interference; CRISPRi; CRISPR/Cas9; RNAi; knock-down; gene therapy; retinal disease; transcriptional repression; dCas9; KRAB

1. Introduction

Inherited retinal diseases are an irreversible and devastating cause of blindness for an estimated 2 million individuals worldwide [1]. They are the result of genetic mutations that generally affect photoreceptors, the light-sensitive retinal cells at the back of the eye, typically causing progressive loss of sight over several years or decades. Over 250 individual genes have been implicated in inherited retinal disease, with autosomal recessive, autosomal dominant and X-linked inheritance patterns observed [2]. As most are monogenic disorders, gene therapy offers a potential treatment.

The eye has several advantages as a gene therapy site. It is easily accessible using ophthalmic surgical techniques allowing direct delivery to the target organ using local anaesthesia; it is immune privileged which reduces the likelihood of immune responses or rejection, and the presence of the blood retina barrier helps to prevent systemic spread of the introduced material [3–5]. These factors have driven dozens of gene therapy clinical trials, culminating in the first FDA approved ocular gene therapy treatment in 2017 [6,7].

Retinal gene therapy clinical trials have focused on treating recessive or X-linked loss-of-function mutations through gene augmentation, where a wild-type copy of a gene is introduced into affected cells. For successful treatment of dominant gain-of-function mutations, the pathogenic gene must be silenced [3,8]. Both the CRISPR/Cas9 (Clustered Regularly Interspaced Short Palindromic Repeats/CRISPR associated protein 9) system and CRISPR interference (CRISPRi) can be used to silence pathogenic genes. The CRISPR/Cas9 system is a naturally occurring bacterial defence mechanism against invading viruses. The bacteria contain two specialized RNA molecules called crRNA and tracrRNA, which form a complex with the endonuclease protein Cas9. This complex is guided to viral DNA that share sequence homology

with crRNA. Cas9 requires a DNA element called a Protospacer Adjacent Motif (PAM) site immediately downstream of the crRNA binding sequence in order to bind to and cleave the DNA. The PAM site is a short nucleotide sequence (usually 3 to 8 bp long), the exact sequence requirements of which vary with bacterial species (for example *Streptococcus pyogenes* Cas9 has the PAM site 5′-NGG-3′). Following binding, Cas9 will cleave both strands, preventing viral colonization [9–12] (Figure 1a).

This system is used within biological research to disrupt genes of interest. The target gene is screened for PAM sites, and then a single guide RNA (gRNA, which is an artificial amalgamation that links both the crRNA and tracrRNA) is designed to match the region immediately upstream of this. By providing the cell with both the gRNA and Cas9, Cas9 will induce a double stranded break in the target gene. The cell then attempts to repair this break, but in the absence of a DNA template, this process is extremely error prone. This causes small insertions and deletions to be incorporated at the DNA break site, resulting in frame shifts or premature stop codons within the DNA [10,13] (Figure 1b).

CRISPRi uses a modified version of the Cas9 protein. The native Cas9 protein contains two DNA cleavage domains called HNH and RuvC, which cleave the gRNA complementary and gRNA non-complementary DNA strands, respectively [14]. By changing a single amino acid at each domain (for the *Streptococcus pyogenes* Cas9, the amino acid changes are D10A and H840A [15]), the Cas9 becomes catalytically inactive. This "dead" dCas9 can still bind to DNA but can no longer cleave it. The dCas9 causes transcriptional repression of the target gene. This is either through blocking the passage of RNA polymerase or through a dCas9-fusion protein altering the histone state of the gene (See Opportunities for Gene Regulation in Eukaryotes and Mechanisms of CRISPRi) (Figure 1c–d).

This review will outline the technique of CRISPRi, how it might be applied to treat dominantly inherited retinal dystrophies, and discuss important considerations for its clinical use.

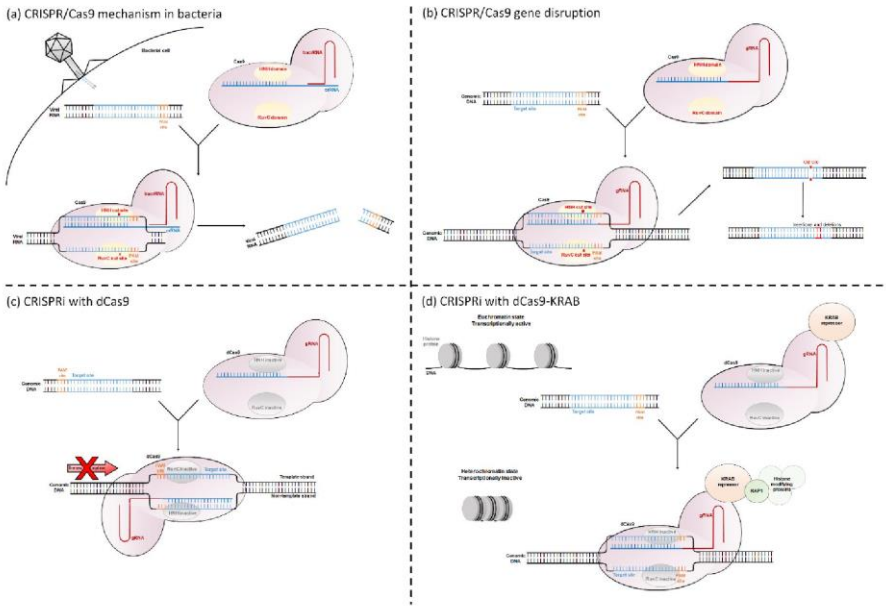

Figure 1. Mechanisms of CRISPR/Cas9 and CRISPRi. (**a**) CRISPR/Cas9 mechanism as a bacterial defence against invading viruses. (**b**) Using CRISPR/Cas9 to disrupt target genes. (**c**) Using CRISPRi with dCas9 to block transcription initiation or transcriptional elongation. (**d**) CRISPRi using a dCas9-KRAB fusion protein to alter the chromatin state of the gene.

2. Opportunities for Gene Regulation in Eukaryotes

The regulation of gene expression within eukaryotes is complex and occurs at multiple levels within the cell. Each of these levels offers an opportunity for expression to be manipulated with molecular techniques (see Table 1). The following is a brief introduction to the main regulatory systems in eukaryotic cells that can be targeted with interference methods.

Regulation begins at a DNA level, where cells can alter the rate of transcription from the gene's promoter. Transcription initiation varies between genes, but generally, transcription factors form a complex with RNA polymerase II, which allows it to bind to the transcriptional start site (TSS) [16]. Following binding, the interaction with distal regulatory elements dictates whether transcription will begin [17,18].

During early development of multi-cellular organisms, promoters can be permanently inactivated via an epigenetic mechanism called DNA methylation. Regions of DNA called "CpG islands" are common in eukaryotic promoters and contain repetitive sequences of 5′-CG-3′. DNA methyltransferase adds a methyl group to cytosines, which results in permanent silencing of that gene, which is inherited by daughter cells [19].

Following successful transcription of the DNA and subsequent processing, mRNA is translated into an amino acid chain. The lifespan of the mRNA molecule determines how much protein is produced (a longer half-life produces more protein), and cells employ a range of mechanisms to trigger or prevent degradation of the mRNA molecule. RNA interference (RNAi) acts to either block translation or trigger early degradation of the mRNA [20]. In RNAi, short double stranded micro-RNAs are produced that are complementary to the target mRNA. Micro-RNAs associate with the RNA-induced silencing complex and bind to the target mRNA, which is then either cleaved and rapidly degraded, or has its translation inhibited. This results in gene suppression.

The final level of gene regulation is at a histone level. Within the nucleus of a cell, the DNA is wound around histone proteins. In an open confirmation (euchromatin), the genes are active. In a tightly wound state (heterochromatin), transcription factors and RNA polymerase II cannot access the genes, making them inactive. The histone proteins have tails that can be chemically "tagged", changing their confirmation and therefore altering DNA accessibility. Transcription factors recruit histone modifying proteins, such as histone acetyltransferase or histone deacetylase, altering the transcription rate of the gene [21].

Table 1. Molecular methods used to target different gene regulation systems in eukaryotes.

Gene Regulation	Method
Gene transcription	CRISPRi
DNA methylation	dCas9-methyltransferase
mRNA lifespan/gene translation	RNAi
Histone state	CRISPRi

3. Mechanisms of CRISPRi

Targeting a genetic locus with CRISPRi requires only three main components. The first component is a PAM site in the DNA target region. The second component is a gRNA, which is designed with a region that is homologous to the area immediately 5′ adjacent to the chosen PAM site. The third component is the dCas9 protein, which forms a complex with the gRNA. The gRNA portion of the dCas9:gRNA complex will bind to the target DNA via sequence homology while dCas9 binds to the adjacent PAM site [10].

The basic CRISPRi mechanism uses the dCas9 protein to sterically block key regions of the target gene, preventing access of crucial transcriptional proteins. This reduces transcription and therefore downregulates expression. CRISPRi is either targeted to the TSS to prevent initiation of transcription or to downstream transcribed regions to block transcriptional elongation [15,22] (Figure 1c).

When blocking transcription initiation, either strand of DNA can be targeted. Large-scale analysis studies have identified the optimal binding site for blocking transcription initiation using CRISPRi as −50 to +250 base pairs relative to the TSS [23,24].

During transcriptional elongation, RNA polymerase II unwinds double stranded DNA and uses the template strand (also called the non-coding strand, reverse strand, or anti-sense strand) to create mRNA. gRNAs targeted to the template strand have reduced knock-down [15,22,25], although knock-down targeting this strand has been observed [23,26]. This could be due to RNA polymerase II unwinding the gRNA:DNA complex as they are "facing" each other. When the gRNA is targeted to the non-template strand of DNA the dCas9:gRNA complex acts as a physical barrier to the passage of RNA polymerase II, preventing further transcription [15,22]. Unlike targeting the TSS, there is currently no consensus on which regions of DNA are optimal and there is high variability between genes [24,27].

To increase the impact of CRISPRi, a 2013 study fused dCas9 with a range of transcriptional repressor domains [25]. These domains are typically eukaryotic protein domains which regulate transcription. The Krüppel Associated Box (KRAB) repressor is most commonly used. It interacts with the scaffold protein KAP1, which recruits histone modifying proteins, ultimately creating a tightly-wound, inactive heterochromatin histone state [28] (Figure 1d). Gilbert et al. found that addition of KRAB significantly increased the repression of genes at most tested loci, with one site reducing the ubiquitous EGFP expression by 15-fold in a GFP+HEK293 cell line [25]. Unlike when using dCas9 alone to block transcriptional elongation, dCas9-KRAB can be targeted to either strand of the DNA, dramatically increasing the potential target sites [27].

Although not typically defined as CRISPRi, it is worth noting that dCas9 can be fused to various proteins, which alter the epigenome of the cell and can result in down- or up- regulation of target genes. dCas9 has been successfully fused to proteins which alter the chemical tags on histone molecules: fusion to methyltransferase domains inactivates genes, and fusion to proteins, which remove methyl groups, activates repressed genes [29,30]. For a recent review on this, see [29].

4. Alternatives to CRISPRi

4.1. CRISPRi vs. CRISPR/Cas9

CRISPR/Cas9 causes permanent changes to the genome, whereas CRISPRi does not. After binding to DNA, Cas9 cleaves it, introducing small insertions and deletions into the target site, which alter the amino acid sequence and cause premature stop codons [10]. CRISPRi, on the other hand, does not alter the DNA sequence and will only affect transcription while dCas9 and gRNA are present. Experiments using inducible promoters have demonstrated that the effects of CRISPRi can be reversed following termination of dCas9 expression. In mRFP-expressing *E. coli* cells transduced with a plasmid carrying dCas9, suppressed mRFP fluorescence levels returned to baseline 300 min after switching off dCas9 expression [15]. In eukaryotic K562 cell lines stably transduced with dCas9-KRAB, target mRNA and protein expression returned to baseline 6 days after switching off dCas9-KRAB expression [23]. This provides safety benefits for gene therapies as CRISPRi treatment could be reversed if driven with an inducible promoter.

CRISPR/Cas9 and CRISPRi have different optimal target requirements. CRISPR/Cas9 is most successful when targeted to the exon of a gene, as insertions and deletions in introns can be removed through splicing leaving an unaltered coding sequence [31]. CRISPRi, on the other hand, can in theory be targeted anywhere in the transcribed region. In practice, however, the optimal target site for CRISPRi is quite narrow, at −50 to +250 relative to the TSS [23,24]. If there is a particular locus of the gene that is being targeted, it may only be possible using either CRISPR/Cas9 or CRISPRi.

While CRISPRi can be highly efficient for some targets, with one paper reporting a 1000-fold repression of the mRNA target, it is generally accepted that the active cutting form of CRISPR/Cas9 is more efficient at knocking down target gene expression than CRISPRi [15,27,32]. This is likely because the efficiency of CRISPRi gene repression is not only dictated by the gRNA:DNA binding, as with

active Cas9, but by the ability of that locus to successfully block transcription [23]. This makes the knock-down rates seen with CRISPRi highly variable across the sequence of a gene [15,23,24].

CRISPRi may have greater specificity than CRISPR/Cas9. Both systems rely on sequence homology between their gRNA and DNA, and the presence of an immediately adjacent PAM site to bind. Off-target binding occurs when DNA with partial homology to the gRNA sequence is adjacent to a PAM site. CRISPR/Cas9 has variable tolerance for mismatches between its gRNA and target DNA sequence and off-target effects are common; some have been reported at sites with a 5 bp gRNA:DNA mismatch [10,33–36]. This has led to the development of "high-fidelity" Cas9 species, which are engineered to have reduced off-target activity; in some cases, they have no detectable off-target effects [37–40]. CRISPRi, on the other hand, has very low tolerance for gRNA:DNA mismatches [23]. One paper reported that a 1 bp mismatch at every gRNA position prevented CRISPRi activity with their tested gRNA (although they noted a trend of gRNA:DNA mismatches at sites distal to the PAM being better tolerated, as observed for active Cas9) [9,10,34,35,41]. Another paper reported that a single gRNA:DNA mismatch significantly reduced the knock-down rate at every gRNA position, while a combination of two or more mismatches was enough to abolish knock-down entirely [23]. This might be due to the different mechanisms between CRISPR/Cas9 and CRISPRi: CRISPR/Cas9 may be able to cleave DNA whilst in contact with it only briefly, which might be the case with mismatched nucleotides, whereas for CRISPRi to be effective, it is likely to need to be in contact with the DNA target for considerably longer. In support of this notion, genome-wide analyses of the effects of CRISPRi commonly report no detected off-target effects on the cell's transcriptome [15,25,42] (see Table 2).

4.2. CRISPRi vs. RNAi

Until the creation of inactive dCas9, RNAi was the leading technique for suppressing gene expression in eukaryotic cells. It utilizes the cells natural RNAi pathway (see Opportunities for Gene Regulation in Eukaryotes). In RNAi, a short RNA sequence complementary to the target is introduced to the cell. It associates with the RNA-induced silencing complex and binds to the target mRNA via sequence homology. This triggers a pathway that will cause either mRNA degradation or a reduction in translation [20].

RNAi is arguably a simpler technique than CRISPRi, requiring only successful cellular delivery of a short double stranded RNA molecule. In ocular diseases, chemically modified RNA molecules are delivered directly to the eye without a delivery vehicle [43]. It has been used for gene knock-down since 2001 and is well characterized, with numerous therapies in clinical trials (including treatments for ocular diseases such as age-related macular degeneration, non-arteritic anterior ischaemic optic neuropathy, and dry eye disease) and two FDA-approved treatments for hereditary transthyretin-mediated amyloidosis and acute hepatic porphyria [43,44].

While RNAi reduces translation, CRISPRi reduces transcription. As it binds to DNA, rather than mRNA, the CRISPRi system has access to more potential binding sites in the untranscribed regions of DNA, such as the promoter and distal regulatory elements. It can also be targeted to introns, which are not accessible to RNAi as it generally targets mRNA [42].

Efficiency and specificity of the treatment strategies have been compared. Off-target effects of CRISPRi are rare, with multiple studies reporting no significant off-target effects detectable with RNA-Seq [23,25,27,41]. With RNAi on the other hand, off-target effects are commonly reported [15,45–47]. Wide-scale studies have identified that CRISPRi and RNAi have comparable efficiencies, but these are highly variable and target-specific [46]. At an individual gene level, CRISPRi is often able to outperform RNAi, with one study achieving CRISPRi-mediated protein knock-down of almost 90% for the 4 tested genes, compared to more variable knock-down with RNAi [41] (see Table 2).

Table 2. Comparison of CRISPRi, CRISPR/Cas9 and RNAi methods for knock-down of eukaryotic genes. + indicates lower levels, ++ indicates higher levels.

Feature	CRISPRi	CRISPR/Cas9	RNAi
Target	DNA	DNA	mRNA
Requirements	gRNA complementary to target. dCas9 protein	gRNA complementary to target. Cas9 protein	Short interfering RNA complementary to target
Efficiency	+	++	+
Specificity	++	+	+

5. Clinical Treatment Strategies

CRISPRi allows highly specific and efficient gene repression and is therefore a promising clinical treatment if targeted to genes involved in disease pathology. This has high applicability in retinal diseases but there is currently only one published in vivo study targeting the retina [48]. The two main therapeutic strategies being explored across diseases are in vivo knock-down of a target gene, in which the CRISPRi construct is applied directly to the target organ, and ex vivo knock-down, where CRISPRi is applied to cells, which are then transplanted into a patient. Pre-clinical studies in animal models using CRISPRi to target human disease are outlined in Table 3. CRISPRi has also proven a useful tool for biological research in vivo for creating knock-down mouse models [49] and identifying gene function [41,50], but these are not discussed here.

5.1. In Vivo Knock-Down

CRISPRi can be used to knock-down expression of genes involved in retinal disease by delivering the construct with gene therapy via a subretinal injection.

5.1.1. Targeting the Pathogenic Mutation

For diseases caused by dominant gain-of-function mutations, such as retinitis pigmentosa caused by rhodopsin mutations, CRISPRi must be targeted exclusively to the pathogenic allele. This can be done in two ways: targeting the pathogenic mutation directly or targeting a single nucleotide polymorphism (SNP) on the same allele as the pathogenic mutation. The mutation or SNP must either generate a novel PAM site or be in the gRNA binding region. Generating a PAM site not present on the non-targeted allele allows the gRNA:dCas9 complex to bind specifically to the target allele. A mutation or SNP in the binding region of the gRNA creates a mismatch of at least 1 bp with the wild type strand. As discussed in "CRISPRi vs. CRISPR/Cas9", CRISPRi is extremely sensitive to mismatches between its gRNA and the target DNA, with 1 bp mismatches often sufficient to prevent dCas9 binding and therefore gene repression [23,41].

Allele-specific targeting of the pathogenic mutation has been used to treat in vivo models of autosomal dominant retinitis pigmentosa with active CRISPR/Cas9. Bakondi et al. and Li et al. targeted pathogenic mutations in *Rho* occurring in the PAM site and gRNA binding region, respectively. In both cases, only the pathogenic allele was disrupted, resulting in significantly improved visual outcomes [51,52]. Bakondi et al. measured increased retinal preservation and a 35% improvement in optokinetic response, a surrogate measurement for visual function, in the treated eye of S334ter-3 rats compared to the untreated eye. Li et al. found significantly more photoreceptor cells in the CRISPR-treated retinal areas of P23H mice, indicating the retinal degeneration was slowed.

5.1.2. Cellular Reprogramming

Cellular reprogramming aims to convert a diseased cell type into a cell type that is unaffected by the pathogenic mutation [53]. This was potentially demonstrated with CRISPRi to treat autosomal recessive retinitis pigmentosa in the Rd10 mouse model. Rd10 mice contain a mutation in the *Pde6β* gene, which causes complete rod cell death by P60 but allows relative preservation of cone cells.

Moreno et al. targeted the rod cell transcription factor *Nrl*, which is a regulator determining rod cell fate over cone cell fate in photoreceptors. The treated mice developed a more cone-like phenotype, which was associated with increased photoreceptor cell layers and visual acuity [48]. While patients treated in this way would lose vision characteristics driven by rod cells, such as night vision, relative preservation of cone cells may allow patients to maintain visual acuity and central vision.

5.1.3. Treating Disease Pathways

A final strategy for in vivo knock-down is targeting genes that drive damaging disease pathways, therefore slowing the disease progression. This technique is useful for polygenic conditions where targeting a single pathogenic gene is not possible.

CRISPRi has been used in this way to treat familial hypercholesterolemia and obesity in mouse models in vivo by knocking down genes that are involved in the disease pathology. In treating familial hypercholesterolemia, the gene *Pcsk9*, which functions in the regulation of low-density lipoprotein receptor degradation, was targeted. Over 80% reduction in PCSK9 protein was achieved in the liver, and a significant reduction in serum low-density lipoproteins was found in the treated mice [54]. For the treatment of obesity, the expression of lipid chaperone protein *Fabp4* was significantly reduced in the high-fat diet-induced mice, which lead to a reduction in body weight, fat mass, and blood glucose levels in the CRISPRi-treated mice [26].

Wet age-related macular degeneration can lead to the loss of the central visual field due to the development of choroidal neovascularization. Current treatment of wet age-related macular degeneration uses drugs to block growth factors that contribute to this disease pathway, such as vascular endothelial growth factor. Disruption of this pathway using RNAi and CRISPR/Cas9 has been demonstrated in principle, achieving potentially significant therapeutic effects, and similarly, CRISPRi could be used to knock-down key genes [55,56].

5.2. Ex Vivo Knock-Down

As well as downregulating a target gene in vivo, CRISPRi has demonstrated effectiveness at suppressing gene function in stem cell-derived cells for implantation into patients [57]. In a paper aiming to improve the low rates of calvarial bone healing, CRISPRi was used alongside CRISPR activation to repress and activate genes involved in the inhibition and promotion of cartilage formation, respectively. dCas9-KRAB reduced its target *PPAR-γ* expression by 30.3% in bone marrow-derived mesenchymal stem cells. The cells were then cultured into engineered cartilage and implanted into calvarial bone defects in rats. The CRISPR-untreated cartilage had negligible bone growth, while the CRISPR-treated cartilage saw significant bone repair, filling 28.6% and 23.3% of the original defect area [58].

This method has application in retinal diseases, where late stage patients have wide-spread loss of retinal cells causing significant gaps in their field of vision. In cases of autologous transplantation, CRISPRi could be used to suppress the pathogenic gene in induced pluripotent stem cells (iPSCs) pre-implantation before reprogramming into the desired retinal cell type, and autologous transplantation. The potential of this treatment has been demonstrated with successful CRISPR/Cas9 gene correction of pathogenic retinal mutations in iPSCs for retinitis pigmentosa and Leber congenital amaurosis [59–61]. Following correction of three different *RPGR* frame shift mutations in patient iPSCs, Deng et al. cultured the iPSCs into retinal organoids and found that the X-linked retinitis pigmentosa phenotype was completely alleviated [60].

Clinical studies using stem cell-derived cells for the treatment of inherited retinal disease are currently underway. Among them, Stargardt disease and retinitis pigmentosa are being investigated, with stem-cell-derived retinal pigment epithelium cells, and retinal progenitor cells, respectively, injected into patient's eyes. Initial results have documented good tolerance of the introduced cells, with some indications of symptom improvement, although full results are not yet published [62].

Table 3. In vivo gene therapy CRISPRi studies.

Reference	Treatment Method	Condition	gRNA Target	Experimental Methodology	Results
Moreno et al. 2018 [48]	In vivo knock-down Cellular reprogramming	Autosomal recessive retinitis pigmentosa	*Nrl*	Dual subretinal injection of AAV.gRNA.dSpCas9-KRAB.N-terminus and AAV.dSpCas9-KRAB C-terminus into Rd10 mouse.	Rods developed a more "cone-like" phenotype. Increased photoreceptor layer thickness. Significantly improved visual function.
Thakore et al. 2018 [54]	In vivo knock-down Treating disease pathways	High LDL cholesterol (familial hypercholesterolemia)	*Pcsk9*	Dual injection of AAV.dSaCas9-KRAB and AAV.gRNA into mouse tail vein.	80% reduction in target protein. Significant reduction in serum LDL cholesterol.
Chung et al. 2019 [26]	In vivo knock-down Treating disease pathways	Obesity	*Fabp4*	Intraperitoneal injection of ATS-9R peptide and dSpCas9.gRNA plasmid oligoplex into HFD-induced obesity and diabetes model mice.	Significant reduction in target mRNA. Improved disease symptoms including decrease in body weight, fat mass, and blood glucose.
Yoshida et al. 2018 [57]	In vivo knock-down Treating disease pathways (Experimental methodology required ex vivo knock-down)	Lung squamous cell carcinoma	ΔNp63	Lentiviral delivery of dSpCas9-KRAB.gRNA to EBC2 lung SCC cells. Xenograft then injected into adult mice.	Tumour growth significantly repressed
Truong et al. 2019 [58]	Ex vivo knock-down	Calvarial bone healing	*PPAR-γ* (repression) and *Sox9* (activation)	Bacilloviral delivery of all-in-one CRISPRai construct into rat bone marrow-derived mesenchymal stem cells. These were implanted into rat calvarial bone defects.	Significant increase in calvarial bone healing.

6. Challenges to Clinical Application

6.1. Target Selection and Efficacy

As covered in "CRISPRi vs. RNAi", optimally designed CRISPRi has comparable efficiency to RNAi, the technique previously favored to knock-down clinically relevant genes [46]. Unfortunately, CRISPRi knock-down is highly variable throughout the gene as not all regions will block transcription effectively [15]. Outside the optimal −50 to +250 (relative to TSS) target region, one paper found only 56% of gRNAs achieved knock-down of over 20% [24]. While the −50 to +250 region gives plenty of potential target sites for a knock-down and replace strategy, it is relatively limited if the strategy involves targeting a specific region of the gene, for example targeting the pathogenic mutation for allele-specific knock-down.

Improvements have been made to methods for predicting successful target sites. The FANTOM5/CAGE atlas is a database annotating regulatory elements of mammalian genomes. By identifying the transcriptional start site using this software and then using traditional CRISPR software to analyse the gRNA:DNA binding success, gRNA efficiency predictions were significantly improved [24].

Gene repression rates can often be increased with the addition of the KRAB repressor [25,27]. A triple fusion protein of dCas9, KRAB repressor, and MeCP2 repressor domain (which initiates chromatin remodelling via a different pathway from the KRAB repressor) was found to further increase gene repression [27].

When targeting pathogenic gain-of-function mutations, it is useful to note that wild type phenotypes can often be restored with less than 100% knock-down of the mutant gene. In Bakondi et al. 2016, for example, retinal morphology was significantly improved in a rat model of autosomal dominant retinitis pigmentosa with CRISPR/Cas9 editing rates of 33% and 36%. Photoreceptor layers were increased from 1 layer in the control group to 8 layers in the CRISPR-treated group [51]. Even partial reduction in the expression of toxic genes may slow the rate of degeneration and result in preservation of visual function and delay of vision loss [53,55,63,64].

6.2. Delivery to the Retina

Once a CRISPRi construct is created, the next challenge is successfully delivering it to the target cell. Clinical retinal gene therapy trials to date have used Adeno-Associated Virus (AAV). AAV vectors

are non-integrating and offer strong expression, an excellent safety profile, and the ability to effectively transduce photoreceptors and RPE when subretinally injected [65]. The main limitation of AAV is its roughly 4.7 kb DNA packaging capacity. Cas9s have a relatively large coding sequence and in vivo experiments using the traditionally favoured 4104 bp SpCas9 have adopted a dual vector approach to overcome this [66]. Multiple shorter variants of Cas9 have been identified which can be packaged into a single AAV along with their regulatory elements, and a gRNA [55,67–69]. In particular, Cas9 species from *Staphylococcus aureus*, *Streptococcus thermophiles*, *Neisseria meningitides*, and *Campylobacter jejuni* are all under 3.5 kb, and their inactive dCas9 form has been used in vitro experiments [70]. The 3159 bp *Staphylococcus aureus* Cas9 has also been used in in vivo CRISPRi studies and successfully reduced target protein expression by 80% [48].

Lentiviruses are integrating vectors with high efficiency of transgene expression. Unfortunately, efficient transduction of photoreceptors is currently limited to newborn animals [7,71,72]. The integration site is also difficult to predict, which raises concerns of off-target effects and potential oncogenesis. For these reasons, lentivirus is usually unsuitable for in vivo knock-down but is frequently used for ex vivo knock-down, where all potential off-target effects can be screened before the cells are transplanted into the patient.

Non-viral delivery methods include ribonucleoproteins (RNPs) or plasmid DNA. RNPs consist of a Cas9 protein bound to a gRNA, which is delivered to cells through lipid-based transfection or electroporation. While RNPs have successfully induced CRISPR-mediated gene disruption in mouse RPE cells, none of the neural retina took up the RNP successfully [73]. The turnover rate of RNP in the eye was very high, with all Cas9 protein degraded 3 days after injection, making it unsuitable for CRISPRi delivery. Multiple studies have used plasmid electroporation to deliver CRISPR/Cas9 into newborn rat retinas with successful transduction in multiple retinal layers [51,74,75]. Despite this, therapeutic application is limited as delivery to post-mitotic cells (as in adult retinas) appears to be less efficient [72].

6.3. Immune Response

Immune responses to gene therapy are a concern in the field. Reactions to the transgene, transgene product or the packaging method can cause inflammation, reduced efficacy, and pose health risks to patients. Advantageously, the eye benefits from immune privilege. The blood-ocular barrier allows the eye to function as a separate microenvironment, altering immune cell activity, suppressing inflammation, and improving tolerance of introduced foreign elements [76]. Unfortunately, this system is not impenetrable, and breakdown of the blood-ocular barrier can introduce adaptive immune cells to the eye [77]. Intraocular inflammation has been reported in multiple AAV gene therapy trials, and therefore, the potential immune response to introduced CRISPRi elements must be considered [78–80].

The two most popular Cas9 species are from pathogenic bacteria: SaCas9 from *Staphylococcus aureus* and SpCas9 from *Streptococcus pyogenes*. It is therefore unsurprising that antibodies and cytotoxic T cells against SaCas9 and SpCas9 have been documented in healthy humans [81–83]. If activated, these could destroy Cas9 proteins found extracellularly or kill cells expressing Cas9 internally.

Immune responses also occur against gRNAs that are transcribed in vitro and used in RNPs. These gRNAs contain a 5′-triphosphate group which is associated with viruses and triggers the type-I interferon-mediated innate immune response within the cell. In one study, this caused cytotoxicity of both the treated and surrounding untreated cells in vitro but was completed alleviated by chemically converting the viral 5′-triphosphate group to a 5′-hydroxyl group [84].

No immune response experiments have been conducted with dCas9, although the response is assumed to be similar to that from Cas9. Successful CRISPRi requires long term stable expression of dCas9, which gives a wide window for potentially dangerous immune responses to occur, so this area must be researched thoroughly.

7. Conclusions

CRISPRi is a promising tool for the treatment of inherited retinal diseases. CRISPRi has a strong safety profile, as off-target repression is extremely rare, and the effects are completely reversed upon degradation of dCas9 or gRNA. Its low tolerance of gRNA:DNA mismatches makes it especially useful for allele-specific knock-down of dominant toxic gain-of-function mutations. While its efficiency can be highly variable, strong gene repression is achievable, and advances in fusion protein modifications and target site predictions are improving experimental outcomes.

Author Contributions: Conceptualization, R.E.M., C.F.P.; writing—original draft preparation, C.F.P.; writing—review and editing, C.F.P., L.E.F., M.E.M., R.E.M.; supervision, M.E.M., R.E.M. All authors have read and agreed to the published version of the manuscript.

Funding: This research was funded by support from the Royal College of Surgeons of Edinburgh, the Mabel Churn Scholarship, the Rhodes Trust, the North Harbour Club Charitable Trust, the Amar-Franses & Foster-Jenkins Trust and the NIHR Oxford Biomedical Research Centre.

Conflicts of Interest: The authors declare no conflict of interest. The funders had no role in the design of the study; in the collection, analyses, or interpretation of data; in the writing of the manuscript, or in the decision to publish the results. The views expressed are those of the authors and not necessarily those of the NIHR or the Department of Health and Social Care.

Abbreviations

AAV	Adeno-associated virus
CRISPRi	CRISPR interference
gRNA	Guide RNA
iPSCs	Induced pluripotent stem cells
KRAB	Krüppel associated box
RNAi	RNA interference
RNP	Ribonucleoprotein
SNP	Single nucleotide polymorphism
TSS	Transcriptional start site

References

1. Berger, W.; Kloeckener-Gruissem, B.; Neidhardt, J. The molecular basis of human retinal and vitreoretinal diseases. *Prog. Retin. Eye Res.* **2010**, *29*, 335–375. [CrossRef] [PubMed]
2. Hafler, B.P. Clinical progress in inherited retinal degenerations: Gene therapy clinical trials and advances in genetic sequencing. *Retina* **2017**, *37*, 417–423. [CrossRef]
3. Grob, S.; Finn, A.; Papakostas, T.; Eliott, D. Clinical trials in retinal dystrophies. *Middle East Afr. J. Ophthalmol.* **2016**, *23*, 49–59. [PubMed]
4. Benhar, I.; London, A.; Schwartz, M. The privileged immunity of immune privileged organs: The case of the eye. *Front. Immunol.* **2012**, *3*, 296. [CrossRef] [PubMed]
5. Lipinski, D.M.; Thake, M.; MacLaren, R.E. Clinical applications of retinal gene therapy. *Prog. Retin. Eye Res.* **2013**, *32*, 22–47. [CrossRef]
6. Kumaran, N.; Michaelides, M.; Smith, A.J.; Ali, R.R.; Bainbridge, J.W.B. Retinal gene therapy. *Br. Med. Bull.* **2018**, *126*, 13–25. [CrossRef]
7. Trapani, I.; Auricchio, A. Has retinal gene therapy come of age? From bench to bedside and back to bench. *Hum. Mol. Genet.* **2019**, *28*, R108–R118. [CrossRef]
8. Boye, S.E.; Boye, S.L.; Lewin, A.S.; Hauswirth, W.W. A comprehensive review of retinal gene therapy. *Mol. Ther.* **2013**, *21*, 509–519. [CrossRef]
9. Cong, L.; Ran, F.A.; Cox, D.; Lin, S.; Barretto, R.; Habib, N.; Hsu, P.D.; Wu, X.; Jiang, W.; Marraffini, L.A.; et al. Multiplex genome engineering using CRISPR/Cas systems. *Science* **2013**, *339*, 819–823. [CrossRef]
10. Jinek, M.; Chylinski, K.; Fonfara, I.; Hauer, M.; Doudna, J.A.; Charpentier, E. A Programmable Dual-RNA—Guided DNA endonuclease in adaptive bacterial immunity. *Science* **2012**, *337*, 816–822. [CrossRef]

11. Mojica, F.J.M.; Díez-Villaseñor, C.; García-Martínez, J.; Almendros, C. Short motif sequences determine the targets of the prokaryotic CRISPR defence system. *Microbiology* **2009**, *155*, 733–740. [CrossRef] [PubMed]
12. Anders, C.; Niewoehner, O.; Duerst, A.; Jinek, M. Structural basis of PAM-dependent target DNA recognition by the Cas9 endonuclease. *Nature* **2014**, *513*, 569–573. [CrossRef] [PubMed]
13. Ran, F.A.; Hsu, P.D.; Lin, C.Y.; Gootenberg, J.S.; Konermann, S.; Trevino, A.E.; Scott, D.A.; Inoue, A.; Matoba, S.; Zhang, Y.; et al. Double nicking by RNA-guided CRISPR cas9 for enhanced genome editing specificity. *Cell* **2013**, *154*, 1380–1389. [CrossRef]
14. Nishimasu, H.; Ran, F.A.; Hsu, P.D.; Konermann, S.; Shehata, S.I.; Dohmae, N.; Ishitani, R.; Zhang, F.; Nureki, O. Crystal structure of Cas9 in complex with guide RNA and target DNA. *Cell* **2014**, *156*, 935–949. [CrossRef] [PubMed]
15. Qi, L.S.; Larson, M.H.; Gilbert, L.A.; Doudna, J.A.; Weissman, J.S.; Arkin, A.P.; Lim, W.A. Repurposing CRISPR as an RNA-γuided platform for sequence-specific control of gene expression. *Cell* **2013**, *152*, 1173–1183. [CrossRef]
16. Sainsbury, S.; Bernecky, C.; Cramer, P. Structural basis of transcription initiation by RNA polymerase II. *Nat. Rev. Mol. Cell Biol.* **2015**, *16*, 129–143. [CrossRef]
17. Yao, L.; Berman, B.P.; Farnham, P.J. Demystifying the secret mission of enhancers: Linking distal regulatory elements to target genes. *Crit. Rev. Biochem. Mol. Biol.* **2015**, *50*, 550–573. [CrossRef]
18. Heintzman, N.D.; Ren, B. Finding distal regulatory elements in the human genome. *Curr. Opin. Genet. Dev.* **2009**, *19*, 541–549. [CrossRef]
19. Schübeler, D. Function and information content of DNA methylation. *Nature* **2015**, *517*, 321–326. [CrossRef]
20. Bobbin, M.L.; Rossi, J.J. RNA Interference (RNAi)-Based Therapeutics: Delivering on the Promise? *Annu. Rev. Pharmacol. Toxicol.* **2016**, *56*, 103–122. [CrossRef]
21. Lawrence, M.; Daujat, S.; Schneider, R. Lateral Thinking: How Histone Modifications Regulate Gene Expression. *Trends Genet.* **2016**, *32*, 42–56. [CrossRef] [PubMed]
22. Larson, M.H.; Gilbert, L.A.; Wang, X.; Lim, W.A.; Weissman, J.S.; Qi, L.S. CRISPR interference (CRISPRi) for sequence-specific control of gene expression. *Nat. Protoc.* **2013**, *8*, 2180–2196. [CrossRef] [PubMed]
23. Gilbert, L.A.; Horlbeck, M.A.; Adamson, B.; Villalta, J.E.; Chen, Y.; Whitehead, E.H.; Guimaraes, C.; Panning, B.; Ploegh, H.L.; Bassik, M.C.; et al. Genome-Scale CRISPR-Mediated Control of Gene Repression and Activation. *Cell* **2014**, *159*, 647–661. [CrossRef] [PubMed]
24. Radzisheuskaya, A.; Shlyueva, D.; Müller, I.; Helin, K. Optimizing sgRNA position markedly improves the efficiency of CRISPR/dCas9-mediated transcriptional repression. *Nucleic Acids Res.* **2016**, *44*, e141. [CrossRef] [PubMed]
25. Gilbert, L.A.; Larson, M.H.; Morsut, L.; Liu, Z.; Brar, G.A.; Torres, S.E.; Stern-Ginossar, N.; Brandman, O.; Whitehead, E.H.; Doudna, J.A.; et al. CRISPR-mediated modular RNA-guided regulation of transcription in eukaryotes. *Cell* **2013**, *154*, 442. [CrossRef] [PubMed]
26. Chung, J.Y.; Ul Ain, Q.; Song, Y.; Yong, S.B.; Kim, Y.H. Targeted delivery of CRISPR interference system against Fabp4 to white adipocytes ameliorates obesity, inflammation, hepatic steatosis, and insulin resistance. *Genome Res.* **2019**, *29*, 1442–1452. [CrossRef]
27. Yeo, N.C.; Chavez, A.; Lance-Byrne, A.; Chan, Y.; Menn, D.; Milanova, D.; Kuo, C.C.; Guo, X.; Sharma, S.; Tung, A.; et al. An enhanced CRISPR repressor for targeted mammalian gene regulation. *Nat. Methods* **2018**, *15*, 611–616. [CrossRef]
28. Lupo, A.; Cesaro, E.; Montano, G.; Zurlo, D.; Izzo, P.; Costanzo, P. KRAB-Zinc Finger Proteins: A Repressor Family Displaying Multiple Biological Functions. *Curr. Genom.* **2013**, *14*, 268–278. [CrossRef]
29. Lau, C.H.; Suh, Y. In vivo epigenome editing and transcriptional modulation using CRISPR technology. *Transgenic Res.* **2018**, *27*, 489–509. [CrossRef]
30. Liu, X.S.; Wu, H.; Ji, X.; Stelzer, Y.; Wu, X.; Czauderna, S.; Shu, J.; Dadon, D.; Young, R.A.; Jaenisch, R. Editing DNA Methylation in the Mammalian Genome. *Cell* **2016**, *167*, 233–247.e17. [CrossRef]
31. Peddle, C.F.; Maclaren, R.E. The Application of CRISPR/Cas9 for the Treatment of Retinal Diseases. *Yale J. Biol. Med.* **2017**, *90*, 533–541.
32. Evers, B.; Jastrzebski, K.; Heijmans, J.P.M.; Grernrum, W.; Beijersbergen, R.L.; Bernards, R. CRISPR knockout screening outperforms shRNA and CRISPRi in identifying essential genes. *Nat. Biotechnol.* **2016**, *34*, 631–633. [CrossRef]

33. Wyman, J.; Changeux, J.P.; Filmer, D.; Jovin, T.M.; Baehr, W.; Holbrook, J.J.; Dattagupta, N.; Crothers, D.M.; Hatfield, G.W.; Bruinsma, R.; et al. Multiplex Genome Engineering Using CRISPR/Cas Systems. *Science* **2013**, *339*, 819–824.
34. Hsu, P.D.; Scott, D.A.; Weinstein, J.A.; Ran, F.A.; Konermann, S.; Agarwala, V.; Li, Y.; Fine, E.J.; Wu, X.; Shalem, O.; et al. DNA targeting specificity of RNA-guided Cas9 nucleases. *Nat. Biotechnol.* **2013**, *31*, 827–832. [CrossRef] [PubMed]
35. Jiang, W.; Bikard, D.; Cox, D.; Zhang, F.; Marraffini, L.A. RNA-guided editing of bacterial genomes using CRISPR-Cas systems. *Nat. Biotechnol.* **2013**, *31*, 233–239. [CrossRef] [PubMed]
36. Fu, Y.; Foden, J.A.; Khayter, C.; Maeder, M.L.; Reyon, D.; Joung, J.K.; Sander, J.D. High-frequency off-target mutagenesis induced by CRISPR-Cas nucleases in human cells. *Nat. Biotechnol.* **2013**, *31*, 822–826. [CrossRef]
37. Slaymaker, I.M.; Gao, L.; Zetsche, B.; Scott, D.A.; Yan, W.X.; Zhang, F. Rationally engineered Cas9 nucleases with improved specificity. *Science* **2016**, *351*, 84–88. [CrossRef]
38. Kleinstiver, B.P.; Pattanayak, V.; Prew, M.S.; Tsai, S.Q.; Nguyen, N.T.; Zheng, Z.; Joung, J.K. High-fidelity CRISPR-Cas9 nucleases with no detectable genome-wide off-target effects. *Nature* **2016**, *529*, 490–495. [CrossRef] [PubMed]
39. Ikeda, A.; Fujii, W.; Sugiura, K.; Naito, K. High-fidelity endonuclease variant HypaCas9 facilitates accurate allele-specific gene modification in mouse zygotes. *Commun. Biol.* **2019**, *2*, 371–377. [CrossRef] [PubMed]
40. Casini, A.; Olivieri, M.; Petris, G.; Montagna, C.; Reginato, G.; Maule, G.; Lorenzin, F.; Prandi, D.; Romanel, A.; Demichelis, F.; et al. A highly specific SpCas9 variant is identified by in vivo screening in yeast. *Nat. Biotechnol.* **2018**, *36*, 265–271. [CrossRef]
41. Zheng, Y.; Shen, W.; Zhang, J.; Yang, B.; Liu, Y.N.; Qi, H.; Yu, X.; Lu, S.Y.; Chen, Y.; Xu, Y.Z.; et al. CRISPR interference-based specific and efficient gene inactivation in the brain. *Nat. Neurosci.* **2018**, *21*, 894. [CrossRef] [PubMed]
42. Thakore, P.I.; D'Ippolito, A.M.; Song, L.; Safi, A.; Shivakumar, N.K.; Kabadi, A.M.; Reddy, T.E.; Crawford, G.E.; Gersbach, C.A. Highly specific epigenome editing by CRISPR-Cas9 repressors for silencing of distal regulatory elements. *Nat. Methods* **2015**, *12*, 1143–1149. [CrossRef] [PubMed]
43. Setten, R.L.; Rossi, J.J.; Han, S. ping The current state and future directions of RNAi-based therapeutics. *Nat. Rev. Drug Discov.* **2019**, *18*, 421–446. [CrossRef] [PubMed]
44. Mullard, A. RNAi agents score an approval and drive an acquisition. *Nat. Rev. Drug Discov.* **2019**, *19*, 10. [CrossRef]
45. Svoboda, P. Off-targeting and other non-specific effects of RNAi experiments in mammalian cells. *Curr. Opin. Mol. Ther.* **2007**, *9*, 248–257.
46. Smith, I.; Greenside, P.G.; Natoli, T.; Lahr, D.L.; Wadden, D.; Tirosh, I.; Narayan, R.; Root, D.E.; Golub, T.R.; Subramanian, A.; et al. Evaluation of RNAi and CRISPR technologies by large-scale gene expression profiling in the Connectivity Map. *PLoS Biol.* **2017**, *15*, 1–23. [CrossRef]
47. Stojic, L.; Lun, A.T.L.; Mangei, J.; Mascalchi, P.; Quarantotti, V.; Barr, A.R.; Bakal, C.; Marioni, J.C.; Gergely, F.; Odom, D.T. Specificity of RNAi, LNA and CRISPRi as loss-of-function methods in transcriptional analysis. *Nucleic Acids Res.* **2018**, *46*, 5950–5966. [CrossRef]
48. Moreno, A.M.; Fu, X.; Zhu, J.; Katrekar, D.; Shih, Y.R.V.; Marlett, J.; Cabotaje, J.; Tat, J.; Naughton, J.; Lisowski, L.; et al. In Situ Gene Therapy via AAV-CRISPR-Cas9-Mediated Targeted Gene Regulation. *Mol. Ther.* **2018**, *26*, 1818–1827. [CrossRef]
49. MacLeod, R.S.; Cawley, K.M.; Gubrij, I.; Nookaew, I.; Onal, M.; O'Brien, C.A. Effective CRISPR interference of an endogenous gene via a single transgene in mice. *Sci. Rep.* **2019**, *9*, 17312. [CrossRef]
50. Cho, S.W.; Xu, J.; Sun, R.; Mumbach, M.R.; Carter, A.C.; Chen, Y.G.; Yost, K.E.; Kim, J.; He, J.; Nevins, S.A.; et al. Promoter of lncRNA Gene PVT1 Is a Tumor-Suppressor DNA Boundary Element. *Cell* **2018**, *173*, 1398–1412.e22. [CrossRef]
51. Bakondi, B.; Lv, W.; Lu, B.; Jones, M.K.; Tsai, Y.; Kim, K.J.; Levy, R.; Akhtar, A.A.; Breunig, J.J.; Svendsen, C.N.; et al. In vivo CRISPR/Cas9 gene editing corrects retinal dystrophy in the S334ter-3 rat model of autosomal dominant retinitis pigmentosa. *Mol. Ther.* **2016**, *24*, 556–563. [CrossRef] [PubMed]
52. Li, P.; Kleinstiver, B.P.; Leon, M.Y.; Prew, M.S.; Navarro-Gomez, D.; Greenwald, S.H.; Pierce, E.A.; Joung, J.K.; Liu, Q. Allele-Specific CRISPR-Cas9 Genome Editing of the Single-Base P23H Mutation for Rhodopsin-Associated Dominant Retinitis Pigmentosa. *Cris. J.* **2018**, *1*, 55–64. [CrossRef] [PubMed]

53. Zhu, J.; Ming, C.; Fu, X.; Duan, Y.; Hoang, D.A.; Rutgard, J.; Zhang, R.; Wang, W.; Hou, R.; Zhang, D.; et al. Gene and mutation independent therapy via CRISPR-Cas9 mediated cellular reprogramming in rod photoreceptors. *Cell Res.* **2017**, *27*, 830–833. [CrossRef] [PubMed]
54. Thakore, P.I.; Kwon, J.B.; Nelson, C.E.; Rouse, D.C.; Gemberling, M.P.; Oliver, M.L.; Gersbach, C.A. RNA-guided transcriptional silencing in vivo with S. aureus CRISPR-Cas9 repressors. *Nat. Commun.* **2018**, *9*, 1674. [CrossRef] [PubMed]
55. Kim, E.; Koo, T.; Park, S.W.; Kim, D.; Kim, K.; Cho, H.Y.; Song, D.W.; Lee, K.J.; Jung, M.H.; Kim, S.; et al. In vivo genome editing with a small Cas9 orthologue derived from Campylobacter jejuni. *Nat. Commun.* **2017**, *8*, 14500. [CrossRef]
56. Garba, A.O.; Mousa, S.A. Bevasiranib for the Treatment of Wet, Age-Related Macular Degeneration. *Ophthalmol Eye Dis.* **2010**, *2*, 75–83. [CrossRef]
57. Yoshida, M.; Yokota, E.; Sakuma, T.; Yamatsuji, T.; Takigawa, N.; Ushijima, T.; Yamamoto, T.; Fukazawa, T.; Naomoto, Y. Development of an integrated CRISPRi targeting ^Np63 for treatment of squamous cell carcinoma. *Oncotarget* **2018**, *9*, 29220–29232. [CrossRef]
58. Truong, V.A.; Hsu, M.N.; Kieu Nguyen, N.T.; Lin, M.W.; Shen, C.C.; Lin, C.Y.; Hu, Y.C. CRISPRai for simultaneous gene activation and inhibition to promote stem cell chondrogenesis and calvarial bone regeneration. *Nucleic Acids Res.* **2019**, *47*, e74. [CrossRef]
59. Bassuk, A.G.; Zheng, A.; Li, Y.; Tsang, S.H.; Mahajan, V.B. Precision Medicine: Genetic Repair of Retinitis Pigmentosa in Patient-Derived Stem Cells. *Sci. Rep.* **2016**, *6*, 19969. [CrossRef]
60. Deng, W.L.; Gao, M.L.; Lei, X.L.; Lv, J.N.; Zhao, H.; He, K.W.; Xia, X.X.; Li, L.Y.; Chen, Y.C.; Li, Y.P.; et al. Gene Correction Reverses Ciliopathy and Photoreceptor Loss in iPSC-Derived Retinal Organoids from Retinitis Pigmentosa Patients. *Stem Cell Rep.* **2018**, *10*, 1267–1281. [CrossRef]
61. Burnight, E.R.; Gupta, M.; Wiley, L.A.; Anfinson, K.R.; Tran, A.; Triboulet, R.; Hoffmann, J.M.; Klaahsen, D.L.; Andorf, J.L.; Jiao, C.; et al. Using CRISPR-Cas9 to Generate Gene-Corrected Autologous iPSCs for the Treatment of Inherited Retinal Degeneration. *Mol. Ther.* **2017**, *25*, 1999–2013. [CrossRef] [PubMed]
62. Terrell, D.; Comander, J. Current Stem-Cell Approaches for the Treatment of Inherited Retinal Degenerations. *Semin. Ophthalmol.* **2019**, *34*, 287–292. [CrossRef] [PubMed]
63. Yu, W.; Mookherjee, S.; Chaitankar, V.; Hiriyanna, S.; Kim, J.W.; Brooks, M.; Ataeijannati, Y.; Sun, X.; Dong, L.; Li, T.; et al. Nrl knockdown by AAV-delivered CRISPR/Cas9 prevents retinal degeneration in mice. *Nat. Commun.* **2017**, *8*, 14716. [CrossRef] [PubMed]
64. Suzuki, K.; Tsunekawa, Y.; Hernandez-Benitez, R.; Wu, J.; Zhu, J.; Kim, E.J.; Hatanaka, F.; Yamamoto, M.; Araoka, T.; Li, Z.; et al. In vivo genome editing via CRISPR/Cas9 mediated homology-independent targeted integration. *Nature* **2016**, *540*, 144–149. [CrossRef] [PubMed]
65. Wang, D.; Tai, P.W.L.; Gao, G. Adeno-associated virus vector as a platform for gene therapy delivery. *Nat. Rev. Drug Discov.* **2019**, *18*, 358–378. [CrossRef]
66. Friedland, A.E.; Baral, R.; Singhal, P.; Loveluck, K.; Shen, S.; Sanchez, M.; Marco, E.; Gotta, G.M.; Maeder, M.L.; Kennedy, E.M.; et al. Characterization of Staphylococcus aureus Cas9: A smaller Cas9 for all-in-one adeno-associated virus delivery and paired nickase applications. *Genome Biol.* **2015**, *16*, 1–10. [CrossRef]
67. Hou, Z.; Zhang, Y.; Propson, N.E.; Howden, S.E.; Chu, L.F.; Sontheimer, E.J.; Thomson, J.A. Efficient genome engineering in human pluripotent stem cells using Cas9 from Neisseria meningitidis. *Proc. Natl. Acad. Sci. USA* **2013**, *110*, 15644–15649. [CrossRef]
68. Ran, F.A.; Cong, L.; Yan, W.X.; Scott, D.A.; Gootenberg, J.S.; Kriz, A.J.; Zetsche, B.; Shalem, O.; Wu, X.; Makarova, K.S.; et al. In vivo genome editing using Staphylococcus aureus Cas9. *Nature* **2015**, *520*, 186–191. [CrossRef]
69. Harrington, L.B.; Paez-Espino, D.; Staahl, B.T.; Chen, J.S.; Ma, E.; Kyrpides, N.C.; Doudna, J.A. A thermostable Cas9 with increased lifetime in human plasma. *Nat. Commun.* **2017**, *8*, 1424. [CrossRef]
70. Murovec, J.; Pirc, Ž.; Yang, B. New variants of CRISPR RNA-guided genome editing enzymes. *Plant Biotechnol. J.* **2017**, *15*, 917–926. [CrossRef]
71. Schlimgen, R.; Howard, J.; Wooley, D.; Thompson, M.; Baden, L.R.; Yang, O.O.; Christiani, D.C.; Mostoslavsky, G.; Diamond, D.V.; Duane, E.G.; et al. Risks associated with lentiviral vector exposures and prevention strategies. *J. Occup. Environ. Med.* **2016**, *58*, 1159–1166.
72. Yu, W.; Wu, Z. In Vivo applications of CRISPR-based genome editing in the retina. *Front. Cell Dev. Biol.* **2018**, *6*, 6. [CrossRef] [PubMed]

73. Kim, K.; Park, S.W.; Kim, J.H.; Lee, S.H.; Kim, D.; Koo, T.; Kim, K.E.; Kim, J.H.; Kim, J.S. Genome surgery using Cas9 ribonucleoproteins for the treatment of age-related macular degeneration. *Genome Res.* **2017**, *27*, 419–426. [CrossRef] [PubMed]
74. Latella, M.C.; Di Salvo, M.T.; Cocchiarella, F.; Benati, D.; Grisendi, G.; Comitato, A.; Marigo, V.; Recchia, A. In vivo Editing of the Human Mutant Rhodopsin Gene by Electroporation of Plasmid-based CRISPR/Cas9 in the Mouse Retina. *Mol. Ther. Nucleic Acids* **2016**, *5*, e389. [CrossRef] [PubMed]
75. Dhande, O.S.; Crair, M.C. Transfection of mouse retinal ganglion cells by in vivo electroporation. *J. Vis. Exp.* **2011**, *50*, e2678. [CrossRef] [PubMed]
76. Taylor, A.W. Ocular Immune Privilege and Transplantation. *Front. Immunol.* **2016**, *7*, 58. [CrossRef] [PubMed]
77. Chandler, L.C.; Barnard, A.R.; Caddy, S.L.; Patrício, M.I.; Mcclements, M.E.; Fu, H.; Rada, C.; Maclaren, R.E.; Xue, K. Enhancement of Adeno-Associated Virus-Mediated Gene Therapy Using Hydroxychloroquine in Murine and Human Tissues. *Mol. Ther. Methods Clin. Dev.* **2019**, *14*, 77–89. [CrossRef]
78. Bainbridge, J.W.B.; Mehat, M.S.; Sundaram, V.; Robbie, S.J.; Barker, S.E.; Ripamonti, C.; Georgiadis, A.; Mowat, F.M.; Beattie, S.G.; Gardner, P.J.; et al. Long-term effect of gene therapy on Leber's congenital amaurosis. *N. Engl. J. Med.* **2015**, *372*, 1887–1897. [CrossRef]
79. Guy, J.; Feuer, W.J.; Davis, J.L.; Porciatti, V.; Gonzalez, P.J.; Koilkonda, R.D.; Yuan, H.; Hauswirth, W.W.; Lam, B.L. Gene Therapy for Leber Hereditary Optic Neuropathy: Low- and Medium-Dose Visual Results. *Ophthalmology* **2017**, *124*, 1621–1634. [CrossRef]
80. Xue, K.; Jolly, J.K.; Barnard, A.R.; Rudenko, A.; Salvetti, A.P.; Patrício, M.I.; Edwards, T.L.; Groppe, M.; Orlans, H.O.; Tolmachova, T.; et al. Beneficial effects on vision in patients undergoing retinal gene therapy for choroideremia. *Nat. Med.* **2018**, *24*, 1507–1512. [CrossRef]
81. Charlesworth, C.T.; Deshpande, P.S.; Dever, D.P.; Camarena, J.; Lemgart, V.T.; Cromer, M.K.; Vakulskas, C.A.; Collingwood, M.A.; Zhang, L.; Bode, N.M.; et al. Identification of preexisting adaptive immunity to Cas9 proteins in humans. *Nat. Med.* **2019**, *25*, 249–254. [CrossRef] [PubMed]
82. Simhadri, V.L.; McGill, J.; McMahon, S.; Wang, J.; Jiang, H.; Sauna, Z.E. Prevalence of Pre-existing Antibodies to CRISPR-Associated Nuclease Cas9 in the USA Population. *Mol. Ther. Methods Clin. Dev.* **2018**, *10*, 105–112. [CrossRef] [PubMed]
83. Wagner, D.L.; Amini, L.; Wendering, D.J.; Burkhardt, L.M.; Akyüz, L.; Reinke, P.; Volk, H.D.; Schmueck-Henneresse, M. High prevalence of Streptococcus pyogenes Cas9-reactive T cells within the adult human population. *Nat. Med.* **2019**, *25*, 242–248. [CrossRef] [PubMed]
84. Kim, S.; Koo, T.; Jee, H.G.; Cho, H.Y.; Lee, G.; Lim, D.G.; Shin, H.S.; Kim, J.S. CRISPR RNAs trigger innate immune responses in human cells. *Genome Res.* **2018**, *28*, 367–373. [CrossRef] [PubMed]